

**DESIGN OF PEPTIDES WITH TARGETED APATITE AND HUMAN BONE
Marrow Stromal Cell Adhesion for Bone Tissue Engineering**

by

Sharon Janell Segvich

A dissertation submitted in partial fulfillment
of the requirements for the degree of
Doctor of Philosophy
(Biomedical Engineering)
in The University of Michigan
2008

Doctoral Committee:

Professor David H. Kohn, Chair
Professor Renny T. Franceschi
Associate Professor Udo Becker
Associate Professor Yvonne L. Kapila
Associate Professor Shuichi Takayama

© Sharon Janell Segvich

All rights reserved

2008

To Scott, for your infinite patience

ACKNOWLEDGEMENTS

I would like to thank Dave Kohn for being my advisor and mentor. You gave me the freedom to explore my own research and with that came confidence, experience, and more questions. Thank you for your patience when I was learning and your guidance when needed. I am grateful for our candid conversations that have schooled me not only in science, but also in many aspects of life. If I am ever honored with a Pulitzer Prize, I will be sure to dedicate it to you and your red pen.

The expertise of my thesis committee that contributed to the success of my work should be acknowledged. To Udo Becker, Renny Franceschi, Yvonne Kapila, and Shuichi Takayama, thank you for your time, advice, and resources. Your guidance has made me a better researcher and a more thorough reviewer, hopefully both of which I can take with me in my next endeavors.

To Hayes C. Smith, thank you for sticking by my side for three years. You're superb SBF making skills, eclectic music taste, compassion for others, and shared appreciation for delicious iced tea made working with you easy and fun. I wish you could have been around when all the work started to come together. It wouldn't have if it weren't for all of our hard work at the beginning. You are by far, one of my favorite people, and it was a pleasure being your "boss" for a while.

I would also like to thank Subhashis Biswas for his efforts in developing the apatite force field. I appreciate all of your efforts and am glad we became friends along the way.

As an ambitious graduate student, I pursued many things that would have never happened without the help and support from many people all over the college. I am grateful for the first experiences I had in grad school with the Skeletal Engineering Group directed by Scott Hollister. A special thank you to Alisha Diggs for always having a big

smile, having time to press disks, and introducing me to some of your other talented colleagues. For microCT and BET help, thank you to Colleen Flanagan, Jeff Meganck, Worajit Setthapun, and Xiaoyin Chen. Thanks also to Jen Mahoney and Henriette Remmer of the Protein Core for always accommodating my peptide requests.

As a grad student, you spend a lot of your time in lab. So, to my labmates Linh Luong, Ricky Rossello, Kyungsup Shin, Erin Gatenby, and Janani Ramaswamy, you made lab bearable, sometimes even fun, and entertained my social coordinator events. We've braved rides at Cedar Point, eaten hot dogs at Tiger Stadium, and farmed a co-ed softball team that went by the name of 'The Kohnheads'. Thanks for all the support, advice, and seemingly endless conversations of how to get out of grad school. Your hard work always made me work harder.

For the behind-the-scene staff that was there to ensure paperwork was completed, deadlines were met, and conference arrangements were seamless. Thank you Liz Rodriguiz, Maria Steele, Pat Schultz, Kim Huner, and Wanda Snyder.

To Teresa Patterson, an angel in disguise. I admire your combination of strength and spirit, and I aspire to be able to project your positive attitude and good karma.

To Joey Wallace and Nadder Sahar, a couple of characters that made me appreciate ricotta is NOT a cheese and realize I have an uncanny ability to make homemade Prince halloween costumes. You two are my best friends from grad school, and I know we will continue to harass one another throughout life. If you guys weren't around to ponder ideas, dispel frustrations, or share successes, I imagine grad school would have been tougher. Thank you for always treating me like one of the guys. You are extended family now, so I expect more good food, football watching, and vacations to come. I'm always here if you need anything or want to get a drink at The Arena.

To Liz McKinley and Graeme Dickinson, for always believing in never losing touch and me. When things are out of sight, they often are out of mind, but you were always there to remind me that life exists outside of school.

To my parents, your silent support throughout all my years of college has not gone unnoticed. I respect your sacrificed time and energy over the years. I am forever grateful for the trips you made to Ann Arbor (especially those with Freeda), when I could not escape. You have taught me more in life by showing than you ever could with words. Thanks for being such great parents, ja cie Kocham to both of you. To Mark, Jen, and Dyann, thank you for keeping tabs on me and putting up with my professional student lifestyle. To Big O and Little E, thanks for always making me smile and laugh (and find every park imaginable in Ann Arbor). To Uncle Ronnie, your spirit is the greatest gift any uncle could give to his niece. To my new family, the Millers', thank you for taking me in as one of your own. I am excited to become an official member of the family and know that we have many more memorable times ahead of us.

Last, I would like to thank Scott Miller, my better half, my best friend, and partner in life. Thank you for being the most patient, fun-loving, and understanding person I know. Over the years, we have realized we make one heck of a team. You have always supported my crazy ideas and equally crazy lifestyle. Wherever we end up, may there always be laughter, spirit, and love.

TABLE OF CONTENTS

DEDICATION.....	ii
ACKNOWLEDGEMENTS	iii
LIST OF FIGURES.....	ix
LIST OF TABLES.....	xiii
LIST OF APPENDICES	xiv
ABSTRACT	xv
CHAPTER ONE INTRODUCTION	1
Biomimetics and Biomineralization	1
Basic Bone Biology	2
Bone-like Mineral and Hydroxyapatite Structure	2
Bone Tissue Engineering	4
Protein Engineering	6
Surface Modification via Peptides to Increase Biological Function	
Surface Adsorption and Quantification of Peptides	
Phage Display	10
Modeling Apatite	11
Modeling Approaches	
Modeling Inorganic-Organic Interactions	
Hypothesis and Aims	14
CHAPTER TWO IDENTIFICATION OF PREFERENTIAL BINDING	
PEPTIDES ON APATITE-BASED MATERIALS AND AN	
INVESTIGATION OF THEIR SURFACE ADSORPTION.....	26
Introduction	26
Materials and Methods.....	29
Preparation of Biomimetic Films and Apatite Disks	
Identification and Sequencing of BLM and HA Binding Peptides	
Peptide Selection	
Phage Binding ELISA	
Synthetic Peptide Adsorption Assay	
Statistics	
Material Characterization	
Results	35

Identification of High Affinity Phage Towards Apatite-based Materials	
S and V Adsorb Consistently With the Highest Affinity on the Apatite-based Materials	
Adsorption of Preferential Binding Peptides on Apatite-based Materials Depends on Substrate Composition and Morphology	
Discussion	39
Acknowledgements.....	43
CHAPTER THREE PEPTIDES DESIGNED TO ADHERE TO BOTH APATITE AND HUMAN BONE MARROW STROMAL CELLS IMPROVE CELL ATTACHMENT ON BONE-LIKE MINERAL	56
Introduction	56
Materials and Methods.....	60
Preparation of Bone-like Mineral Films and Apatite Disks	
Cells	
Phage Display on hBMSCs	
RELIC Analysis	
Peptide Synthesis and Adsorption	
Cell Attachment Assay	
Statistics	
Results.....	68
Identification of Preferential Cell Adhesion Sequences to hBMSCs via Phage Display	
Adsorption of Dual-Functioning Peptides on Apatite Materials	
Dual-Functioning Peptide Influences hBMSC Adhesion to Bone-Like Mineral	
Discussion	70
Acknowledgements.....	75
CHAPTER FOUR UNIFORM DEPOSITION OF PROTEIN INCORPORATED MINERAL LAYER ON THREE-DIMENSIONAL POROUS POLYMER SCAFFOLDS.....	86
Introduction	86
Materials and Methods.....	89
Scaffold Fabrication	
Simulated Body Fluid Preparation	
Mineralization of Scaffolds in the Filtration System	
BSA Coprecipitation	
MicroCT Analysis of Mineralized Scaffolds	
X-ray Diffraction Analysis	
FTIR Analysis	

BSA Quantification	
Confocal Microscopy	
Statistics	
Results	94
Uniform, Continuous Mineral Precipitated Throughout the Depth of Filtered Scaffolds	
Uniform and Increased BSA Incorporation in Filtered Scaffolds	
Discussion	95
Acknowledgements	100
CHAPTER FIVE SUMMARY AND FUTURE WORK.....	110
The Identification of Peptide Sequences for Bone Tissue Engineering	111
Dual-Functioning Peptide Performance.....	112
The Effect of Surface Composition and Morphology on Peptide Adsorption....	113
Phosphorylation as a Method to Tailor Peptide Adhesion.....	114
Inducing Fluid Flow Improves Mineralization in Three-Dimensional Scaffolds	116
Future Studies.....	116
Broader Applications of Dual-Functioning Peptides.....	119
APPENDICES	123
BIBLIOGRAPHY	184

LIST OF FIGURES

Figure 1.1: Hierarchical Bone Structure.....	19
Figure 1.2: Hydroxyapatite Lattice Structure.	20
Figure 1.3: Thermodynamic Conditions for Film Formation.	21
Figure 1.4: Steps Involved in Cell Adhesion.	22
Figure 1.5: Phage Display Schematic.....	23
Figure 2.1: Schematic displaying the tri-fold analysis approach used to identify peptides that preferentially adhere to BLM and HA.	45
Figure 2.2: INFO content values calculated in RELIC for NEB background and phage subset identified as high affinity binders to apatite-based materials.	46
Figure 2.3: Modified ELISA results for 10 representative peptides on 4 substrates showing a higher absorbance value at OD 410 with a higher concentration of phage.....	47
Figure 2.4 Adsorption of peptides EEEEEEEPRGDT [E], APWHLSSQYSRT [A], STLPIPHFSRE [S], and VTKHLNQISQSY [V] on (a) tissue culture polystyrene (TCPS), (b) sintered disks from 5.6% carbonated apatite powder (CA5), (c) sintered disks from 10.5% carbonated apatite powder (CA10), (d) sintered disks from hydroxyapatite powder (HA), and (e) bone-like mineral (BLM).....	48
Figure 2.5 Representative SEM images showing low and high magnification morphologies of the four apatite-based materials: (a) sintered disks from hydroxyapatite powder (HA), (b) sintered disks from 5.6% carbonated apatite powder (CA5), (c) bone-like mineral films (BLM), and (d) sintered disks from 10% carbonated apatite powder (CA10).	49
Figure 2.6: Representative FT-IR spectra for bone-like mineral (BLM), sintered disks from 5.6% carbonated apatite powder (CA5), sintered disks from 10.5% carbonated apatite powder (CA10), and sintered disks from hydroxyapatite powder (HA) substrates.....	50
Figure 2.7: X-ray diffraction patterns for bone-like mineral (BLM), sintered disks from 10.5% carbonated apatite powder (CA10), sintered disks from	

5.6% carbonated apatite powder (CA5), sintered disks from hydroxyapatite powder (HA), and a calcium phosphate standard (CaP Std).	51
Figure 2.8: Peptide adsorption data normalized to sample dimensions (MacroSA) shows that peptides A and S have increased adsorption on CA5 and CA10 when compared with BLM (For A, CA5 $p=0.006$, CA10 $p=0.001$; For S, CA5 $p=0.001$, CA10 $p<0.001$).....	52
Figure 2.9: Peptide adsorption data normalized to sample dimensions (MicroSA).	53
Figure 3.1: Schematic displaying data analysis progression used to identify peptides that preferentially adhere to clonally derived hBMSCs.....	76
Figure 3.2: Consensus sequences from the MOTIF1 program showing (S/T)(I/V)LS and NHT as the 4- and 3-mer motifs having the most frequent hits.....	77
Figure 3.3: INFO content values calculated in RELIC for NEB background and phage subset identified as preferential binders to clonally derived hBMSCs.	78
Figure 3.4: Representative confocal images from the immunohistochemistry with the phage containing the sequences LLADTTHHRPWT (a) and DPIYALSWGMA (b) showing positive FITC signal at 488nm for the hBMSC introduced to the phage. Images are compressed z-stacks taken for 20 μ m at 2 μ m intervals.	79
Figure 3.5: Adsorption of five dual-functioning peptides (L-VTK, D-VTK, RGDV, RGEV, and E) on four substrates (BLM, HA, CA5, and TCPS).	81
Figure 3.6: (a) hBMSC adhesion on BLM for all five peptides tested. L-VTK and D-VTK had a positive influence on cell attachment compared to BLM devoid of peptide. RGDV, RGEV, and E had low levels of cell attachment compared to the BLM control. (b) hBMSC adhesion on TCPS for all five peptides tested. L-VTK and RGEV were the only peptides that showed increased cell attachment compared to the TCPS devoid of peptide. All experiments were performed in duplicate, with each experiment having $n=6$	82
Figure 3.7: Cell adhesion normalized to amount of peptide adsorbed on BLM.....	83

Figure 4.1: Schematic showing the filtration device.....	101
Figure 4.2: Representative MicroCT images of the filtration group (a-c) and the submerged control group (d-f).	102
Figure 4.3: Mineral Volume % (MV%) for the filtration, floating control, and submerged control groups demonstrated the filtration group mineralized the greatest amount. (* - p = 0.029 vs. both controls).....	103
Figure 4.4: Volumetric mineral analysis of the MicroCT images (threshold = 1000) showing the filtration scaffolds have a uniform mineral profile throughout all 6 regions of the scaffolds analyzed.....	104
Figure 4.5: FTIR spectra for filtration, floating control, and submerged control groups showing the mineral deposited on the scaffolds was characteristic of hydroxyapatite with carbonate peaks (ν_{3c} P-O 1032 cm^{-1} , ν_1 P-O 962 cm^{-1} , ν_{4a} O-P-O 602 cm^{-1} , and ν_{4c} O-P-O 561 cm^{-1} [filtration group only]) and carbonated apatite (ν_1 CO_3^{2-} 1465 cm^{-1} [filtration and floating control groups])......	105
Figure 4.6: XRD spectra for all three groups (filtration, floating control, submerged control) show characteristic apatite peaks between 25.9°-26.8°, between 31.8°-32.7°, at 40.1°, and between 45°-55° when compared to the hydroxyapatite standard.	106
Figure 4.7: Quantitative coprecipitated BSA values (μg) showing greater protein incorporation in the filtered scaffolds.....	107
Figure 4.8: Representative confocal microscopy images of transverse sections of filtration (a) and submerged control (b) groups coprecipitated with BSA for 3 days.	108
Figure 4.9: Mineral Volume % (MV%) for the filtration and submerged control coprecipitation groups demonstrated the filtration group mineralized the greatest amount. (* - p < 0.001). MV% was calculated from MicroCT data using MicroView® at a threshold of 1000.....	109
Figure 5.1: Adsorption of VTK vs. VTK-phos on apatite-based substrates.....	121
Figure 5.2: Cell attachment data reported in Figure 3.7 with the addition of VTK-phos.....	122
Figure A.1: Hydroxyapatite lattice cluster set-ups.....	127

Figure B.1: Standard curve for peptide APWHLSSQYSRT [A] (MW = 1431.7 g/mol) determined via UV spectroscopy at A205.....	157
Figure B.2: Standard curve for peptide EEEEEEEPRGDT [E] (MW = 1447.6 g/mol) determined via UV spectroscopy at A220.....	158
Figure B.3: Standard curve for peptide STLPIPEFSHRE [S] (MW = 1411.7 g/mol) determined via UV spectroscopy at A205.....	159
Figure B.4: Standard curve for peptide VTKHLNQISQSY [V] (MW = 1416.7 g/mol) determined via UV spectroscopy at A205.....	160
Figure B.5: Standard curve for peptide GGDPIYALSWSGMAGGGSVTKHLNQISQSY (MW = 3081.2 g/mol) determined via UV spectroscopy at A205.....	161
Figure B.6: Standard curve for peptide GLLADTTHHRPWTGGGSVTKHLNQISQSY (MW = 3218.0 g/mol) determined via UV spectroscopy at A205.....	162
Figure B.7: Standard curve for peptide GGRGDGGGSVTKHLNQISQSY (MW = 2117.6 g/mol) determined via UV spectroscopy at A205.	163
Figure B.8: Standard curve for peptide GGRGEGGGSVTKHLNQISQSY (MW = 2131.6 g/mol) determined via UV spectroscopy at A205.	164
Figure B.9: Standard curve for peptide EEEEEEEPRGDT (MW = 1447.6 g/mol) determined via UV spectroscopy at A205.	165
Figure B.10: Standard curve for peptide VTKHLNQIS(p)QS(p)Y (MW = 1576. g/mol) determined via UV spectroscopy at A205.....	166

LIST OF TABLES

Table 1.1: Formulas and Names for Common Non-Stoichiometric Apatite Phases.....	24
Table 1.2: Ion Concentrations Present in the Supersaturated Ionic Solution (SBF).....	25
Table 2.1: Peptide Sequences Identified via Phage Display with Preferential Adsorption Towards Apatite-Based Materials.....	54
Table 2.2: Summary of Computational Modeling Data for Peptides A, S, and V on Hydroxyapatite (001) Surface and Step Surface.....	55
Table 3.1: Immunohistochemistry Scoring for hBMSC with Phage Treated with and without Saponin.....	84
Table 3.2: Dual-functioning Peptide Sequences Containing Both an Apatite Seeking Portion (underlined) and a Cell Adhesive or Control Sequence (bold).....	85
Table A.1: HYDROXYAPATITE Force Field Potential Parameters Used in Molecular Modeling of the 19 Phage Derived Peptides on Hydroxyapatite Surface and Surface Step.....	128
Table A.2: Comparison of Experimentally Determined and Computational (Using Table A.1 Force Field Values) Cell Parameters and Fractional Units.....	129
Table A.3: Peptide Charge Assignments Based on Peptide Composition.....	130
Table A.4: Molecular Modeling Results for 19 Phage Display Derived Apatite-Binding Peptides on (001) HA Plane and [010] Step on (001) HA Plane for Both Neutral and Charged Peptides.....	131
Table B.1: Standard Curve Dilution Scheme for Peptide Adsorption.....	167
Table B.2: Cell Standard Curve Scheme for Cell Attachment Assay.....	168

LIST OF APPENDICES

APPENDIX A: Computational Modeling	123
APPENDIX B: Phage Display and Peptide Protocols	132
APPENDIX C: Bioreactor Protocol and MATLAB Program	169
APPENDIX D: Papers and Presentations	181

ABSTRACT

The restoration and repair of orofacial and large bone defects resulting from extreme trauma, disease, or genetic inheritance is a clinical challenge in need of new solutions, as current grafting techniques can result in donor site morbidity, graft rejection, and/or inadequate bone formation and quality. Because bone is a complex organ, its hierarchical structure may only be restored in such defects if a temporary material guides tissue formation. Bone tissue engineering explores combinations of materials, biological signals, and cell sources to achieve guided tissue formation with structure-function properties matching those of native tissue.

By using nature's building blocks, or amino acids, as a design platform to synthesize multi-dimensional biomolecules in the form of peptides, biological function can be influenced. The idea is to provide specificity to induce a desired biological activity. In addition, coating a material with biomimetic bone-like mineral can provide a surface morphology and composition similar to the native hydroxyapatite in bone. While bone-like mineral can increase bone growth *in vivo*, the tissue formed is not uniform or spatially controlled, suggesting the need for better-designed scaffolding to spatiotemporally influence bone tissue development.

No studies have investigated the potential impact biomolecule-laden bone-like mineral has on influencing cell behavior. The work presented in this thesis is first to design dual-functioning peptides to increase *in vitro* cell attachment on bone-like mineral. Using a combinatorial phage library, computational modeling, and biological assays, specific peptide sequences that preferentially adsorb to bone-like mineral and attach to clonally derived human bone marrow stromal cells (hBMSCs) were identified. When combined, these sequences formed a dual-functioning peptide that exhibited an increased ability to attach hBMSCs compared to previous peptide designs. Additionally, a

bioreactor was designed to coat three-dimensional porous scaffolds with uniform, continuous bone-like mineral, addressing a need for improved biomimetic coating fabrication techniques. The presented strategies can influence guided bone growth and advance the current methodologies in bone engineering. This work provides a new paradigm for peptide development linking organics to inorganics, not only for bone tissue engineered constructs, but also for any system requiring temporary or guided adhesion.

CHAPTER ONE

INTRODUCTION

Science is often inspired by nature, and the fields of biomimetics and biomineralization are no exception. Examples found in nature that have inspired man-made materials include calcium phosphate derived bones and teeth and calcium carbonate containing mollusk shells. Hard tissues produced by organisms are created in shapes and structures at multiple levels of dimensional scale that are non-trivial to synthetically reproduce. To understand the depth of complexity, one must first understand the concepts of biomimetics and biomineralization.

Biomimetics and Biomineralization

The field of biomimetics aims to replicate the formation, structure, and function of biological entities. In other words, biomimetics uses the process of mimicry to achieve a desired functional effect in a man-made material. Biomineralization is the process by which minerals, or ordered inorganic-organic structures, are fabricated by living organisms. Biominerals are typically composite structures comprised of a precipitated inorganic structure intertwined with an organic molecular phase. A structural hierarchy exists within biominerals from the macroscopic level down to the nanoscopic level. The inorganic phase of natural biominerals can range from single crystals to semi-crystalline and amorphous phases. Another striking feature of the development of biominerals in nature is that they are formed at ambient or physiological temperatures and pressures. The structural control that produces the unique morphologies of biominerals has been unmatched by any synthetic material. The organic components found within biominerals have an amazing ability to direct nucleation and growth of the inorganic mineral.

Specific organic molecules produced by the organism can inhibit or promote crystal face growth to achieve a complex structure with extraordinary mechanical properties.

We can apply knowledge from biomimetics towards the field of bone tissue engineering, which seeks to replace damaged bone tissue by restoring and/or improving the complex inorganic-organic bone structure (Langer and Vacanti, 1993). The work presented in this thesis aims to improve the materials and methods used in guided bone repair; however, before attempting to do so, pertinent knowledge on bone composition and structure is reviewed.

Basic Bone Biology

Bones serve a variety of functions including both a structural role (supporting body weight, enabling movement, and protecting organs) and a biological role (storing calcium, maintaining calcium homeostasis, and producing red blood cells) (Gunn, 1996). Bone extracellular matrix is composed of 50-70% inorganic mineral, 20-40% organic components (collagen, non-collagenous proteins, lipids, and vascular elements), and 5-10% water (Robey and Boskey, 2003). The inorganic mineral phase is a form of hydroxyapatite ($\text{Ca}_{10}(\text{PO}_4)_6(\text{OH})_2$) that is typically carbonated at 2-7 wt% (Posner et al., 1984). The mechanical strength and density of bone are derived from the ability of the organism to assemble hydroxyapatite imbedded within an organic matrix (Figure 1.1). The mineralization of bone consists of ordering the *c*-axis of hydroxyapatite crystals parallel with Type I collagen molecules. Precipitation of the apatite onto collagen occurs when the ion activity product (IAP) of the surrounding fluid or solution exceeds the solubility product of the precipitating phase (Boskey, 1999). Experimentally reproducing the hydroxyapatite structure often results in incorrect stoichiometric chemistries; thus, the term bone-like mineral (BLM) will be used to represent the biomimetic apatite phase formed synthetically from a supersaturated ionic solution at 37°C.

Bone-like Mineral and Hydroxyapatite Structure

The composition of hydroxyapatite is typically written as $\text{Ca}_{10}(\text{PO}_4)_6(\text{OH})_2$, denoting that two formula units are represented within the unit cell. The unit cell

parameters for hydroxyapatite can vary ($a=b=9.32-9.64 \text{ \AA}$ and $c=6.78-6.90 \text{ \AA}$) (Nesse, 2000). Pure hydroxyapatite has a monoclinic structure, even though fluorapatite ($\text{Ca}_5(\text{PO}_4)_3\text{F}$) is defined as hexagonal, because the non-spherical hydroxyl groups within the channel position prevent a required mirror plane in the hexagonal structure definition (Figure 1.2). The hydroxyapatite lattice can accommodate many chemical substitutions, most commonly Sr, Ba, Cd, Pb in the Ca position, V, As, S, Si, Ge, CO_3 in the P position, and F, Cl, O, Br, CO_3 in the OH position (Aoki, 1991). Certain types of substitution can elicit an increase or decrease in the unit cell dimensions of apatite. Slight changes to the chemical composition of hydroxyapatite can influence solubility, hardness, and thermal stability, among other structural and optical properties (Wopenka and Pasteris, 2005). As an example, fluoride substitutes readily for hydroxyl ions in tooth enamel, increasing the apatite's resistance to dissolution in acidic environments (e.g. soft drinks). If a perfect hydroxyapatite crystal is not formed during crystallization, other phases with varied stoichiometries could form (Table 1.1) (Ben-Nissan et al., 1995; Wopenka and Pasteris, 2005).

Often, supersaturated solutions can precipitate hydroxyapatite that is deficient in calcium, resulting in a less stable form of hydroxyapatite more susceptible to the inclusion of impurities (e.g. carbonated apatite). In synthetic apatites, Type A substitution (e.g. CO_3^{2-} substitutes at the OH^- site) occurs at high processing temperatures, whereas environments with low temperatures facilitate Type B substitutions (e.g. CO_3^{2-} substitutes at the PO_4^{3-} site) (Astala and Stott, 2005; Barralet et al., 1998). Carbonated apatite samples are investigated for their ability to adsorb biological molecules in the form of peptides in Aim 2. The apatite-based samples sintered at 1350°C are expected to possess Type A CO_3^{2-} substitutions when carbonate is detected, whereas the apatite-based mineral precipitated on polymer films at 37°C possess Type B CO_3^{2-} substitutions.

Biomimetically precipitating bone-like mineral onto a substrate begins with the nucleation of bone-like apatite precursors from a supersaturated ionic solution, often called simulated body fluid. Simulated body fluid (SBF) is comprised of similar ion

concentrations as those found in human serum (Table 1.2) (Kokubo, 1996). By controlling the pH, temperature, and ionic concentration within the solution, the nucleation of precursors can be controlled. Homogenous precipitation can also occur if these factors are changed, leaving a precipitated phase within the solution. However, the objective of biomineralizing substrates with bone-like mineral is to coat the material via heterogeneous precipitation. In order to maintain film formation, the thermodynamics of the system must be held between homogeneous precipitation and the solute saturation limit (Figure 1.3) (Bunker et al., 1994). To drive heterogeneous precipitation, the net energy between a nucleated precursor and the substrate must be less than the net energy of the nucleated precursor within the ionic solution (Bunker et al., 1994). A biomimetic layer of BLM precipitated on organic, biodegradable polymer films and scaffolds serve as the apatite-based substrate investigated throughout this thesis.

Bone Tissue Engineering

The restoration and repair of orofacial defects resulting from disease, trauma, or genetic inheritance is still a major clinical challenge (Feinberg et al., 2005; Muschler and Midura, 2002; Parikh, 2002; Wiesmann et al., 2004). Autogenous bone grafting is the current method used in repairing skeletal defects; however, limitations of donor site morbidity, graft rejection, inadequate bone formation and quality often result (Ducheyne and Qiu, 1999; Parikh, 2002; Yaszemski et al., 1996). Current concepts in bone tissue engineering strive to induce bone formation using a combination of scaffolding, cells, and biological signals (Garcia and Reyes, 2005; Hubbell, 1999; Maskarinec and Tirrell, 2005; Shin et al., 2003). Three approaches have been identified in the tissue engineering field: conduction, induction, and cell transplantation (Alsberg et al., 2001; Hirano and Mooney, 2004). Initial research has focused on the conduction approach to recruit host cells towards an implanted material and initiate bone regeneration. Inductive approaches of incorporating cell-recruiting factors/molecules in or on the implant are used to improve the quality and amount of bone formation (Chen and Mooney, 2003). In parallel, explanted cells, such as bone marrow stromal cells (BMSCs), seeded on substrates and then implanted to direct bone formation has been explored (Rose and Oreffo, 2002). An

advantage to using BMSCs is that they are readily available in most patients in need of bone defect repair, allowing for autologous expansion *ex vivo*. The expansion capability of BMSC is also advantageous, as these cells secrete paracrine factors that promote osteogenic growth and differentiation. Other cells seeded on these constructs have consisted of established bone cell lines, cells capable of genetic manipulation or viral infection, and stem cells. In Aim 1 of this thesis, phage panning experiments are used to identify peptide sequences that preferentially bind to a population of clonally derived human bone marrow stromal cells (hBMSCs). These peptide sequences are then linked to an apatite-seeking sequence and jointly investigated for their potential to increase hBMSC attachment to BLM in Aim 3.

The organic, biodegradable class of polymers named the poly(α -hydroxyesters) that include poly-L-lactic acid (PLLA), polyglycolic acid (PGA), and polylactic-co-glycolic acid (PLGA), have been fabricated into inter-connected, porous structures (Chen et al., 2000; Ma and Langer, 1999; Mikos et al., 1994) and studied for osteogenic potential as bone graft materials (Ishaug et al., 1994). PLGA as a substrate material is well established because it is easily fabricated into two- and three-dimensional structures that degrade in the body within 6-24 months, depending on the ratio of PLLA to PGA. To control the function of explanted cells and direct new tissue growth, a consensus of desired scaffold properties has emerged. The implanted scaffold needs to be biocompatible, non-toxic, biodegradable, and structurally sound (Liu and Ma, 2004; Wiesmann et al., 2004; Yaszemski et al., 1996). Additional features identified include ideal pore size for osseointegration and vascularization, ability to control material degradation rate to match tissue formation rate, and incorporation and controlled release of biomolecules. While poly(α -hydroxyesters) possess the biodegradability necessary for an implant material to guide bone growth, the surface composition and mechanical integrity of PLGA are not the same as that of native bone or the ceramic and metallic materials used for bone implants.

The technique of biomimetically precipitating apatite onto the surface of a biomaterial was introduced on titanium implants to induce implant-bone osseointegration

(Abe et al., 1990). Using the biomimetic technique in bone scaffolding has evolved into mineralizing biodegradable polymeric scaffolds with the intent of tailoring calcium-phosphate ratios to evoke particular cell responses. The design goals of using a biomimetic technique to precipitate a mineral layer on bone scaffolding aim to reduce the time of apatite formation, to tailor calcium-phosphate ratios, and to mineralize the interior of three-dimensional scaffolding (Oliveira et al., 2003). Altering compositional or surface characteristics of the material can alter biological responses, such as increased tissue growth or cell death (apoptosis). Biomimetically precipitated apatite is hypothesized to recruit host cells as well as have the ability to control the differentiation of explanted cells towards a bone phenotype (Luong et al., 2006). Still, the technique of biomimetically precipitating apatite is an alternative to high temperature ceramic processing methods (Habibovic et al., 2002) that also increases the mechanical integrity of PLGA scaffolding (Murphy et al., 2000). While continuous growth of apatite on three-dimensional (3D) PLGA scaffolds is attainable, the apatite precipitated is not uniform, does not completely cover the surface of the scaffold, and takes at least 16 days to precipitate (Murphy and Mooney, 2002; Murphy et al., 2000; Zhang and Ma, 2004). To increase the amount of bone growth in three dimensions, a PLGA scaffold uniformly coated with biomimetically-precipitated apatite is necessary, particularly for thick porous constructs (> 2 mm in thickness). In Aim 4, flow induction via a bioreactor capable of three-dimensional mineralization of PLGA scaffolds addresses this current limitation in the field of bone tissue engineering. Increased mineral coverage in three-dimensions would prove useful not only for PLGA porous scaffolds, but also metallic or other polymeric materials used in bone scaffolding design.

Protein Engineering

The complex role of proteins in bone formation continues to stimulate new research regarding which specific proteins are agonists or antagonists to bone growth and/or resorption. As proteins are identified and their functions are elucidated, they can be implemented in bone scaffold designs via protein engineering to control a specific cell function. Protein engineering employs rational design of protein polymers using

enzymes, cells, or synthetic methods. An ultimate goal of protein engineering is to use nature's building blocks, or amino acids, as a design platform to synthesize multi-dimensional biomolecules that contain multiple levels of organization that influence biological function. In Aim 1, phage panning, computational modeling, and biological assays are used to identify amino acid sequences that bind to apatite-based materials and hBMSCs, independently. The apatite-binding and hBMSC-binding sequences are then linked, and the peptide design is tested for its ability to increase cell attachment with and without the designed peptides on BLM in Aim 3.

Surface Modification via Peptides to Increase Biological Function

A strategy in controlling cell function includes presenting biomolecules on the bone-like apatite surface. Growth factors and peptides have been ionically or covalently attached to surfaces to increase cell adhesion, and ultimately, the amount of bone growth. While several proteins enhance cell adhesion, proteins are subject to isolation and prone to degradation (Hersel et al., 2003). Proteins can also change conformation or orientation because they possess sections with varying hydrophobicities that control cellular functions other than adhesion. On the other hand, peptides can mimic the same response as a protein while being smaller, cheaper, and less susceptible to degradation. Peptides have a greater potential for controlling initial biological activity, because they can contain specific target amino acid sequences and can permit control of hydrophilic properties through sequence design (Ladner et al., 2004). Identifying peptide sequences on apatite could prove beneficial in designing molecules for guided bone repair.

Understanding the steps involved in cell adhesion is imperative when trying to link the influence of a peptide. Cell adhesion progresses in four steps: cell attachment, cell spreading, production of organized actin filaments, and focal adhesion formation (Figure 1.4) (LeBaron and Athanasiou, 2000). The importance of cell adhesion has been demonstrated in a variety of tissues including the differentiation of myoblasts (Menko and Boettiger, 1987), terminal keratinocytes (Adams and Watt, 1990), mammary epithelium (Streuli et al., 1991), and osteoblasts (Damsky, 1999). Since cell attachment is the first step of adhesion, Aim 3 of this work strives to show hBMSC cell attachment

can be increased with the design of peptides that both adhere to apatite and to hBMSCs. Establishing cell attachment is essential in guided bone repair, as the subsequent phenotypic differentiation cannot occur if cells do not attach.

Identification of short recognition sequences has motivated the development of bioactive materials that can recruit a certain cell population to adhere to a material surface via specific integrin mediated bonding. One peptide that interacts with a variety of cell adhesion receptors, including those on osteoblasts, is the RGD (Arg-Gly-Asp) sequence (Hersel et al., 2003). The RGD binding sequence, first found in fibronectin, is an adhesion sequence that interacts with multiple adhesion receptors including the $\alpha_v\beta_3$ integrin that binds not only to vitronectin and fibronectin, but to the bone proteins osteopontin and bone sialoprotein (Hersel et al., 2003). RGD sequences can act as inhibitors of cell adhesion if present in solution, even though they promote cellular adhesion when adsorbed on a material surface (Ruoslahti, 1996). Utilizing the RGD sequence is one way to create a more attractive surface for cells to regenerate bone. Other peptide sequences mimic sections of extracellular matrix proteins that include bone sialoprotein (Fujisawa et al., 1997), osteopontin (Gilbert et al., 2000; Shin et al., 2004a; Shin et al., 2004b), fibronectin (Huebsch et al., 1996), statherin (Gilbert et al., 2000; Shaw et al., 2000a), elastin (Simionescu et al., 2005), and osteonectin (Fujisawa et al., 1996) and have been examined for increased cell attachment, proliferation, and differentiation. Peptide sequences have also been designed to increase cellular adhesion to titanium (Ferris et al., 1999; Verrier et al., 2002), to provide conformational stability via cyclic RGD sequences (Pallu et al., 2003), or to model non-RGD adhesion mechanisms of the heparin binding domain (Dalton et al., 1995; Dee et al., 1998). A limited list of adhesion peptide sequences, other than RGD, involved in cell integrin-ligand binding includes PSHRN (Benoit and Anseth, 2005), FHRRIKA (Rezania and Healy, 1999) and YIGSR (Massia and Hubbell, 1990).

Peptides have been designed to bind to PLGA, sintered hydroxyapatite, and glass, but have not yet been designed to adhere to biomimetic BLM. BLM as an apatite-based coating has potential to impact current bone biomaterials as it has been shown to increase

bone growth *in vivo*, increase murine bone marrow stromal cells spreading *in vitro*, and controls surface dissolution behavior via tailored SBF solutions, making it an attractive candidate to investigate (Kohn et al., 2005; Leonova et al., 2006; Shin et al., 2007). Hydroxyapatite binding sites have been divided into two classes: those involved in post-translational modifications (phosphorylated amino acid and gammacarboxyglutamic acid sequences) and consecutive basic amino acid sequences (poly-Glu, poly-Asp) (Fujisawa et al., 1996). While these peptide design guidelines are a starting point for BLM peptide design, the approach of identifying peptide sequences that preferentially bind to apatite-based materials via combinatorial libraries is a novel one that is tested in Aim 1. The peptide sequences identified using the combinatorial libraries are tested against a peptide designed using conventional methods of joining RGD with a polyglutamic acid chain (EEEEEEPRGDT or E₇PRGDT). It is possible that the non-specific RGD sequence may not be appropriate for all cell sources, particularly those used for bone regeneration, and alternative methods of peptide design and discovery are necessary to apply protein engineering principles towards a BLM coated scaffold.

Regardless of material, engineered peptides need to be presented on the substrate surface in a manner that will stimulate bone tissue formation. Peptides are typically presented on the surface of apatite-based substrates using surface adsorption, as ceramics are not as conducive to surface modifications as polymer or metals. Since BLM and other apatite-based materials are used throughout the aims tested, surface adsorption is the main method of peptide adhesion throughout this thesis.

Surface Adsorption and Quantification of Peptides

Surface adsorption is a simple way to introduce peptides onto a substrate. The preparation of peptide solutions prior to adsorption onto a substrate includes reconstituting the peptide in water or a buffer solution. The concentration the peptide depends on the aim of the experiment, but a typical range of concentrations used is between 1-250 µg/mL. Therefore, the amount of peptide that physically adsorbs to the surface should be accurately quantified to better elucidate the role of peptide concentration on the observed biological response. Properties of the substrate that can

influence peptide adsorption include chemistry, morphology, and surface charge. Consistent peptide adsorption can only occur when substrate properties, peptide concentrations, and solution contents do not vary. Too much or too little peptide can have no effect or can cause adverse cell behavior. Amino acid analysis, a method that determines the quantity of each amino acid in solution, is one of the most accurate quantification techniques. However, since amino acid analysis is expensive to perform on large sample sets, peptide concentrations are approximated by fluorescence or absorbance characterization (Barber et al., 2005). When a direct peptide quantification method is not published, researchers often report initial peptide concentrations of the solutions used in the experiment. Peptide adsorption assays are utilized in Aims 1, 2, and 3 of the work presented, and as such, care was taken to develop reliable methods of detecting peptide adsorption. UV Spectrophotometry was used to quantify peptide present for standard curves (Appendix B) and peptides adsorbed on multiple apatite-based materials. The initial peptide concentration introduced to the substrates was also analyzed via amino acid analysis.

Another aspect of investigating the interaction between cells and a substrate includes determining the strength of cell adhesion to the surface. Decreased cell adhesion can result from changing a single amino acid in a peptide sequence, particularly when the change is within a region of the peptide known to contribute to cell adhesion mechanisms (e.g. replacing the aspartic acid in RGD with a glutamic acid, making it RGE) (Rezania et al., 1997). These initial results indicate that cell adhesion strength is increased when an RGD peptide is present on the surface, mainly because of increased cell spreading. In the presented work, peptides designed with RGD and RGE sequences were used as controls and are investigated in Aim 3 for their ability to influence hBMSC attachment compared with dual-functioning peptides designed in Aim 1.

Phage Display

A complete set of sequences known to adhere to the variety of materials used in bone tissue engineering would provide better design guidelines when designing a biomaterial. Aim 1 of this thesis describes the use combinatorial phage display

technology to elucidate specific sequences or sequence patterns that adhere to apatite-based materials and a population of clonally derived hBMSC. Phage display technologies introduce a combinatorial library (on the order of 10^9 sequences) of 7-mer or 12-mer linear peptide sequences to a molecule, ligand, or material. The concept behind phage display is to create an oligonucleotide insertion mutation on the gene of a virus (typically M13 bacteriophage) allowing a library of sequences to be expressed on the exterior protein coat of the phage (Rodi and Makowski, 1999). After several rounds of panning, or expanding and reintroducing the sequences that adhere, consensus sequences emerge and are identified by DNA sequencing (Figure 1.5). Although this technology has been mostly used in identifying enzyme substrates and inhibitors, DNA and protein binding peptides, tissue specific peptides, and receptors (Ladner et al., 2004; Marks and Marks, 1996; Uchiyama et al., 2005), the principle of the technique can be applied to identifying peptides that have high specificity to biomaterials. The phage display technique has proven effective for a variety of inorganic substrates such as silver, palladium, platinum, titanium, and carbon nanotubes, in addition to organic plastics (Adey et al., 1995; Kriplani and Kay, 2005). Moreover, the usefulness of phage display in cell adhesion research has been shown through the isolation of integrin receptor sequences that bind to RGD (Pasqualini et al., 1995). Peptide sequences identified from panning experiments introducing a combinatorial 12-mer phage library on apatite-based substrates and hBMSCs are analyzed in Aim 1 using a bioinformatics tool, RELIC (REceptor LIgand Contacts) (Mandava et al., 2004), specifically designed to analyze data generated using phage display libraries (Makowski and Soares, 2003; Rodi et al., 2004).

Modeling Apatite

The experimental techniques utilized to investigate peptide secondary structure and structure-function relationships that are responsible for adhesion receptor specificity (Reyes and Garcia, 2003b; Stayton et al., 2003) are often expensive and time consuming; therefore, molecular modeling is being used to investigate organic-inorganic interactions. Modeling is useful in investigating protein-substrate and peptide-substrate interactions in calcite, calcium oxalate, and apatite systems (Dahlin et al., 1998; Fujisawa and Kuboki,

1998; Qiu et al., 2004). Molecular modeling is also used to model carbonate substitution within the hydroxyapatite lattice. Because synthetic apatite, including BLM formed from SBF, is often carbonated, models determining favored carbonate substitution locations within the lattice are useful. Using extracted model information, the composition and type of carbonate substitutions can be tailored when fabricating synthetic apatite. Simulated inorganic lattice structures and organic-inorganic interfaces can be observed at varied temperatures, pressures, and levels of hydration. Utilizing a model provides insight to unobservable interactions and can compliment bench-top experimental analysis. In the presented work, molecular modeling was used to investigate the behavior of a group of peptides isolated from phage panning in Aim 1 on apatite-based materials on a hydroxyapatite lattice. Modeling data of peptide adsorption behavior on the (001) hydroxyapatite face and a [010] step on the (001) hydroxyapatite face, aimed to isolate peptide sequences having the highest adsorption energies to the hydroxyapatite lattice.

Modeling Approaches

In order to represent accurate lattice structures, the positions and bond angles of all of the atoms in the lattice and the locations of substitutions are important parameters needed in both *ab initio* and empirical modeling. Empirical modeling performs simulations on crystal structures with experimentally defined lattice parameters (via molecular mechanics), whereas *ab initio* modeling performs simulations on atoms to determine their positions with respect to one another (via quantum mechanics). Prior to modeling with organic-inorganic interactions, an inorganic lattice structure must first be defined and well understood.

Molecular modeling can be performed on a cluster or periodic structure. A molecular mechanics, or empirical, approach requires a force field, developed either *ab initio* or experimentally, and a structure. A force field defines the molecular mechanics of the system in question using parameterized analytical expressions (Cygan RT, 2001). Molecular modeling using empirical methods utilizes molecular mechanics to perform calculations during the simulations. Molecular mechanics simulations use Newtonian physics in a time dependent manner to calculate the forces on a system. Energy

minimizations, conformational analyses, lattice dynamics, molecular dynamics, and Monte Carlo simulations are examples of molecular mechanics modeling (Cygan RT, 2001). Molecular dynamics is an atomistic simulation technique that uses Newton's Law of Motion with updated atom positions and velocities during numerical calculation. While running molecular dynamics increases computing times, it has the advantage that it can also be applied to fluids (Parker et al., 2001). Because the various approaches to modeling a system evaluate the energy of a system, they have similar outputs including: structure information, physical properties, thermodynamic data, kinetic information, and spectroscopy predictions (Gale and Rohl, 2003).

The development of the General Utility Lattice Program (GULP) has enabled simulations on solid-state structures and structural defects (Gale and Rohl, 2003). GULP can be utilized to develop force fields. An example of the types of potential energy terms that can be included within a force field are bonded energy terms (bond stretching, angle bending, and dihedral torsion) and non-bonded energy terms (van der Waals, and/or Coulombic interactions) (Equation 1).

$$E_{\text{Total}} = E_{\text{non-bonded energy terms}} + E_{\text{bonded energy terms}} \quad [1]$$

The Universal Force Field (UFF) is a force field applicable to a range of molecular systems used in both inorganic and organic simulations (Rappe et al., 1992). However, the UFF cannot be solely utilized in these applications, because it does not define molecular interactions between the inorganic lattice and the organic molecules. As a result, an accurate force field describing interactions between the inorganic apatite lattice and organic molecules is also essential. Much effort has been put into modeling the different stoichiometric and structural variations of apatite in order to reveal unrecognized alternatives that were not defined when the definition of apatite was recorded over 70 years ago (Hughes et al., 1989; Hughes et al., 1990). Rigid and flexible models of fluorapatite and hydroxyapatite have also been produced (Hauptmann et al., 2003).

Modeling Inorganic-Organic Interactions

Evidence of acidic proteins participating in bone precipitation has led investigators to consider the involvement of acidic peptides or acidic portions of proteins on nascent bone crystal formation and existing bone apatite crystals (Dahlin et al., 1998; Fujisawa and Kuboki, 1998; Gilbert et al., 2000; Moradianoldak et al., 1992; Sarig, 2004). Evidence that bone proteins contain large portions of aspartic and glutamic acid residues has also supported the hypothesis that acidic regions are participating during bone formation. Presence of glutamic and aspartic acids is thought to be the mechanism of association of negatively charged peptides with the apatite mineral (Glimcher, 1984; Moradianoldak et al., 1992; Sahai, 2005). Because the apatite lattice is complex and conformations of all of the bone proteins thought to be involved are unknown, it has been difficult to pinpoint the exact interactions between the organic and inorganic components of the system. To complicate things, some bone proteins have been identified as both promoters and inhibitors of bone formation (Robey and Boskey, 2003). Modeling the interaction of an entire protein requires intense computer calculations, which is time consuming. Thus, modeling peptides or small proteins (≤ 30 kDa) is a feasible alternative.

In Aim 1, computational modeling strives to elucidate peptide sequences with high adsorption energies on a hydroxyapatite lattice. The peptide-hydroxyapatite computational model used aimed to provide a high-throughput validation technique where multiple interactions can be investigated prior to *in vitro* or *in vivo* testing.

Hypothesis and Aims

The clinical need for improved strategies for guided bone growth exists. In addition, the incorporation of biological molecules is important in synthetic materials in directing cellular behavior. The aims of this thesis were structured to improve biomolecular design and biomimetic coating techniques used to regenerate bone. Multi-disciplinary tools were implemented to investigate the global hypothesis guiding this research.

Global Hypothesis: Dual-functioning peptide sequences designed to both specifically adhere to apatite-based materials and human bone marrow stromal cells (hBMSC) will increase cell attachment on bone-like mineral.

To test this global hypothesis, phage display, a modified ELISA, and computational modeling were combined to derive peptide sequences specific to apatite-based materials. Peptide sequences from a combinatorial library population that preferentially bind to hBMSCs were also found using phage display and immunohistochemistry techniques. Combining the apatite-binding sequence with the hBMSC preferential binding sequence yielded dual-functioning peptides that were tested for their cell attachment properties using a centrifugation assay. Furthermore, a bioreactor system was designed to nucleate and precipitate a uniform, continuous bone-like mineral layer on three-dimensional PLGA porous scaffolds. Four aims were addressed in the presented work.

Hypothesis 1a: Amino acid sequences that strongly adhere to biomimetically-precipitated apatite, or bone-like mineral, and hBMSCs are identifiable using preferential adherence experiments, such as a combinatorial phage library.

Hypothesis 1b: Computational modeling peptide sequences from the apatite-adherent phage in Aim 1 can elucidate peptides with favorable binding energies on a hydroxyapatite lattice.

Aim 1: Design dual-functioning adhesion peptides that adsorb to biomimetic apatite and promote hBMSC attachment. Phage display technology determined 12-mer peptide sequences that have the specificity to adsorb to biomimetic apatite through multiple rounds of panning. Peptide sequences obtained through DNA analysis were analyzed using the bioinformatics tool (RELIC) specifically designed to analyze data generated using phage display libraries. A modified ELISA verified that the isolated phage sequences were preferentially being adsorbed to the apatite-based materials. The adsorption potential of designed peptides on apatite via computational modeling were determined using molecular simulations (Cerius² and Materials Studio v3.1) on a

hydroxyapatite step defect in the [010] direction on the (001) face, in addition to a hydroxyapatite slab structure on (001) face. The computational modeling was used to identify sequences with favorable binding energies. A subset of 2-4 peptides based on validation via RELIC analysis, ELISA, and computational modeling, was further evaluated in Aim 3. Immunohistochemistry was used to verify identified phage binding on hBMSCs. Generated sequences were compared to protein sequences available on the Protein Database (PDB) to identify specific regions of proteins that may be involved in cell adhesion.

Hypothesis 2: Because the incorporation of carbonate into the hydroxyapatite lattice can alter surface charge periodicity, carbonate incorporated in hydroxyapatite will decrease adsorption of apatite-adherent peptides derived in Aim 1.

Aim 2: Investigate the adsorption of synthetic, apatite-adherent peptides on apatite-based materials. Four apatite-based materials with a range of CO_3^{2-} from 0-5wt% and differing carbonate substitutions were fabricated. Absorbance readings via UV Spectrophotometry quantified the amount of peptide adsorbed to each material. Material characterization methods (scanning electron microscopy, Fourier-transform infrared spectroscopy, x-ray diffraction, 'Brunauer-Emmett-Teller' method) were performed on all apatite-based substrates to verify compositions and surface areas. Peptide adsorption was normalized to each material using surface area data to elucidate the effect of CO_3^{2-} incorporation on peptide adsorption.

Hypothesis 3: Adsorbing peptide sequences designed in Aim 1 onto bone-like mineral will improve initial hBMSC attachment compared to bone-like mineral devoid of peptide.

Aim 3: Determine if functionalizing biomimetic apatite with the designed dual-functioning adhesion peptide sequences increases hBMSC attachment. Bone like-mineral coated PLGA films were used to investigate the potential advantage of adsorbed peptides to improve initial cell adhesion. Absorbance readings on a UV Spectrophotometer were used to quantify the amount of peptide adsorbed to each material. The number of

attached hBMSCs to control and peptide-laden samples was determined using centrifugation and WST-1 assays, where the WST-1 assay only detected living cells.

Hypothesis 4: Induction of fluid flow through the pores of a polymer scaffold will provide a favorable thermodynamic environment for a uniform, continuous layer of bone-like mineral to nucleate and precipitate.

Aim 4: Develop a method of uniformly coating a continuous layer of bone-like mineral on the surface of porous structures. A bioreactor capable of holding multiple porous scaffolds was constructed capable of inducing fluid flow through the pores of the scaffolds. A model protein, bovine serum albumin, was coprecipitated to demonstrate feasibility of biomolecular incorporation. Uniform, continuous mineral formation and protein incorporation throughout the thickness of the scaffolds were characterized using confocal microscopy, micro-computed tomography, Fourier transform infrared spectroscopy, x-ray diffraction, and the bicinchoninic (BCA) protein quantification assay.

Chapter Two discusses the identification and validation of peptide sequences that adhere to apatite-based materials as presented in Aim 1. Through a rigorous, tri-fold validation combining bioinformatics, an established biological assay, and computational modeling, three 12-mer peptide sequences, were identified as preferential apatite-binding peptides. The hypothesis in Aim 2, discussing how the incorporation of carbonate into the hydroxyapatite lattice can alter surface charge periodicity and therefore peptide adsorption is also discussed in Chapter Two. Chapter Three presents data testing Aims 1 and 3, identifying hBMSC preferential binding-sequences, in addition to the adsorption and cell adhesion trends of the dual-functioning peptides, respectively. The dual-functioning peptides influence on cell attachment to bone-like mineral compared to the peptide E₇PRGDT is also presented. This method of identifying preferential binding sequences to cell populations is a new approach to selecting or recruiting specific cell populations *in vitro* or *in vivo*. Finally, data corresponding to the bioreactor design and validation hypothesized in Aim 4 are presented in Chapter Four. Inducing fluid flow

through the pores of hydrophobic polymeric scaffolds to improve mineral nucleation and precipitation throughout the thickness is tested.

The collected work presented provides alternative design methods that can implement peptide sequences capable of improving initial hBMSC adhesion. This work is first to present detailed methods on how peptides can be rationally designed using phage display, established biological assays, and computational modeling. Furthermore, while advancing the current biomolecular design paradigm, this work also improves upon traditional methods used in fabricating BLM coatings on current bone regenerative materials. Ultimately, the peptide design scheme presented can be used in disciplines unrelated to bone to improve tissue development in other areas of the body, be used in multi-tissue platforms that involve bone (e.g. bone-tendon research), or be used even in non-biomedical applications.

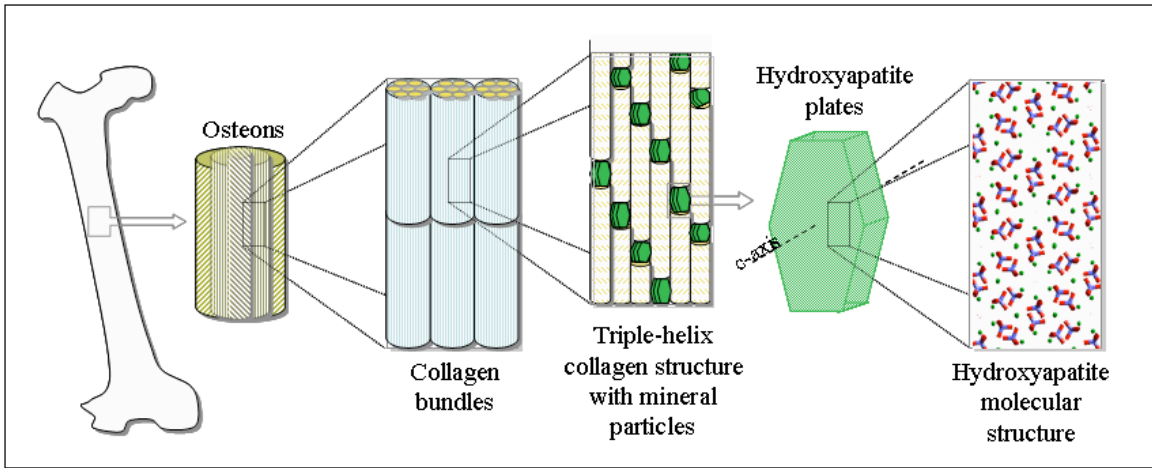


Figure 1.1: Hierarchical Bone Structure. The schematic shows some of the many levels of hierarchy found in bone, from the macroscopic whole bone down to the atomic level arrangement of calcium and phosphate ions to form hydroxyapatite, the main inorganic phase. Organic collagen molecules serve as templates during bone formation and remodeling for appropriate thermodynamic conditions to occur, allowing hydroxyapatite nucleation and precipitation to ensue.

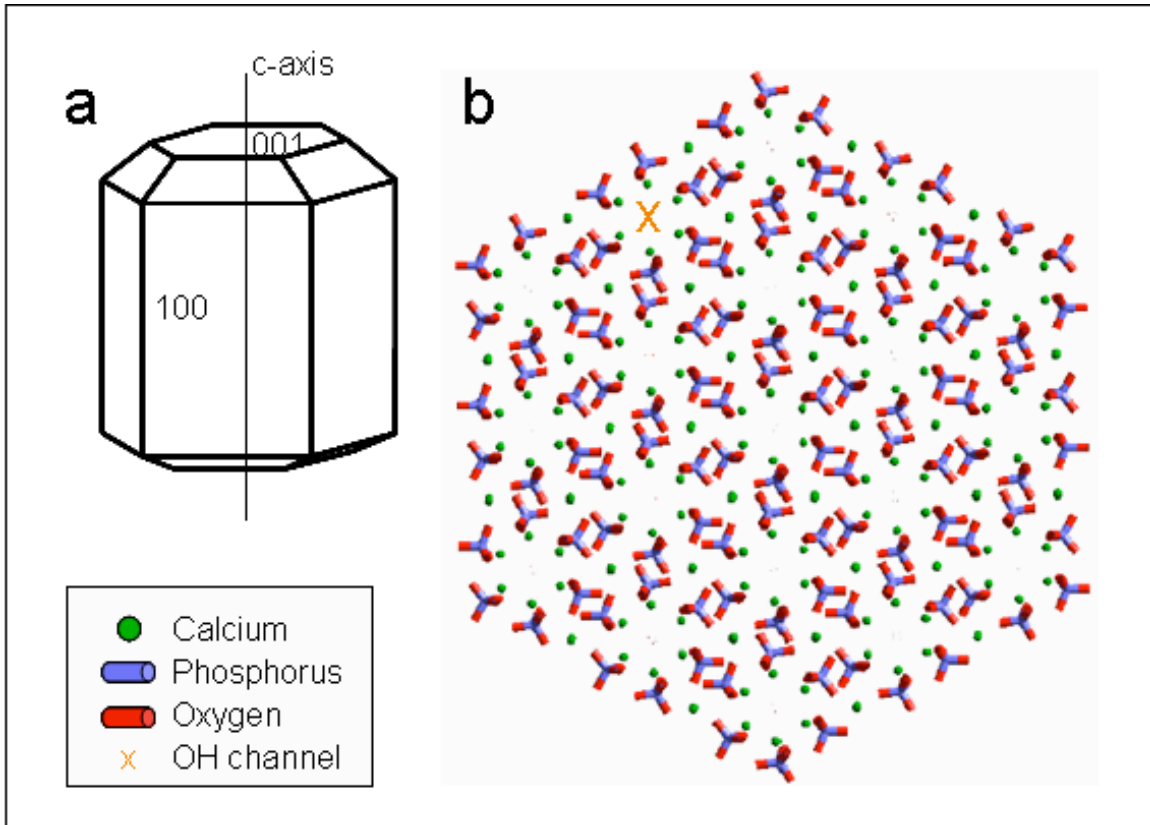


Figure 1.2: Hydroxyapatite Lattice Structure. Hydroxyapatite, $\text{Ca}_{10}(\text{PO}_4)_6(\text{OH})_2$, is the main inorganic phase present in bones and teeth. The hexagonal symmetry is evident when looking at the (001), and the unit cell parameters fall between $a=b=9.32\text{-}9.64 \text{ \AA}$ and $c=6.78\text{-}6.90 \text{ \AA}$, with $\alpha = \gamma = 90^\circ$, $\beta = 150^\circ$ (Nesse, 2000). The OH^- ions are situated in the middle of the hexagonal channels of Ca^{2+} ions, as indicated in the figure by the X. Synthetic formation of hydroxyapatite often produces impurities in the form of carbonate substitutions. Type A substitution, where CO_3^{2-} substitutes at the OH^- channel site, occurs at high processing temperatures, whereas environments with low temperatures facilitate Type B substitutions, where CO_3^{2-} substitutes at the PO_4^{3-} site (Astala and Stott, 2005; Barralet et al., 1998).

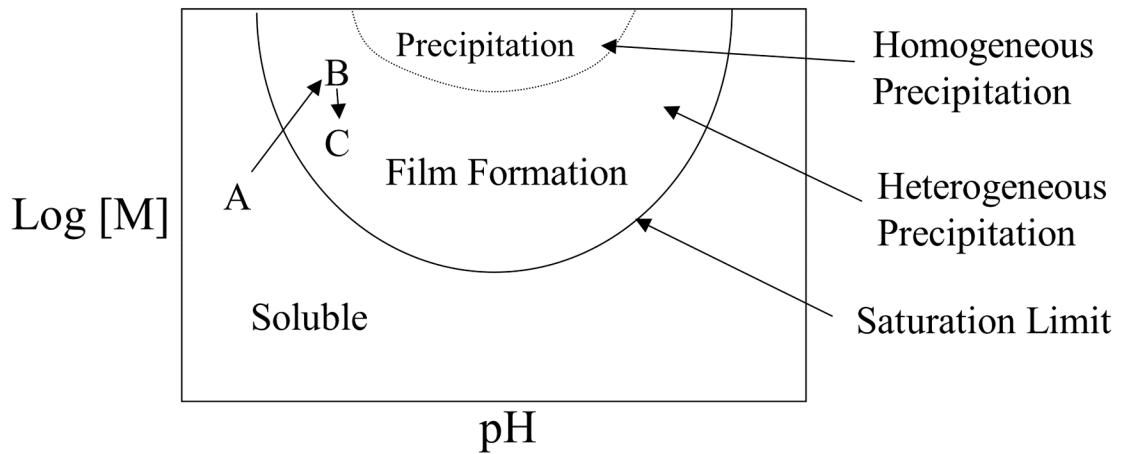


Figure 1.3: Thermodynamic Conditions for Film Formation. General solubility diagram for the formation of films in water (adapted from Bunker et al., 1994). Solutes are dissolved in water (A) in concentrations that create a supersaturated solution (B). During film formation, heterogeneous precipitation is occurring on the substrate, depleting the solution from some solute (C). This process is regulated by the concentration of solute present in solution, pH, and temperature. Therefore, this schematic provides a two-dimensional design domain at 37°C for heterogeneous bone-like mineral deposition. For a bone-like mineral to precipitate heterogeneously on a substrate the product of the concentrations of Ca^{2+} , PO_4^{3-} , and OH^- must be greater than 10^{-114}M , or $[\text{Ca}]^5[\text{PO}_4]^3[\text{OH}]^2 \geq 10^{-114}\text{M}$.

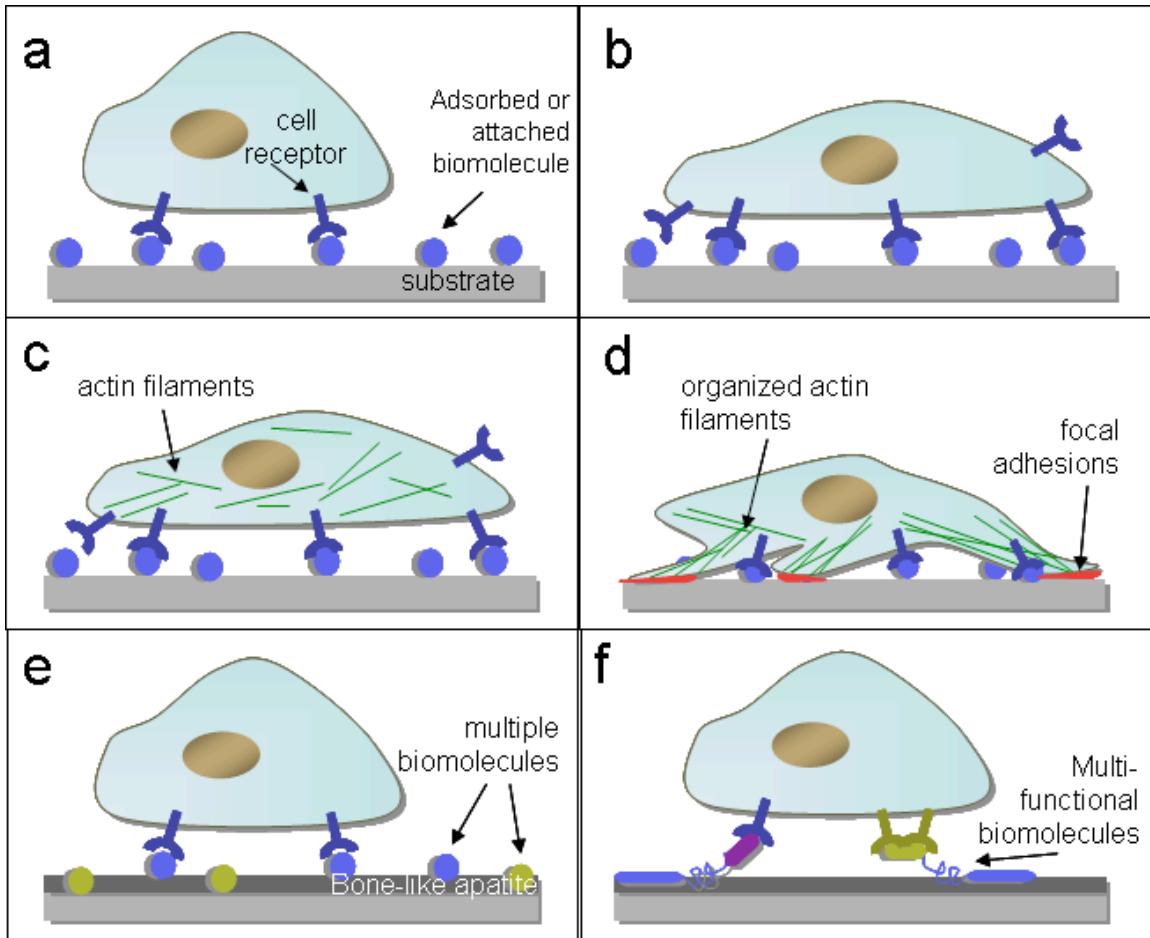


Figure 1.4: Steps Involved in Cell Adhesion. (a) Cell adhesion to a material begins when cell receptors recognize adsorbed or attached biomolecules. (b) The cell begins to spread out after recognizing the biomolecules. (c) Actin filaments, or organized protein structures, begin to form after the cell flattens. (d) The organization of actin filaments allows focal adhesions to form. (e) The bone-like apatite can contain and present multiple biomolecules that can initiate the beginning stages of cell adhesion. (f) Development of second generation biomolecules will allow specified cell receptors to attach to the biomolecules present on the material.

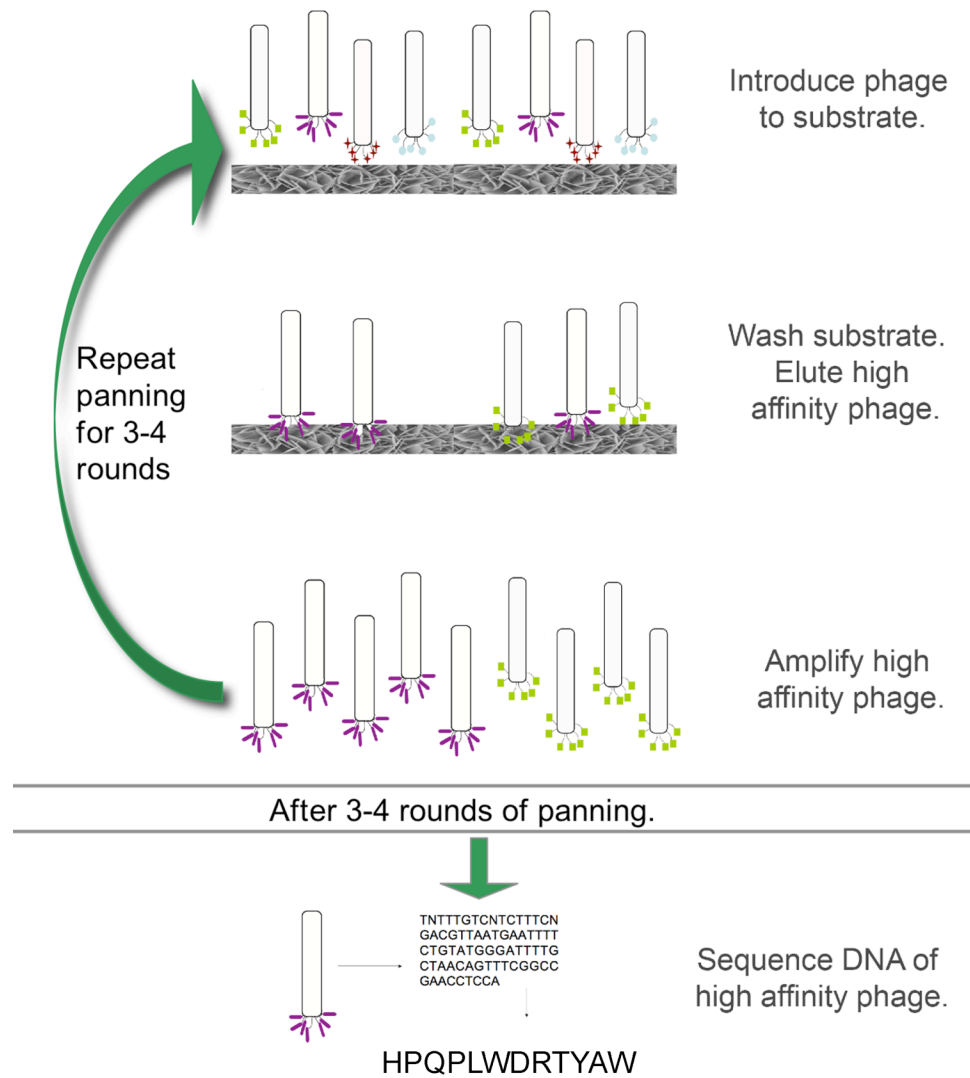


Figure 1.5: Phage Display Schematic. A combinatorial library housing $\sim 10^9$ different 12-mer peptides on the protein coat of bacteriophage, or phage, is introduced to a substrate of interest. The substrate is rigorously washed, and the high affinity phage are eluted and amplified, constituting one round of panning. The amplified high affinity phage are reintroduced to the substrate for successive rounds of panning to eliminate non-specific binding phage. After multiple rounds of panning, the DNA of the phage are sequenced and the 12-mer peptides with high affinity to the substrate are identified.

Table 1.1: Formulas and Names for Common Non-Stoichiometric Apatite Phases (Ben-Nissan et al., 1995; Wopenka and Pasteris, 2005)

Formula	Ca/P Ratio	Type of Mineral
$\text{Ca}_{10}(\text{PO}_4)_6(\text{OH})_2$	1.67	Hydroxyapatite (HA)
$\text{Ca}_{10}(\text{PO}_4)_6\text{F}_2$	1.67	Fluorapatite
$\text{Ca}_{10}(\text{PO}_4)_6\text{Cl}_2$	1.67	Chlorapatite
$\text{Ca}_{10}(\text{PO}_4)_6\text{CO}_3$	1.67	A-type Carbonated Apatite, Unhydroxylated
$\text{Ca}_{10-x}[(\text{PO}_4)_{6-2x}(\text{CO}_3)_{2x}](\text{OH})_2$	≥ 1.67	B-type Carbonated Hydroxyapatite (Dahllite)
$\text{Ca}_{10-x}[(\text{PO}_4)_{6-2x}(\text{CO}_3)_{2x}]\text{CO}_3$	≥ 1.67	Mixed A-type and B-type Carbonated Apatite
$\text{Ca}_{10-x}[(\text{PO}_4)_{6-x}(\text{HPO}_4)_x](\text{OH})_{2-x}$	≤ 1.67	HPO_4 Containing Apatite
$\text{Ca}(\text{H}_2\text{PO}_4)_2 \cdot \text{H}_2\text{O}$	0.50	Monohydrate Calcium Phosphate (MCPH)
$\text{Ca}(\text{H}_2\text{PO}_4)_2$	0.50	Monocalcium Phosphate (MCP)
$\text{Ca}(\text{HPO}_4) \cdot 2\text{H}_2\text{O}$	1.00	Dicalcium Phosphate Dihydrate (DCPD)
α - and β - $\text{Ca}_3(\text{PO}_4)_2$	1.50	Tricalcium Phosphate (TCP)
$\text{Ca}_4\text{H}(\text{PO}_4)_3 \cdot 2.5\text{H}_2\text{O}$	1.33	Octacalcium Phosphate (OCP)

Table 1.2: Ion Concentrations Present in the Supersaturated Ionic Solution (SBF) (Kokubo, 1996)

	Na^+	K^+	Mg^{2+}	Ca^{2+}	Cl^-	HCO_3^-	HPO_4^{2-}	SO_4^{2-}
Human blood plasma	142.0	5.0	1.5	2.5	103.0	27.0	1.0	0.5
1 X SBF	145.2	5.0	1.5	2.5	152.0	4.2	1.0	0.5
1 X Modified SBF	145.2	6.0	1.5	5.0	157.0	4.2	2.0	0.5
2 X SBF	284.0	10.0	3.0	5.0	297.6	8.4	2.0	1.0
4 X SBF	568.0	20.0	6.0	10.0	595.2	16.8	4.0	2.0

CHAPTER TWO

IDENTIFICATION OF PREFERENTIAL BINDING PEPTIDES ON APATITE-BASED MATERIALS AND AN INVESTIGATION OF THEIR SURFACE ADSORPTION

Introduction

Understanding biomimetic principles of replicating the formation and structure of tissues can aid in restoring organ function. Repair and restoration of orofacial and long-bone defects caused by trauma or disease could benefit from advances, as current grafting methods have limitations of donor site morbidity, graft rejection, and/or inadequate bone formation and quality (Ducheyne and Qiu, 1999; Feinberg et al., 2005; Muschler and Midura, 2002; Parikh, 2002; Wiesmann et al., 2004; Yaszemski et al., 1996).

Concepts in bone tissue engineering strive to induce bone formation using a combination of scaffolding, biological signals, and cells (Alsberg et al., 2001; Garcia and Reyes, 2005; Hubbell, 1999; Maskarinec and Tirrell, 2005; Shin et al., 2003). A number of scaffold materials, such as biodegradable polymers (Chen et al., 2000; Ishaug et al., 1994; Ma and Langer, 1999; Mikos et al., 1994), titanium (Ferris et al., 1999; Verrier et al., 2002), calcium phosphate-based ceramics (Barrere et al., 2003; Ignatius et al., 2001; LeGeros, 1991; de Groot et al., 1998) and glass (Garcia et al., 1998; Lobel and Hench, 1998) have been investigated for their ability to elicit the formation of bone tissue with or without donor cells. The variety of material choice stems from the requirements that bone implant materials should demonstrate biocompatibility, mechanical integrity, and biodegradability (Liu and Ma, 2004; Wiesmann et al., 2004; Yaszemski et al., 1996). Both the composition and the surface morphology of an implanted material influence

protein adsorption and the subsequent cell adhesion (Anselme et al., 2000; Garcia et al., 1998; Healy et al., 1996; Kilpadi et al., 2001; Prime and Whitesides, 1991; Redey et al., 1999). Cell adhesion is important for survival, proliferation, and differentiation of multiple cell types, including osteoblasts (Adams and Watt, 1990; Damsky, 1999; Menko and Boettiger, 1987; Streuli et al., 1991).

While both proteins and peptides can promote cell adhesion on biomaterials, peptides have advantages over proteins in that they are smaller, cheaper, less susceptible to degradation, and can be fabricated quickly which increases availability, all while containing specific target amino acid sequences (Hersel et al., 2003; Ladner et al., 2004). Furthermore, peptide fabrication does not involve purification from an animal source, eliminating the chance of an immune response in the recipient. These advantages led to the development of peptide sequences that mimic sections of extracellular matrix proteins, including bone sialoprotein (Fujisawa et al., 1997), osteopontin (Gilbert et al., 2000; Shin et al., 2004b), fibronectin (Huebsch et al., 1996), statherin (Gilbert et al., 2000; Shaw et al., 2000a; Shaw et al., 2000b), elastin (Simionescu et al., 2005), and osteonectin (Fujisawa et al., 1996) for improved cell adhesion, proliferation and osteoblastic differentiation. Peptide sequences, other than the common cell adhesion sequence RGD (Hersel et al., 2003), involved in integrin-ligand binding that have been identified from extracellular matrix proteins are limited, but include PSHRN (Benoit and Anseth, 2005), FHRRKA (Rezania and Healy, 1999), and YIGSR (Massia and Hubbell, 1990). Research investigating the effect of peptide composition and density on cell adhesion to poly-lactic-co-glycolic-acidic (PLGA) polymers, glass, and sintered hydroxyapatite has shown that optimal peptide quantities and conformations are required to elicit a cellular response.

Hydroxyapatite (HA) can fill bone defects and accelerate osseointegration (Geesink, 2002). HA can also be made osteoinductive by incorporation, attachment, or adsorption of biological factors such as growth factors, DNA, proteins, and peptides (Alsberg et al., 2001). However, the efficacy of incorporated biological factors is limited by processing conditions (e.g. >1000°C sintering temperatures); hence, biomimetic

formation of bone-like mineral (BLM) via incubation in supersaturated solutions maintaining ion concentrations appropriate for heterogeneous precipitation (Kokubo, 1995) is an attractive alternative because the benign processing temperature of 37°C permits the retention of biomolecular function. The biomimetic method of forming BLM on a biodegradable polymeric substrate provides a conductive apatite layer with controlled stoichiometries (Shin et al., 2007), that induces increased osteogenesis *in vivo* (Kohn et al., 2005) and that provides a template for coprecipitation and adsorption of biological molecules (Luong et al., 2006; Segvich et al., 2008b).

While the BLM can increase osteogenesis *in vivo*, the additional bone growth is not uniform or spatially controlled, suggesting the need for exogenous factors to spatiotemporally influence tissue development. Since the surface of hydroxyapatite-based materials are not easily modified with surface treatments that form functional hydroxyl-, amino-, or carboxyl- groups, such as on polymers and metals, peptides designed to adsorb to these materials are a logical alternative. The long strings of acidic amino acids found in extracellular bone matrix protein sequences in a previous peptide design proved effective in increasing cell attachment to apatite (Itoh et al., 2002). Peptides have been derived from bone extracellular matrix proteins (Dee et al., 1998; Dettin et al., 2005; Fujisawa et al., 1997), but have not been designed to preferentially attach to a biomaterial of specific composition. Furthermore, none of these peptides have been investigated on BLM.

The technique of phage display panning is effective in isolating specific peptide sequences attracted to inorganic substrates such as silver, palladium, platinum, titanium, and carbon nanotubes, in addition to organic plastic (Adey et al., 1995; Kriplani and Kay, 2005). Phage display technology has been mostly used in identifying enzyme substrates and inhibitors, DNA and protein binding peptides, and tissue specific peptides (Ladner et al., 2004; Marks and Marks, 1996; Uchiyama et al., 2005). An objective of this work was to identify high affinity peptide sequences to apatite to provide insight into the design of functional peptides that preferentially adsorb to apatite-based materials. A combinatorial phage display library was used to elucidate specific 12-mer linear peptide sequences that

have preferential adsorption properties on BLM and sintered hydroxyapatite (HA). The preferential affinity of the identified peptides towards apatite-based materials was confirmed with a modified ELISA and synthetic peptide adsorption assays. Another objective of this work was to test the hypothesis that a change in surface morphology and/or the presence of carbonate within apatite will alter the adsorption of peptides identified as having high affinity towards apatite-based materials. Surface morphology changes and carbonate incorporation can alter charge distribution on the apatite surface, both of which could alter peptide adsorption. To achieve this second objective, morphologies (scanning electron microscopy) and surface areas (“Brunauer-Emmett-Teller” Method, or BET) obtained for four apatite-based materials (BLM, sintered hydroxyapatite disks, and two sintered carbonated apatite disks) were used to normalize peptide adsorption data to account for changes from substrate composition and/or morphology. Composition and morphology of the apatite-based materials were further characterized using x-ray diffraction (XRD), and Fourier Transform Infrared Spectroscopy (FTIR).

Materials and Methods

Reagents and solutions were obtained for all experiments from Sigma-Aldrich unless otherwise noted.

Preparation of Biomimetic Films and Apatite Disks

A 5 w/v% 85:15 polylactic-co-glycolic acid (PLGA, Alkermes)-chloroform solution was cast on 15mm diameter glass slides and dried overnight. The PLGA films were etched in 0.5M NaOH for 7 minutes and rinsed in Millipore water (ddH₂O). Etched films were soaked in modified simulated body fluid (mSBF) for 5 days at 37°C (Kokubo, 1995). The mSBF was made by dissolving the following reagents in Millipore water at 25°C and titrating to pH 6.8 using NaOH: 141 mM NaCl, 4.0 mM KCl, 0.5 mM MgSO₄, 1.0 mM MgCl₂, 4.2 mM NaHCO₃, 5.0 mM CaCl₂•2H₂O, and 2.0 mM KH₂PO₄. The mSBF, a supersaturated solution that enables self-assembly of a carbonated apatite layer onto the polymer substrate, was changed daily to maintain supersaturation. Mineralized

films were rinsed with ddH₂O, dried under a hood, and desiccated until use. Hydroxyapatite disks (10 mm diameter x 4 mm thick) were pressed from powder (Plasma Biotol Ltd. P220) at 1 metric ton for 1 minute and sintered at 1350°C for 1 hour (heating rate of 10°C/minute). The sintered disks were sonicated in 10mM HCl, then in ddH₂O. The BLM films and HA disks were placed in 24-well plates and soaked in ddH₂O overnight prior to phage panning.

Carbonated apatite disks were made from 5.6% (CA5) and 10.5% (CA10) carbonated apatite powders (generous gift from Dr. Mary Tecklenburg). Carbonated apatite disks (8-10mm diameter x 2-4mm thick) were pressed from powders at 0.5 metric ton for 1 minute and sintered at 1350°C for 1 hour (heating rate of 10°C/minute). Carbonated disks were also sonicated in 10mM HCl, then in ddH₂O. All sintered disks (CA5, CA10, and HA) were autoclaved prior to use. Macroscopic dimensions of all disks were measured with calipers.

Identification and Sequencing of BLM and HA Binding Peptides

Peptide sequences with preferential binding to apatite-based materials were identified by screening the Ph.D.12™ Phage Display Library (New England Biolabs, #E8110S), consisting of 10⁹ different phage with 12-mer amino acid linear peptide inserts, against BLM films and HA sintered disks. A streptavidin control was run in parallel with the two apatite-based materials. The ddH₂O was removed and replaced with blocking buffer (Tris-HCl Buffer Solution with 0.1% or 0.5% Tween (TBST) and bovine serum albumin (BSA)) and incubated at 4°C for 1 hour. The blocking buffer was discarded and the substrates were washed 6X with TBST (0.1%). An aliquot of the original Ph.D.12™ library containing 10¹¹ pfu (plaque-forming units) diluted in 1mL of TBST (0.1%) was introduced to each substrate and gently rocked (LabLine 4625) for 40 minutes at room temperature. Non-binding phage were discarded and the substrates were washed 10X with TBST (0.1%). The phage bound to the substrates were eluted with 1mL of Glycine/HCl, pH 2.2, with 1 mg/mL BSA for 10 minutes at room temperature

while being gently rocked. The eluted phage were collected and neutralized with 1M Tris-HCl, pH 9.1.

A small amount of the phage eluate was titered to determine the number of phage bound to each substrate. The rest of the eluate was amplified with *E. coli* (ER2738) by culturing the bacteria and phage in 20mL Lurie broth with vigorous shaking for 4.5 hours at 37°C. The culture was centrifuged for 10 minutes at 10,000 rpm (Sorvall SS-34) at 4°C. The supernatant was transferred to a fresh tube, respun, and the upper 80% of the final supernatant was placed into a fresh tube and allowed to precipitate with 1/6 the volume of PEG/NaCl (20 w/v% polyethylene glycol-8000 in 2.5M NaCl) solution. The phage were allowed to precipitate at 4°C overnight. The PEG precipitation was spun for 15 minutes at 10,000 rpm at 4°C, decanted and briefly respun. The pellet was suspended in Tris-HCl Buffered Solution (TBS) and transferred to a microcentrifuge tube, respun in a microcentrifuge for 5 minutes at 10,000 rpm at 4°C. The supernatant was precipitated with 1/6 the volume of PEG/NaCl solution for 60 minutes on ice, recentrifuged for 10 minutes at 10,000 rpm at 4°C, and the pellet was resuspended in TBS with 0.02% NaN₃. A small amount of the purified phage eluate was titered to determine the number of amplified phage. This amplified and purified phage elute was used in the next round of panning. Subsequent rounds of panning introduced at least 10⁹ pfu as the input phage concentration. Three to four rounds of panning were performed for each substrate. The entire experiment was repeated 3 times, and a streptavidin control yielding the HPQ consensus sequence was run in parallel each time.

Titering was performed with appropriate serial dilutions for both the eluted phage and amplified phage after each round of panning. Agar plates treated with IPTG (isopropyl-b-D-thiogalactoside) and Xgal (5-bromo-4-chloro-3-indoyl-b-D-thiogalactoside) were able to visually identify correct plaques using blue/white screening. Individual plaques picked from plates having no more than ~100 plaques were amplified by infecting a log phase *E. Coli* culture. Amplified phage from selected phage plaques were purified by PEG/NaCl precipitation. Single stranded DNA was isolated using an iodide buffer extraction, cleaned in ethanol, and resuspended in DNase/RNase free water.

The DNA was sequenced via dideoxy chain termination method using a DNA sequencer (Applied Biosystems, 3730XL DNA Analyzer, UM DNA Core) with the NEB -96 gIII sequencing primer provided in the kit.

Peptide Selection

A tri-fold analysis, involving a bioinformatic tool, biological ELISA, and computational model, was devised to determine the peptides with greatest potential to adhere to apatite-based materials. The computational model was previously published and not discussed in the present work (Segvich et al., 2008a). The bioinformatics tool REceptor LIgand Contacts (RELIC) (<http://relic.bio.anl.gov/index.aspx>) (Makowski and Soares, 2003; Mandava et al., 2004; Rodi et al., 2004) was used to analyze the data from the phage display runs. The programs DNA2PRO, AAFREQ, and INFO determined peptide translation sequences from DNA code, amino acid frequency as a function of position, and information numbers for each peptide reflecting the probability of selecting individual phage by chance, respectively. The AAFREQ analysis did not show amino acid specificity by position (data not included). The most informative data was obtained using the INFO program. The INFO program calculates an information measure for each peptide identified that expresses the probability that each peptide occurs by chance (Information measure = $-\ln[\text{probability}]$). For example, a high information measure can be indicative of an uncommon sequence with a low growth rate during amplification; whereas, a low information measure could represent a phage sequence likely to appear based on composition and/or high growth rates. The program INFO was run with subtraction of a random selection of phage from the parent library (12R, 441 random sequences from NEB 12-mer Ph.D. kit).

Phage Binding ELISA

To determine the binding efficiency of the identified phage to the bone-like substrate materials, an ELISA was performed on BLM films, HA disks, PLGA films, and tissue culture polystyrene (TCPS) wells. The substrates were soaked in ddH₂O overnight in 24-well plates. The ddH₂O was removed and replaced with blocking buffer (TBST

(0.1%) w/BSA) and incubated at 4°C for 1 hour. For each plate with samples, a second 24-well plate was blocked and used to prepare serial dilutions for each individual phage. The blocking buffer was discarded and the substrates were washed 6X with TBST (0.1%). In the blocked plate, dilutions of individual phage were prepared in TBST (0.1%) in the concentrations of 10^6 , 10^7 , 10^8 , and 10^{10} pfu (n=1 per dilution). Each phage concentration was introduced to the four substrates and incubated at room temperature for 1.5 hours with gentle rocking (LabLine 4625). The non-binding phage were discarded and the substrates were washed 6X with TBST (0.1%). HRP-conjugated anti-M13 antibody (GE Healthcare, #27-9421-01) was prepared in 1:5000 ratio in blocking buffer and added to each well. The substrates were washed again 6X with TBST (0.1%). Immediately prior to detection, a 30% H₂O₂ (Corco, Fairless Hills, PA #1403)-ABTS (2',2'-azino-bis(3-ethylbenz-thiazoline-6-sulphonic acid) diammonium salt) solution in a 0.05M citric acid solution at pH 4.0, was added to each well and allowed to incubate at room temperature for 50 minutes. For each sample, an aliquot of each well was read on a UV Spectrophotometer (Biorad SmartSpec 3000) at 410nm.

Synthetic Peptide Adsorption Assay

Three high affinity peptides identified (APWHLSSQYSRT [A], VTKHLNQISQSY [V], and STLPIPHEFSRE [S]) and a positive control peptide (E₇PRGDT [E]) (Fujisawa et al., 1997), were fabricated on a Rainin Symphony synthesizer and determined as >86% pure via HPLC (Synthetic peptides were provided by The University of Michigan Protein Structure Facility, Dr. Henriette Remmer, director). Amino acid analysis was performed to verify peptide concentration for standard curves created with UV absorbance at 205nm and 220 or 225nm wavelengths (BioRad Smartspec 3000). Standard curves for APWHLSSQYSRT, VTKHLNQISQSY, and STLPIPHEFSRE were also generated using UV Spectrophotometry at 280nm, 274nm, and 257 nm, respectively. Each peptide was reconstituted in ddH₂O and diluted to ~500µg/mL in 50mM Trizma buffer (T7818, pH=7.5). In 24-well tissue culture dishes, BLM films, HA disks, CA5 disks, CA10 disks, and blank TCPS wells were soaked in ddH₂O overnight at 4°C (n=5). Prior to introducing 1mL of the peptide or

buffer solutions for negative controls, plates were allowed to warm to room temperature and then the overnight solution was removed. The plates were agitated on a Titer Plate Shaker at ~80rpm for 3 hours at room temperature. The films and disks were rinsed with ddH₂O and then soaked in a 10mM HCl solution for 18 hours at room temperature on the same shaker. Aliquots of the HCl solution were read on a UV spectrophotometer.

Statistics

All data are presented as mean values \pm one standard deviation. Non-parametric one-way ANOVAs run with the Dunnetts T3 post-hoc test determined the effect of substrate on peptide adsorption. The effect of peptide on substrate was also calculated with this statistical test. Statistical significance was defined as $p < 0.05$.

Material Characterization

Scanning Electron Microscopy (SEM): Morphologies of all apatite-based materials were examined using scanning electron microscopy (Philips XL30 FEG Scanning Electron Microscope, UM EMAL). Samples from each group (n=2) were coated gold coated and examined at 10-15 kV.

Surface Area Determination (BET): Single Point BET surface area at $P/P_0 = 0.1$ was determined for all apatite-based materials on a surface area and porosity analyzer (Micrometrics ASAP 2020). At least 1g of material was used and data acquisition was performed in duplicate. Peptide adsorption data for all apatite-based substrates were normalized to their respective surface areas using sample dimensions (MacroSA) and BET analysis data (MicroSA). The well area of TCPS was used for both MacroSA and MicroSA normalizations.

Fourier Transform Infrared Spectroscopy (FTIR): Characteristic peaks for apatite were detected using a Fourier Transform Infrared Spectroscopy (Spectrum BX FT-IR, Perkin Elmer). A 300:1 ratio of KBr to apatite sample was used prepare a pellet and analyze all of the apatite-based materials (n=3). Spectra were recorded from 400 to 4000 cm^{-1} and baseline corrected. The wt% CO_3^{2-} incorporation range was determined using

FTIR spectra for each substrate using two established methods (Featherstone et al., 1984; LeGeros, 1991) taking the peak height ratio of $1450\text{cm}^{-1}/569\text{cm}^{-1}$ or $1410\text{cm}^{-1}/600\text{cm}^{-1}$.

X-ray Diffraction Analysis (XRD): XRD spectra were obtained from a representative sample of each composition using a Rigaku Miniflex X-ray Diffractometer with a fixed incidence of 4.2° . A range of $10\text{-}90^\circ$ was scanned using a step size of 0.1° and a scan rate of $1^\circ/\text{minute}$. All spectra were normalized to their respective maximum peaks. Hydroxyapatite from Sigma-Aldrich (#289396) was scanned as a calcium phosphate standard.

Results

Identification of High Affinity Phage Towards Apatite-based Materials

Of the $\sim 10^9$ phage present in the original library, 243 were identified as binders to apatite (Figure 2.1). The streptavidin control yielded the HPQ consensus sequence signifying successful panning in all experiments. Within the 243 apatite-binding phage identified, 19 sequences appeared in repeated experiments after DNA sequencing. Of these 19 sequences, 17 were found in more than one experiment on the same substrate, either BLM or HA. Of these 17 phage clones, 7 phage had high affinity towards both BLM and HA (bold – Table 2.1). While the frequency data showing 7 sequences bound to both BLM and HA in multiple experiments provided evidence that these sequences were specific to apatite, further validation was required to verify this. Bioinformatic analysis, computational modeling, and an ELISA were therefore used to analyze the entire set or subsets of the original 243 clones identified.

All 243 phage sequences identified as binders to BLM and/or HA were analyzed with the INFO program provided by RELIC. When the phage set identified as adsorbing to the BLM and/or HA was compared to a RELIC provided NEB Background phage set, the BLM/HA data showed a shift towards higher information content (Figure 2.2). To isolate this subset of phage valued with high information content, regions of greater occurrence were partitioned from information content ranges 0-28.3, 33.0-35.8, and 36.5-40.0. These ranges were chosen as regions that exhibited higher occurrence levels within

the apatite-based material phage set when compared to the NEB background. Sixty-eight sequences were partitioned and deemed “high information clones”.

A representative set of 10 clones from the original 243 clones was chosen for ELISA analysis (labeled with \diamond in Table 2.1). Of the ten, 6 occurred as repeats, whereas 4 occurred only once. Both repeated and single-occurrence phage were tested to identify if the repeated phage occurred in higher frequencies than the single-occurrence phage, because of advantageous growth properties in the Lurie Broth. Phage dilutions of 10^8 and 10^{10} pfu resulted in positive ELISA readings, with stronger positive signals for the 10^{10} dilution (Figure 2.3). Favorable phage binding was not observed for VSPLSFGSPRYP and WSPAPHVIMGTT, two of the four single-occurrence phage. Of the 6 repeats tested, four showed positive ELISA results. For the phage with positive ELISA results, TCPS and PLGA films showed consistently low background adsorption for all concentrations tested, illustrating the specificity of the phage identified as binders to BLM and HA.

From the original frequency data encompassing all 243 identified clones, the 19 phage sequences that appeared in repeated experiments were also analyzed via computational modeling on a hydroxyapatite lattice (data reported (Segvich et al., 2008a), but A, S, and V data reported here in Table 2.2, so the integrated role of the model along with the bioinformatics and ELISA can be illustrated) (Table 2.2). Peptides identified as having high peptide adsorption energies, or more negative energies, as neutral or charged peptides were deemed as having greater binding potential. A neutral peptide is given an overall charge of zero prior to any energy minimization, whereas a charged peptide is assigned a peptide-appropriate overall charge (e.g. VTKHLNQISQSY would be assigned an overall charge of +1). At a pH 7.5, the net charges for A, S, and V were estimated as +1, -1, and +1, respectively. The isoelectric points for A, S, and V were estimated from amino acid contributions of C, D, E, H, K, R, Y, and the amino- and carboxy- termini as 9.9, 5.3, and 9.7, respectively. In deciding which peptides to synthetically fabricate for the peptide adsorption experiments, the results from the RELIC analysis, modified ELISA, individual clone frequency over the three phage experiments, and computational

modeling were evaluated (Figure 2.1). Of the six peptides that exhibited positive ELISA signals, sequences were only considered if present in the top 5 ranking of any of the computational models run, eliminating NMNTHIHKDRPP and SMRLPLLSSHAL. From the remaining sequences, only those deemed as high information clones from the INFO analysis were chosen, eliminating ALTLHPQPLDHP. Three phage sequences, APWHLSSQYSRT [A], STLPIPEFSRE [S], and VTKHLNQISQSY [V], emerged as having superior behavior compared to the other sequences.

S and V Adsorb Consistently With the Highest Affinity on the Apatite-based Materials

Peptides S and V adsorb in statistically greater amounts on the apatite-based materials in comparison to peptide A, (For S vs. A, BLM $p=0.001$, CA5 $p<0.001$, CA10 $p<0.001$, HA $p=0.038$; For V vs. A, BLM $p=0.006$, CA5 $p=0.033$, CA10 $p=0.029$) (Figure 2.4). Peptides S and V also have significantly higher adsorption to CA5 and CA10 disks in comparison to peptide E (For S vs. E, CA5 $p=0.005$, CA10 $p=0.004$; For V vs. E, CA5 $p=0.026$, CA10 $p=0.010$). Peptide adsorption to HA disks was less specific, as the only significant difference was between peptides A and S, $p=0.038$. The BLM was the only material which supported a greater adsorption of peptide V when compared to peptide S, $p=0.006$. Consistently low peptide adsorption to TCPS was found for all peptides, verifying specificity to calcium phosphate substrates. These results suggest that peptide adsorption is not only dependent on substrate composition, but also on the peptide composition.

Adsorption of Preferential Binding Peptides on Apatite-based Materials Depends on Substrate Composition and Morphology

HA, CA5, and CA10 had similar surface feature sizes, whereas the bone-like mineral revealed a smaller plate-like structure with evident spherical areas of nucleation and growth (Figure 2.5). Higher magnification images of the surfaces (Figure 2.5 insets) illustrate the characteristic plate-like features on the bone-like mineral and more granular surface features on the HA, CA5, and CA10 disks. BET surface areas for BLM, HA, CA5, and CA10 were 121.55, 0.05, 0.11, and 0.19m²/g, respectively.

All of the apatite-based materials show phosphate adsorption bands correlating with hydroxyapatite at ca. 1087, 1032, 602, and 574 cm^{-1} (Figure 2.6). Carbonate peaks at ca. 1455 and 875 cm^{-1} were detected for BLM, CA5, and CA10. The carbonate peaks in BLM indicate that a Type B carbonate substitution is occurring during formation, whereas the small but distinct peak that both CA5 and CA10 exhibited, taken into account with the fabrication temperature of 1350°C, is indicative of Type A carbonate substitution (Liao et al., 1999).

XRD characteristic peaks correlating with hydroxyapatite (PDF 9-432) existed in all of the materials at or around 2θ (crystal family plane) = 25.9° (200), 31.8° (211), 34.0 (202), 39.8° (310), 46.7° (222), 49.4° (213), and 53.1° (401, 303) (Figure 2.7). Narrow, distinct peaks were observed in the HA, CA5, and CA10 spectra as a result of the high sintering temperature during disk fabrication. Additional HA peaks were evident for HA, CA5, and CA10 at or $\pm 0.2^\circ$ for 2θ (crystal family plane) = 32.2° (122) and 32.9° (300). The BLM peaks were broadened in comparison to the sintered disks, revealing that either a less crystalline apatite or a nano-crystalline phase forms over the 5 day soak in the supersaturated ion solution at 37°C. Small 2θ peaks at 29.7° and 37.3° were found for the sintered disks pressed from carbonated apatite powders, CA5 and CA10. These small peaks are most likely a combination of calcium oxide (CaO) and/or α -TCP that did not completely revert back to hydroxyapatite during cooling (Liao et al., 1999). These peaks are not present in the HA spectrum. This inconsistency leads to the interpretation that these peaks result from the incorporation of carbonate into the powder prior to sintering the CA5 and CA10 disks. Because the height of this peak is small in relation to the highest apatite peak, the amounts of calcium oxide and/or α -TCP present on the surface are thought to be minimal.

When normalized to MacroSA, Figure 2.8, adsorption of A and S were significantly greater on carbonated disks (CA5, CA10) versus the BLM (For A, CA5 $p=0.006$, CA10 $p=0.001$; For S, CA5 $p=0.001$, CA10 $p<0.001$). Differences between the carbonated disks and HA disks also existed for peptide S (CA5 $p=0.004$, CA10 $p=0.001$). Because the surface area of BLM is three orders of magnitude greater than the sintered

disks, the MicroSA normalized peptide adsorption values (Figure 2.9) are in the picogram range and are significantly lower than other apatite-based materials, $p < 0.050$. Despite CA5 and CA10 possessing similar carbonate content, the CA5 disks had a significantly higher ability to adsorb peptide S, $p = 0.007$. Moreover, a trend of decreased adsorption to CA10 versus CA5 or HA was seen for A, V, and E. For MacroSA and MicroSA normalization, apatite groups HA, CA5, and CA10 were significantly different, $p < 0.050$, in comparison to TCPS for A, S, and V, again indicating the peptides are specific to calcium phosphate substrates.

Discussion

This work is the first to present detailed methods, to our knowledge, that identify peptide sequences with preferential adsorption towards synthetic bone-like mineral or apatite substrates. Phage display libraries expressing combinations of linear or cyclic peptide inserts have isolated sequences with high affinity towards inert materials (Adey et al., 1995; Whaley et al., 2000), cell lines cultured *in vitro* (Samoylova et al., 2002; Zhang et al., 2001), and cell/organ targets *in vivo* (Pasqualini et al., 1995). Three 7-mer peptide sequences have been reported as specific to hydroxyapatite, but the review presenting this data lacked methods on the preparation of the hydroxyapatite substrate (Tamerler and Sarikaya, 2007). Through repetitive experimentation and a rigorous, tri-fold validation technique, three peptides APWHLSSQYSRT [A], STLPIPHFSRE [S], and VTKHLNQISQSY [V] were identified to exhibit preferential adsorption towards apatite-based materials.

Many of the hydroxyapatite binding sequences identified have been from non-collagenous bone-related proteins present in the extracellular matrix of bone and/or proteins present in saliva. These proteins include, but are not limited to, bone sialoprotein, osteopontin and osteonectin (Shin et al., 2003), and a number of these proteins have a high proportion of acidic amino acids, such as glutamic and aspartic acids. In comparison to the bone sialoprotein derived peptide E with seven acidic amino acids, peptides A, S, and V that did not contain strings of acidic amino acids adsorbed in comparable, if not increased amounts on all the apatite-based materials and with lower

variability (Figure 2.4). Therefore, phage display derived sequences may offer an alternative to peptide identification compared to protein sequence searching and ultimately, contribute to peptide design that can enhance the bioactivity of implanted materials.

Adsorbed or covalently attached peptide sequences have been shown to mediate cell adhesion, as functionalizing biomaterials with the ubiquitous RGD (Gly-Arg-Asp) sequence increases cell adhesion (Hersel et al., 2003). Other peptide sequences have been designed to increase cellular adhesion to titanium (Ferris et al., 1999; Verrier et al., 2002), to contain cyclic RGD sequences (Pallu et al., 2003), or to be modeled from the heparin binding domain (Dalton et al., 1995; Dee et al., 1998). However, these cell adhesive sequences were not designed based on preferential affinity towards a specific material. Weakly attached surface molecules can be redistributed by cells attempting to attach to a surface (Choquet et al., 1997; Pelham and Wang, 1998), and softer substrates can cause the disorganization of actin filaments (Pelham and Wang, 1998). In both cases, effective formation of focal adhesions will not occur, demonstrating the need to consider both the substrate material and cell source in the peptide design. Furthermore, a cell-influencing sequence can be linked to the peptides to specify cell behavior, such as attachment.

Not only do the surface peptides need to withstand contractile forces from attached cells, the peptide concentration presented on the material surface should be optimized for a specific cellular behavior (Hubbell, 1999). Adjusting the initial peptide concentration introduced to an apatite-based substrate can provide the specific surface density required for the promotion of cell adhesion. To ensure appropriate surface densities are present for the cells, the amount of peptide adsorbed to the surface must be quantified, as the peptide adsorption can change depending on substrate charge and morphology. The presented work highlights the adsorption capacity through quantification of the high affinity peptides to various apatite-based materials.

Normalization of peptide adsorbed to MacroSA (Figure 2.8) provided insight towards the amount of peptide that would be required to coat apatite-based implants.

Slight carbonate incorporation in the CA5 and CA10 groups increased adsorption of peptides S and A compared with HA. The MacroSA normalization data also indicate that a sintered apatite coating on an implant may be more capable of adsorbing S and A peptides compared with a BLM coating. However, the additional factor of peptide surface density must be considered, as extracellular matrix mineralization varies with adhesive peptide surface densities (Rezania and Healy, 1999).

Normalization of peptide adsorbed to MicroSA (Figure 2.9) was performed to investigate the effects carbonate incorporation and morphology have on the amount of peptide adsorbed. Slight changes in carbonate percentage did not influence peptide adsorption. This result does not rule out that a larger change in carbonate incorporation affect peptide adsorption. The range of carbonate present in the studied materials did vary (CA5 and CA10 vs. HA); however, at the same morphological scale, the carbonate differences were minimal (~2wt%). A trend of decreased adsorption to CA10 in comparison to CA5 and HA was shown across all peptides. CA5 adsorbed significantly higher amounts of peptide S compared with CA10, indicating that a morphological difference, not a compositional difference, was evident for this case only. The morphology difference between CA5 and CA10 could change the charge distribution on the apatite surface, promoting peptide adsorption. Better control of the surface morphology accompanied by larger differences in carbonate content would better investigate if carbonate incorporation has an effect on peptide adsorption.

Both material composition and surface morphology influence protein adsorption (Kilpadi et al., 2001; Rosengren et al., 2002; Zeng et al., 1999) and the resulting cell adhesion and proliferation (Healy et al., 1996; McFarland et al., 2000; Keselowsky et al., 2003). Calcium phosphates exhibit the ability to adsorb more protein than other materials, which has led to the suggestion that Ca^{2+} and PO_4^{3-} present themselves as preferential binding sites for proteins (Zeng et al., 1999). Changes in surface morphology (e.g. pore size) also affect protein adsorption. Microporosity has been shown to increase protein adsorption, but decrease cellular differentiation (Anselme et al., 2000; Rouahi et al., 2006). Taken together, these studies suggest that with a certain composition and

morphology, calcium phosphates allow a preferred charge pattern that promotes protein binding. Identifying peptides that preferentially adsorb to apatite-based materials without disrupting the charge distribution that may prove beneficial *in vivo* by allowing protein adsorption to transpire. Despite BLM being classified as a calcium phosphate with a distinct nano-morphology, BLM has not been investigated in biomolecular adsorption studies. The presented data parallels the literature discussing factors that affect protein adsorption and offers a new perspective on peptide adsorption to BLM.

Phage display combinatorial libraries offer potential in isolating binding peptide sequences from a vast library, making otherwise unfathomable experiments possible (Rodi and Makowski, 1999; Scott and Craig, 1994; Uchiyama et al., 2005). Phage libraries can express an unequal representation of each amino acid within the library, are not able to include every peptide combination possible, and oftentimes omit important post-translational modifications such as phosphorylation of serine residues in the parent library. The results from the presented phage display experiments did not preferentially isolate peptide sequences with long strings of acidic amino acids, as the peptides isolated from the phage display had an average overall charge of ± 1 . This unexpected result could have occurred because poly-acidic peptide sequences were not initially present in the parent library, or because the identified sequences bound with greater affinity than poly-acidic peptide sequences. Nonetheless, the array of peptides presented in these libraries provided the opportunity to identify sequences specific to the apatite-based materials. Furthermore, the A, S, and V peptides identified in this study contain amino acid residues that can be phosphorylated. Phosphorylating the serine, threonine, and/or tyrosine residues on peptides A, S, and V would increase the negative charge on these peptide sequences, possibly enhancing their adsorption to apatite. It is possible with phage display techniques to identify high adsorbing, non-modified sequences that could achieve even higher affinity after synthetic phosphorylation.

While the lack of controlled peptide adsorption was taken into account when analyzing carbonate effect on adsorption by normalizing peptide adsorbed by its respective surface area (micro or macro), we do not report saturation curves, and cannot

conclusively say that peptide saturation was attained. However, increased fluorescence intensities with increased concentrations of FITC-labeled E₇RGD peptide on HA disks shows a strong intensity visible at 100µg/mL (Sawyer et al., 2005b). Since the initial peptide concentrations used in these studies were ~500µg/mL, we can only speculate that saturation was achieved.

The work described in this chapter provides a stimulus to explore alternative methods to better engineer current tissue repair constructs. For example, apatite-binding peptides can be combined with soft tissue or ligament binding recognition sequences to help re-establish tissue interfaces in the tooth-gum and bone-ligament systems, respectively. The presented work also strives to emphasize that a multitude of factors influence not only protein or peptide adsorption, but other biomolecules such as growth factors and DNA as well. Therefore, it is imperative to fully characterize the substrate material to better understand how the material will regulate biomolecular adsorption or incorporation prior to the addition of cells.

Three peptides, APWHLSSQYSRT [A], STLPIPEFSRE [S], and VTKHLNQISQSY [V], were identified as high affinity binders specific to apatite-based materials. The morphology of the apatite-based materials influenced synthetic peptide adsorption more than slight changes (2%) in carbonate content. Because the identified peptides have preferential adsorption to apatite, their use can now be investigated in a variety of bone-based research including bone and dentin tissue engineering, tendon and ligament repair, and enamel formation.

Acknowledgements

I would like to acknowledge my co-authors on this work, Dr. David H. Kohn and Hayes C. Smith. This work is supported by the National Institutes of Health and the Department of Energy: DE 015411 and DE07057. Thanks so Udo Becker and Subhashis Biswas for all of the modeling help and analysis. I would also like to thank Alisha Diggs for help with disk preparation, Henriette Remmer and Jen Mahoney for their support that the UM Peptide Core, UM EMAL for their continued support of scanning electron

microscopy, and Xiaoyin Chen for his expertise in the BET analysis. Thanks to Dr. Mary Tecklenberg for supplying the carbonated apatite powders.

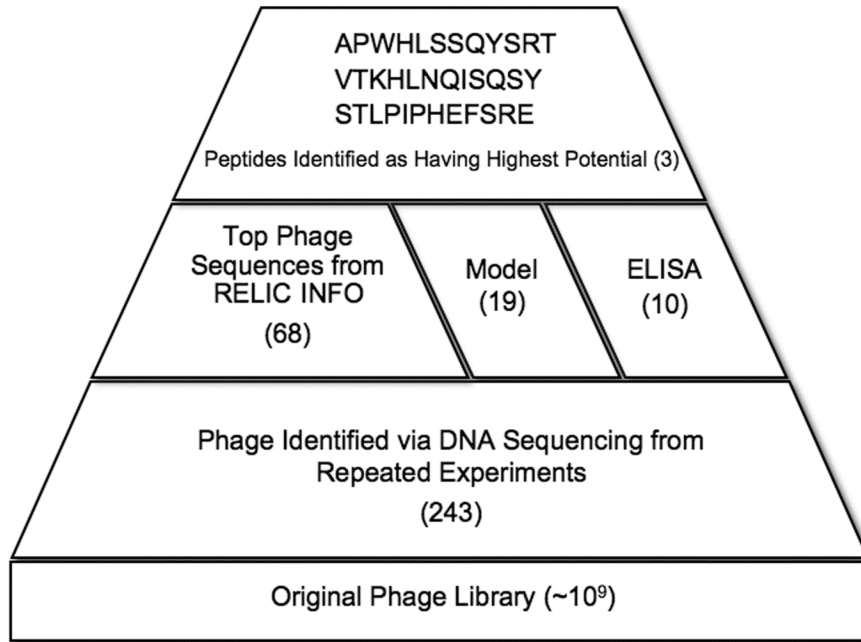


Figure 2.1: Schematic displaying the tri-fold analysis approach used to identify peptides that preferentially adhere to BLM and HA.

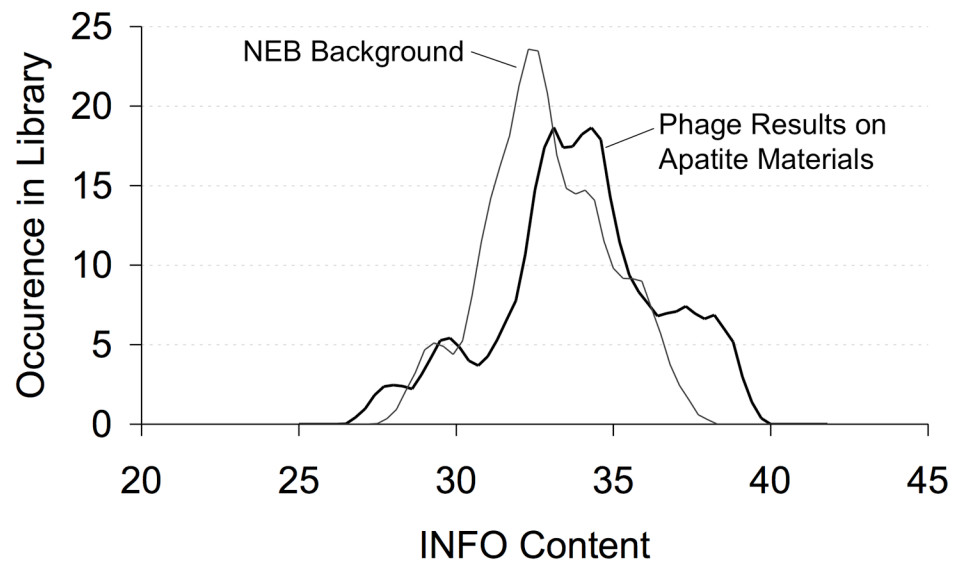
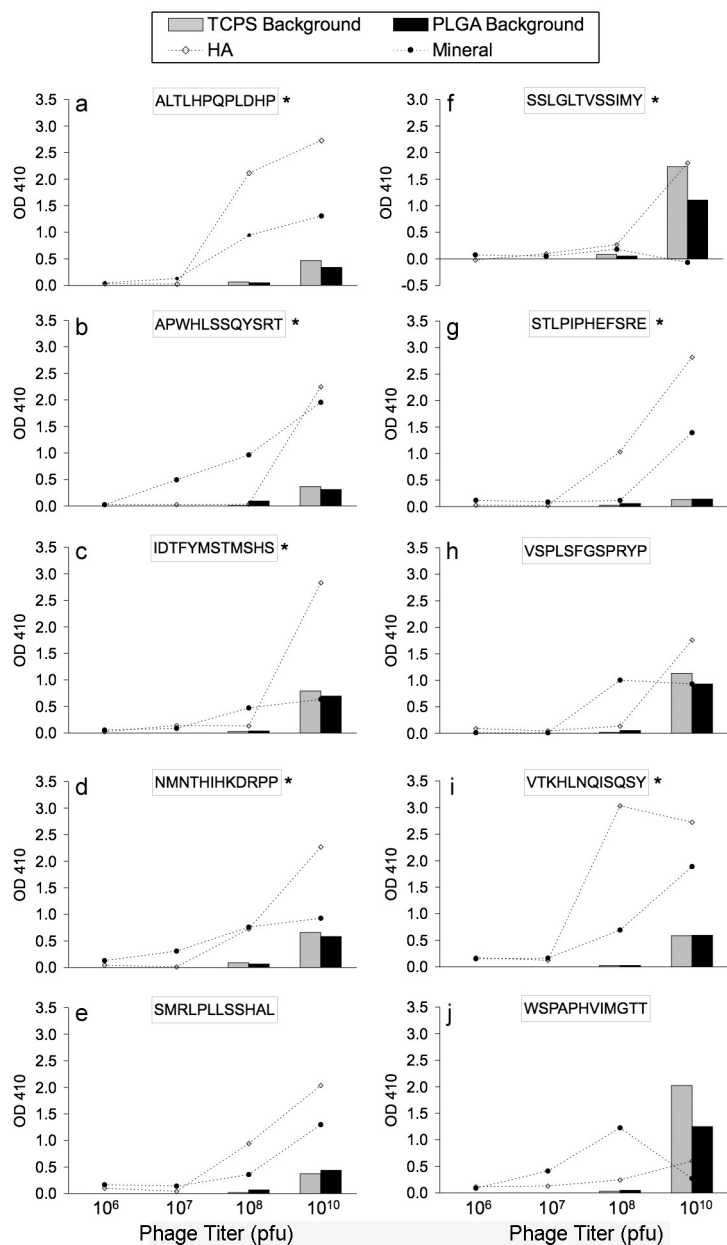


Figure 2.2: INFO content values calculated in RELIC for NEB background and phage subset identified as high affinity binders to apatite-based materials. High information content correlates to a lower incidence of being selected by chance. The phage subset shows a shift towards a higher information content signifying this subset was selected based on the binding affinity towards HA and BLM.



* Phage Sequences Modeled on Hydroxyapatite Lattice

Figure 2.3: Modified ELISA results for 10 representative peptides on 4 substrates showing a higher absorbance value at OD 410 with a higher concentration of phage. PLGA and TCPS background adsorption of each phage was minimal in 6 of 10 phage sequences tested. An example of a phage with high background is shown for peptide WSPAPHVIMGTT. Positive readings on the modified ELISA supports that the phage identified are indeed specific to apatite-based materials. (*) Indicates peptide sequences that were computationally modeled.

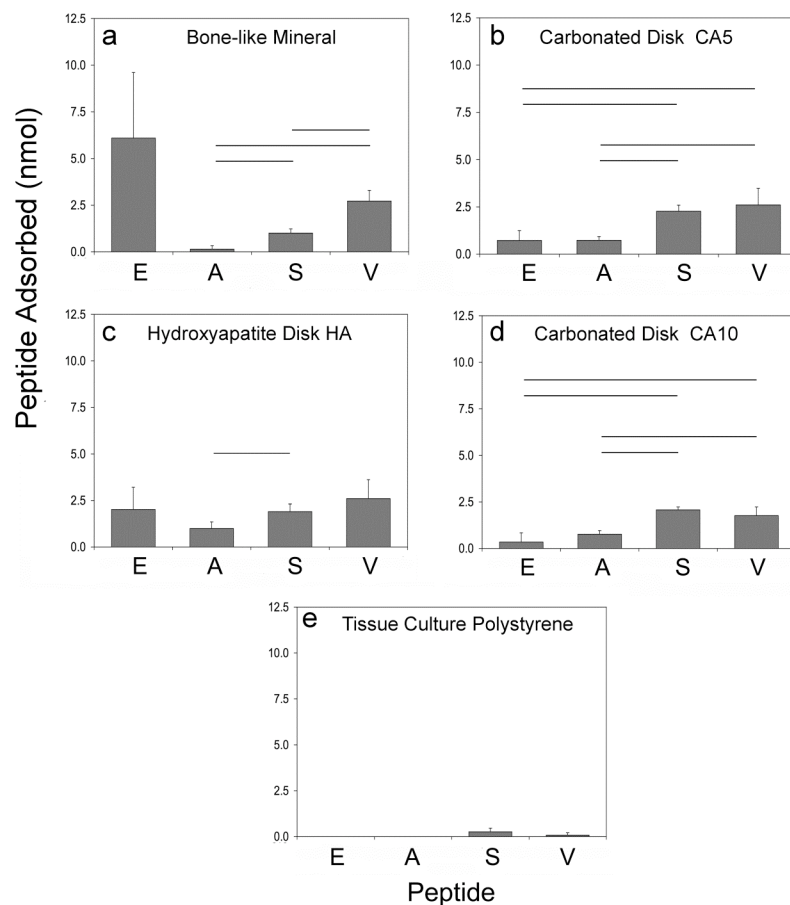


Figure 2.4 Adsorption of peptides EEEEEEEPRGDT [E], APWHLSSQYSRT [A], STLPIPHFSRE [S], and VTKHLNQISQSY [V] on (a) bone-like mineral (BLM), (b) sintered disks from 5.6% carbonated apatite powder (CA5), (c) sintered disks from hydroxyapatite powder (HA), (d) sintered disks from 10.5% carbonated apatite powder (CA10), and (e) tissue culture polystyrene (TCPS). Peptides S and V showed better adherence to all apatite-based materials in comparison to A, (For S vs. A, BLM $p=0.001$, CA5 $p<0.001$, CA10 $p<0.001$, HA $p=0.038$; For V vs. A, BLM $p=0.006$, CA5 $p=0.033$, CA10 $p=0.029$), and to both carbonated disks CA5 and CA10 in comparison to E, (For S vs. E, CA5 $p=0.005$, CA10 $p=0.004$; For V vs. E, CA5 $p=0.026$, CA10 $p=0.010$). Differences between S and V were also only seen on bone-like mineral, $p=0.006$. These results suggest that peptide adsorption is not only dependent on substrate composition, but also on the peptide composition. Horizontal bars denote statistical differences.

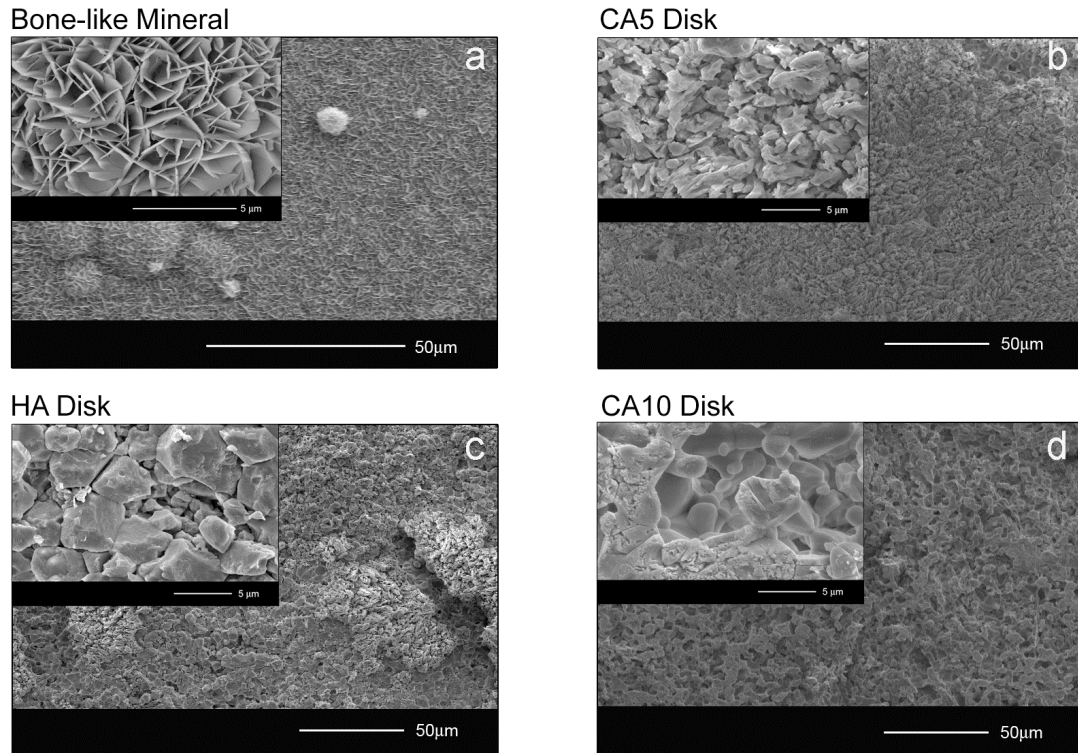


Figure 2.5 Representative SEM images showing low and high magnification morphologies of the four apatite-based materials: (a) bone-like mineral (BLM), (b) sintered disks from 5.6% carbonated apatite powder (CA5), (c) sintered disks from hydroxyapatite powder (HA), and (d) sintered disks from 10% carbonated apatite powder (CA10). These higher magnification images show that the bone-like mineral has small surface features that relate to the bone-like mineral having a 100X higher surface area than the other three apatite-based materials. (Original images taken at U of M EMAL)

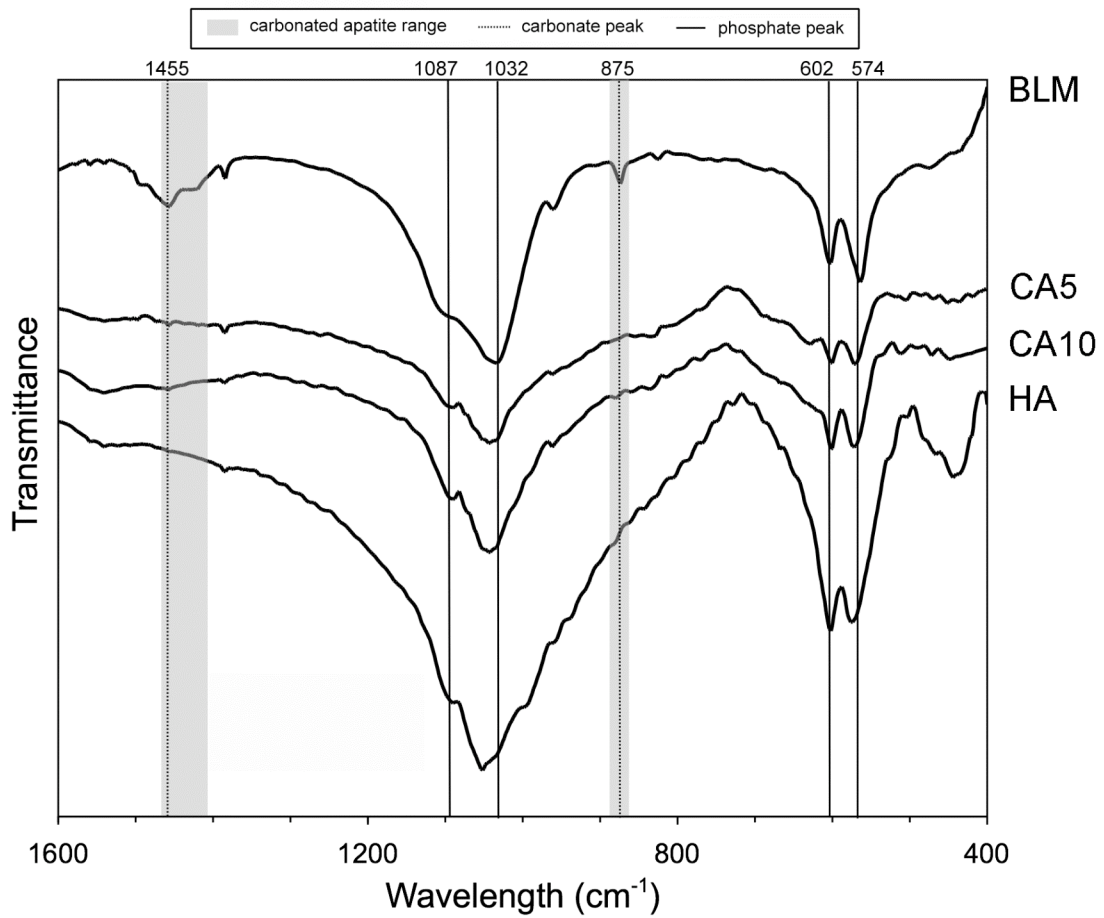


Figure 2.6: Representative FT-IR spectra for bone-like mineral (BLM), sintered disks from 5.6% carbonated apatite powder (CA5), sintered disks from 10.5% carbonated apatite powder (CA10), and sintered disks from hydroxyapatite powder (HA) substrates. Phosphate peaks are found for all samples at 1031, 600, and 561 cm^{-1} and a carbonate peaks are found at 875 or 1456 cm^{-1} .

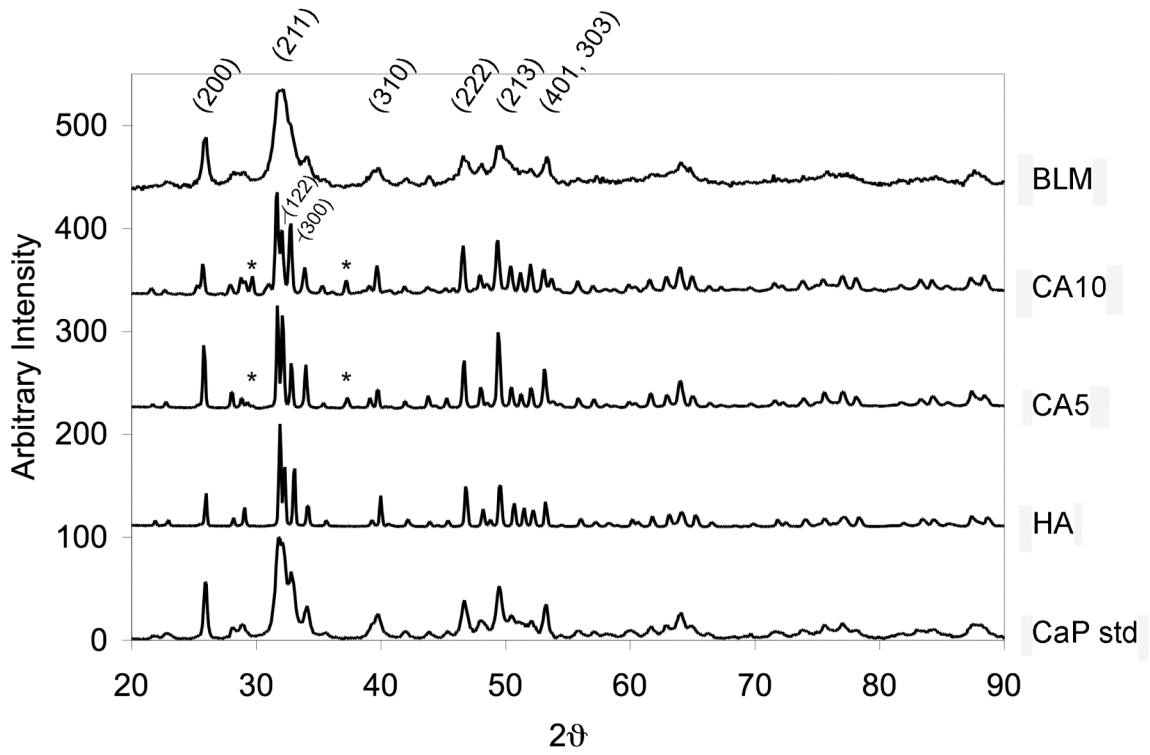


Figure 2.7: X-ray diffraction patterns for bone-like mineral (BLM), sintered disks from 10.5% carbonated apatite powder (CA10), sintered disks from 5.6% carbonated apatite powder (CA5), sintered disks from hydroxyapatite powder (HA), and a calcium phosphate standard (CaP Std). The bone-like mineral was less crystalline than the sintered disks; however, all samples showed characteristic hydroxyapatite peaks (labeled). The disks sintered from carbonate powder, CA10 and CA5, revealed small peaks at $2\theta = 29.7$ and 37.3° (*), which reflect traces of calcium oxide and/or α -TCP.

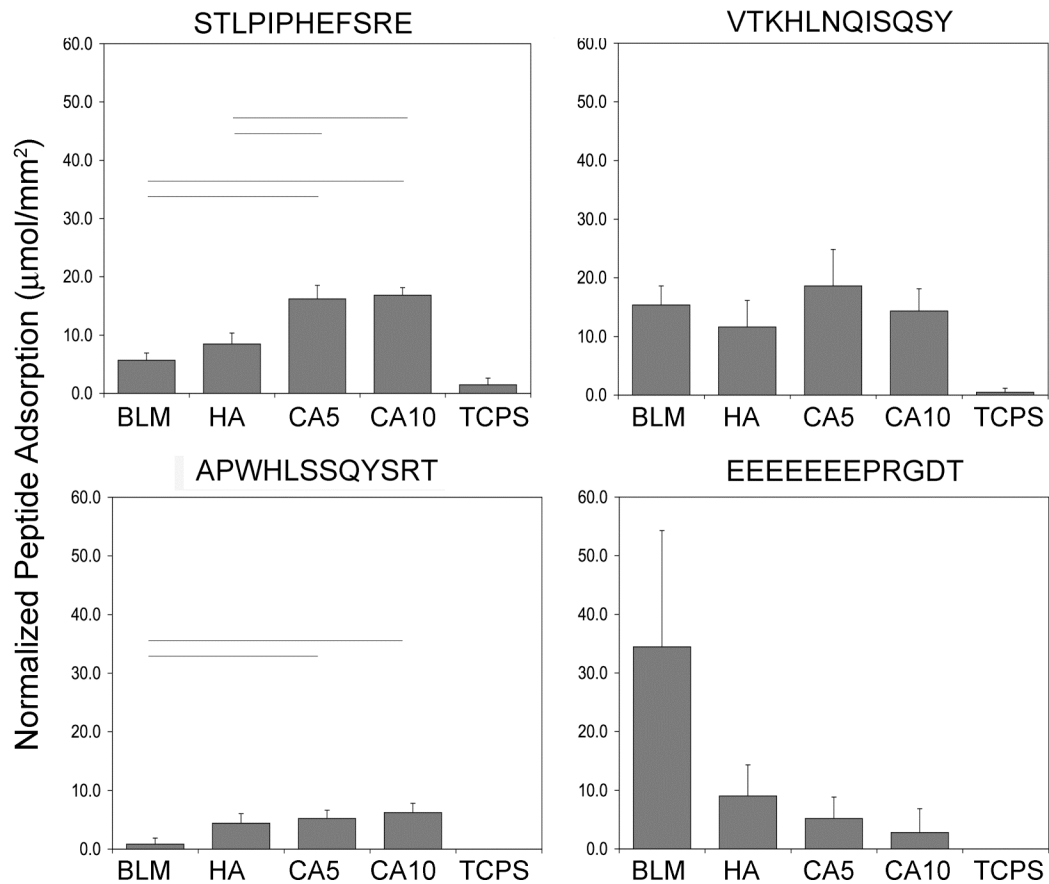


Figure 2.8: Peptide adsorption data normalized to sample dimensions (MacroSA) shows that peptides A and S have increased adsorption on CA5 and CA10 when compared with BLM (For A, CA5 $p=0.006$, CA10 $p=0.001$; For S, CA5 $p=0.001$, CA10 $p<0.001$). Differences for peptide S were also evident between HA and the carbonated disks (CA5 $p=0.004$, CA10 $p=0.001$). Apatite groups HA, CA5, and CA10 were significantly different, $p<0.050$, in comparison to TCPS for A, S, and V. Horizontal lines represent statistical significance.

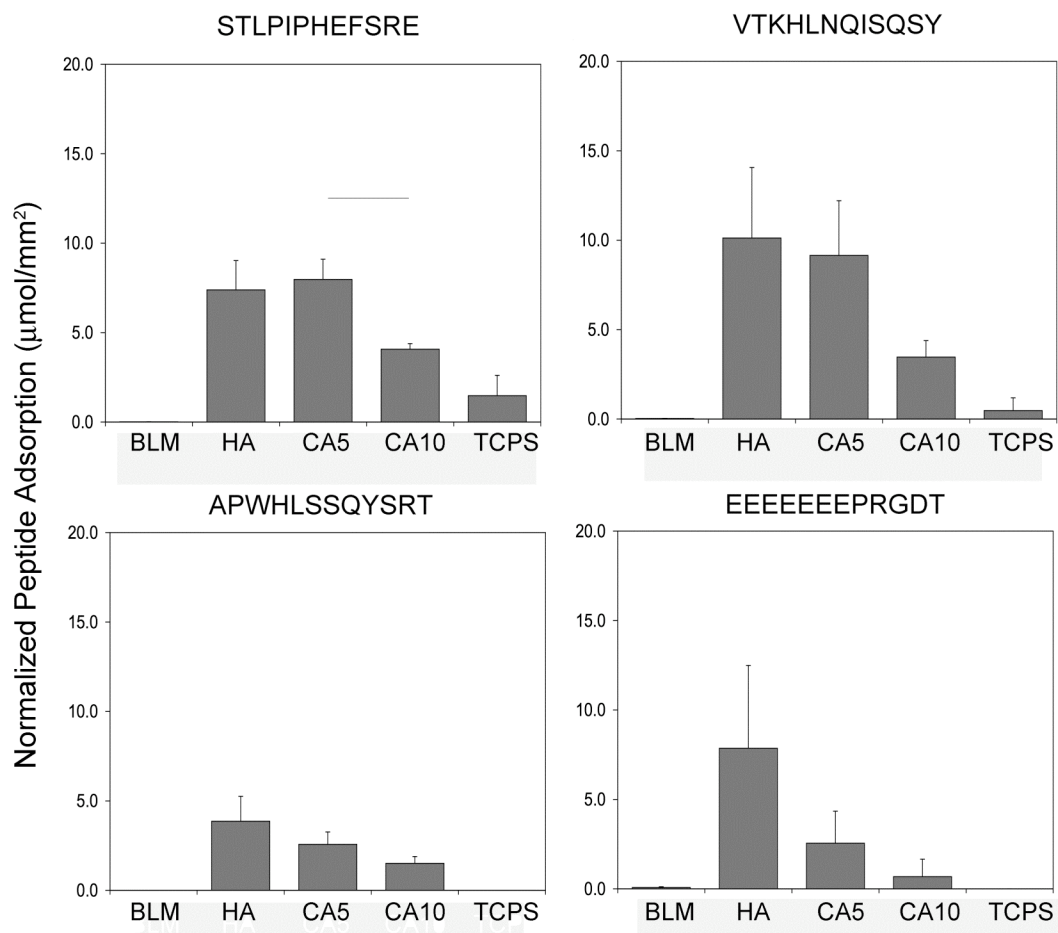


Figure 2.9: Peptide adsorption data normalized to sample dimensions (MicroSA). Despite CA5 and CA10 possessing similar carbonate content, the CA5 disks had a higher affinity to adsorb peptide S, $p=0.007$. Trends of decreased adsorption to CA10 versus CA5 or HA were seen for peptides A, V, and E. Apatite groups HA, CA5, and CA10 were significantly different, $p<0.050$, in comparison to TCPS for A, S, and V. Horizontal lines represent statistical significance.

Table 2.1: Peptide Sequences Identified via Phage Display with Preferential Adsorption Towards Apatite-Based Materials

Identified Phage Sequences	# clones	Frequency (% of total clones)
APWHLSSQYSRT [◇]	53	21.8
IDTFYMSTMSHS ^{**◇}	21	8.6
ALTLHPQPLDHP [◇]	12	4.9
TALATSSTYDPH	12	4.9
VTKHLNQISQSY ^{**◇}	6	2.5
WSSGMTPTDTGAP ^{**}	6	2.5
ALSSSSNTTTRV	4	1.6
SSLGLTVSSIMY [◇]	3	1.2
NMNTHIHKDRPP ^{**◇}	2	0.8
SMRLPLLSSHAL ^{**◇}	1	0.4
VSPLSFGSPRYP ^{**◇}	1	0.4
WSPAPHYIMGTT ^{**◇}	1	0.4
STLPIPHEFSRE ^{**◇}	1	0.4

bold - Sequences occurring on both BLM and HA

** - Identified as a high information clone via INFO

◇ - Clone ran in modified ELISA

Table 2.2: Summary of Computational Modeling Data for Peptides A, S, and V on Hydroxyapatite (001) Surface and Step Surface

Adsorption on (001) plane				Adsorption on [010] step in (001)			
	Peptide	Peptide Adsorption Energy (kcal/mol)	pI		Peptide	Peptide Adsorption Energy (kcal/mol)	pI
Neutral	VTKHLNQLSQSY	-336.9	9.7	Neutral	VTKHLNQLSQSY	-705.6	9.7
	APWHLSSQYSRT	-279.6	9.9		APWHLSSQYSRT	-680.8	9.9
	STLPIPEFSRE	-239.3	5.3		STLPIPEFSRE	-677.3	5.3
Charged	VTKHLNQLSQSY	-288.2	9.7	Charged	STLPIPEFSRE	-919.2	5.3
	STLPIPEFSRE	-263.9	5.3		VTKHLNQLSQSY	-449.6	9.7
	APWHLSSQYSRT	-247.0	9.9		APWHLSSQYSRT	-368.8	9.9

CHAPTER THREE

PEPTIDES DESIGNED TO ADHERE TO BOTH APATITE AND HUMAN BONE MARROW STROMAL CELLS IMPROVE CELL ATTACHMENT ON BONE-LIKE MINERAL

Introduction

The current concepts in bone tissue engineering aim to replace large defects with new bone tissue having properties that mimic native tissue through a combination of scaffolding, cells, and/or biological signals (Alsberg et al., 2001; Garcia and Reyes, 2005; Hubbell, 1999; Maskarinec and Tirrell, 2005; Shin et al., 2003). Improvements in the materials and methods used in bone repair are needed to overcome clinical limitations of autogenous bone grafting, such as graft rejection, donor site morbidity, and inadequate bone formation (Ducheyne and Qiu, 1999; Parikh, 2002; Yaszemski et al., 1996). In addition to osteoconductivity of implantable materials, exogenous signals or cell sources capable of osteogenic differentiation are required to attain directed bone formation both *in vitro* and *in vivo* (Abiraman et al., 2002; Liu et al., 2005; Shimaoka et al., 2004). Research identifying and incorporating biological molecules has been ongoing in parallel with research isolating and manipulating appropriate cell sources for use in bone engineered systems (Chen and Mooney, 2003; Rose and Oreffo, 2002).

Cellular adhesion can dictate the success of an implanted construct. Cells can be seeded on a construct *ex vivo* or a specific cell population can be recruited *in vivo*; however, either scenario requires cell attachment to ensure cell viability with subsequent proliferation and differentiation. Understanding the steps involved in cell adhesion is imperative when trying to incorporate biological signals that can promote adhesion in

scaffold design. Cell adhesion progresses in four steps: cell attachment, cell spreading, production of organized actin filaments, and focal adhesion formation (LeBaron and Athanasiou, 2000). The importance of cell adhesion has been demonstrated in a variety of cells and tissues including the differentiation of myoblasts (Menko and Boettiger, 1987), terminal keratinocytes (Adams and Watt, 1990), mammary epithelium (Streuli et al., 1991), and osteoblasts (Damsky, 1999). The establishment of an integrin mediated bond between a cell and a protein initiates a cascade of signals that provides structural support and phenotypic influence (Garcia and Boettiger, 1999). When a material is implanted in the body, extracellular matrix proteins such as fibronectin and vitronectin adsorb onto the material and initiate integrin-ligand binding of cells to the material (Garcia and Boettiger, 1999). However, proteins are subject to isolation and prone to degradation (Hersel et al., 2003). Proteins can also change conformation or orientation, because they possess sections with varying hydrophobicities that address cellular functions other than adhesion.

Identification of short cell recognition sequences has motivated the development of peptide-laden bioactive materials that can recruit a certain cell population to adhere to a material surface via specific integrin mediated bonding. Peptides can effectively mimic the same response as a protein while being smaller, cheaper, and less susceptible to degradation. Peptides have a greater potential for controlling initial biological activity, because they can contain specific target amino acid sequences and can permit control of hydrophilic properties through sequence design (Ladner et al., 2004). One peptide that interacts with a variety of cell adhesion receptors, including those on osteoblasts, is the RGD (Arg-Gly-Asp) sequence (Hersel et al., 2003). The RGD binding sequence is an adhesion sequence that interacts with multiple adhesion receptors including the $\alpha_v\beta_3$ integrin that binds not only to vitronectin and fibronectin, but to the bone proteins osteopontin and bone sialoprotein (Hersel et al., 2003). RGD sequences can act as inhibitors of cell adhesion if present in solution, even though they have been shown to promote cellular adhesion when adsorbed on some material surfaces (Ruoslahti, 1996). In addition, RGD adsorption, when combined with other adhesive extracellular bone

matrix proteins on a hydroxyapatite surface, proved detrimental to human mesenchymal stem cell adhesion and survival (Hennessy et al., 2008), suggesting RGD presence *in vivo* could hinder tissue growth. Therefore, non-RGD adhesion sequences are an attractive alternative that could prove more effective in establishing initial cell attachment. Such peptide alternatives could also offer increased specificity towards a specific cell source as compared to the ubiquitous RGD.

Since the osteoconductivity of a bone implant is improved if made or coated with an apatite-based material (Abe et al., 1990; Kohn DH et al., 2005), it is of interest to design peptide sequences with preferential adsorption to apatite. Inorganic-organic hybrid systems that employ bone-like mineral coatings to biodegradable polymers are often used to improve the osteoconductivity of materials compositionally dissimilar to apatite. A bone-like mineral (BLM) coating can be achieved by soaking the polymer in a supersaturated ionic solution capable of heterogeneously precipitating a film of apatite. However, compared with polymers, apatite-based materials are less tolerant to surface modifications that allow covalent molecular attachment. Therefore, apatite-based materials must rely on their inherent material properties to allow consistent, ionic adhesion of peptides. Post-translational modifications and poly-acidic peptide strings are two strategies used to encourage peptide adhesion to apatite-based materials (Fujisawa et al., 1996; Fujisawa et al., 1997). While these design strategies have been used to fabricate sequences, such as E₇PRGDT, that aim to increase cell adhesion, sequences discovered via peptide selection from a combinatorial library of sequences could provide alternative sequences that prove to be better at increasing cell adhesion.

Combinatorial phage display libraries can be utilized to identify 12-mer peptide sequences with preferential binding to apatite-based materials (refer to Chapter Two), including bone-like mineral. Phage display is a useful technique in identifying peptide sequences not only specific to tissues (kidney tubules (Odermatt et al., 2001), breast vasculature (Essler and Ruoslahti, 2002), muscle (Samoylova and Smith, 1999), bone marrow (Nowakowski et al., 2004)) and malignant cell types (Morita et al., 2006; Samoylova et al., 2003), but also to inorganic materials such as platinum (Seker et al.,

2007), silver (Naik et al., 2002a; Naik et al., 2002b), and semiconductors (Lee et al., 2002; Mao et al., 2003; Whaley et al., 2000). Specific to bone, phage display has been utilized *in vitro* to identify potential osteoblast binding sites during the resorption-formation process in remodeling bone (Sheu et al., 2002). It has also been suggested that 7-mer peptide sequences have been identified on hydroxyapatite substrates, but limited information on the substrate preparation or properties is reported (Sarıkaya et al., 2003; Tamerler et al., 2003). The limited peptide research on bone-like mineral led the pursuit of sequences that preferentially bind to BLM. Since bone-like mineral is a synthetic form of apatite synthetically fabricated at benign physiologic conditions (pH=6.8, 37°C), BLM is capable of biomolecular incorporation and positively influencing cell spreading (Leonova et al., 2006; Luong et al., 2006; Segvich et al., 2008b), making it an important apatite-based substrate to investigate. Specifically, the sequence VTKHLNQISQSY, was identified as a preferential apatite-binder having increased ability to bind to hydroxyapatite and carbonated apatite materials compared with the previously reported ability of bone sialoprotein derived peptide E₇PRGDT (refer to Chapter Two).

The goal of the work presented in this chapter was to identify peptide sequences that preferentially bind to clonally derived hBMSC cells that can then be implemented in a dual-functioning peptide design to promote hBMSC cell attachment on apatite-based substrates. The hypothesis that dual-functioning peptides adsorbed to BLM will increase hBMSC attachment compared to BLM devoid of peptide was tested. To identify peptides that preferentially bind to hBMSC, a combinatorial phage display library was used. Data from the phage display experiments were analyzed using the bioinformatics tool RELIC and immunohistochemistry techniques, and as a result, two 12-mer peptide sequences, LLADTTHHRPWT [L] and DPIYALSWGMA [D], were identified as preferential binding peptides to the hBMSC population used in this study. Dual-functioning peptides were built using the hBMSC binding sequences combined with the previously identified VTKHLNQISQSY [VTK] apatite-binding peptide. The intent of this work is to demonstrate the feasibility of using such peptides to create a linkage between inorganic and organic constituents, in this case BLM and hBMSCs.

Materials and Methods

Reagents and solutions were obtained for all experiments from Sigma-Aldrich unless otherwise noted.

Preparation of Bone-like Mineral Films and Apatite Disks

A 5 w/v% 85:15 polylactic-co-glycolic acid (PLGA, Alkermes)-chloroform solution was cast on 15mm diameter glass slides and dried overnight. The PLGA films were etched in 0.5M NaOH for 7 minutes and rinsed in Millipore water (ddH₂O). Etched films were soaked in modified simulated body fluid (mSBF) for 5 days at 37°C. The mSBF was made by dissolving the following reagents in Millipore water at 25°C and titrating to pH 6.8 using NaOH: 141 mM NaCl, 4.0 mM KCl, 0.5 mM MgSO₄, 1.0 mM MgCl₂, 4.2 mM NaHCO₃, 5.0 mM CaCl₂•2H₂O, and 2.0 mM KH₂PO₄. The mSBF, a supersaturated solution that enables self-assembly of a carbonated apatite layer onto the polymer substrate, was changed daily to maintain supersaturation. Following a 5 day soak in mSBF, films with a precipitated bone-like mineral (BLM) layer were rinsed with ddH₂O, dried under a hood, and desiccated until use.

Hydroxyapatite disks (HA) (10 mm diameter x 4 mm thick) were pressed from powder (Plasma Biotol Ltd. P220) at 1 metric ton for 1 minute and sintered at 1350°C for 5 hours (heating rate of 10°C/minute). Carbonated apatite disks were made from 5.6% (CA5) carbonated apatite powders (generous gift from Dr. Mary Tecklenburg). Carbonated apatite disks (8-10mm diameter x 2-4mm thick) were pressed from powder at 0.5 metric ton for 1 minute and sintered at 1350°C for 1 hour (heating rate of 10°C/minute). Both hydroxyapatite and carbonated apatite disks were sonicated clean in 10mM HCl, then in ddH₂O. The HA and CA5 disks contained 0-1.1% and 1.5-2.1% CO₃²⁻, respectively (refer to Chapter Two). All disks were autoclaved prior to use. Macroscopic dimensions of all disks were measured with calipers.

Cells

Clonally derived human bone marrow stromal cells (hBMSC), a generous gift from NIH, were maintained in alpha minimum essential media (α -MEM) (Gibco, #12561) with glutamine containing 20% fetal bovine serum (FBS) and antibiotics (100 U/mL penicillin, 0.1 mg/mL streptomycin (P/S)) (Gibco, #15140) at 37°C in a 5% CO₂ incubator. Media consisting of α -MEM with supplements (both FBS and antibiotics) is referred to as 'normal media'. Media consisting of α -MEM without supplements (no FBS nor antibiotics) was used where appropriate in the following experiments and is denoted as ' α -MEM without supplements'. Cells were passaged or plated when they reached 80-90% confluence. Media was replaced every 2-3 days.

Phage Display on hBMSCs

Peptide sequences were identified by screening the Ph.D.12TM Phage Display Library (New England Biolabs, #E8110S), consisting of 10⁹ different phage with 12-mer amino acid linear peptide inserts, against clonally derived hBMSC (Passage 3-6). 2x10⁴ hBMSCs were plated in 2 wells of a 6-well dish and cultured for 6 days in normal media at 37°C and 5%CO₂. After 6 days of culture, the NEB 12-mer peptide library was prescreened against sintered HA disks prior to introduction to the cells, to preferentially screen for sequences attracted to the cells and not the apatite. A streptavidin control was run in a separate dish per the manufacturers protocol.

Prior to phage introduction to the cells, the sintered HA disks and streptavidin control were incubated in ddH₂O and 1.5mg/mL streptavidin in 0.1 M NaHCO₃, respectively, overnight at 4°C in a humidified container. The following day, the ddH₂O or 0.1M NaHCO₃ was removed and replaced with blocking buffer and incubated at 4°C for 1 hour. Blocking buffer solution consisted of TBST (0.1%) (Tris-HCl buffered solution 50mM Tris-HCl pH 7.5, 150mM NaCl with 0.1% Tween-20) w/BSA for HA disks, TBST (0.1%) w/BSA + 0.1 μ g/mL streptavidin for control. The blocking buffer was discarded, and the substrates were washed 6X with TBST (0.1%). An aliquot of the original Ph.D.12TM library containing 10¹¹ pfu (plaque-forming units) diluted in 1mL of

TBS for HA disks and TBST (0.1%) for streptavidin control was introduced to each substrate and gently rocked (LabLine 4625) for 40 minutes at room temperature.

Non-binding phage on the HA disks were harvested and set aside. Plated cells in 6-well dishes were rinsed 2X with phosphate buffered solution (PBS, Gibco #10010) and pre-blocked with α -MEM without supplements containing 0.1% BSA at 37°C and 5% CO₂ for 30 minutes. The aliquot of phage harvested from the HA disks were then introduced to the cells (n=2) in 1mL of α -MEM without supplements containing 0.1% BSA for 1 hour at 37°C and 5% CO₂. Non-binding phage to the cells was then discarded, and the cells were washed 5X in cold PBS. The phage bound to the cells were eluted with 1mL of Glycine/HCl, pH 2.2, with 1 mg/mL BSA for 10 minutes at room temperature while being gently rocked. The eluted phage was collected and neutralized with 1M Tris-HCl, pH 9.1.

Non-binding phage was discarded for the streptavidin control plate, which was then washed 10X with TBST (0.1%). Bound phage were eluted from the control plate using 0.1mM biotin in TBS for 30 minutes at room temperature.

A small amount of each phage eluate was titered to determine the number of phage bound to each substrate. The rest of the eluate was amplified in *E. coli* (ER2738) by culturing the bacteria and phage in 20mL Lurie broth with vigorous shaking for 4.5 hours. The culture was centrifuged for 10 minutes at 10,000 rpm (Sorvall SS-34) at 4°C. The supernatant was transferred to a fresh tube, respun, and the upper 80% of the final supernatant was placed into a fresh tube and allowed to precipitate with 1/6 the volume of PEG/NaCl solution (20 w/v% polyethylene glycol-8000 in 2.5M NaCl). The phage were allowed to precipitate at 4°C overnight. The PEG precipitation was spun for 15 minutes at 10,000 rpm at 4°C, decanted and briefly respun. The pellet was suspended in TBS and transferred to a microcentrifuge tube, respun in a microcentrifuge for 5 minutes at 10,000 rpm at 4°C. The supernatant was precipitated with 1/6 the volume of PEG/NaCl solution for 60 minutes on ice, recentrifuged for 10 minutes at 10,000 rpm at 4°C, and the pellet was resuspended in TBS with 0.02% NaN₃. A small amount of the purified phage eluate was titered to determine the number of amplified phage. This amplified and purified

phage eluate was used in the next round of panning. Subsequent rounds of panning introduced at least 10^9 pfu as the input phage. Three rounds of panning were performed for each sample.

Titering was performed with appropriate serial dilutions for both the eluted phage and amplified phage after each round of panning. Agar plates treated with IPTG (isopropyl-b-D-thiogalactoside) and Xgal (5-bromo-4-chloro-3-indoyl-b-D-thiogalactoside) were able to visually identify correct plaques using blue/white screening. For the cell samples, a total of 60 individual plaques picked from plates having no more than ~100 plaques were individually amplified by infecting 1mL of a log phase *E.coli* culture. A fraction of the amplified phage stock from selected phage plaques were purified by PEG/NaCl precipitation. Single stranded DNA was isolated using an iodide buffer extraction, cleaned in ethanol, and resuspended in DNase/RNase free water. The DNA was sequenced via dideoxy chain termination method using a DNA sequencer (Applied Biosystems, 3730XL DNA Analyzer) with the NEB -96 gIII sequencing primer provided in the kit. The remainder of the amplified phage stock for 20 selected phage plaques was amplified again by infecting 20mL of a log phase *E. coli* (ER2738 in Lurie broth) with vigorous shaking for 4.5 hours. The culture was centrifuged for 10 minutes at 10,000 rpm (Sorvall SS-34) at 4°C. The supernatant was transferred to a fresh tube, respun, and the upper 80% of the final supernatant was placed into a fresh tube and allowed to precipitate with 1/6 the volume of PEG/NaCl solution. The phage were allowed to precipitate at 4°C overnight. The PEG precipitation was spun for 15 minutes at 10,000 rpm at 4°C, decanted and briefly respun. The pellet was suspended in TBS and transferred to a microcentrifuge tube, respun in a microcentrifuge for 5 minutes at 10,000 rpm at 4°C. The supernatant was precipitated with 1/6 the volume of PEG/NaCl solution for 60 minutes on ice, recentrifuged for 10 minutes at 10,000 rpm at 4°C. Each pellet was suspended in 50uL of DNase, RNase free water and stored at 4°C until used for immunohistochemistry.

RELIC Analysis

The bioinformatics tool REceptor LIgand Contacts (RELIC) (<http://relic.bio.anl.gov/index.aspx>) (Makowski and Soares, 2003; Mandava et al., 2004; Rodi et al., 2004) was used to analyze the data from the phage display. The programs DNA2PRO, MOTIF1, and INFO determined peptide translation sequences from DNA code, continuous conserved motifs within the peptide population allowing for conservative substitutions, and information numbers for each peptide reflecting the probability of selecting individual phage by chance, respectively. For example, a high information measure can be indicative of an uncommon sequence with a low growth rate during amplification; whereas, a low information measure could represent a phage sequence likely to appear based on composition and/or high growth rates. The phage display experiment on hBMSCs yielded 50 peptides, which were subsequently used in the MOTIF1 and INFO programs. The program MOTIF1 searched for 3-mer and 4-mer continuous conserved motifs. The program INFO was run with subtraction of a random selection of phage from the parent library (12R, 441 random sequences from NEB 12-mer Ph.D. kit).

Immunohistochemistry

1×10^4 hBMSC cells (Passage 5-6) were plated in each well of 4-well chamber glass slides (Nunc Lab-Tek Chamber Slide Systems, Fisher #1256521) in normal α -MEM. Cells were allowed to attach and grow until confluent. Prior to phage introduction, the media was removed and the cells were incubated with 500 μ L of normal α -MEM containing 0.1% BSA overnight at 37°C in 5% CO₂. Chosen individual phage plaques (Table 3.1) that had been amplified and isolated were introduced to this culture medium in a concentration of 0.5×10^{11} pfu/100 μ L and allowed to mix gently for 2 hours at 37°C in 5% CO₂. The media with phage was removed, and the cells were washed 6X with PBS. The cells were then fixed in 4% paraformaldehyde (Electron Microscopy Sciences #15710) in PBS for 10 minutes and washed 2X with PBS. Half of the fixed slides for each peptide were treated with 0.1% saponin in PBS with 0.1% BSA for 15

minutes. All fixed slides were incubated with mouse anti-M13 monoclonal antibody (GE Healthcare, #27-9420-01) diluted to 1:250 in PBS for 1 hour. The cells were washed 3X with PBS, and then incubated with FITC-conjugated sheep anti-mouse IgG (Jackson ImmunoResearch Laboratories, Inc., #515-095-003) diluted 1:250 in PBS for 1 hour, covered from light. The cells were again washed 3X in PBS and allowed to soak in PBS overnight. The antibody solution, PBS wash solution, and PBS overnight soak solution for the saponin treated slides contained 0.1% saponin.

Cells were covered with a glass coverslide after preparing in Vectashield (Vector Laboratories H-1200), and were subsequently viewed on a confocal laser-scanning microscope at an excitation wavelength of 488nm (Nikon TE 3000 Inverted Microscope). A BioRad Radiance 2000 LaserSharp program was used to image 20 μ m into the depth of the cells at 2 μ m intervals under 20x magnification. An excitation wavelength of 568nm was used to obtain similar series of images to identify the cells in the background without exciting the FITC attached to the phage. Each series of images was compiled in the LaserSharp program to obtain images showing adhesion of phage onto or into cells. Controls were run each day images were collected on the confocal microscope. Controls included: cells without phage receiving both antibody and FITC and cells only to detect any background fluorescence. Two samples for each phage and each condition were imaged. Three individual scorers blinded to the phage number and saponin treatment scored each image on a scale of 0-3 (3 having the most stain present). The scores were averaged, and phage having the highest stain present in both saponin treatments were further considered.

Peptide Synthesis and Adsorption

The two identified preferential hBMSB binding sequences (Figure 3.1) were combined with the previously identified apatite-based material binding sequence VTKHLNQISQSY [VTK] to build the dual-functioning peptides **GGLLADTTHHRPWTGGGS**VTKHLNQISQSY [L-VTK, MW = 3218.0 g/mol] and **GGDPIYALSWSGMAGGGS**VTKHLNQISQSY [D-VTK, MW = 3081.2 g/mol] (Table 3.2) (refer to Chapter Two) (bold – cell adhesive sequence, underline – apatite-based

material adhesive sequence). The idea of the dual-functioning peptide stems from the apatite-based binding sequence being able to anchor the peptide to BLM, while the cell binding sequence accessible to the hBMSCs to increase cell adhesion. Two peptides with RGD sequences, one with a glutamic acid tail (EEEEEEEEPRGDT [E, MW = 1447.6 g/mol]) and the other with the V peptide (GGRGDGGGSVTKHLNQISQSY [RGDV, MW = 2117.6 g/mol]) were also fabricated to use as positive controls. A peptide with RGE and V (GGRGEGGGSVTKHLNQISQSY [RGEV, MW = 2131.6 g/mol]) was built as a negative control against cell-attachment. The peptide sequences were fabricated on a Rainin Symphony synthesizer and determined as >86% pure via high performance liquid chromatography (HPLC) (UM Protein Core). Amino acid analysis was performed to verify initial peptide concentration read at A205nm with UV spectrophotometry (UM Protein Core). Standard curves for all peptides were also generated using UV spectrophotometry (BioRad Smartspec 3000) at 205nm and 274nm (except EEEEEEEPRGDT for 274nm). Each peptide was reconstituted in ddH₂O and diluted to ~500µg/mL in 50mM Trizma buffer (Sigma, pH=7.5). In 24-well tissue culture dishes, blank tissue culture polystyrene (TCPS) wells, BLM films, HA disks and CA5 disks were soaked in Trizma buffer overnight at 4°C (n=5). Prior to introducing 1mL of the peptide or buffer solutions for negative controls, plates were allowed to come to room temperature, and then the overnight solution was removed. The plates were agitated on a Titer Plate Shaker at ~80rpm for 3 hours at room temperature. The films and disks were rinsed with 1X with Trizma and then soaked in a 10mM HCl solution for 18 hours at room temperature on the same shaker. Aliquots of the HCl solution were read on a UV spectrophotometer at 205nm and 274nm wavelengths.

Cell Attachment Assay

hBMSC cell attachment was tested with and without peptides on BLM and TCPS substrates. Both BLM films (n=6) and TCPS wells (n=6) were soaked in Trizma buffer overnight at 4°C in a humidified container, prior to peptide adsorption. The same method of peptide adsorption was followed as previously stated. After the peptides were allowed to adsorb for 3 hours, the peptide solution was removed and the films and wells were

rinsed 1X with Trizma buffer solution (#T7818). The control samples, devoid of peptide, received a 3 hour soak in Trizma buffer solution, and were then treated the same as the peptide groups. All films and wells were blocked with denatured BSA (dBSA) (1% BSA in PBS heated to 80°C for 6 minutes) for 1 hour, followed by 1X rinse with PBS. A concentration of 5×10^4 hBMSCs (Passages 5-8) suspended in α -MEM without supplements were seeded in all wells and allowed to attach for 1 hour at 37°C in 5% CO₂. A cell standard curve prepared in 500 μ L of α -MEM without supplements was plated in a separate 24-well dish and incubated at 37°C in 5% CO₂ at the same time cells were introduced to the films and wells. After the 1 hour cell attachment, the α -MEM without supplements was removed and the plates were centrifuged upside-down at 300rpm for 5 minutes (Eppendorf 5810R). The films and wells were rinsed 1X with PBS, 500 μ L of α -MEM without supplements was added to each well, and 50 μ L of WST-1 reagent (CloneTech #630118) was added to each well. 50 μ L of WST-1 was also added to each well in the cell standard curve. All plates were incubated at 37°C in 5% CO₂ for 3 hours. After 3 hours, the plates were shaken for 1 minute, and a 100 μ L aliquot was removed from each well, transferred to a 96-well plate, and read on a UV Microplate reader at 420nm wavelength (Genios Tecan). The WST-1 assay detects live cells only. Background values from films and wells without peptide were subtracted out for each run prior to normalization. Percent cell adhesion was calculated by dividing the number of cells adhered by the number of initial cells seeded. Initial cell seeding numbers were determined from an average of n=4 individually plated wells. For BLM samples with peptide present, the percent cell adhesion was then normalized to the amount of peptide adsorbed to the mineral film. All substrates were run with n=6, and each experiment was performed in duplicate.

Statistics

Statistical analysis was performed using SPSS (16.0). Data are reported as mean \pm one standard deviation. To determine differences in peptide adsorption to a given substrate, a one-way analysis of variance (ANOVA) was run with the Dunnetts T3 post-

hoc multiple comparisons test. Significance was determined by if the p -value < 0.05 . To detect differences in cell attachment normalized to nmol of peptide adsorbed on BLM for each peptide tested, an Independent Samples t-test was run with significance determined by a p -value < 0.05 .

Results

Identification of Preferential Cell Adhesion Sequences to hBMSCs via Phage Display

Three rounds of phage panning on duplicate samples of hBMSC populations yielded a total of 50 sequences that were DNA sequenced and analyzed using the RELIC software. One sequence, LLADTTHHRPWT, was identified in both replicates of the phage experiment on the hBMSC populations. From the 50 sequences identified, the MOTIF1 program identified continuous motif sequences 3 and 4 amino acids long as NHT, and (S/T)(I/V)LS, respectively (Figure 3.2). Peptides DPIYALSWGMA and LLADTTHHRPWT are included to show sequence homology with the 4- and 3-mer motifs identified. The motif NHT or equivalent was present in 6% of the total peptides identified, whereas (S/T)(I/V)LS was present in 12%. The streptavidin control run yielded the consensus HPQ sequence, signaling successful panning.

The INFO analysis revealed a shift towards higher information content in the phage identified as binders to hBMSCs compared to the NEB background (Figure 3.3). Higher information content describes a peptide sequence less likely to occur by chance. For the analyzed set of 50 peptides, a peptide sequence was deemed a higher information clone if the information measure was calculated as greater than 33.5, where 27 of 50 peptides identified were labeled as high information clones. The shift towards higher information content shows the successive rounds of panning isolated a unique pool of phage bound to the hBMSCs; however, the results from both the MOTIF1 and INFO show that one unique sequence was not identified. Rather, multiple sequences with high information and shared motifs were identified. A subset of 20 sequences, 10 higher information clones and 10 lower information clones, were analyzed using immunohistochemistry techniques.

The peptide sequence, DPIYALSWGMA, had the highest combined score, where the combined IHC score (Table 3.1) was taken as the addition of scores with saponin and without saponin. Both the groups with and without saponin for each phage sequence tested was an average of three independent scores on $n=2$. On average, the higher information clones showed evidence of more staining, and hence, more phage binding to the hBMSCs. The higher information clones had an average combined score of 3.50 ± 1.01 , whereas the lower information clones had an average combined score of 2.23 ± 1.20 . Peptides 11 and 13 could not be scored for samples without saponin and were not taken into account when calculating the averages. The sequence, LLADTTHRPWT that occurred in both wells of hBMSCs also showed positive scoring. When the frequency data, the RELIC INFO analysis, and IHC are taken collectively, the two sequences that showed the most promise as preferential binding sequences to the hBMSCs were DPIYALSWGMA [D] and LLADTTHRPWT [L]. Peptides D and L show positive binding to hBMSCs with and without saponin (Figure 3.4). Confocal image stacks acquired after excitation at wavelength 568nm to view cell location are also shown.

Adsorption of Dual-Functioning Peptides on Apatite Materials

On BLM, D-VTK showed superior binding compared to all other peptides with the VTK apatite-binding anchor (Figure 3.5) (For BLM D-VTK vs: L-VTK $p=0.019$, RGDV $p=0.016$, RGEV $p=0.019$; For HA D-VTK vs: L-VTK $p=0.031$, RGEV $p=0.003$; For CA5 D-VTK vs: L-VTK $p=0.003$, RGEV $p<0.001$). The peptide E, also displayed high binding, although not significant, to BLM compared with L-VTK, RGDV, and RGEV, despite having a large standard deviation. This adsorption and standard deviation is consistent with previously reported values for E (Refer to Chapter Two). The adsorption of VTK peptide alone (previously reported average adsorption of VTK in nmol on BLM, HA, CA5, and TCPS were 2.72 ± 0.57 , 2.60 ± 1.01 , 2.61 ± 0.87 , and 0.08 ± 0.13 , respectively) was consistently higher than the dual-functioning peptides for each substrate tested. Adsorption of the dual-functioning peptides was minimal, or at the

limits of the peptide detection method, for TCPS. This data reinforces the substrate selectivity of the VTK portion of the dual-functioning peptides.

Dual-Functioning Peptide Influences hBMSC Adhesion to Bone-Like Mineral

Peptides L-VTK and D-VTK showed increased cell adhesion on BLM compared to RGDV, RGEV, and E (Figure 3.6). The nature of the cell adhesion assay limits the number of peptides analyzed in one experiment; thus, a no peptide control was run in parallel for each experiment (white bars in Figures 3.6a,b). On TCPS, L-VTK and RGEV had a positive influence on cell attachment compared to D-VTK, RGDV, and E. For both substrates, peptide E consistently showed low adhesion values, signaling that no more hBMSCs attached compared to the appropriate control when this peptide was adsorbed. Because the initial amount of peptide adsorbed to the BLM is not easily controlled via chemical alteration of the ceramic substrate, adhesion data were normalized to the amount of peptide adsorbed on each material. This normalization was only calculated for BLM (Figure 3.7), as some of the peptide adsorption values for TCPS were at the detection limits of the technique, which could produce erroneous values. Peptide L-VTK increased the ability of the hBMSCs to attach the most out of all the peptides tested. Surprisingly, RGEV also showed the ability to positively influence hBMSC adhesion to BLM. (L-VTK vs. D-VTK $p=0.046$, For E vs: L-VTK $p=0.006$, D-VTK $p<0.001$, RGDV $p=0.029$, RGEV $p=0.026$)

Discussion

Peptide sequences with an inherent preference to adsorb to the surface of apatite were identified within a peptide combinatorial library via phage display (refer to Chapter Two). The identified peptide sequences are not useful biologically unless they promote desired cell functions, such as adhesion or proliferation. In the present work, the phage display technique was also able to isolate peptides that preferentially bind to a clonally derived hBMSC population (Figure 3.4), which when combined with the apatite-binding peptide sequence, improved hBMSC attachment to bone-like mineral, particularly for L-VTK (Figure 3.7). The efficacy of the presented peptides is not limited to bone tissue

engineering applications, as this work illustrates that dual-functioning peptides can be designed, in general, to link inorganic substrates to organic sources.

The efficacy of the ubiquitous cell adhesive sequence Arg-Lys-Asp (RGD), whether ionically or covalently bound to a plastic, metal, or ceramic, on cell adhesion has been studied extensively (Bearinger et al., 1998; Benoit and Anseth, 2005; Cavalcanti-Adam et al., 2002; Ferris et al., 1999; Hennessy et al., 2008; Houseman and Mrksich, 2001; Hu et al., 2003; Itoh et al., 2002; Koo et al., 2002; Maheshwari et al., 2000; Mardilovich and Kokkoli, 2004; Massia and Hubbell, 1990; Niu et al., 2005; Okamoto et al., 1998; Rapuano et al., 2004; Sawyer et al., 2005a; Sawyer et al., 2005b; Shin et al., 2002; Shin et al., 2004a; Tosatti et al., 2004; VandeVondele et al., 2003). While RGD can promote cell adhesion and proliferation when used in appropriate concentrations, recent experiments have reported that coating RGD on the surface of implanted hydroxyapatite may have negative implications, such as the lack of osseointegration, on bone-implant integration (Hennessy et al., 2008). Additionally, passive adsorption of RGD on HA substrates decreased mesenchymal cell adhesion compared to HA substrates having the RGD sequence with a polyglutamate motif attached. Linking the cell-binding peptides tested to the apatite-binding peptide VTK allows the VTK peptide to anchor the cell-binding peptide to the apatite surface, so passive adsorption of the cell-binding peptide is avoided.

The dual-functioning peptides designed in this study showed a positive effect on the ability to adhere hBMSCs on BLM compared to the E peptide having a glutamic-acid tail for apatite adhesion and RGD for cell adhesion (Figure 3.7). In fact, the E peptide had the highest mean adsorption on BLM (Figure 3.5), but did not improve cell attachment. The D-VTK peptide had adsorption values on the same order as the E peptide, but was able to positively influence cell attachment, suggesting that the composition of the D-VTK peptide promoted hBMSC attachment. The E peptide data contradicts previous reports that state E₇PRGDT has the ability to increase cell adhesion of murine KUSA/A1 osteoblast cells (Itoh et al., 2002) and human mesenchymal stem cells (Sawyer et al., 2005b) on HA, although both studies performed their experiments on

sintered hydroxyapatite samples. Neither study quantified the amount of peptide on the surface of their HA samples, and both studies used serial washing as a method of cell detachment, making it difficult to compare the results to those reported in this study. Cell adhesion methods using centrifugation eliminate any questions of reproducibility and sensitivity than washing methods (Garcia and Gallant, 2003; Reyes and Garcia, 2003a). Also, slight changes in substrate morphology can influence peptide adhesion at similar initial adsorption concentrations (refer to Chapter Two). While adhesive proteins may contain acidic and RGD amino acid sequences, isolating these portions of proteins as peptides may not be beneficial on all substrates and/or cell sources. Alternatively, acidic peptides may have lower ionic binding strength to the BLM than the other peptides tested, creating a weaker acidic peptide-BLM bond that could be broken more easily during the centrifugation step in the cell attachment assay. This suggests that the D-VTK and L-VTK peptides favorably interact with the BLM surface compared with E, again indicating that the phage derived sequences identified prove advantageous in promoting cell attachment on BLM.

Surprisingly, no difference in cell adhesion to the BLM was seen between the positive control, RGDV, or the negative control, RGEV (Figure 3.7). The attachment of the VTK peptide could have interfered with the binding or presentation of RGD and RGE to the cells. If this were the case, the cell attachment that did occur could have resulted, because the VTK sequence contains a peptide sequence that influences cell attachment to the BLM. VTK alone would have to be investigated to rule out the influence this apatite-seeking sequence. Likewise, the hBMSC population studied may not be influenced by the RGD or RGE sequences as much as other cell sources, decreasing the response of the hBMSCs to RGD or RGE. The unresponsiveness of hBMSCs to RGD was shown in a previous study that showed immobilized linear and cyclic RGD containing peptides on hydroxyapatite displayed no effect of the peptide on initial adhesion of hBMSCs after 1 hour incubation (Durrieu et al., 2004).

Increased cell adhesion to TCPS coated with L-VTK and RGEV was seen (Figure 3.6b), despite negligible amounts of these peptides being adsorbed (Figure 3.5). The

inability to accurately quantify peptide at the nanogram level is a limitation of using the UV absorbance technique for peptide adsorption. Traces of these peptides could have been undetected on the TCPS, allowing small amounts to influence hBMSC attachment. Alternative explanations could be that the L-VTK and RGEV peptides alter the surface charge of the TCPS, yielding an altered surface for the hBMSCs to attach, or the VTK peptide is influencing cell attachment.

While the lack of controlled peptide adsorption was taken into account by normalizing cell adhesion to the amount of peptide adsorbed, we do not report saturation curves, as this would be an expensive experiment for the concentrations and materials used, and cannot conclusively say that peptide saturation was attained. However, increased fluorescence intensities with increased concentrations of FITC-labeled E₇RGD peptide on HA disks shows a strong intensity visible at 100µg/mL (Sawyer et al., 2005b). Since the initial peptide concentrations used in these studies were ~500µg/mL, we can only speculate that saturation was achieved.

Increased hBMSC attachment resulting from the presence of the dual-functioning peptide, L-VTK, on bone-like mineral demonstrates the feasibility of rational peptide design using phage display technology. The surface modification limitations for ceramic materials have impeded the development of functionalization methods that can control peptide concentrations present on the surface of apatite-based materials. This was addressed in the current study by normalizing the cell adhesion data with the adsorbed peptide amounts. Only recently have methods of silanization been used to covalently link peptides to apatite surfaces (Durrieu et al., 2004); however, it is not known if chemical alteration of the apatite surface will affect cell behavior.

Peptide design has focused on identifying portions of known bone extracellular matrix proteins (e.g. osteonectin (Fujisawa et al., 1996), bone sialoprotein (Fujisawa et al., 1997), statherin (Gilbert et al., 2000)) that are potential apatite binders via ionic binding, such as phosphorylated sites or long strings of acidic amino acids (Fujisawa et al., 1997; Itoh et al., 2002; Sarig, 2004; Sawyer et al., 2005b). In both cases, these peptide regions on proteins are thought to adhere to the apatite in bone due to their

negative charge in a biological environment, which is typically at neutral pH. It has been suggested both experimentally and computationally that this negative charge is attracted to the calcium ions on the surface of the apatite (Boanini et al., 2006; Fujisawa and Kuboki, 1991; Fujisawa and Kuboki, 1998; Fujisawa et al., 1997; Gilbert et al., 2000; Gilbert et al., 2003; Pan et al., 2007). The design scheme of using negatively charged peptides works if the apatite surface maintains a periodic surface charge with calcium ions available. Bone-like mineral precipitated from a 1X or 1Xmodified SBF solution possesses spherical rosette clusters with plate-like features at the nanometer scale (Luong et al., 2006; Murphy and Mooney, 2002; Murphy et al., 2000). The unique morphology of BLM could alter the charge distribution on its surface, limiting the benefits of acidic peptides. Peptide E displayed increased adsorption on BLM compared to the other peptides tested, but also had the largest standard deviation making the adsorption of this acidic peptide to BLM less predictable. The HA plates in BLM coatings are positioned close to one another, so that even if the correct surface charge periodicity is present on one plate, the overall charge periodicity on a cluster of plates may provide an unattractive surface for long strings of negatively charged peptides. Further, identifying non-acidic peptide sequences that preferentially bind to apatite materials may provide an advantage in that they may not bind to free calcium sites on the surface of the material, allowing serum proteins, when present, to concurrently adsorb and promote other cell functions. It has been suggested that HA is more osteoconductive than other materials because of its ability to adsorb increased amounts of adhesive proteins when introduced to serum (Kilpadi et al., 2001).

Two hBMSC binding peptides, DPIYALSWGMA and LLADTTHHRPWT, were identified via phage display and linked to a previously identified apatite-binding peptide VTK. The combined peptide D-VTK showed superior ability to adsorb onto the three apatite-based materials tested when compared to the other peptides possessing the VTK anchor. Both D-VTK and L-VTK were able to increase the attachment of hBMSCs on BLM compared to E. When cell attachment was normalized to peptide adsorbed, L-VTK proved most influential on hBMSC attachment to BLM.

The phage display technique utilized in Chapters Two and Three to isolate preferential binding sequences to apatite-based materials and a clonally derived hBMSC population, respectively, illustrates the wide-range of advantageous information that can be harnessed using phage display. A peptide combining the sequences identified, L-VTK, increased hBMSC attachment to BLM, validating the new proposed design approach. This technique can potentially be used to isolate populations of cells, a concept that would provide great control over bone engineered scaffolds. Additionally, multiple permutations can be investigated to apply this design rationale not only to bone engineering, but also to cartilage, ligament, tendon, and soft tissue research.

Acknowledgements

I would like to acknowledge my co-authors on this work, David H. Kohn and Hayes C. Smith. Sources of funding for this work came from the National Institute of Health and the Department of Energy: NIH R01 DE 015411 and DE07057. I would also like to thank Dr. Kristy Warner, Dr. Ben Zeitlin, and Janani Ramaswamy for their advice and support during this work. Thanks to Sergei Kuznetsov for generously providing the clonally derived human bone marrow stromal cells, and to Dr. Mary Tecklenberg for the carbonate apatite powder.

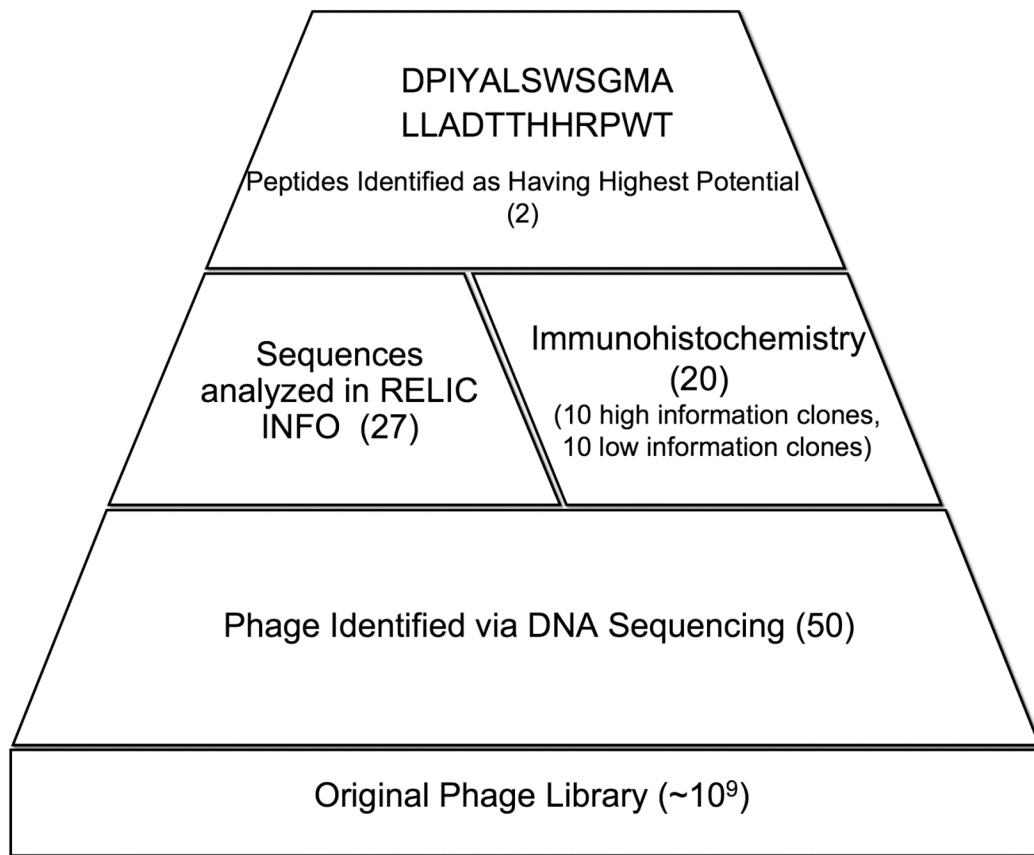


Figure 3.1: Schematic displaying data analysis progression used to identify peptides that preferentially adhere to clonally derived hBMSCs.

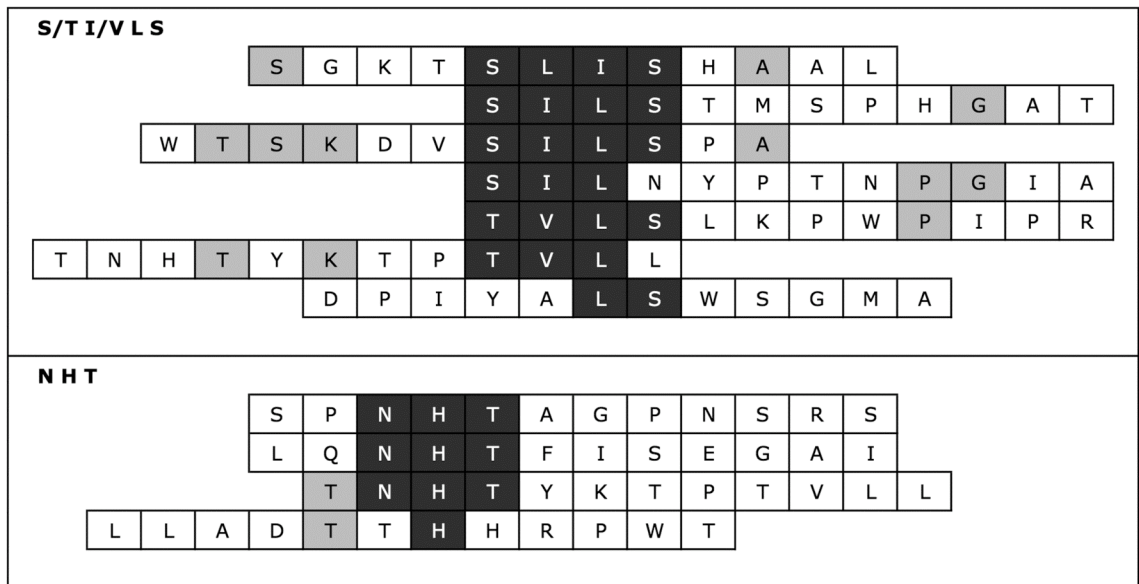


Figure 3.2: Consensus sequences from the MOTIF1 program showing (S/T)(I/V)LS and NHT as the 4- and 3-mer motifs having the most frequent hits. The RELIC program MOTIF1 was run with 50 peptide sequences identified from three rounds of phage display panning on clonally derived hBMSCs. Peptides DPIYALSWSGMA and LLADTTHHRPWT are included to show sequence homology with the 4- and 3-mer motifs identified via MOTIF1.

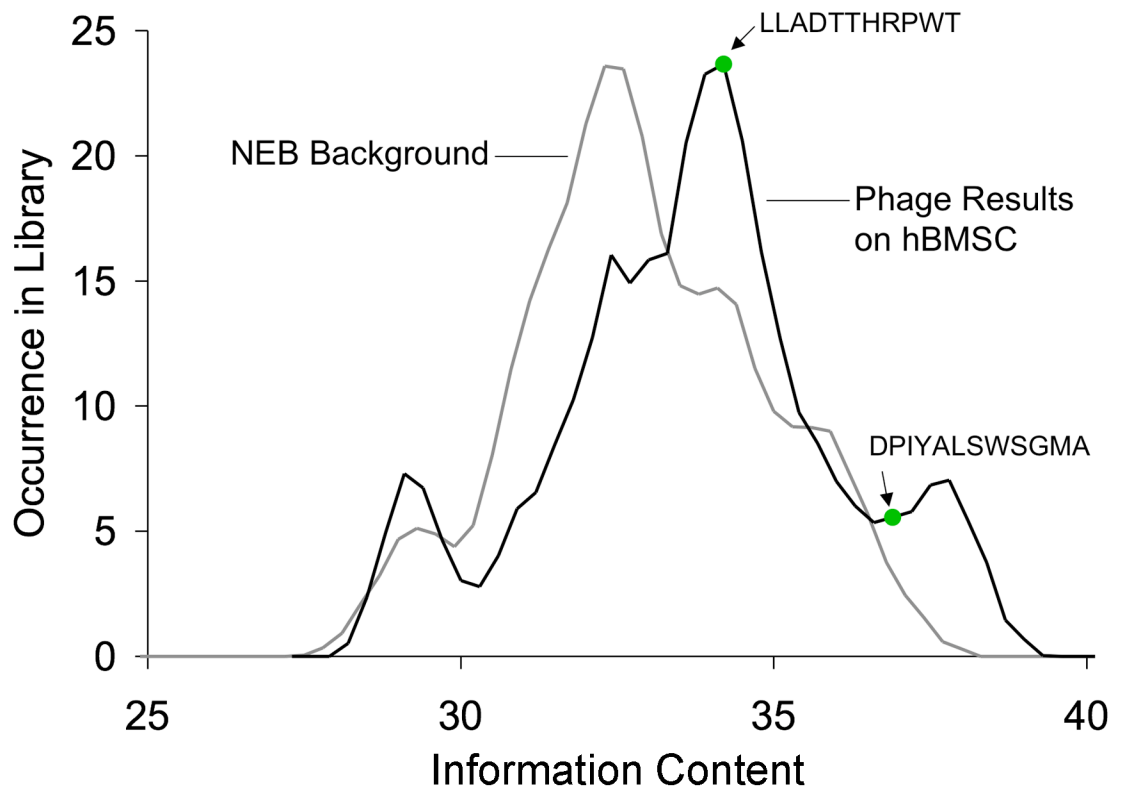


Figure 3.3: INFO content values calculated in RELIC for NEB background and phage subset identified as preferential binders to clonally derived hBMSCs. High information content correlates to a lower incidence of being selected by chance. The phage subset shows a shift towards a higher information content signifying this subset was selected based on the binding affinity to hBMSCs. The INFO values of the two phage sequences, LLADTTHRPWT and DPIYALSWGMA, used in the final dual-functioning peptide design are labeled on the graph.

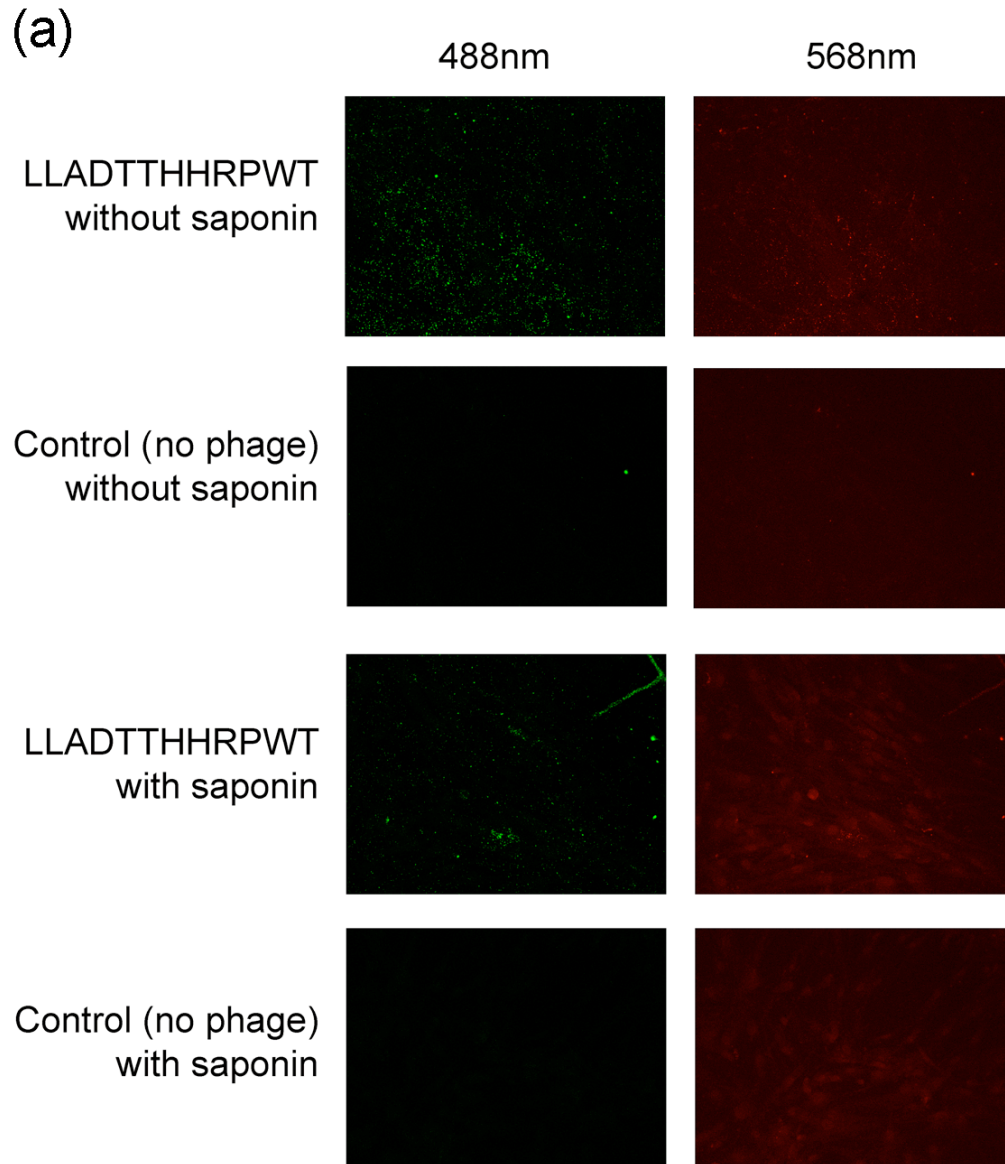


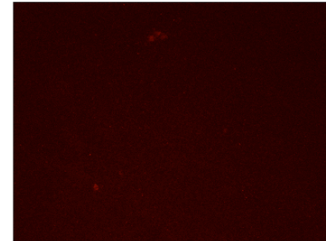
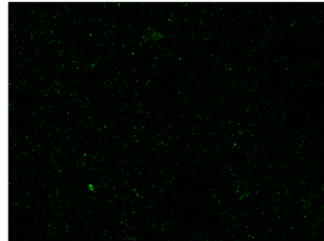
Figure 3.4: Representative confocal images from the immunohistochemistry with the phage containing the sequences LLADTTHHRPWT (a) and DPIYALSWGMA (b) showing positive FITC signal at 488nm for the hBMSC introduced to the phage. Images are compressed z-stacks taken for 20 μ m at 2 μ m intervals. Compiled images taken with the red laser at 568nm show the location of the cells on the slides for the hBMSCs treated with saponin. Note phage binding is located only in regions where cells are present. Sequence DPIYALSWGMA had the highest overall score from all of the phage analyzed by immunohistochemistry.

(b)

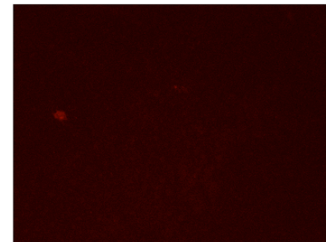
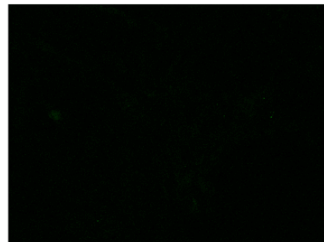
488nm

568nm

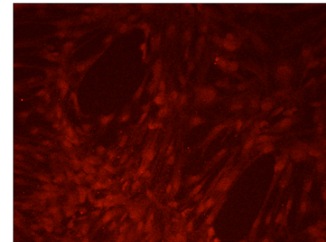
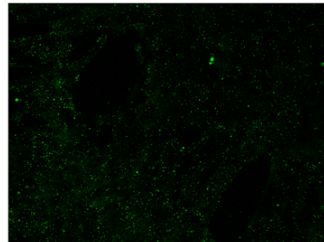
DPIYALSWGMA
without saponin



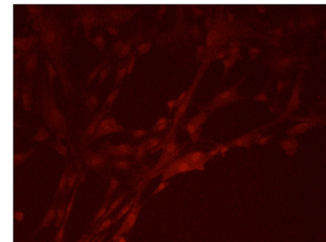
Control (no phage)
without saponin



DPIYALSWGMA
with saponin



Control (no phage)
with saponin



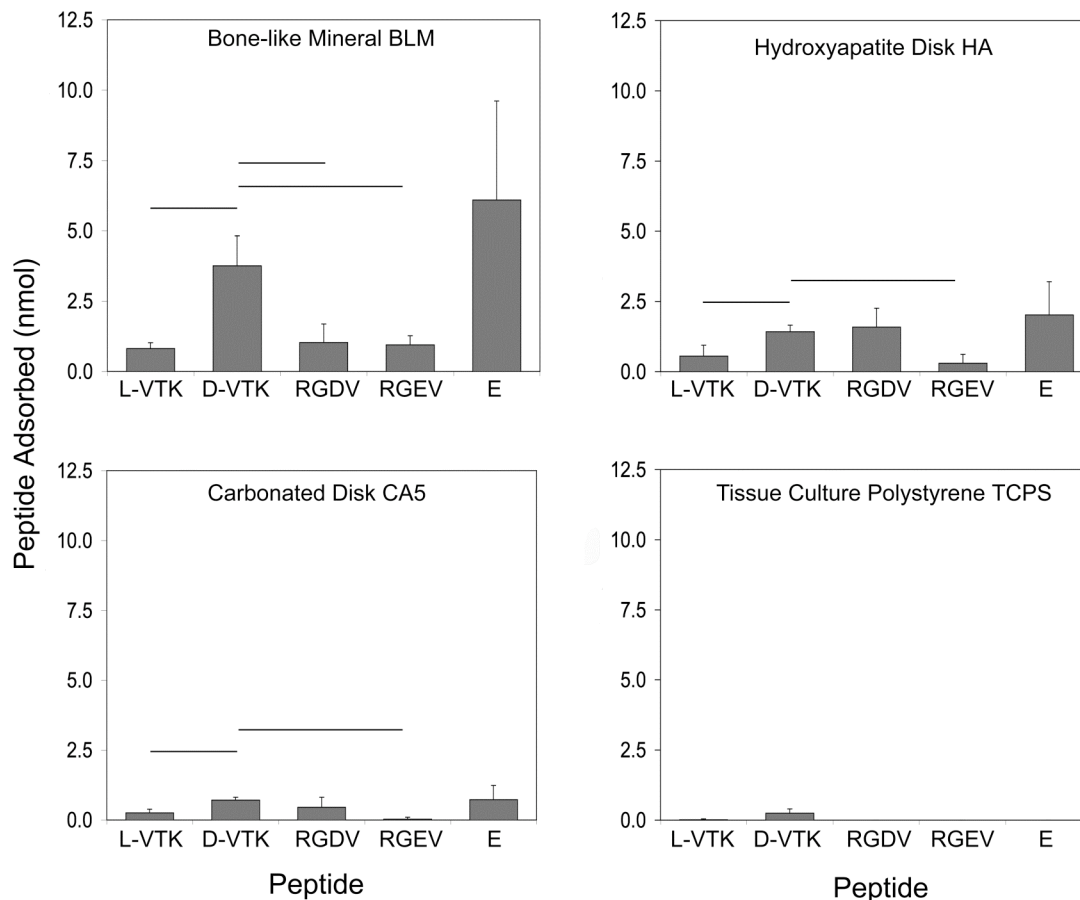


Figure 3.5: Adsorption of five dual-functioning peptides (L-VTK, D-VTK, RGDV, RGEV, and E) on four substrates (BLM, HA, CA5, and TCPS). Adsorption of phage display derived peptide D-VTK was significantly higher than L-VTK, RGEV, and RGDV on BLM and L-VTK and RGEV on HA and CA5 ((For BLM D-VTK vs: L-VTK $p=0.019$, RGDV $p=0.016$, RGEV $p=0.019$; For HA D-VTK vs: L-VTK $p=0.031$, RGEV $p=0.003$; For CA5 D-VTK vs: L-VTK $p=0.003$, RGEV $p<0.001$)). Adsorption of all peptides was higher on the apatite-based materials displaying the specificity of the peptides to apatite versus TCPS. Horizontal bars represent statistical differences.

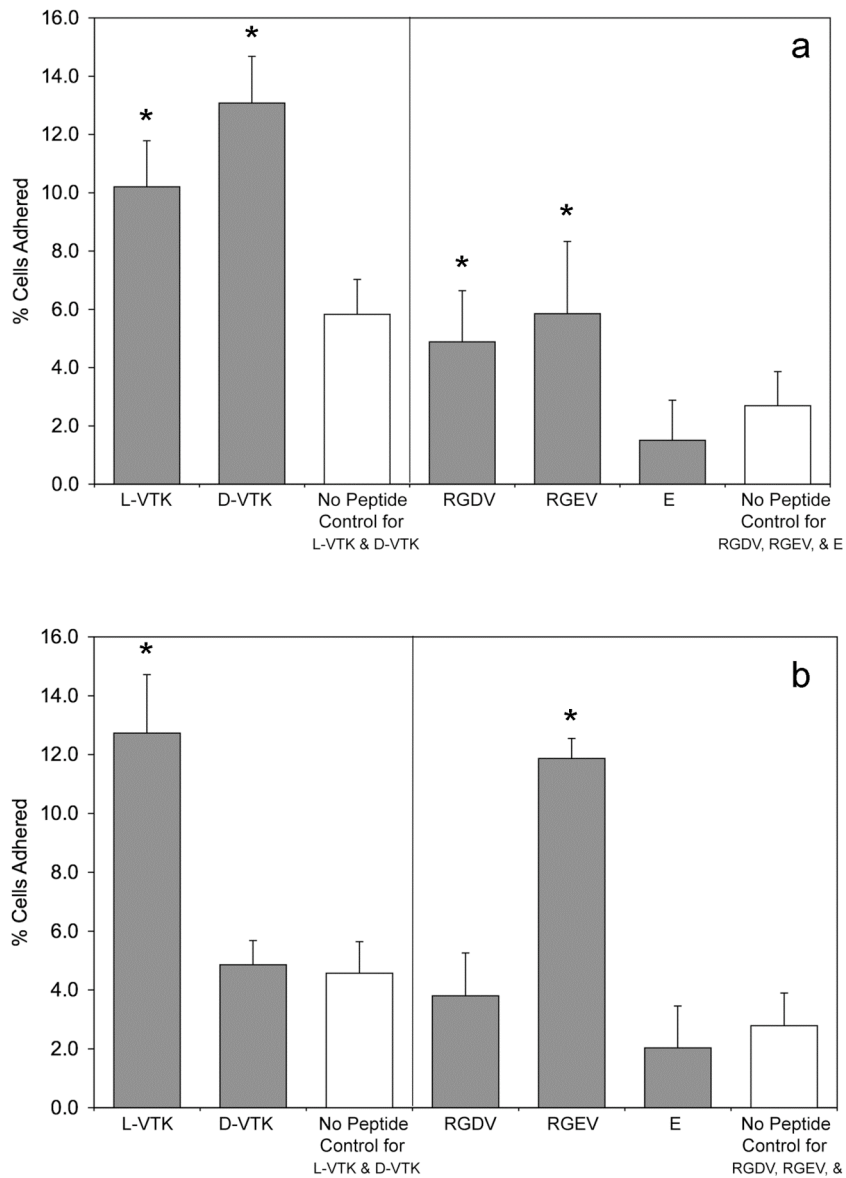


Figure 3.6: (a) hBMSC adhesion on BLM for all five peptides tested. L-VTK and D-VTK had a positive influence on cell attachment compared to BLM devoid of peptide. RGDV, RGEV, and E had low levels of cell attachment compared to the BLM control. (b) hBMSC adhesion on TCPS for all five peptides tested. L-VTK and RGEV were the only peptides that showed increased cell attachment compared to the TCPS devoid of peptide. All experiments were performed in duplicate, with each experiment having n=6. * - Statistical difference vs. appropriate control, $p < 0.05$.

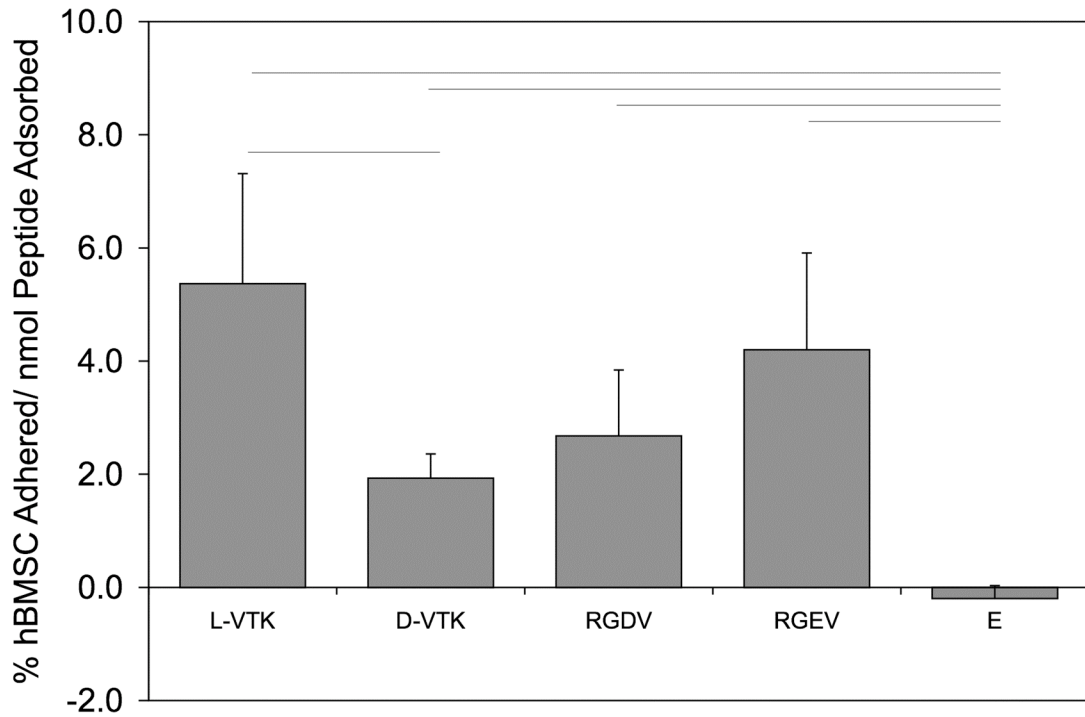


Figure 3.7: Cell adhesion normalized to amount of peptide adsorbed on BLM. Appropriate background adhesion to BLM devoid of peptide was subtracted prior to normalization. L-VTK was statistically more effective at improving cell attachment than D-VTK and E. L-VTK also displayed a greater mean compared with RGDV or RGEV (L-VTK vs. D-VTK $p=0.046$, For E vs: L-VTK $p=0.006$, D-VTK $p<0.001$, RGDV $p=0.029$, RGEV $p=0.026$). Peptide E showed no effect on cell adhesion. Horizontal bars indicate statistical differences.

Table 3.1 Immunohistochemistry Scoring for hBMSC with Phage Treated with and without Saponin

Phage with Peptide Sequence Tested	Information Level	Average Score Without Saponin	Average Score With Saponin	Combined Score
YPLRPNAESLRF	high	1.00	1.50	2.50
DPIYALSWGMA*	high	2.17	2.83	<u>5.00</u>
NATHLTADHVNK	high	1.67	2.00	3.67
YPSAPPQWLTNT	high	1.50	1.67	3.17
AQHRSWDGFSH	high	0.00	1.50	1.50
LPLYTSPDKPGK	high	1.67	2.00	3.67
SILNYPTNPGIA	high	2.33	2.17	4.50
LLADTTHHRPWT	high	2.00	1.50	3.50
HPIRVQPDWGFL	high	1.83	1.33	3.17
VETHTTQWLITEV	high	1.83	2.50	4.33
TPMGRPHPETPA	low	**	1.33	1.33
SGKTSLISHAAL	low	0.00	0.17	0.17
NHLPLPPPAATM	low	**	1.17	1.17
SDTQMPPAXGRA	low	0.33	2.17	2.50
GYLPLHSITYRP	low	1.83	1.50	3.33
QLLEPVNLSTGP	low	1.83	1.33	3.17
WHPPKGLSPLPD	low	0.67	1.33	2.00
FRLPGSLINHPQ	low	1.33	2.17	3.50
SILSTMSPHGAT	low	0.00	0.83	0.83
NYNPHNPFPPAP	low	1.67	0.67	2.33

* Peptide sequence chosen as best preferential binder to hBMSC

** Cells washed away during rinsing and could not be scored

Table 3.2 Dual-functioning Peptide Sequences Containing Both an Apatite Seeking Portion (underlined) and a Cell Adhesive or Control Sequence (bold)

Peptide Sequence	Code
GGLLADTTHHRPWTGGGS <u>VTKHLNQISQSY</u>	L-VTK
GGDPIYALSWSGMAGGGS <u>VTKHLNQISQSY</u>	D-VTK
GGRGDGGGS <u>VTKHLNQISQSY</u>	RGDV
GGRGEGGGS <u>VTKHLNQISQSY</u>	RGEV
<u>EEEEEEE</u> PRGDT	E

CHAPTER FOUR

UNIFORM DEPOSITION OF PROTEIN INCORPORATED MINERAL LAYER ON THREE-DIMENSIONAL POROUS POLYMER SCAFFOLDS

Introduction

The restoration and repair of orofacial and long-bone defects resulting from disease, trauma, or genetic inheritance is still a major clinical challenge (Feinberg et al., 2005; Muschler and Midura, 2002; Parikh, 2002; Wiesmann et al., 2004). Autogenous bone grafting is a current method used in repairing skeletal defects. However, limitations including donor site morbidity, graft rejection, and inadequate bone formation or quality often result (Parikh, 2002; Yaszemski et al., 1996). Current approaches in bone tissue engineering strive to overcome these limitations and induce bone formation using a combination of an extracellular matrix analogue, cells, and/or biological signals (Garcia and Reyes, 2005; Hubbell, 1999; Maskarinec and Tirrell, 2005; Shin et al., 2003).

Three approaches are used in tissue engineering: conduction, induction, and cell transplantation (Alsberg et al., 2001; Hirano and Mooney, 2004). Initial research has focused on a conductive approach that aims to recruit host cells towards an implanted material and initiate bone ingrowth or regeneration. Research using inductive approaches of incorporating cell-recruiting or cell-directing molecules in or on the implant has increased to improve the rate, amount, and quality of bone being regenerated (Chen and Mooney, 2003). In parallel, control of the location and direction of bone growth via transplantation of bone cell lines, genetically manipulated cells, or stem cells on these constructs has been explored (Rose and Oreffo, 2002). Cells are typically seeded on highly porous (> 90%) scaffolds fabricated from biodegradable materials. To control cell responses, such as adhesion, the material can be modified via surface alterations or coatings.

Specific to bone scaffolding, strategies to increase the quantity and quality of regenerated bone include using organic/inorganic hybrid materials that promote bone healing and remodeling. For example, the technique of biomimetically precipitating a bone-like mineral layer onto porous polymer scaffolding provides cells a calcium phosphate material surface that is chemically similar to the composition of natural bone. This technique of biomimetically precipitating apatite onto the surface of a biomaterial was first researched on silica rich Bioglass® (Ogino et al., 1980) and was subsequently introduced on titanium hip implants to enhance implant-bone osseointegration (Abe et al., 1990). Biomimetic deposition of bone-like mineral occurs at biological temperatures, making it an attractive alternative to high temperature processing methods such as plasma spray and sputtering techniques (Habibovic et al., 2002; de Groot et al., 1998). The biomimetic technique in bone tissue engineering has evolved into mineralizing biodegradable polymeric scaffolds with the intent of tailoring calcium-phosphate ratios to evoke particular cell behavior while also increasing scaffold mechanical integrity (Murphy et al., 2000). The presence of bone-like mineral is hypothesized to recruit host cells as well as to have the ability to control the differentiation of transplanted cells towards a bone phenotype (Luong et al., 2006).

Surface pre-treatments that create negatively charged surface groups to accelerate mineral nucleation benefit both 2D and 3D materials. While growth of bone-like mineral on polylactic-co-glycolic acid (PLGA) is attainable when a pre-mineralization hydrolysis (Murphy and Mooney, 2002) or aminolysis (Croll et al., 2004) treatment is used, the apatite precipitated on 3D PLGA scaffolds is often discontinuous and can take up to 16 days to form (Murphy et al., 2000; Zhang and Ma, 2004). The lack of mineral continuity in 3D exists for both materials that do and do not receive surface pre-treatments, supporting the need for innovations to improve current processing techniques. The design goals of using second generation biomimetically mineralized materials therefore, aim to reduce the time of apatite formation and to uniformly mineralize the interstices of 3D scaffolding, while controlling calcium phosphate ratios (Oliveira et al., 2003). To clarify terminology used, a dense substrate amenable to mineralization, such as a polymer

or titanium surface is considered a 2D surface; however, when the substrate becomes porous and mineralization can occur through its thickness, the result is a 3D structure or scaffold.

In addition to a bone-like mineral layer providing a more conductive surface, the incorporation of inductive agents such as proteins or growth factors into the mineral can expose cells to spatiotemporally controlled biomolecular cues that can further promote and direct osteogenesis. Methods of incorporating proteins include covalent attachment, adsorption, and entrapment and are less than ideal for sustained release. A promising alternative to these methods is the coprecipitation of proteins and bone-like mineral. Depositing a protein-mineral layer on a porous scaffold provides a system that can deliver protein while allowing tissue ingrowth in 3D. Another advantage to coprecipitation is the ability to deposit bone-like mineral and proteins at physiological temperatures, minimizing potential processing parameters that could alter the biological activity of the incorporated biomolecules (Liu et al., 2005; Wen et al., 1997; Wen et al., 1999). A third advantage to coprecipitation is the ability to incorporate different biomolecules at different stages of mineral deposition, which provides a means of controlling release kinetics (Azevedo et al., 2005; Luong et al., 2006). Coprecipitation also leads to more sustained biomolecule release compared to adsorption, increases potential loading capacity, and is able to be used in conjunction with adsorption to further control biomolecular release (Liu et al., 2001; Luong et al., 2006). While coprecipitation is an effective means of incorporating biomolecules in bone-like mineral on dense, permanent implants, to be effective in tissue regeneration there is a need to rapidly and uniformly coat pores through the thickness of 3D scaffolding.

To study the effects of surface mineralization and biomolecular incorporation on bone growth in three dimensions, a scaffold uniformly and continuously coated with bone-like mineral or bone-like mineral with protein is necessary. Therefore, a filtration system was designed to induce flow of simulated body fluid (SBF), an ionic solution with similar ion concentrations as body serum, through the pores of polymer scaffolding to achieve mineralization throughout the thickness within 5 days. The goals of this study

were to demonstrate: 1) the filtration system is capable of coating the pores of a 3D scaffold with a uniform, continuous bone-like mineral layer and 2) a model biomolecule, BSA, is capable of being incorporated throughout the 3D mineral layer. The hypothesis that flow of simulated body fluid through porous scaffolding will initiate mineralization within the pores of 3D scaffolds and induce the formation of a uniform mineral layer in 3D is tested. Furthermore, the capability of precipitating a continuous mineral-protein layer in 3D is also investigated. A combination of micro-computed tomography (MicroCT), x-ray diffraction (XRD), protein quantification, and confocal microscopy is utilized to illustrate uniform, continuous mineralization and protein incorporation throughout the thickness of 3D scaffolds.

Materials and Methods

Scaffold Fabrication

The scaffolds were fabricated using a salt-leaching method. NaCl was sieved to 425-600 μm in diameter and packed into 10 mm diameter wells in a Delrin® (filtration group) or Teflon® (control groups) mold. A 5 wt% 85:15 polylactic-co-glycolic acid (iv = 0.73 dL/g, Alkermes)-chloroform solution was added to each well. The scaffolds were covered with aluminum foil and dried under a chemical fume hood for at least 36 hours. The mold was then placed in distilled water (dH_2O) to leach out the salt particles for at least 36 hours. The scaffolds were treated with 0.5 M NaOH for 7 minutes and rinsed with dH_2O . The final thickness of the scaffolds was approximately 2 mm.

Simulated Body Fluid Preparation

Chemicals for making SBF were purchased from Sigma-Aldrich unless otherwise noted. The chemicals and concentrations used to make 1x SBF include 141 mM NaCl, 4.0 mM KCl, 0.5 mM MgSO_4 , 1.0 mM MgCl_2 , 4.2 mM NaHCO_3 , 5.0 mM $\text{CaCl}_2 \cdot 2\text{H}_2\text{O}$, and 2.0 mM KH_2PO_4 (Kokubo, 1995). To prepare 2x SBF and 4x SBF, the concentrations were doubled and quadrupled, respectively. All SBF solutions were prepared at 25°C using dH_2O . The 2x SBF was titrated to pH 6.8, and the 4x SBF was

titrated to pH 6.4 using 1 M NaOH. These pH values were used to avoid homogenous precipitation. Both 2x SBF and 4x SBF were buffered with Tris-HCl. All SBF solutions were filtered using a 0.22 μm filter prior to use, and 0.005% sodium azide was added to prevent bacterial contamination.

Mineralization of Scaffolds in the Filtration System

The Delrin® mold with salt-leached scaffolds (n=4) was attached to the actuator of an Instron 8521 servo-hydraulic system and lowered into the aluminum base housing the SBF (Figure 4.1). The filtration system base is filled with SBF such that the scaffolds within the Delrin® mold are submerged with all surfaces being exposed to the SBF throughout the experiment. SBF solutions were warmed to 37°C prior to adding to the base. Initially, 1 L of 4x SBF (pH=6.4) was used for 12 hours, being replenished with fresh solution after 6 hours. Subsequently, 1 L of 2x SBF (pH=6.8) replaced the 4x SBF and was replenished every 12 hours. The SBF was changed to sustain the appropriate ion concentration levels in addition to maintaining the pH of 6.4 or 6.8, which is conducive to heterogeneous precipitation of bone like mineral onto the scaffolds. The pH values of new (fresh SBF) and used (SBF being replenished) SBF were measured using a pH meter (Mettler Toledo MP230). A fatigue regimen was programmed on the Instron 8521 to cycle the mold with the scaffolds at an amplitude of 25.4 mm at 0.011 Hz for 5 days. A temperature controller (Extech Instruments, Model 48VTR) maintained a solution temperature of 37°C \pm 1°C. Two static control groups, submerged control (n=4) and floating control (n=4), were subjected to the same SBF regimen (0.5 L SBF instead of 1 L) in a 37°C incubator for 5 days. The submerged group scaffolds were prepared in a Teflon® mold. The scaffolds in the floating static group were cast in a Teflon® mold, removed, and mineralized in 50 mL conical tubes containing 50 mL of SBF. The 5 day mineralization experiment was repeated twice for all of the groups.

BSA Coprecipitation

The Delrin® mold with salt-leached scaffolds (n=8) was attached to the Instron 8521 system and lowered into the aluminum base housing the SBF or SBF:FITC-BSA.

Fluoroisothiocyanate (FITC) conjugated BSA (Sigma-Aldrich, A9771) and BSA (Sigma-Aldrich, A3294) were used to prepare SBF:FITC-BSA solutions with a 1:5 ratio of FITC-BSA to BSA for a total protein concentration of 200 $\mu\text{g/mL}$. The SBF for these solutions was filtered using a 0.22 μm filter prior to the addition of FITC-BSA or BSA. Initially, 1 L of 4x SBF (pH = 6.4) was used for 12 hours, being replenished with fresh solution after 6 hours. Subsequently, 1 L of 2x SBF:FITC-BSA (pH = 6.8) replaced the 4x SBF and was replenished every 12 hours. The SBF:FITC-BSA was changed to sustain the appropriate ion concentration levels, to replenish the FITC-BSA supply, and to maintain a pH of 6.8. A fatigue regimen was programmed on the Instron 8521 to cycle the mold with the scaffolds at an amplitude of 25.4 mm at 0.011 Hz for a total of 3 days. The temperature controller maintained a solution temperature of $37^{\circ}\text{C} \pm 1^{\circ}\text{C}$. A submerged static group (n=8) was prepared in a Teflon[®] mold and subjected to the same SBF and SBF:FITC-BSA regimen in a 37°C incubator for 3 days. The floating control group was excluded from this experiment, because the MicroCT analysis for this group showed the least amount of mineral volume % in the previously described 5 day mineralization experiment. An equal volume of SBF was used for the control and experimental groups to maintain similar FITC-BSA concentrations. The coprecipitation experiment was repeated twice for both groups.

MicroCT Analysis of Mineralized Scaffolds

After 5 or 3 days of mineralization, all scaffolds were removed, rinsed in dH₂O, and dried under a chemical fume hood. Scaffolds were scanned (n=4 for 5 day mineralized scaffolds, n=8 for 3 day coprecipitated mineralized scaffolds) in a MicroCT system (EVS MS8X-130, 16 μm voxel size) to obtain mineral volume % (MV%) and 3D rendered images (MicroView[®], GE Systems). MicroCT scans were obtained at 75 mA and 75 mV for 400 frames using an aluminum filter. All reconstructed images were rendered in MicroView[®] using the Isosurface tool at a threshold of 1000 with the smoothing filter on, and at a surface quality factor of 0.55. A MV % profile for each group (filtration, submerged control, and floating control) was calculated using a volumetric shrinkage program written in MATLAB. This program calculates the

centroid of each scaffold from a user-defined region of interest volume in MicroView, and subsequently uses spline calculations to determine a 16.7% volume shrinkage from the original volume. Analysis of progressively smaller concentric volumes resulted in 6 different shells of equal volumes per scaffold. The term ‘innermost shell’ refers to the innermost volume, which is cylindrical in shape. The other five volumes calculated were concentric cylindrical shells. The mineral volume % was calculated for each shell to compare the mineral gradient within and between the scaffold groups.

X-ray Diffraction Analysis

XRD spectra were obtained using a Rigaku Miniflex X-ray Diffractometer with a fixed incidence of 4.2° . A range of $10-90^\circ$ was scanned using a step size of 0.1° and a scan rate of $1^\circ/\text{min}$. The top surface of all of the scaffolds was scanned, unless otherwise noted. The raw data of a representative sample were plotted for all groups to compare the different conditions, which included filtration 5 days (n=2), filtration 3 days (n=1), filtration 1 day (n=1), submerged control (5 days, n=2), and filtration control (5 days, n=2). The filtration samples retrieved after 1 day, 3 days, and 5 days were analyzed to evaluate time dependent changes in mineral. A blank PLGA scaffold was also scanned to detect background from the substrate material. To investigate if the mineral formed in the center of the filtration scaffolds was similar to the mineral formed on the surface, 5 day filtration scaffolds were transversely cut and analyzed (Filtration Center 5 Days, n=2). Hydroxyapatite (Sigma-Aldrich #289396) and 6wt% carbonated apatite (generous gift from Dr. Mike Morris, University of Michigan) were scanned as standards.

FTIR Analysis

Characteristic peaks for apatite were detected using a Fourier Transform Infrared Spectroscopy (Spectrum BX FT-IR, Perkin Elmer). A 300:1 ratio of KBr to deposited mineral was used to prepare a pellet and analyze the filtration, submerged control, and filtration control groups (n=2). Spectra were recorded from 400 to 4000 cm^{-1} and baseline corrected.

BSA Quantification

The amount of BSA coprecipitated onto the scaffolds (n=8) was detected using a UV spectrophotometer (SmartSpec 3000, BioRad). Each scaffold was demineralized in 10 mM HCl. An aliquot of the demineralization solution was measured at a wavelength of 494 nm to detect the FITC conjugated to the BSA. Concentrations of coprecipitated FITC-BSA were determined from a standard curve prepared with a 1:5 ratio of FITC-BSA to BSA. The calibration curve was constructed for the FITC-BSA:BSA solution using serial dilutions in 1x PBS. Protein densities were calculated using values for the amount of mineral precipitated from MicroCT analyses and the amount of BSA coprecipitated from the quantitative UV spectrophotometry.

Confocal Microscopy

A 1-2 mm thick center cross-section from protein incorporated scaffolds was cut to expose the 2 mm depth of the scaffolds (n=4). Each section, rectangular in shape (10 mm x 2 mm x 1-2 mm), was sandwiched between a glass slide and glued cover slip and viewed using confocal microscopy (Nikon TE 3000 Inverted Microscope) at an excitation wavelength of 488 nm. A BioRad Radiance 2000 LaserSharp program was used to image 750 μm into the 1-2 mm section at 3 μm intervals under 10x magnification. The series of images was compiled in the LaserSharp program to yield images showing FITC-BSA incorporation throughout the 750 μm . Multiple images were obtained across each sample and were mosaic-tiled together. The center cross-sections from scaffolds mineralized via filtration (5 day mineralization using the previously described 4x SBF/2x SBF regimen) without fluorescent-labeled protein were also investigated to characterize any mineral autofluorescence.

Statistics

The effect of filtration on MV% was determined using a One-Way Analysis of Variance (ANOVA) on Ranks with Student-Newman-Keuls post-hoc evaluation. Significant differences in MV% between the concentric volumes within each group were also determined using a One-Way Analysis of Variance (ANOVA) on Ranks. The

effects of filtration on MV% and on FITC-BSA incorporation for the BSA-scaffolds were determined using a Student's t-test. Significance was defined as $p < 0.05$, and all statistics were calculated using SigmaStat v3.1.

Results

Uniform, Continuous Mineral Precipitated Throughout the Depth of Filtered Scaffolds

Filtration of SBF through the scaffold pores significantly increased the mineral deposition compared to both the submerged and floating static control groups (Figures 4.2 and 4.3). The qualitative 3D MicroCT renderings for the filtration and submerged control groups show increased mineral within the filtration group (Figure 4.2). The cross-section images (Figure 4.2c-f) also confirmed that mineral was present throughout the thickness of the filtration scaffolds. The floating control group 3D renderings did not show any mineralization (images not shown). The MV% in the filtration scaffolds was significantly greater than both control groups (floating control $p=0.029$, submerged control $p=0.029$). There was also an even distribution of mineral throughout the filtration scaffolds compared with both control groups, which had $>60\%$ of the precipitated mineral in the two outermost shell volumes (Figure 4.4). If the average amount of mineral precipitated ($\sim 8\%$, Figure 4.3) on the filtration scaffolds is combined with the initial amount of PLGA present (5%), the scaffold porosity would decrease, on average, from 95% to approximately 87% for the filtration scaffolds.

The mineral deposited on the scaffolds showed characteristic FITR peaks for both hydroxyapatite (ν_{3c} P-O 1032 cm^{-1} , ν_1 P-O 962 cm^{-1} , ν_{4a} O-P-O 602 cm^{-1} , and ν_{4c} O-P-O 561 cm^{-1} [filtration group only]) and carbonated apatite (ν_1 $\text{CO}_3^{(2-)}$ 1465 cm^{-1} [filtration and floating control groups]) (Figure 4.5) (Koutsopoulos, 2002). XRD spectra for all of the groups also show apatite characteristic 2θ peaks between 25.9° - 26.8° , between 31.8° - 32.7° , at 40.1° , and between 45° - 55° (Figure 4.6) (Koutsopoulos, 2002). The XRD spectra further reveal that the peaks from the filtration scaffolds are consistent over the 5 days of mineralization, providing evidence that the mineral being precipitated on days 1 and 3 is similar to the mineral being precipitated on day 5. Last, XRD analysis confirms

that the type of mineral deposited was similar in all three experimental groups (filtration, submerged control, and floating control).

Uniform and Increased BSA Incorporation in Filtered Scaffolds

A ten-fold increase in protein incorporation (Figure 4.7) was established in the scaffolds mineralized using the filtration device. Confocal microscopy supported the increased protein incorporation within the filtration group, in addition to showing uniform precipitation throughout the thickness of the scaffolds (Figure 4.8). The confocal microscopy methods followed in these (Figure 4.8c) and other experiments revealed no interfering autofluorescence from the PLGA or the mineral (Luong et al., 2006). Similar to the 5 day filtration mineralized scaffolds, a greater amount of mineral was deposited on the 3 day coprecipitated filtration scaffolds compared to the static controls, $p < 0.001$ (Figure 4.9).

Discussion

Using the filtration system developed, a uniform 3D substrate surface that mimics the inorganic composition of bone was created, providing a microenvironment that could potentially enhance osteogenesis (Kohn et al., 2005). Designing a biomaterial that can enhance the ability of cells to attach and proliferate is an imperative aspect of controlling cellular microenvironment. Seeding cells on 3D scaffolding as a first step in controlling cell function however, is not trivial (Toh et al., 2005). Non-uniform apatite coverage on scaffolding is preventative of uniform cell seeding. By establishing a technique that can consistently provide uniform and continuous mineral coverage of 3D porous scaffolding, it is hypothesized that cell seeding uniformity will be enhanced and uniform osteogenesis will be more likely to occur.

The precipitation of a continuous mineral film onto pore surfaces of the polymer substrate was the goal of the initial filtration experiment. Appropriate ion concentrations are necessary for calcium phosphate growth (Feng et al., 2000), particularly within the internal pores of a 3D scaffold. In order to maintain film formation, the thermodynamics of the SBF must be held below the homogenous precipitation limit and above the solute

saturation limit (Bunker et al., 1994). If these conditions are not met, then no or minimal mineral will form (Bunker et al., 1994; Murphy and Mooney, 2002). To provide the pore surfaces within the interstices of the scaffolds appropriate ion concentrations for film formation to occur, the delivery method of SBF can be enhanced. Flow perfusion bioreactors have already shown that increased mass transfer in 3D is responsible for increases in cell numbers, resulting in uniform tissue growth (Bancroft et al., 2003). Additionally, the flow conditions and resulting shear stresses that occur within these bioreactors have been modeled (Porter et al., 2005). By facilitating flow of the SBF through the scaffold pores, an appropriate ion concentration was expected to occur within the interstices of the scaffolds allowing mineral to form throughout the thickness.

To further accelerate mineral nucleation on all pore surfaces, the PLGA polymer surface was treated with NaOH, facilitating alkaline hydrolysis that increases the number of free carboxylic acid groups on the surface. This treatment accelerates heterogeneous precipitation of a bone-like mineral by creating an environment where free carboxylic acid groups that can interact with ions in solution are formed at a greater rate than just by hydrolysis in SBF (Murphy and Mooney, 2002). The presence of negatively charged surface groups provides a substrate more capable of apatite nucleation compared to positively charged surfaces (Tanahashi and Matsuda, 1997).

The enhancements to the SBF delivery and more rapid functionalization of the polymer surface together indicate that an appropriate ion concentration was established within the filtration scaffolds. While both control scaffold groups were treated with NaOH, neither group showed continuous mineralization through the scaffold thickness, showing that the improvement to SBF delivery via flow is responsible for the continuous mineralization seen within the filtration scaffolds. Maintaining this appropriate ionic environment depends on temperature, pH, and the concentration of the solutes. Efforts to control the temperature and pH were enforced by the use of a temperature controller held at $37^{\circ}\text{C} \pm 1^{\circ}\text{C}$ and frequent replacement of the SBF solution. The pH values of both the new and used SBF were monitored every time the SBF was changed (every 6 hours for 4x SBF and every 12 hours for 2x SBF), and the filtration group had an average increase

in pH of 0.47 ± 0.09 , whereas the submerged group had an average increase of 0.37 ± 0.07 . The pH changes reported are the maximum values that the pH had increased over a 12 hour period and are likely to occur for a small percentage of each incubation period, because the SBF is replenished in a timely fashion. These pH changes keep the pH value of the solution between 6.4 and 6.8 when the scaffolds are submerged in 4x SBF and between 6.8 and 7.2 when the scaffolds are submerged in 2x SBF. The pH changes that occurred are thought to be greater than pH changes resulting solely from ion depletion, because the SBF in all groups is not completely sealed from the atmosphere nor titrated to maintain a constant pH.

Despite fluctuations in pH, the mineral precipitated in the filtration, submerged control, and floating control groups all show characteristic XRD peaks of carbonated apatite. The mineral formed at 1, 3, and 5 days using the filtration system is similar (Figure 4.6). The 1 day filtration spectrum had the lowest intensity above the background, suggesting that the mineral could be less crystalline than the mineral formed at later times. This indicates that a more amorphous apatite phase or a nano-crystalline phase could be forming during the first day of precipitation. This XRD spectrum after 1 day of mineralization is consistent with spectra of apatite precipitated on PLLA and PGA films after 24 hours in a 5x SBF solution (Chen et al., 2005). Spatially, the mineral precipitated on the outer scaffold surface (filtration 5 days) showed similar peaks as the mineral precipitated within the center of the scaffold (filtration center 5 days), supporting the deposition of uniform mineral throughout the filtration scaffolds. Because most forms of calcium phosphate that differ by a few percent in carbonate substitution have overlapping peaks, it is difficult to discern the specific type of apatite or calcium phosphate being formed in these experiments from the XRD spectra. However, carbonated apatite characteristic peaks were detected for the filtration and floating control groups in FTIR analysis, providing evidence that a carbonated apatite is being precipitated onto the scaffolds. The decreased resolution of the precipitated bone-like apatite compared to the hydroxyapatite and carbonated apatite standards could result from either the precipitated mineral being crystalline but having nanometer-range crystal

size or the precipitated mineral containing a large fraction of an amorphous phase (Posner et al., 1984). A slight peak shift to higher 2θ values was seen for the submerged control and filtration (3 days) samples compared to the rest of the samples, which could be indicative of chloride substitutions within the apatite being formed (Koutsopoulos, 2002).

A model protein, BSA, was successfully incorporated into the mineral layer within 3 days. A ten-fold increase of protein incorporation was found in the coprecipitated scaffolds via filtration compared to the submerged control scaffolds (Figure 4.7). More protein incorporation in the filtration coprecipitation group is attributed to increased mineral formation on these scaffolds (Figure 4.8). The amount of protein coprecipitated within the filtration and submerged control groups ($1308 \pm 464 \mu\text{g}$ and $139 \pm 45 \mu\text{g}$, respectively) are comparable to previous coprecipitation reports that incorporated biomolecules within mineral or polymeric materials (Kim et al., 2003; Luong et al., 2006; Shea et al., 1999). Additionally, the scaffolds coprecipitated via filtration displayed uniform protein incorporation throughout the scaffold thickness, whereas the scaffolds coprecipitated via submersion showed protein incorporation only on the outer surfaces (Figure 4.9). This uniform incorporation would allow uniform biomolecular release throughout the scaffold in an *in vitro* or *in vivo* setting.

The protein densities for the filtration and submerged control groups were $345 \pm 164 \mu\text{g}/\text{mm}^3$ and $1260 \pm 410 \mu\text{g}/\text{mm}^3$, respectively. The increased density within the submerged control is likely attributed to a static mineralization that allowed the BSA to adsorb to the surface of the scaffold prior to mineralization, whereas in the filtration group fluid movement limited BSA adsorption. However, cells transplanted onto coprecipitated scaffolds could favor a lower protein loading density. Coprecipitated inorganic coatings have shown to be effective on a dense 3D materials (Liu et al., 2004; Liu et al., 2005; Stigter et al., 2002), and spatial control of the organic constituents within the coating of a film has been achieved (Luong et al., 2006); however, to our knowledge, this is the first investigation of coprecipitation of mineral with protein on a 3D porous template. The aim of using the filtration method is to spatially localize biomolecules that promote bone formation into a more effective bone engineered template.

When coating implant materials, such as titanium hip replacements, the 2D surface is coated with a thick mineral layer to ensure the coating is present on the implant after the surgery. However, the design strategy of coating the pores of a 3D scaffold for tissue engineering differs from coating a 2D surface, because a main objective of coating a 3D scaffold is to retain porosity. Therefore, current coating techniques would not be effective in uniformly coating all pore surfaces within a 3D scaffold with a thin mineral layer, demonstrating the need for a method to uniformly coat pore surfaces of 3D scaffolds without compromising porosity.

Techniques to precipitate a uniform, continuous calcium phosphate layer on porous polymer scaffolds via pre-mineralization aminolysis or hydrolysis have not been able to establish a continuous mineral layer in a time effective manner. Even with longer precipitation times, the mineral layer is not continuous throughout the thickness. The result is a thicker layer of mineral around the periphery of the scaffold, which can lead to pore occlusion and compromise cell function. An increase in the volume fraction of regenerated bone occurs on statically mineralized PLGA scaffolds having a 250-425 μm pore size range, compared to PLGA controls (Kohn et al., 2005). In the presented work, the scaffold pore size ranged from 425-600 μm , so, as an example, a 20 μm thick layer of mineral would decrease the pore size range to 405-580 μm , which is larger than the pore size reported by Kohn et al. but within an identified range for bone ingrowth (Hollister et al., 2005). Ultimately, the presence of continuous bone-like mineral throughout the polymer scaffolds is expected to lead to more continuous in vivo osteogenesis.

Although the initial design of the system enables a batch of sixteen 10 mm diameter scaffolds, mineralization of twenty-five 5 mm diameter scaffolds has also proved feasible (data not shown). Moreover, this system is not limited to PLGA scaffolds. Any material capable of being constrained in the Delrin® mold can be utilized with scaffold diameter and thickness as variable parameters.

In summary, incorporating a bone-like apatite mineral layer on polymer scaffolds in an environment conducive to biomolecular incorporation has the potential to increase the ability of cell recognition, attachment, and regeneration in vivo. A filtration device

designed to force SBF through the pores of scaffolds enabled a uniform, continuous bone-like mineral layer to form throughout, and uniform mineral coverage could be attained in only 4-5 days. Additionally, a model protein, BSA, was coprecipitated uniformly in the bone-like mineral layer throughout the thickness of the scaffolds. Scaffolds mineralized within the filtration device displayed an increase in mineral volume % and in the amount of incorporated BSA via coprecipitation compared to static mineralization. This filtration system can potentially be used to incorporate cell-signaling biomolecules, such as growth factors or DNA, to promote in vivo osteogenesis, in addition to just serving as a technology to develop conductive materials.

Acknowledgements

I would like to thank my co-authors on this manuscript, Dave H. Kohn and Hayes C. Smith. This research is supported by NIH R01 DE 013380, DE 015411 (DHK) and Tissue Engineering at Michigan Grant DE 07057 (SS). The authors would like to thank the University of Michigan Chemistry Machine Shop and the Orthopedic Research Lab Machine Shop for their craftsmanship, in addition to Dr. Scott Hollister for the generous use of the MicroCT. The authors would also like to thank Jeff Meganck for his MATLAB expertise, Ricky Rossello, Colleen Flanagan, and Mike Barker for their helpful advice.

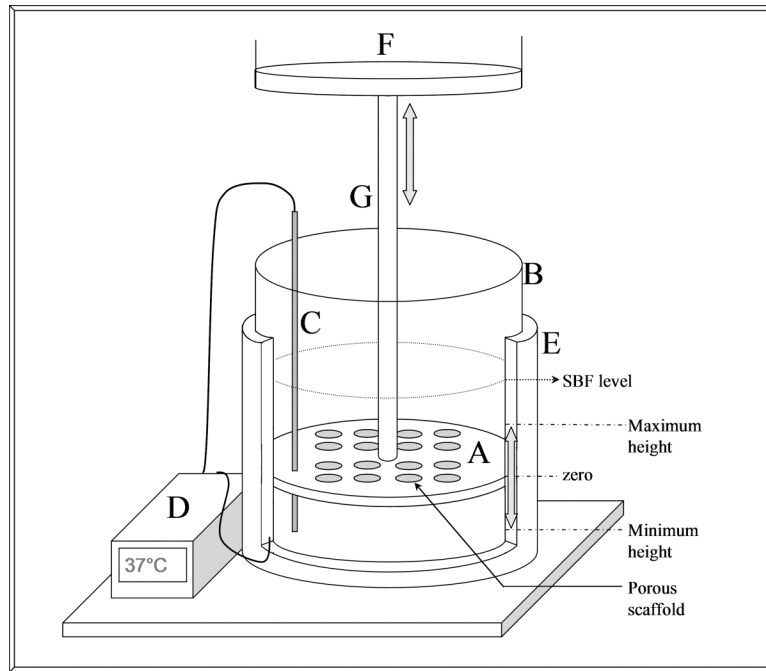


Figure 4.1: Schematic showing the filtration device. The device consists of a Delrin® mold (A), aluminum base (B), thermocouple (C), temperature controller (D), and heating element (E). The Delrin® mold is connected to the actuator of an Instron 8521 servo-hydraulic system (F) and cyclically loaded via an aluminum rod (G). The SBF level and maximum and minimum positions that the Delrin® mold is displaced to are labeled on the figure. Holes in the Delrin® mold that did not have a PLGA scaffold were plugged with rubber stoppers. 1 L of SBF solution is housed in the aluminum base during mineralization. The Delrin® mold can simultaneously cast sixteen 10 mm diameter scaffolds (or twenty-five 5 mm diameter scaffolds, not shown).

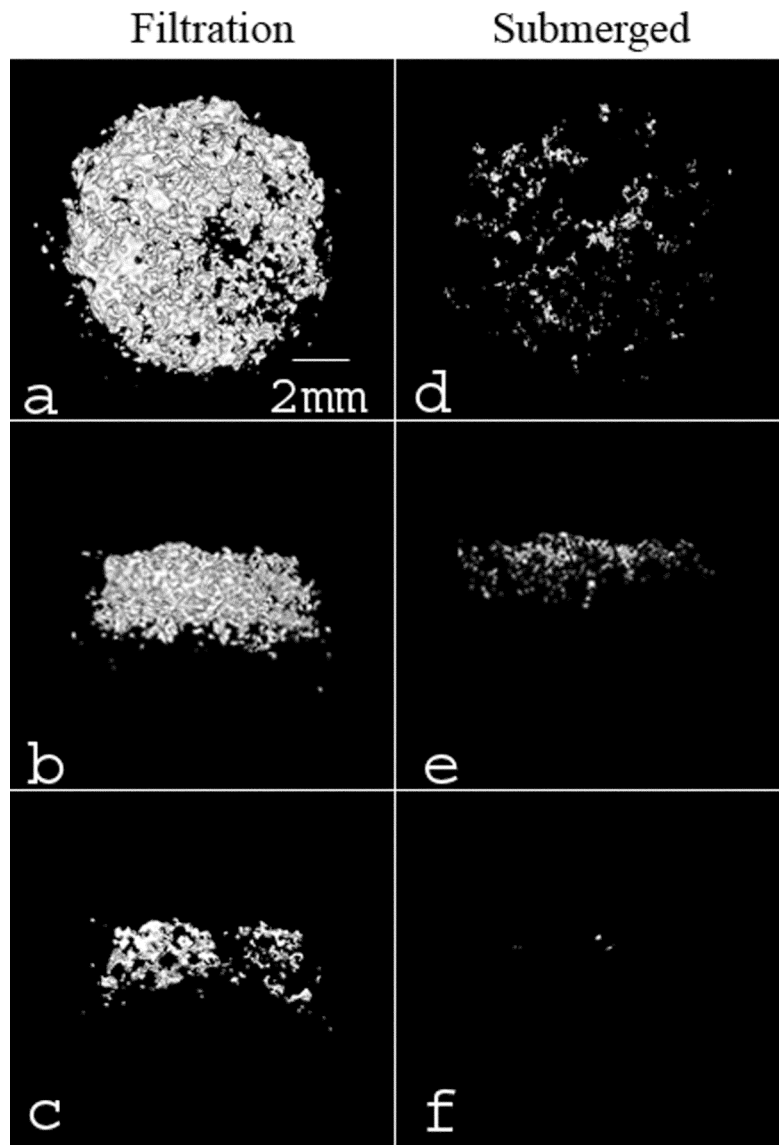


Figure 4.2: Representative MicroCT images of the filtration group (a-c) and the submerged control group (d-f). These images represent top (a,d), side (b,e), and center cross-sections (c,f). A greater amount of mineral formed on the filtration scaffolds in comparison to the submerged control group. Renderings of the floating control group are not shown because mineral present in the images was minimal (<0.2 MV%). All images were created in MicroView® using the Isosurface tool (voxel size = 16 μm , threshold = 1000, surface quality factor = 0.55).

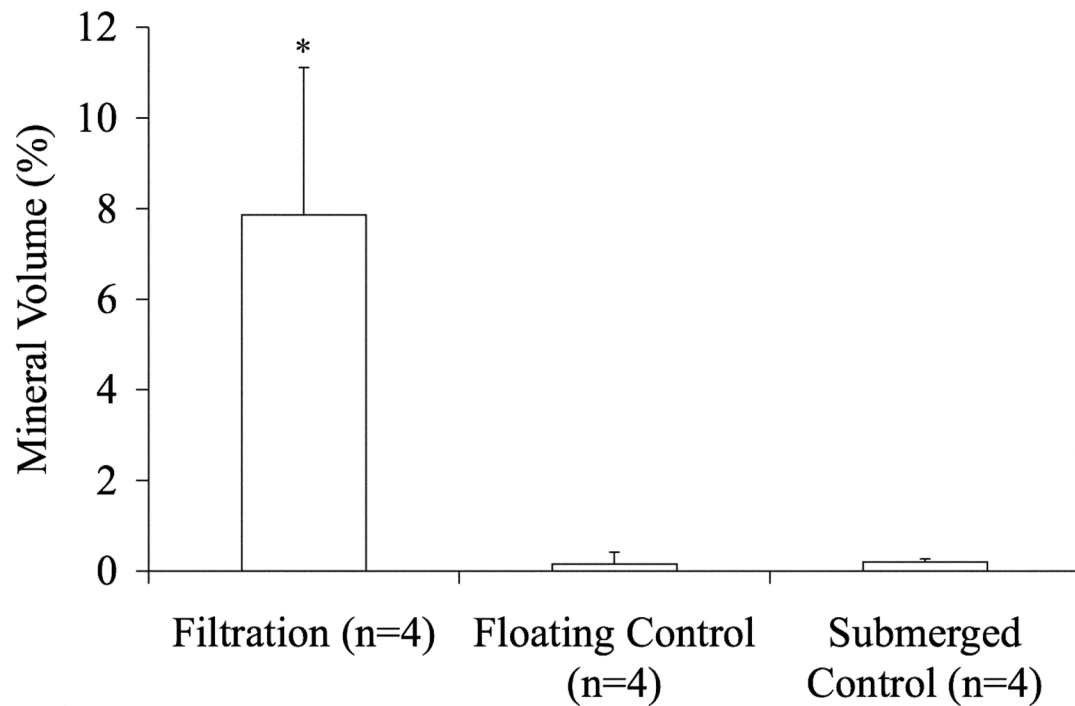


Figure 4.3: Mineral Volume % (MV%) for the filtration, floating control, and submerged control groups demonstrated the filtration group mineralized the greatest amount. (* - $p = 0.029$ vs. both controls). MV% was calculated from MicroCT data using MicroView® at a threshold of 1000.

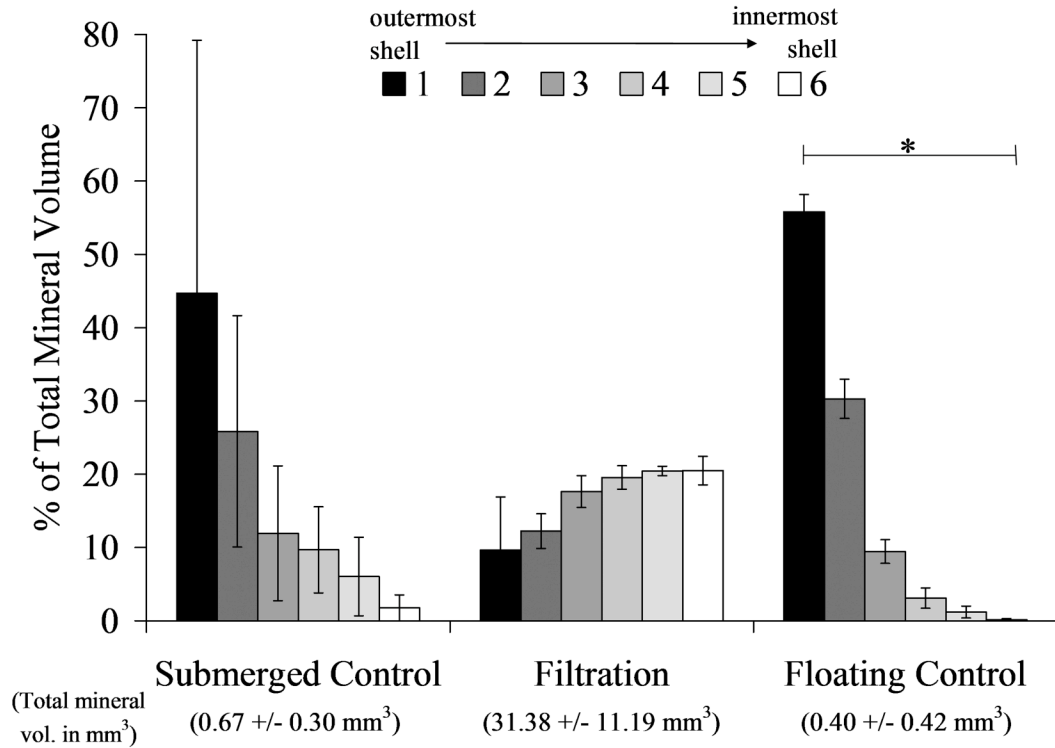


Figure 4.4: Volumetric mineral analysis of the MicroCT images (threshold = 1000) showing the filtration scaffolds have a uniform mineral profile throughout all 6 regions of the scaffolds analyzed. The % of total mineral volume for 6 concentric shell volumes show the control mineralized scaffolds have at minimum 60% of the mineral present in the 2 outer shells (shells 1 and 2). The floating control group shell volumes were statistically different from one another (n=4, p=0.002), whereas the submerged control and filtration groups did not show significance (n=3, p=0.051 and n=4, p=0.104, respectively). * - Statistical significance found, p<0.050.

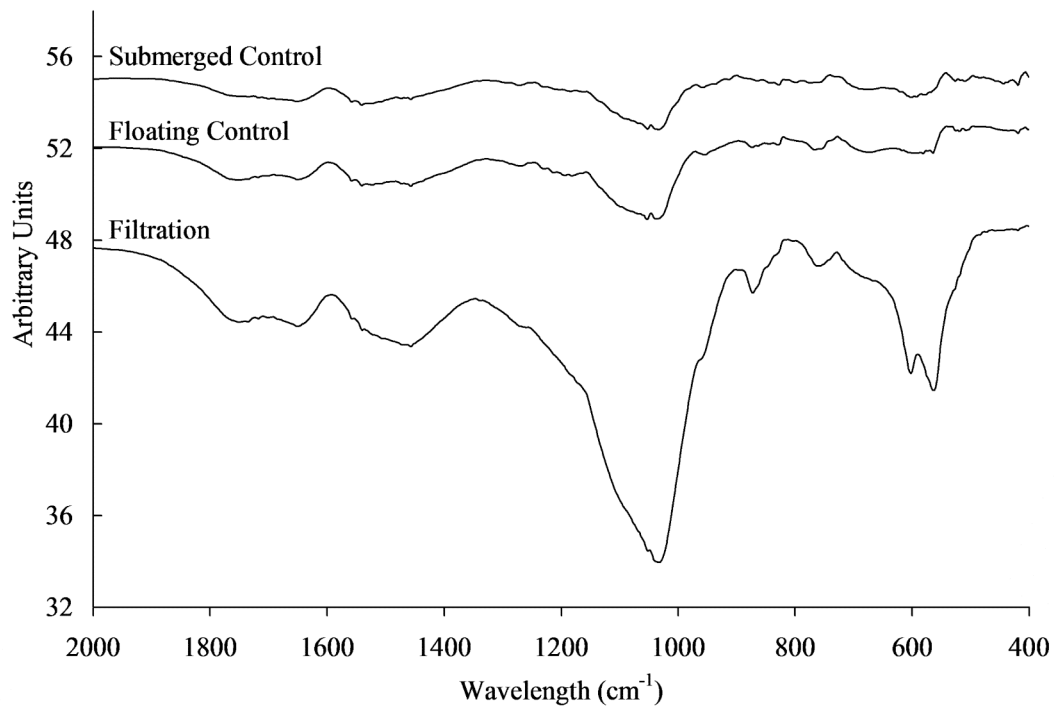


Figure 4.5: FTIR spectra for filtration, floating control, and submerged control groups showing the mineral deposited on the scaffolds was characteristic of hydroxyapatite with carbonate peaks (ν_{3c} P-O 1032 cm^{-1} , ν_1 P-O 962 cm^{-1} , ν_{4a} O-P-O 602 cm^{-1} , and ν_{4c} O-P-O 561 cm^{-1} [filtration group only]) and carbonated apatite (ν_1 CO_3^{2-} 1465 cm^{-1} [filtration and floating control groups]). Stronger peaks for the filtration group indicate the presence of more mineral.

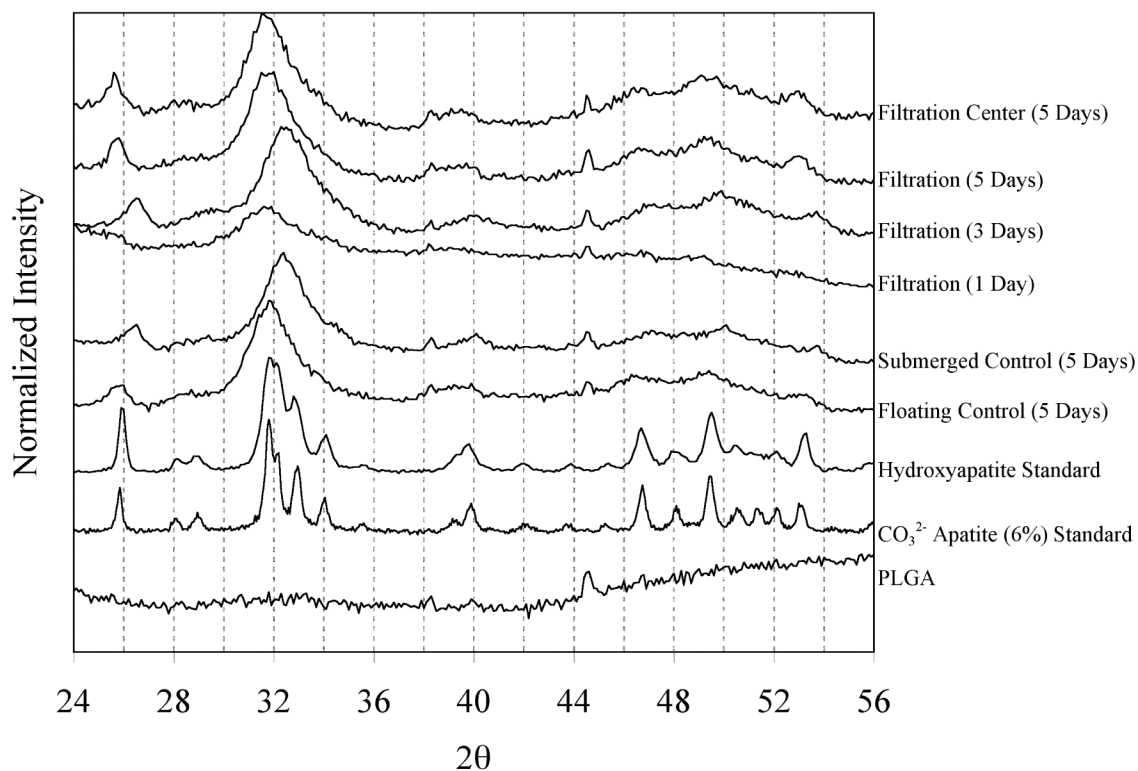


Figure 4.6: XRD spectra for all three groups (filtration, floating control, submerged control) show characteristic apatite peaks between 25.9°-26.8°, between 31.8°-32.7°, at 40.1°, and between 45°-55° when compared to the hydroxyapatite standard. A similar type of mineral was precipitated over the 5 days of filtration (1, 3, and 5 days). To assess if the mineral formed within the center of the filtration scaffolds was similar to the mineral formed on the surface of the filtration scaffolds, 5 day scaffolds were sectioned transversely and analyzed (Filtration Center 5 Days). The mineral formed on the interior surface of 5 day filtration scaffolds showed a similar spectrum to the mineral formed on the outer surface of the same scaffolds at 5 days, verifying that a similar mineral formed throughout the depth of the scaffold.

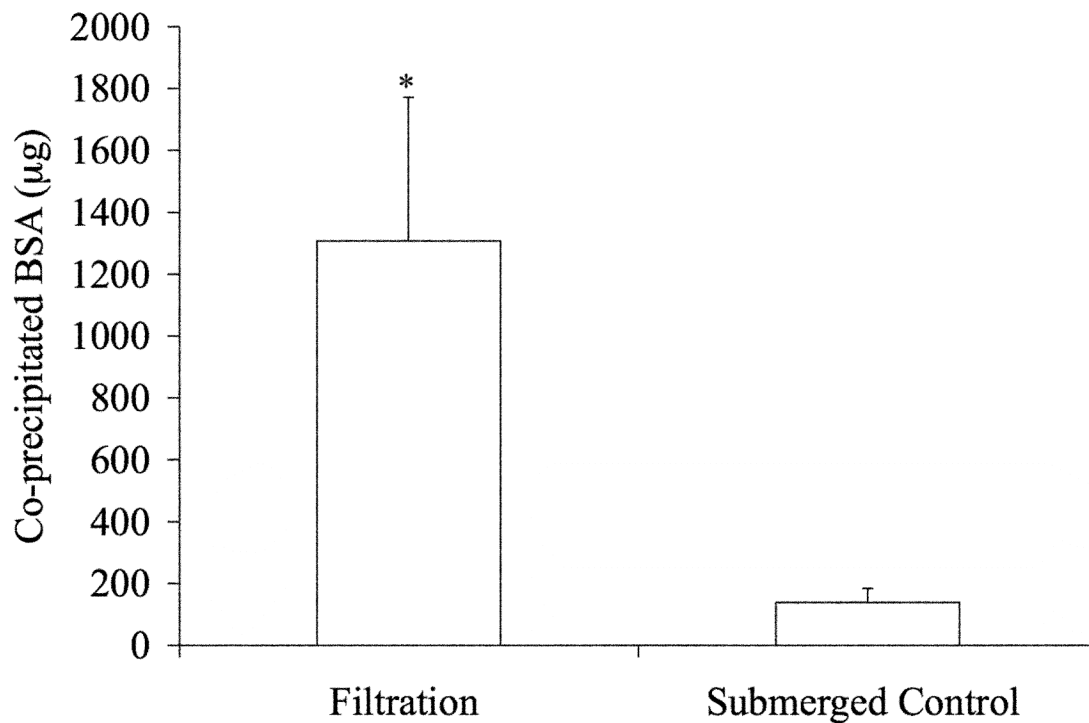


Figure 4.7: Quantitative coprecipitated BSA values (µg) showing greater protein incorporation in the filtered scaffolds. The amount of BSA incorporated was quantified utilizing UV Spectrophotometry at 494nm wavelength to detect the FITC-BSA. (* - Statistically significant compared to submerged control group, $p < 0.001$).

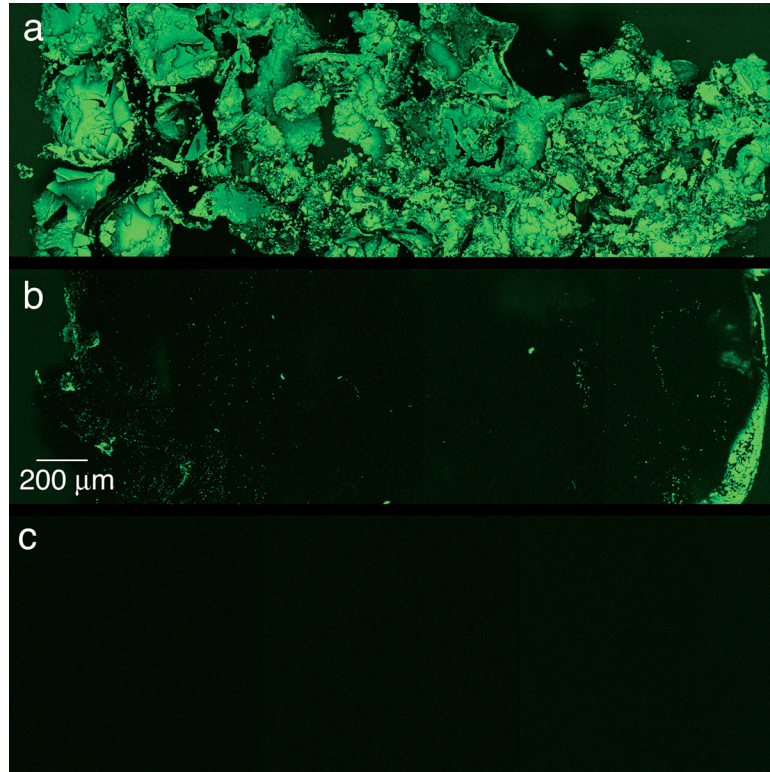


Figure 4.8: Representative confocal microscopy images of transverse sections of filtration (a) and submerged control (b) groups coprecipitated with BSA for 3 days. The mosaic images were compiled from multiple images of the center cross-section for each scaffold in each group (n=4 per group). The incorporation of BSA is shown by the fluorescence of FITC conjugated to the BSA. The filtration scaffolds showed uniform BSA coprecipitation throughout. A typical mineral shell, evidenced by more FITC seen on the left and right edges, is seen for the submerged control group. The presence of a mineral shell also supports less BSA incorporation. Autofluorescence of the mineral was not detected, shown by a representative image of a center cross-section of a scaffold mineralized via filtration for 5 days using the 4x SBF/2x SBF regimen precipitated without protein (c). Original images were taken at 10X.

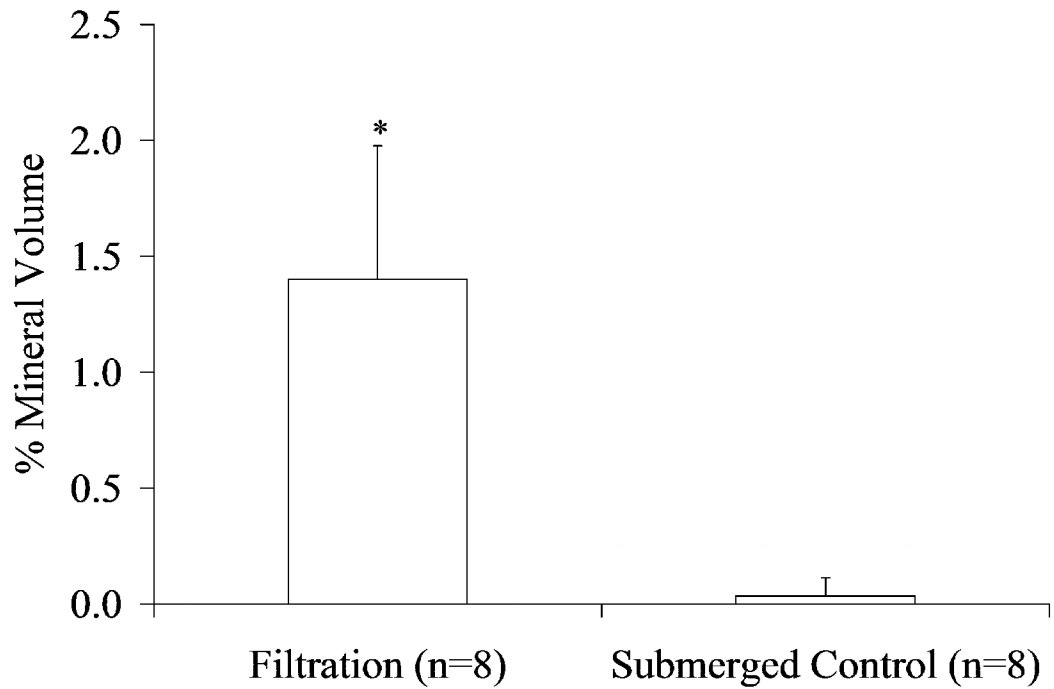


Figure 4.9: Mineral Volume % (MV%) for the filtration and submerged control coprecipitation groups demonstrated the filtration group mineralized the greatest amount. (* - $p < 0.001$). MV% was calculated from MicroCT data using MicroView® at a threshold of 1000.

CHAPTER FIVE

SUMMARY AND FUTURE WORK

The work throughout this dissertation aims to improve the design rationale and methodologies used to engineer bone. The goal that all bone engineers strive to accomplish is complete repair of large defects with new bone tissue having the quality of native bone tissue. As conditions caused by diseases, accidents, and genetic defects still create bone defects too large for the body to heal by itself, we continue to search for better materials and a better understanding of how we can provide influential biological cues to guide bone growth. Current repair techniques for large bone defects include permanent metal implants that provide mechanical integrity, but often lack complete integration at the bone-implant interface, which can cause loosening and require further repair. An ideal implant would be comprised of temporary, biodegradable materials that direct the body to heal itself with or without spatiotemporal cues on or within the implant. Because bone is a complex organ, we look to multiple disciplines to learn how we can integrate biology, chemistry, and materials science not just at the whole bone level, but also at the nanoscopic level. The work presented in this thesis has introduced a new rationale for designing biological molecules in the form of dual-functioning peptides, in addition to improving the apatite coating techniques used on porous implants.

Using a commercially developed phage display combinatorial library on both inorganic apatite and a source of clonally derived human bone marrow stromal cells, short peptide sequences were separately identified as preferential binders towards the apatite and cells (Chapters Two and Three). Combining the two short peptide sequences yielded a dual-functioning peptide that provides improved cell attachment to apatite-based materials. The design rationale for the inorganic-organic hybrid system studied in

this thesis for bone repair can now be explored in other hybrid systems throughout the body. Isolating preferential binding sequences in the form of peptides may prove invaluable when trying to integrate two dissimilar tissues (e.g. bone and cartilage). Furthermore, such peptides can be combined with established pattern processing techniques to direct tissue growth and integration. In general, any organic-inorganic hybrid system requiring the union of two constituents that do not inherently bond could benefit from the presented design strategy.

The Identification of Peptide Sequences for Bone Tissue Engineering

There has been limited use of phage display with the materials and cells used in bone regeneration. Until this work, phage display had been used *in vitro* to identify potential osteoblast binding sites during bone remodeling (Sheu et al., 2002) and there was a brief mention in a review that it was used to identify peptides with affinity towards hydroxyapatite (Sarıkaya et al., 2003; Tamerler et al., 2003). Therefore, using this microbiological technique to discover peptides unique to apatite-based materials and hBMSCs sources was an ambitious, unexplored goal. A tri-fold analysis involving phage display, computational modeling, and ELISA techniques proved successful in identifying peptide sequences with preferential apatite-binding capabilities (Figure 2.4) after multiple rounds of phage panning on two apatite-based materials, bone-like mineral and sintered hydroxyapatite. The unexpected result that peptides identified from the phage experiments did not contain long strings of acidic amino acid sequences may have transpired because such peptides were not present in the parent library. This would be a limitation of the 12-mer phage display library used. It should also be noted that one consensus peptide sequence did not surface in these experiments, suggesting that other peptides identified could be as good at binding to apatite as the peptides STLPIPHEFSRE and VTKHLNQISQSY. However, the rigorous validation techniques combined (shown in Figure 2.1) to isolate these two peptides would support that they have the best ability to preferentially adsorb on apatite-based materials for the experimental conditions tested.

Combinatorial libraries also had not been applied to bone regeneration research on cells, except for one *in vitro* study on osteoblasts. Phage display is capable of

identifying informative peptide sequences on various tissues (e.g. muscle (Samoylova and Smith, 1999), breast vasculature (Essler and Ruoslahti, 2002), bone marrow (Nowakowski et al., 2004)). The same 12-mer combinatorial library used on the apatite materials was introduced to a population of clonally derived human bone marrow stromal cells. This population of cells has the capability of differentiating down an osteoblast lineage resulting in the ability to form bone tissue. Bioinformatic and immunohistochemistry analyses (Figures 3.2 and 3.3) identified two sequences as having the highest potential to bind to the clonally derived human bone marrow stromal cells (LLADTTHHRPWT and DPIYALSWGMA).

Dual-Functioning Peptide Performance

The peptide sequences that preferentially bound to the apatite-based materials and the human bone marrow stromal cell population were combined to build dual-functioning peptides. Adsorption of the VTKHLNQISQSY peptide (Figure 2.4) on multiple apatite-based materials was superior to STLPIPHFSRE, so the VTKHLNQISQSY was used in the final dual-functioning peptide design. The VTKHLNQISQSY sequence was kept at the carboxy-terminus of the peptide design, as this is the configuration that the peptide would see when expressed on the protein coat of the bacteriophage. This meant the identified cell binding sequences LLADTTHHRPWT and DPIYALSWGMA were present towards the amino-terminus of the dual-functioning peptide. Glycine (G) spacers were used at the amino-terminus end and also between the cell and apatite recognition sequences to preserve any peptide conformation and decrease any steric effects from neighboring charges. The adhesion and cell attachment influence of the final dual-functioning peptides were compared with the E₇PRGDT positive control peptide derived from bone-sialoprotein (Chapter Three) that has a positive influence on cell adhesion to hydroxyapatite sintered disks (Itoh et al., 2002; Sawyer et al., 2005b).

The dual-functioning peptide D-VTK had superior binding to bone-like mineral compared to all other peptides tested except E₇PRGDT (Figure 3.5), indicating that the cell sequence DPIYALSWGMA was contributing to the adsorption of the peptide to the apatite-based materials. However, while this peptide exhibited greater adsorption to

bone-like mineral than other peptides, when hBMSC attachment was normalized to the amount of peptide present on the BLM, this peptide proved to be not as effective as L-VTK (Figure 3.7). The positive control peptide E₇PRGDT had a higher mean adsorption to BLM compared with L-VTK; however, E₇PRGDT was not capable of increasing cell attachment to BLM. Previous designs of cell influencing peptides have included polyacidic tails on cell adhesive sequences (e.g. RGD) to increase peptide binding to apatite-based materials (Itoh et al., 2002; Sawyer et al., 2005b). The inability for E₇PRGDT to increase cell attachment is inconsistent with previously published results (Itoh et al., 2002; Sawyer et al., 2005b). Neither study quantified the amount of peptide on the surface of their HA samples, and both studies used serial washing as a method of cell detachment, making it difficult to compare the results to those reported in this study. Developed cell adhesion methods using centrifugation reduce any questions of reproducibility and sensitivity than previously developed washing methods that are dependent on the person pipeting (Garcia and Gallant, 2003; Reyes and Garcia, 2003a). Also, slight changes in substrate morphology can influence peptide adhesion at similar initial adsorption concentrations (Chapter Two). While adhesive proteins may contain acidic and RGD amino acid sequences, isolating these portions of proteins as peptides may not be beneficial on all apatite-based substrates and/or cell sources.

The Effect of Surface Composition and Morphology on Peptide Adsorption

The adsorption of the short peptides identified as preferential binders to apatite-based materials was tested on four apatite substrates. Investigation into whether compositional or morphological changes affect peptide adsorption has merit as changes in percent carbonate of bone with age may effect adsorption of specific proteins/peptides because of this compositional change (Boskey, 1999). Understanding the changing bone composition with age and its effect on the extracellular matrix could help in identifying the mechanisms involved in osteoporosis.

Normalization of peptide adsorbed to MicroSA, quantified via BET, was performed to investigate the effects carbonate incorporation and morphology have on the amount of peptide adsorbed. Slight changes in carbonate percentage did not influence

peptide adsorption for the apatite-based materials studied in these experiments. The range of carbonate present in the materials did vary; however, at the same morphological scale, the carbonate differences were minimal (~2wt%). A trend of decreased adsorption to CA10 in comparison to CA5 and HA was shown across all peptides. These results do not rule out that a larger change in carbonate incorporation could produce an effect on peptide adsorption. CA5 adsorbed significantly higher amounts of peptide S compared with CA10, indicating that a morphological difference, not a compositional difference, was evident for this case only. The morphology difference between CA5 and CA10 could affect peptide adsorption resulting from a change in charge distribution on the apatite surface that promotes peptide adsorption. Better control of the surface morphology accompanied by larger differences in carbonate content would better investigate if higher amounts of carbonate incorporation have an effect on peptide adsorption.

The large surface area for BLM suggests that all of the available sites on the BLM are not saturated with peptide. However, the feature size on the BLM is very small with plates growing to dimensions of 500nm length x 50nm thickness. The distinct morphology of BLM could be inhibiting peptide access to all of the measured surface area, which implies that the BET method could be overestimating the available surface area to which peptides may have access. Or, the BLM morphology could be presenting unfavorable surface charge arrangements, meaning the peptides are able to access all of the measured surface area, but do not because of unfavorable presentation of charge.

Phosphorylation as a Method to Tailor Peptide Adhesion

Since one approach in identifying apatite-binding peptide sequences is to perform post-translational modifications (e.g. phosphorylation) (Goldberg et al., 2001; Pampena et al., 2004; Shaw et al., 2000a) on peptide sequences derived from proteins, it was of interest to see if phosphorylating the VTK peptide identified in the presented work would improve peptide adsorption to apatite-based materials. Phosphorylation introduces a phosphate group onto a serine, threonine, or tyrosine amino acid and serves as a regulatory mechanism on proteins in the body. The addition of a phosphate group on a

peptide can influence its charge and ability to interact with charged surfaces. The VTKHLNQIS(p)QS(p)Y (VTK-phos) peptide was fabricated on a Rainin Symphony synthesizer and determined as >86% pure via HPLC (UM Protein Core). Amino acid analysis was performed to verify VTK-phos peptide concentration for standard curves created with UV absorbance at 205nm, 220nm, and 274nm wavelengths (BioRad Smartspec 3000).

The VTK-phos peptide was reconstituted in ddH₂O and diluted to ~500µg/mL in 50mM Trizma buffer (Sigma, pH=7.5). In 24-well tissue culture dishes, BLM films, HA disks, CA5 disks, CA10 disks, and blank TCPS wells were soaked in ddH₂O overnight at 4°C (n=5). Prior to introducing 1mL of the peptide or buffer solutions for negative controls, plates were allowed to warm to room temperature and then the overnight solution was removed. The plates were agitated on a Titer Plate Shaker at ~80rpm for 3 hours at room temperature. The films and disks were rinsed with ddH₂O and then soaked in a 10mM HCl solution for 18 hours at room temperature on the same shaker. Aliquots of the HCl solution were read on a UV spectrophotometer. The entire experiment was performed in duplicate.

Phosphorylating the two end serines on the VTK peptide led to a 10-fold increase in peptide adsorption on BLM, $p=0.028$ (Figure 5.1). Significant increases in VTK-phos adsorption compared to VTK were also seen for the carbonated disks, CA5 and CA10 (CA5 $p=0.009$, CA10 $p=0.009$). The non-carbonated HA disks did not experience a significant change in peptide adsorption between the phosphorylated and non-phosphorylated VTK peptides. These results have interesting implications on the ability to control adsorption on carbonated apatite, in particular, BLM. The data suggest that phosphorylating available amino acids on peptide sequences can provide a means of increasing peptide concentration to a carbonated apatite surface. Subjecting the VTK-phos to the same cell attachment assay reported in Chapter Three, the VTK-phos peptide alone was not able to increase cell attachment on BLM (Figure 5.2). The opportunity for future research on VTK-phos is discussed further in Future Studies section.

Inducing Fluid Flow Improves Mineralization in Three-Dimensional Scaffolds

The bioreactor, designed in Chapter Four, forced SBF through the pores of highly porous PLGA scaffolds and was able to induce continuous, uniform mineral formation. While the BLM can increase osteogenesis *in vivo*, the additional bone growth is not uniform or spatially controlled, suggesting the need for uniform apatite coverage to direct tissue growth through the thickness of the scaffold. The protocol presented completely mineralized a 2mm thick porous polymer scaffold in 5 days, displaying potential the bioreactor could present in coating biomaterial surfaces. Furthermore, it was demonstrated that a model protein could be incorporated into the BLM coating, allowing more utility in spatiotemporal bone scaffold design. The ability to uniformly and continuously coat porous scaffolds with BLM will advance BLM coatings in three-dimensions. The data presented will hopefully convince those using techniques of biomimetic film deposition on bone engineered constructs to seek a method of providing uniform, continuous film coverage by inducing fluid flow in the interstices of the construct rather than passive static soaking methods that are typically employed. Ultimately, porous scaffolds that enable spatiotemporal release of growth factors and/or DNA can be coated with dual-functioning peptides to increase initial cell attachment *in vitro*. This strategy may provide better-directed bone growth in large defects.

Future Studies

The work presented in this thesis provides a new perspective on how peptides can be designed for bone tissue engineered constructs. By capitalizing on the apatite-based adhesive properties of synthetic peptides identified via phage display, cell adhesive sequences can be joined to improve initial cell attachment to a material. This initial cell attachment is the imperative first step in cell survival, proliferation, and differentiation. The introduction of using phage display on apatite-based materials elucidated sequences that may not have been found using the current approach in the field of deciphering protein sequences. Furthermore, using the combinatorial library approach on a source of human bone marrow stromal cells is the first attempt to isolate sequences that may preferentially bind to the clonally derived hBMSCs tested. The approach of using phage

display to isolate subsets of cells could be used to fabricate the next level of peptide-laden substrates for bone repair. Never in bone material development has phage display been implemented on both the substrate material and the cell source to identify peptide sequences that can influence and improve cell behavior and function. Thus, this work is first to introduce the idea of using phage display to create dual-functioning peptides.

While apatite-binding and preferential hBMSC-binding sequences were identified in this work, many new questions can be studied to understand how the identified sequences can be used to their full potential. It is evident from the work in Chapter Two, that small differences in carbonate percentage between apatite-based materials do not influence peptide adsorption behavior. However, if larger ranges of carbonate differences were established up to 15% carbonate (e.g. 5%, 10%, 15%), peptide adsorption could potentially change. A change in peptide adsorption over larger carbonate percentage differences could indicate protein/peptide adsorption is altered with compositional changes in bone that occur with disease and age. The effect of carbonate incorporation into apatite on protein adsorption is not clearly shown anywhere in the literature. If it is found that large changes in carbonate percentage do not affect peptide adsorption, this could lead researchers to investigate other mechanisms with disease and age that could alter bone remodeling, such as post-translational modifications or changes in the micro-environments near the bone surface. The methodologies for performing peptide adsorption experiments are well outlined throughout this thesis and could be used as a starting point for such experiments.

Furthermore, it was shown that phosphorylating the serine residues present on the VTK peptide dramatically increase its adsorption to BLM. As phosphorylation is important in protein function, the influence of phosphorylation on mineralization and peptide adhesion to apatite-based materials are both exciting areas of research. The location of the phosphorylated serine residues within the VTK peptide, the number of phosphorylated serine residues, and the ability for phosphorylated VTK peptides to increase cell attachment has yet to be determined. Scrambling the VTK sequence with and without phosphorylated residues would identify any specific portions of VTK are

responsible for its adsorption behavior. When the VTK peptide was run in the MATCH program of RELIC against bone protein sequences, it did contain the motif NQIS (Asn-Gln-Ile-Ser), a sequence conserved in small leucine-rich proteins (SLRP) such as fibromodulin, lumican, and decorin. Another motif of the VTK peptide, VTXXL was found in a collagen I protein sequence. Since the VTK peptide was identified as a preferential binder to apatite-based materials, and the SLRPs family of proteins are thought to regulate collagen fibril assembly, which would occur prior to apatite formation, the VTK peptide could be a link between collagen and extracellular bone proteins that allows aggregation of correct ion concentrations for apatite nucleation. Research on the protein decorin has also suggested decorin contains N-linked oligosaccharide attachment sites near the asparagine residue of the NQIS motif (Weber et al., 1996).

While it was not in the scope of this thesis, further work on how the apatite-binding portion of the dual-functioning peptides influences the conformation of the cell-binding portion would provide further support for the increased attachment results for L-VTK. Performing cell attachment experiments on the apatite-binding and cell-binding portions alone would provide more information as to how each sequence influences the other in cell attachment. The increased attachment values for RGDV and RGEV in comparison to D-VTK could result because VTK has an inherent ability to increase cell attachment (Figure 3.7). VTK-phos does not enhance cell attachment (Figure 5.2); however, the non-phosphorylated version could behave differently. To increase our understanding of conformational changes of the dual-functioning peptides, they could also be computationally modeled on larger hydroxyapatite surfaces, in addition to multiple face planes (e.g. (001), (010), and (100)). Incorporating hydration into the model would also prove beneficial, as it would better simulate the experimental scenario.

Further studies investigating the cellular influence that the phage identified cell-binding sequences have on hBMSCs or other cell populations could also be done on TCPS. Because TCPS can be modified to covalently attach peptides in known concentrations, TCPS could be used as a control material to establish consistent peptide

concentrations for different peptide sequences. The cell-identified sequences could be covalently linked at both termini to provide insight as to which end, if only one, is responsible for increased cell attachment. Likewise, the efficacy of increasing initial cell attachment using the peptide L-VTK can also be studied in an *in vivo* subcutaneous bone model in mice or an *in vivo* craniofacial rodent defect model.

Cell work related to advanced stages of cell adhesion, and not just attachment, would also provide insight to the efficacy of the identified peptides. In the presented work, attachment was only allowed during a 1 hour incubation; however, if the incubation time was increased upwards of 3 hours, hBMSC cell adhesion would be able to be quantified. The centrifugation assay utilized in Chapter Three is a harsh assay on the cells, although more consistent than serial washing. Thus, even if focal adhesion assays are performed after 1 hour of attachment, the influence on cell adhesion by the peptides may be masked, as the cells may not behave normally after being subjected to high gravity forces. Perhaps a more appropriate experiment would combine the suggested TCPS work above and incorporate longer cell attachment incubation times to tease out peptide effect on focal adhesion formation.

As the ultimate goal is to develop better bone-guided repair scaffolds, combining the findings of all of the research aims in this thesis would be a step in the right direction. The scaffolds fabricated using the bioreactor designed in Chapter Four, can now be loaded with the dual-functioning peptide L-VTK to influence *in vitro* hBMSC cell attachment during incubation prior to implantation in an *in vivo* model that can determine its potential to increase osteogenesis.

Broader Applications of Dual-Functioning Peptides

As the main goal in this work was to improve materials used in bone repair, the substrate and cell source were appropriately chosen for this application. However, the idea of a dual-functioning peptide can be expanded to other areas of research trying to join two dissimilar materials. For example, the methods used in this thesis can be tailored to bone-tendon or bone-ligament junctions. Other applications where apatite-based peptides can be utilized in the dual-functioning peptide design would be bone-

cartilage and enamel-soft tissue systems. The dual-functioning idea can also be implemented across other bodily system research that aims to join two dissimilar tissues. The cells of each tissue can be panned using the phage display, which could isolate sequences unique to each population of cells, and the two peptide sequences could be joined together to help facilitate a tissue junction.

Outside the realm of biomaterials and tissue engineering, the idea of dual-functioning peptides can be utilized in any discipline trying to join an organic matrix with an inorganic substrate. Examples include bacteria inhibiting sequences being attached to metals and organic films being joined with ceramics or semi-conductors in the aerospace and electronic fields. Surely, the dual-functioning peptide can be tailored for specific applications that require better organic-inorganic bonding.

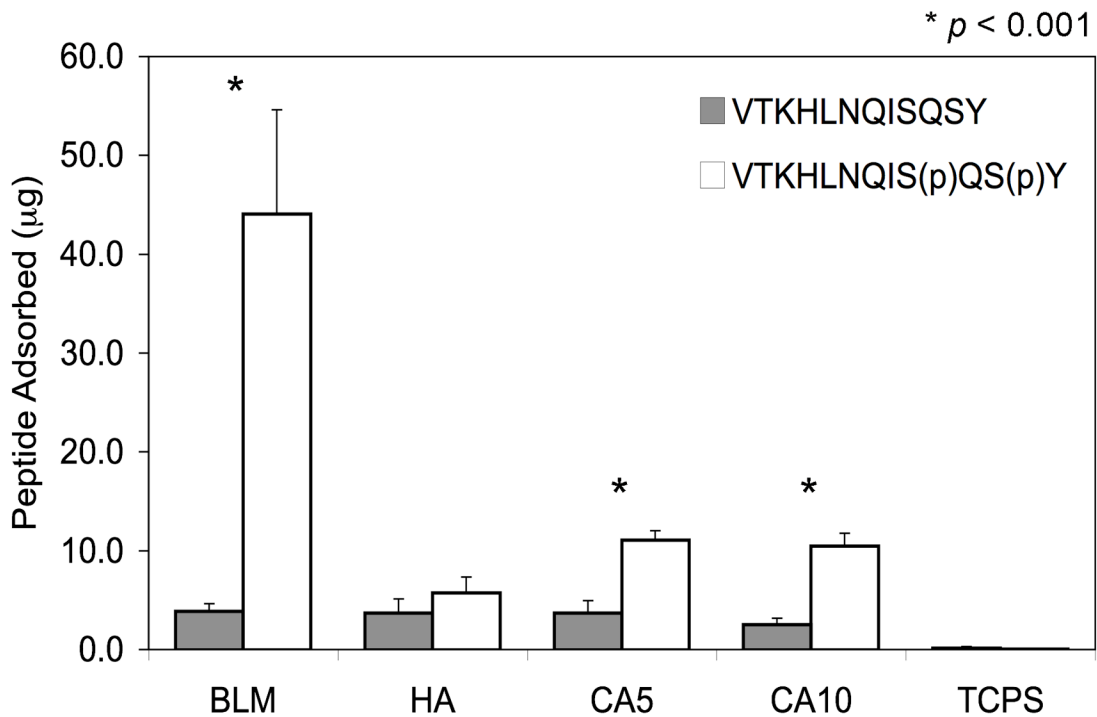


Figure 5.1: Adsorption of VTK vs. VTK-phos on apatite-based substrates. Phosphorylating the end serines on the BLM increased the peptide adsorption to 10-fold greater than non-phosphorylated peptide VTK, $p=0.028$. A similar trend was found on CA5 and CA10 substrates (CA5 $p=0.009$, CA10 $p=0.009$). All data are presented as mean values \pm one standard deviation. Statistics in SigmaStat ran an Independent Samples T-Test to determine differences between VTK and VTK-phos on each material. (*) Indicate statistical significance was found between VTK and VTK-phos.

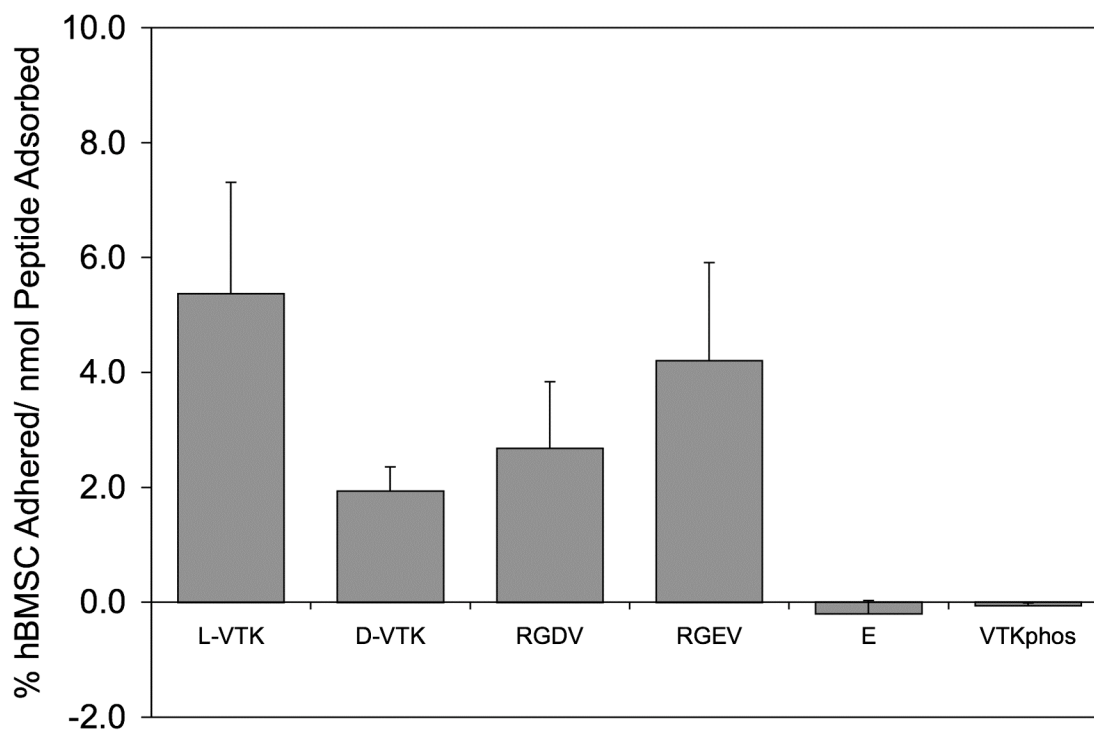


Figure 5.2: Cell attachment data reported in Figure 3.7 with the addition of VTK-phos. VTK-phos alone was not able to increase cell attachment when present on BLM. Attaching a cell adhesive sequence to the VTK-phos would test whether the better adsorptive properties of VTK-phos can influence cell attachment on BLM.

APPENDIX A

COMPUTATIONAL MODELING

Computational Modeling of Peptides on Apatite

Modeling organic molecules has proven useful in a variety of organic-inorganic systems including the investigation of protein-substrate and peptide-substrate interactions in calcite and calcium oxalate (Qiu et al., 2004). Despite a basis of modeling work on the apatite lattice alone (Astala and Stott, 2005; Hauptmann et al., 2003; Mkhonto and de Leeuw, 2002), limited studies have modeled organic molecules on an apatite lattice (Fujisawa and Kuboki, 1998). Using Newtonian physics in a time dependent manner to calculate forces on a system, molecular mechanics simulations allow the calculation of peptide adsorption energies. A greater negative peptide adsorption energy translates into a peptide possessing more potential to favorably adsorb to the lattice. When a step is introduced to the hydroxyapatite lattice, adsorption energies increase, likely because of the altered charge and higher degree of under-coordination of atoms and molecules on the surface of the step. The effect of negatively charged amino acid sequences on adsorption has been suggested as one mechanism of protein/peptide adsorption to hydroxyapatite (Fujisawa et al., 1997). These data provide molecular modeling evidence that given appropriate charge for a neutral pH environment, acidic peptides exhibit favorable binding over basic peptides. Furthermore, the model system used in these experiments provides a high-throughput validation technique where multiple interactions can be investigated prior to further *in vitro* or *in vivo* testing.

Using a HYDROXYAPATITE force field (Biswas, 2007) (HAF) developed from the UNIVERSAL 1.02 force-field (UFF) (Rappe et al., 1992), peptide adsorption energies were calculated from simulations using molecular modeling techniques between HA and 19 peptides that emerged from multiple phage display experiments. The potential parameters used in the HYDROXYAPATITE force field are listed in Table A1,

and non-bonded van der Waals terms generated by fitting the potentials listed in Table A1 to the experimental structure are listed in Table A2. The HYDROXYAPATITE force field is a hybrid force field that has basic properties of the UNIVERSAL1.02 force field with additional terms like off-diagonal van der Waals, bond-stretch, and angle-bend that are added for interaction within the apatite. The experimental terms (Table A2) are in agreement with similar systems studied before (Wierzbicki and Cheung, 2000; de Leeuw, 2004), and provide the basis that this HYDROXYAPATITE force field is appropriate for this study. Cluster calculations are more appropriate for this study than periodic slabs due to the use of charged adsorbates. Coulomb and van der Waals cutoff values were greater than the cluster dimensions, which was large enough (e.g., 200 Å) to include all atom-atom interactions within the cluster.

Hydroxyapatite (001) surfaces and a surface step parallel to [001] were created in Cerius² modeling software. A small dipole moment perpendicular to the [001] step was unavoidable. Charge distribution within each peptide, calculated using a QEq charge equilibration (Rappe and Goddard, 1991), was performed by distributing the appropriate charge of the peptide in a neutral environment, pH 7.2, across the molecule. After assigning charge, the individual atomic charges were kept constant in subsequent calculations to avoid energy fluctuation introduced during energy optimization of the structure of the isolated molecule and of its adsorbate. The charges of atoms in the hydroxyapatite are those listed in Table A1. To find the absolute energy minimum through optimization, molecular dynamics (MD) simulations under constant NVE (constant number of atoms, volume, and energy) at 300K were performed after every energy minimization. Every 100 simulation steps, velocities are rescaled if the averaged temperature goes outside a predefined window around the target temperature. The predefined window of target temperature was between 295 K and 310 K. In each MD simulation, the dynamic step was 0.001ps and total simulation time 700 steps (0.7ps). Energy minimization and the subsequent MD were run 7X for each peptide under each initial start orientation. Each peptide was run as a neutral or appropriately charged

molecule on both a flat (001) apatite plane and a [010] step introduced on the (001) plane (Figure A1). Four initial start orientations were simulated for each peptide on both the flat and step apatite cluster. This resulted in a total of 16 permutations run for each peptide investigated. The atoms in the hydroxyapatite lattice were not allowed to move during any simulations run. The adsorption energy of each peptide (E_{ads}) was calculated using the following equation.

$$E_{\text{ads}} = E_{(\text{peptide}+\text{HA})} - [E_{\text{peptide in vacuum}} + E_{\text{HA}}]$$

The average of the two lowest adsorption energies out of the four initial start orientations run for each peptide, both neutral and charged, was calculated (Table A3). The computationally derived peptide adsorption energies were then ranked for the four set-ups: neutral peptide – (001) HA plane, charged peptide – (001) HA plane, neutral peptide – [010] step on (001) HA plane, and charged peptide – [010] step on (001) HA plane.

It was expected that the peptides with negatively charged R groups for the charged peptides modeled would have higher adsorption trends than those with without basic amino acids in their compositions (Table A.3). This trend has been identified both experimentally and computationally in the literature (Fujisawa et al., 1996; Fujisawa et al., 1997; Sawyer et al., 2005b). This was apparent for the [010] hexagonal step case, where the charged peptides aligned by isoelectric point. This alignment indicated that peptides with low isoelectric points, which would be negative in a neutral pH solution, had higher adsorption energies than peptides with higher isoelectric points. The charged peptides run on the (001) HA plane also saw some alignment in peptide adsorption energy with isoelectric points. The isoelectric points for all peptides were estimated from contributions of C, D, E, H, K, R, Y, the amino- and carboxy- termini as 9.9, 5.3, and 9.7, respectively (Table A.4). The neutral peptides did not indicate any preferential adsorption ranking by isoelectric point. The top five ranking peptides for each of the four scenarios modeled were used, along with ELISA data and frequency results in Chapter

Two, to determine the peptide sequences with the most potential to adsorb favorably on apatite-based materials.

Limitations to the model include the lack of incorporation of water molecules. Addition of hydration to the model would be computationally expensive and would prove inefficient. Therefore, the modeling performed was done to compare relative adsorption energies for different peptides in the same computational set-up. The ability to analyze 19 different peptide sequences in a computational model for two HA crystal set-ups is valuable information that provides insight as to the organic-inorganic interactions that may be occurring at the atomic level. Such interactions are not always detectable in bench-top experiments, and they are often at the limits of peptide analysis techniques.

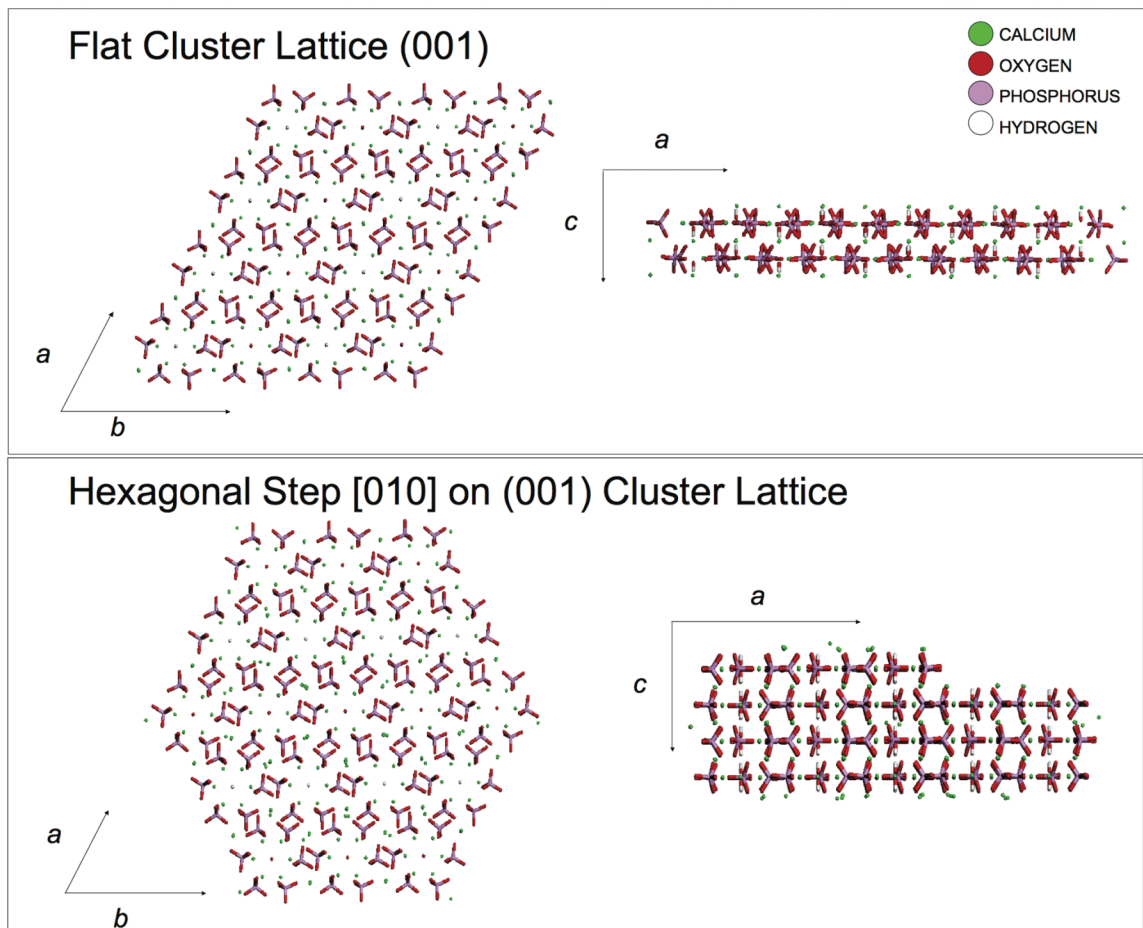


Figure A.1: Hydroxyapatite lattice cluster set-ups. A flat cluster on the (001) HA plane and a hexagonal step introduced on the [010] on the (001) HA plane were used to model the 19 peptide sequences derived from phage display experiments on apatite-based materials. The adsorption energies of all 19 peptides were calculated in a vacuum for both neutral and charged peptide values.

Table A.1: HYDROXYAPATITE Force Field Potential Parameters Used in Molecular Modeling of the 19 Phage Derived Peptides on Hydroxyapatite Surface and Surface Step

<i>Buckingham</i>¹	<i>A</i> (eV)	ρ (Å)	<i>C</i> (eV Å⁶)	<i>r_{cut}</i> (Å)
O _p -O _p	54459.74	0.213	3.47	14
O _p -O _{OH}	347464.33	0.213	3.47	14
Ca-O _{OH}	685.92	0.344	0.00	14
Ca-O _p	1544.03	0.297	0.00	14
<i>Morse</i>²	<i>D</i> (eV)	<i>r₀</i> (Å)	<i>K_β</i> (eV/Å²)	
O _p -P	1.5799	2.03	1.625	
O _{OH} -H	7.1757	3.18	1.199	
<i>Three-body</i>³	<i>K_θ</i> (eV/Å²)	θ_0 (°)		
O _p -P-O _p angle	8.043	109.47		

Charges: P = +1.6927, O_p = -1.0448, Ca = +1.6647, O_{OH} = -1.8647, H = +1.0000

¹ *Buckingham*: $A \exp(-r/\rho) - Cr^{-6}$

² *Morse*: $D[(1-\exp[-a(r-r_0)])^2 - 1]$, $a = (K_\beta/2D)^{1/2}$

³ *Three-body*: $E = K_\theta (\theta - \theta_0)^2$

Table A.2: Comparison of Experimentally Determined and Computational (Using Table A.1 Force Field Values) Cell Parameters and Fractional Units

	Experimental Values ¹			Simulation Values ²		
	x	y	z	x	y	z
Ca	0.667	0.999	0.750	0.668	0.998	0.748
	0.333	0.499	0.250	0.335	0.497	0.249
	0.254	0.750	0.500	0.247	0.750	0.507
	0.993	0.750	0.120	0.992	0.756	0.123
	0.753	0.750	0.630	0.761	0.750	0.635
OH	0.000	0.460	0.250	0.000	0.426	0.251
O	0.000	0.302	0.250	0.000	0.324	0.250
	0.344	0.430	0.551	0.356	0.440	0.564
	0.742	0.430	0.664	0.747	0.416	0.662
	0.915	0.430	0.036	0.913	0.442	0.027
	0.844	0.750	0.836	0.849	0.740	0.842
	0.122	0.750	0.105	0.120	0.767	0.103
	0.413	0.750	0.224	0.413	0.760	0.224
	0.465	0.750	0.421	0.465	0.736	0.422
	0.485	0.750	0.571	0.487	0.757	0.570
	0.671	0.750	0.343	0.664	0.742	0.339
	0.085	0.930	0.965	0.072	0.917	0.951
	0.258	0.930	0.336	0.277	0.943	0.348
	0.657	0.930	0.449	0.666	0.919	0.454
P	0.601	0.750	0.366	0.598	0.746	0.362
	0.030	0.750	0.964	0.029	0.746	0.966
	0.369	0.750	0.419	0.374	0.755	0.423
Hydroxyapatite	a (nm)	b (nm)	c (nm)	α (deg)	β (deg)	γ (deg)
experimental	16.311	6.847	18.834	90	150.000	90
simulation ³	16.317	6.876	18.840	90	150.003	90

¹ Sudarsanan & Young, 1969 (reference³⁵)

² The average difference between the experimental fractional coordinates and the calculated coordinates is 0.0064 fractional units.

³ Typically, apatite is described with hexagonal symmetry (P6₃/m, $a=b=9.424$ Å, $c=6.879$ Å, $\alpha=\beta=90^\circ$,

$\gamma=120^\circ$)³⁵ with undefined orientation of the hydroxide ions and partial occupancies. Here, hydroxyapatite is described with parallel orientation of the hydroxide ions in one row and opposite orientation in the next. This energetically most favorable setup (no partial occupancies) is described in the monoclinic space group P2₁c. In this new space group setting, the OH groups are parallel to the b axis.

Table A.3: Peptide Charge Assignments Based on Peptide Composition

Peptide	pI	+ charges (a)	- charges (b)	Total Peptide Charge (a+b)
alsssntrtrv	11.1	1	0	+1
altlhpqpldhp	6.0	0	1	-1
apwhlssqysrt	9.9	1	0	+1
gapalstppls	11.1	1	0	+1
gtlseklrdtha	7.8	2	1	+1
hgevprfhavhl	8.1	1	1	0
hhnvhltsqnq	8.1	0	0	0
hnffpetpssgp	5.1	0	1	-1
hnpkamfygvns	9.7	1	0	+1
idtfymstmshs	4.9	0	1	-1
nmnthihkdrpp	10.1	2	1	+1
qnmmspiegvri	6.0	1	1	0
sslgltvssimy	5.9	0	0	0
stlpiphefsre	5.3	1	2	-1
talatsstydp	4.9	0	1	-1
vnysmeiplvps	3.3	0	1	-1
vtkhlnqisqsy	9.7	1	0	+1
wssgmtpdtgap	3.1	0	1	-1
yqtsspakqsvg	9.7	1	0	+1

(a) Positive charges considered from contributions of arginine [r] and lysine [k]

(b) Negative charges considered from contributions of glutamic acid [e] and aspartic acid [d]

Table A.4: Molecular Modeling Results for 19 Phage Display Derived Apatite-Binding Peptides on (001) HA Plane and [010] Step on (001) HA Plane for Both Neutral and Charged Peptides

NEUTRAL PEPTIDES

Adsorption on (001) plane

Rank	Peptide	Peptide Adsorption Energy (kcal/mol)	pI
1	vtkhlnqisqsy*	-336.9	9.7
2	vnysmeiplvps	-304.9	3.3
3	alssssnttrv	-288.1	11.1
4	idtfymstmshs*	-284.4	4.9
5	apwhlssqysrt*	-279.6	9.9
6	gtlseklrdtha	-275.7	7.8
7	talatsstydp	-266.8	4.9
8	hgevprfhavhl	-260.7	8.1
9	nmnthihkdrpp*	-249.5	10.1
10	gapalstpplsr	-247.5	11.1
11	stlpiphefsre*	-239.3	5.3
12	sslgltvssimy*	-233.9	5.9
13	hnpkamfygvns	-231.0	9.7
14	yqtsspakqsvg	-227.5	9.7
15	qnmmspiegvri	-223.2	7.0
16	hhnhlltsgnq	-209.0	8.1
17	hnffpetpssgp	-197.6	5.1
18	wssgmtptdgap	-190.6	3.1
19	althpqpdlhp*	-187.1	6.0

Adsorption on [010] step on (001) plane

Rank	Peptide	Peptide Adsorption Energy (kcal/mol)	pI
1	gtlseklrdtha	-727.9	7.8
2	vnysmeiplvps	-713.9	3.3
3	vtkhlnqisqsy*	-705.6	9.7
4	idtfymstmshs*	-696.5	4.9
5	talatsstydp	-688.0	4.9
6	alssssnttrv	-684.0	11.1
7	althpqpdlhp*	-683.9	6.0
8	apwhlssqysrt*	-680.8	9.9
9	stlpiphefsre*	-677.3	5.3
10	hnffpetpssgp	-657.3	5.1
11	hhnhlltsgnq	-654.8	8.1
12	hgevprfhavhl	-653.6	8.1
13	wssgmtptdgap	-622.1	3.1
14	qnmmspiegvri	-610.7	7.0
15	nmnthihkdrpp*	-598.2	10.1
16	sslgltvssimy*	-590.8	5.9
17	gapalstpplsr	-582.7	11.1
18	yqtsspakqsvg	-569.0	9.7
19	hnpkamfygvns	-564.7	9.7

CHARGED PEPTIDES

Adsorption on (001) plane

Rank	Peptide	Peptide Adsorption Energy (kcal/mol)	pI
1	alssssnttrv	-388.3	11.0
2	stlpiphefsre*	-269.4	5.3
3	idtfymstmshs*	-263.1	4.9
4	talatsstydp	-260.7	4.9
5	althpqpdlhp*	-251.3	6.0
6	apwhlssqysrt*	-248.8	9.8
7	hnffpetpssgp	-239.7	5.1
8	wssgmtptdgap	-212.3	3.1
9	qnmmspiegvri	-205.2	7.0
10	hhnhlltsgnq	-190.5	8.1
11	gapalstpplsr	-179.5	11.0
12	sslgltvssimy*	-178.8	5.9
13	gtlseklrdtha	-173.0	7.8
14	nmnthihkdrpp*	-160.6	10.1
15	vtkhlnqisqsy*	-145.2	9.7
16	hgevprfhavhl	-136.8	8.1
17	hnpkamfygvns	-114.7	9.7
18	yqtsspakqsvg	-113.4	9.7
19	vnysmeiplvps	18.7	3.3

Adsorption on [010] step on (001) plane

Rank	Peptide	Peptide Adsorption Energy (kcal/mol)	pI
1	idtfymstmshs*	-872.0	4.9
2	talatsstydp	-848.7	4.9
3	wssgmtptdgap	-848.3	3.1
4	hnffpetpssgp	-822.7	5.1
5	stlpiphefsre*	-794.8	5.3
6	althpqpdlhp*	-713.4	6.0
7	hhnhlltsgnq	-704.5	8.1
8	hgevprfhavhl	-629.2	8.1
9	qnmmspiegvri	-620.0	7.0
10	sslgltvssimy*	-586.2	5.9
11	apwhlssqysrt*	-545.6	9.8
12	vnysmeiplvps	-507.9	3.3
13	vtkhlnqisqsy*	-495.2	9.7
14	gtlseklrdtha	-471.2	7.8
15	nmnthihkdrpp*	-470.2	10.1
16	hnpkamfygvns	-421.0	9.7
17	yqtsspakqsvg	-419.7	9.7
18	alssssnttrv	-405.8	11.0
19	gapalstpplsr	1.0	11.0

* Phage Sequences with ELISA Data

APPENDIX B

PHAGE DISPLAY AND PEPTIDE PROTOCOLS

Phage Display Modified for Panning on hBMSCs

Phage Display on hBMSCs Protocol

Media and Solutions:

LB Medium - Per liter: 10 g Bacto-Tryptone, 5g yeast extract, 5g NaCl. Autoclave, store at room temperature.

LB/IPTG/Xgal plates - 1 liter LB medium + 15 g/L agar. Autoclave, cool to < 70C, add 1 mL IPTG/Xgal and pour into sterile plates. Store plates at 4C in the dark.

Agarose top - Per liter: 10g Bacto-Tryptone, 5g yeast extract, 5g NaCl, 1 g MgCl₂·6H₂O, 7 g agarose. Autoclave, dispense into 50mL aliquots. Store solid at room temperature and microwave as needed.

Tetracycline Stock - 20mg/mL tetracycline in Ethanol. Store at -20C in the dark. Vortex before using

LB-Tet Plates - 1 liter LB medium + 15 g/L agar. Autoclave, cool to <70C, add 1 mL tetracycline stock and pour into sterile plates. Store plates at 4C in the dark. Do not use if brown or black.

Blocking buffer - 0.1M NaHCO₃ (pH=8.6), 5mg/mL BSA, 0.02% NaN₃. Filter sterilize, store at 4C.

TBS - 50mM Tris-HCl (pH=7.5), 150mM NaCl. Autoclave, store at room temperature.

TBST (Wash buffer) - First Round: TBS + 0.1% (v/v) Tween-20, Second Round: TBS + 0.5% (v/v) Tween-20

TBS with NaN₃ - TBS + 0.02% NaN₃

PEG/NaCl - 20% (w/v) polyethylene glycol-8000, 2.5M NaCl. Autoclave, store at room temperature

Iodide Buffer - 10mM Tris-HCl (pH=8.0), 1mM EDTA, 4M NaI. Store at room temperature in the dark

Streptavidin Stock Solution - Dissolve 1.5mg Lyophilized streptavidin in 1mL 10mM sodium phosphate (pH=7.2), 100mM NaCl, 0.02% NaN₃. Store at 4C or -20C

IPTG/Xgal - Mix 1.25 g IPTG (isopropyl b-D-thiogalactoside) and 1g Xgal (5-Bromo-4-chloro-3-indolyl-b-D-galactosie) in 25mL Dimethyl formamide. Solution can be stored at -20C in the dark.

General Buffer (to elute peptide off substrate) - 0.2M Glycine-HCl (pH=2.2), 1 mg/mL BSA

Tris-HCl (pH=9.1)

Materials Needed:

250 Erlenmeyer flask

Tissue Culture plates (75cm²)

Paper towels

Titer plate shaker, LabLine

24 well plates (3 per run)

6-well plates

Aerosol-resistant, sterile pipet tips (1000uL, 200uL, 10uL)

Sterile culture tubes (125 per run)

Mineralize films 5 Days with 1xmod SBF

Cell Materials:

α-MEM (Minimum Essential Media) Gibco #12561

P/S (0.25% Penicillin-Streptomycin) Gibco #15140

FBS (Fetal Bovine Serum) Gibco #

BSA (Bovine Serum Albumin) Sigma #

PBS (Phosphate Buffer Solution, pH 7.4) Gibco #10010

Alpha-MEM with 20% FBS + 1% P/S

Alpha-MEM with 20% FBS + 1% P/S + 10^{-8} M Dexamethasone + 10^{-4} M Ascorbic Acid

Alpha-MEM with 0.1% BSA

Sterile 6-well plates

T-25 flasks

Sterile Millipore containers w/vacuum filter

Bringing up cells:

1. Bring up frozen hBMSC in osteogenic media in 2 T-25 tissue culture flasks.
2. After 1.5 days, switch media to normal alpha-MEM media
3. Passage cells 1:3 (so 2 T-25 → 4 T-25 (in normal media) and 2 6-well dishes (10,000 cells seeded per well)
 - a. For all T-25 continue to use normal alpha-MEM media
 - b. For **one** 6-well dish use normal alpha-MEM media
 - c. For **one** 6-well dish use osteogenic media
4. Allow cells to grow and/or begin differentiation for at least 6 days.
5. When cells in T-25 have reached confluence, freeze 3 T-25 flasks down in freezing media.
6. After cells are ~80-90% confluent from step #4, prep for Day One.

Groups:

- 1) Prescreen against HA → Introduce supernate to undifferentiated cells
- 2) Prescreen against HA → Prescreen #2 against differentiated cells → Introduce supernate to undifferentiated cells
- 3) Streptavidin control incubated at 37C during phage binding (but without any introduction of media)

Day One

1. Incubate HA disks & control overnight at 4C in a humidified container (a sealable plastic box lined with damp paper towels). Store plates until needed. Incubated in 1.5mL ddH₂O for films. Use carbon tab to “glue” samples to bottom of well.
 - a. Streptavidin control solution: 4.2mL 0.1M NaHCO₃ + 300uL of streptavidin stock (1.5mg/mL).
2. Streak out 2 plates ER2738 from the included glycerol culture onto an LB-Tet plate. Invert and incubate at 37C overnight and store wrapped with parafilm at 4C in the dark for a maximum of 1 month.

Day Two

1. Inoculate 10mL LB medium with ER2738. This is the plating culture for titering. Incubate at 37C with vigorous shaking. Takes ~3hrs in past to get to OD~0.5.
 - a. If amplifying eluted phage on the same day, inoculate 20mL LB medium in a 250mL Erlenmeyer flask PER SAMPLE. **Do not use a 50mL tube.** Can leave on bench until ready to use. Can shake for ~15min prior to adding phage.
2. Get ice.
3. Blocking step HA & control
 - a. For HA & control: Pour off the coating solution from each plate and firmly slap it face down onto a clean paper towel to remove residual solution. Fill each plate or well completely with Blocking buffer*. Incubate at least 1 hour at 4C.
 - i. * - Control blocking solution has 0.1ug/mL streptavidin [8uL of 100ug/mL from control initial solution + 8mL of blocking buffer]
4. Discard the blocking solution for HA & control. Wash each plate rapidly 6X with TBST (0.1%). Coat bottom and sides of plate or well by swirling, pour off

the solution, and slap the plate face down on a clean paper towel each time. Work quickly to avoid drying out plates.

5. Introduction of phage for Prescreen #1:
 - a. Dilute 2×10^{11} phage (10uL of original library) with 1mL TBST. Pipet onto HA & control and rock gently (speed 2) for 40 minutes at RT. (30uL phage + 3mL of TBST in 15 mL tube)
 - b. Recover supernate and label.
6. Blocking step for cells (start after phage is introduced to HA & control)
 - a. For cells: Wash differentiated cells grown in osteogenic media 2x with PBS. Incubate these cells with 1mL of alpha-MEM containing 0.1% BSA for 30min at 37C. (2mL Blocking Buffer + 48mL alpha-MEM media = blocking buffer for cells)

For sample that only gets Prescreen #1, continue to step # 8. For Streptavidin control, continue to step #9.

7. Introduction of phage for Prescreen #2:
 - a. Add recovered supernate from HA in step #5 to media containing alpha-MEM with 0.1% BSA on differentiated cells.
 - b. Incubate with gentle agitation for 1 hour at 37C.
 - c. Recover supernate, rinse differentiated cells 1x with 1mL PBS and add this to supernate
 - d. Centrifuge supernate for 10min at 2000g.
 - e. Transfer supernate to a new tube and label
8. Prep Undifferentiated Cells for Phage (2 wells):
 - a. Wash undifferentiated cells in 6-well plates 2x with PBS
 - b. Incubate undifferentiated cells with 1mL of Alpha-MEM with 0.1% BSA[WITHOUT FBS!!] for 30min-1hour at 37C in 5%CO₂.
 - c. Add recovered supernate from HA or Prescreen #2.
 - d. Incubate for 1 hour
9. Discarding Phage:

For control:

- a. Discard nonbinding phage by pouring off and slapping plate face-down onto a clean paper towel.
- b. Wash plates 10X with TBST (0.1%) rapidly Coat bottom and sides of plate or well by swirling, pour off the solution, and slap the plate face down on a clean paper towel each time to prevent cross-contamination. Work quickly to avoid drying out plates.
- c. Elute control with 0.1mM biotin in TBS for **30min**. Do not have to neutralize the control sample. [Biotin solution to elute control: 30uL Biotin stock in 3mL of TBS]

For cells:

- d. Discard supernatant on undifferentiated cells and wash 5x with cold PBS.
- e. Elute bound phage with 1mL of general buffer (Glycine/HCl pH=2.2, 1mg/mL BSA). Rock gently for no more than 10 minutes at RT, Pipet eluate into a microcentrifuge tube.
- f. Neutralize with 150uL 1 M Tris-HCl (pH-9.1). Keep on ice until tittered.
- g. (Optional) Wash cells 2 more x with PBS. Lyse cells in 1mL of 30mM Tris, pH 8, 1mMEDTA for 1 hour on ice to recover cell-associated phage fraction. Set aside phage fraction recovered from cells.

10. Amplification of Phage:

- a. Titer a small amount of the eluate (~1uL) from Groups 1, 2 & 3. [for groups 2 & 3 only amplify the cell surface phage]. Plaques from the first or second round eluate tittering can be sequenced if desired.
- b. Check the inoculated LB media to see if it is at mid-log phase ($OD_{600} \sim 0.5$)
- c. While cells are growing, melt Agarose Top in microwave and dispense 3mL into sterile culture tubes, one per expected dilution. Equilibrate tubes at 55C in water bath until ready for use. Microwave on Power 2 for 2 min. Pre-warm 1 LB/IPTG/Xgal plate per expected dilution at 37C in incubator until ready to use.

- d. Prepare 10-fold dilutions of phage in LB. Use a fresh pipet tip for each dilution.
- i. Unamplified panning eluates: 10^1 - 10^4 for control, $10^2 - 10^5$ for mineral film, HA disk, and TCPS.

	LB	Eluate	
$1:10^1$	18uL	2uL	
$1:10^2$	198uL	2uL	A
$1:10^3$	18uL	2uL A	
$1:10^4$	99uL	1uL A	B
$1:10^5$	18uL	2uL B	
$1:10^6$	99uL	1uL B	

- e. Once culture has reached mid-log phase, dispense 200uL culture into microfuge tubes, 1 for each phage dilution.
- f. Add 10uL of each dilution to each tube, vortex quickly, and incubate at RT for 5min. Microwave agarose on Power 2 for 2 minutes during the 5 min. incubation period.
- g. Lay out a couple of bench pads to keep the counter top warm. Else, the agar will clump. Work with no more than 4 plates at a time.
- h. One at a time, transfer the infected cells to a culture tube containing 45C Agarose Top, vortex quickly, and IMMEDIATELY pour onto a pre-warmed LB/IPTG/Xgal plate. Spread Agarose top by tilting plate. If plates come out clumpy, the agarose was not heated thoroughly.
- i. Allow plates to cool 5 minutes, invert, and incubate overnight at 37C.
- j. Inspect plates and count plaques on plates having $\sim 10^2$ plaques. Multiply each number by the dilution factor for that plate to get the phage titer in plaque forming units (pfu) per 10uL.

11. The rest of the eluate should be amplified: Add the eluate to the 20mL ER2738 culture (should be early log at this point) and incubate at 37C with vigorous shaking for 4.5 hours.
12. Turn on Ultra Centrifuge before leaving – after incubating eluate to be amplified so that the centrifuge is cold after 4.5 hours.
13. Transfer the culture to a centrifuge tube and spin 10 minutes at 10000rpm (Sorvall SS-34, Beckman JA-17, or equivalent) at 4C. Transfer the supernatant to a fresh tube and respin.
14. Pipet the upper 80% of the supernatant (~16mL) to a fresh tube and add 1/6 volume of PEG/NaCl. Allow phage to precipitate at 4C for at least 60 minutes, preferably overnight. Added 2.6mL of PEG/NaCl. Make sure you mix the PEG solution before using it.

Day Three

1. Spin PEG precipitation 15 minutes at 10,000rpm at 4C. Decant supernatant, re-spin briefly, and remove residual supernatant with a pipette. Will barely be able to see pellet.
2. Suspend the pellet in 1mL TBS. Transfer the suspension to a microcentrifuge tube and spin for 5 minutes at 10,000rpm to 4C to pellet residual cells.
3. Transfer the supernatant to a fresh microcentrifuge tube and re-precipitate with 1/6 volume of PEG/NaCl (~17uL). Incubate on ice for 60 minutes. Microcentrifuge for 10 minutes at 4C. Discard supernatant, re-spin briefly, and remove residual supernatant with a micropipet.
4. Suspend the pellet in 200uL TBS, 0.02% NaN₃. Microcentrifuge for 1 minute to pellet any remaining insoluble matter. Transfer the supernatant to a fresh tube. THIS IS THE AMPLIFIED ELUATE.
5. Titer the amplified eluate on LB/IPTG/Xgal plates. Titer a small amount of the eluate (~1uL). Inoculate 10mL LB w/ ER2738
 - a. Check the inoculated LB media to see if it is at mid-log phase (OD₆₀₀~0.5)

- b. While cells are growing, melt Agarose Top in microwave and dispense 3mL into sterile culture tubes, one per expected dilution. Equilibrate tubes at 45C in water bath until ready for use.
- c. Pre-warm 1 LB/IPTG/Xgal plate per expected dilution at 37C in incubator until ready to use.
- d. Prepare 10-fold dilutions of phage in LB. Use a fresh pipet tip for each dilution.
 - i. Amplified phage culture supernatant: 10^8 - 10^{11} (Mineral – 10^9 - 10^{12} , Control 10^9 – 10^{11}). Be sure to vortex well.

	LB	Eluate	
$1:10^2$	99uL	1uL	A
$1:10^4$	99uL	1uL A	B
$1:10^6$	99uL	1uL B	C
$1:10^7$	18uL	2uL C	
$1:10^8$	99uL	1uL C	D
$1:10^9$	18uL	2uL D	
$1:10^{10}$	99uL	1uL D	E
$1:10^{11}$	18uL	2uL E	
$1:10^{12}$	99uL	1uL E	

- e. Once culture has reached mid-log phase, dispense 200uL culture into microfuge tubes, 1 for each phage dilution.
- f. Add 10uL of each dilution to each tube, vortex quickly, and incubate at RT for 1-5min.
- g. Lay out a couple of bench pads to keep the counter top warm. Else, the agar will clump. Work with no more than 4 plates at a time.
- h. One at a time, transfer the infected cells to a culture tube containing 45C Agarose Top, vortex quickly, and IMMEDIATELY pour onto a pre-warmed LB/IPTG/Xgal plate. Spread Agarose top by tilting plate.

- i. Allow plates to cool 5 minutes, invert, and incubate overnight at 37C.
 - j. Inspect plates and count plaques on plates having $\sim 10^2$ plaques. Multiply each number by the dilution factor for that plate to get the phage titer in plaque forming units (pfu) per 10uL.
6. Store plates at 4C
7. Prep another mineralized sample and control for round two.

Day Four

1. Count blue plaques and determine the phage titer. Use this value to calculate an input volume corresponding to 2×10^{11} pfu. If the titer is too low, succeeding rounds of panning can be carried out with as little as 10^9 pfu of input phage. [Last run used all but 10uL because the amplification was low]
Amplified phage in this step has been consistently low. Usually use most of the amplified phage eluate (all but 10uL for freezing).
15. Inoculate 10mL LB medium with ER2738. This is the plating culture for titering. Incubate at 37C with vigorous shaking. Takes ~ 3 hrs in past to get to OD ~ 0.5 .
 - a. If amplifying eluted phage on the same day, inoculate 20mL LB medium in a 250mL Erlenmeyer flask PER SAMPLE. **Do not use a 50mL tube.** Can leave on bench until ready to use. Can shake for ~ 15 min prior to adding phage.
16. Get ice.
17. Blocking step HA & control
 - a. For HA & control: Pour off the coating solution from each plate and firmly slap it face down onto a clean paper towel to remove residual solution. Fill each plate or well completely with Blocking buffer*. Incubate at least 1 hour at 4C.
 - i. * - Control blocking solution has 0.1ug/mL streptavidin [8uL of 100ug/mL from control initial solution + 8mL of blocking buffer]

18. Discard the blocking solution for HA & control. Wash each plate rapidly 6X with TBST (0.1%). Coat bottom and sides of plate or well by swirling, pour off the solution, and slap the plate face down on a clean paper towel each time. Work quickly to avoid drying out plates.
19. Introduction of phage for Prescreen #1:
 - a. Dilute 2×10^{11} phage (10uL of original library) with 1mL TBST. Pipet onto HA & control and rock gently (speed 2) for 40 minutes at RT. (30uL phage + 3mL of TBST in 15 mL tube)
 - b. Recover supernate and label.
20. Blocking step for cells (start after phage is introduced to HA & control)
 - a. For cells: Wash differentiated cells grown in osteogenic media 2x with PBS. Incubate these cells with 1mL of alpha-MEM containing 0.1% BSA for 30min at 37C.

For sample that only gets Prescreen #1, continue to step # 8. For Streptavidin control, continue to step .

21. Introduction of phage for Prescreen #2:
 - a. Add recovered supernate from HA in step #5 to media containing alpha-MEM with 0.1% BSA on differentiated cells.
 - b. Incubate with gentle agitation for 1 hour at 37C.
 - c. Recover supernate, rinse differentiated cells 1x with 1mL PBS and add this to supernate
 - d. Centrifuge supernate for 10min at 2000g.
22. Prep Undifferentiated Cells for Phage:
 - a. Wash undifferentiated cells in 6-well plates 2x with PBS
 - b. Incubate undifferentiated cells with 1mL of Alpha-MEM with 0.1% BSA[WITHOUT FBS!!] for 30min-1hour at 37C in 5%CO₂.
23. Discarding Phage:

For control:

- a. Discard nonbinding phage by pouring off and slapping plate face-down onto a clean paper towel.
- b. Wash plates 10X with TBST (0.1%) rapidly Coat bottom and sides of plate or well by swirling, pour off the solution, and slap the plate face down on a clean paper towel each time to prevent cross-contamination. Work quickly to avoid drying out plates.
- c. Elute control with 0.1mM biotin in TBS for **30min**. Do not have to neutralize the control sample. [Biotin solution to elute control: 30uL Biotin stock in 3mL of TBS]

For cells:

- d. Discard supernatant on undifferentiated cells and wash 5x with cold PBS.
- e. Elute bound phage with 1mL of general buffer (Glycine/HCl pH=2.2, 1mg/mL BSA). Rock gently for no more than 10 minutes at RT, Pipet eluate into a microcentrifuge tube.
- f. Neutralize with 150uL 1 M Tris-HCl (pH-9.1). Keep on ice until tittered.
- g. Wash cells 2 more x with PBS. Lyse cells in 1mL of 30mM Tris, pH 8, 1mMEDTA for 1 hour on ice to recover cell-associated phage fraction. Set aside phage fraction recovered from cells.

24. Amplification of Phage:

- a. Titer a small amount of the eluate (~1uL) from Groups 1, 2 & 3. [for groups 2 & 3 only amplify the cell surface phage]. Plaques from the first or second round eluate titering can be sequenced if desired.
- b. Check the inoculated LB media to see if it is at mid-log phase ($OD_{600} \sim 0.5$)
- c. While cells are growing, melt Agarose Top in microwave and dispense 3mL into sterile culture tubes, one per expected dilution. Equilibrate tubes at 55C in water bath until ready for use. Microwave on Power 2 for 2 min. Pre-warm 1 LB/IPTG/Xgal plate per expected dilution at 37C in incubator until ready to use.

- d. Prepare 10-fold dilutions of phage in LB. Use a fresh pipet tip for each dilution.
- i. Unamplified panning eluates: 10^1 - 10^4 for control, $10^2 - 10^5$ for mineral film, HA disk, and TCPS.

	LB	Eluate	
$1:10^1$	18uL	2uL	
$1:10^2$	198uL	2uL	A
$1:10^3$	18uL	2uL A	
$1:10^4$	99uL	1uL A	B
$1:10^5$	18uL	2uL B	
$1:10^6$	99uL	1uL B	

- e. Once culture has reached mid-log phase, dispense 200uL culture into microfuge tubes, 1 for each phage dilution.
- f. Add 10uL of each dilution to each tube, vortex quickly, and incubate at RT for 5min. Microwave agarose on Power 2 for 2 minutes during the 5 min. incubation period.
- g. Lay out a couple of bench pads to keep the counter top warm. Else, the agar will clump. Work with no more than 4 plates at a time.
- h. One at a time, transfer the infected cells to a culture tube containing 45C Agarose Top, vortex quickly, and IMMEDIATELY pour onto a pre-warmed LB/IPTG/Xgal plate. Spread Agarose top by tilting plate. If plates come out clumpy, the agarose was not heated thoroughly.
- i. Allow plates to cool 5 minutes, invert, and incubate overnight at 37C.
- j. Inspect plates and count plaques on plates having $\sim 10^2$ plaques. Multiply each number by the dilution factor for that plate to get the phage titer in plaque forming units (pfu) per 10uL.

25. The rest of the eluate should be amplified: Add the eluate to the 20mL ER2738 culture (should be early log at this point) and incubate at 37C with vigorous shaking for 4.5 hours.
26. Turn on Ultra Centrifuge before leaving – after incubating eluate to be amplified so that the centrifuge is cold after 4.5 hours.
27. Transfer the culture to a centrifuge tube and spin 10 minutes at 10000rpm (Sorvall SS-34, Beckman JA-17, or equivalent) at 4C. Transfer the supernatant to a fresh tube and respin.
28. Pipet the upper 80% of the supernatant (~16mL) to a fresh tube and add 1/6 volume of PEG/NaCl. Allow phage to precipitate at 4C for at least 60 minutes, preferably overnight. Added 2.6mL of PEG/NaCl. Make sure you mix the PEG solution before using it.

Day Five

8. Spin PEG precipitation 15 minutes at 10,000rpm at 4C. Decant supernatant, re-spin briefly, and remove residual supernatant with a pipette. Will barely be able to see pellet.
9. Suspend the pellet in 1mL TBS. Transfer the suspension to a microcentrifuge tube and spin for 5 minutes at 10,000rpm to 4C to pellet residual cells.
10. Transfer the supernatant to a fresh microcentrifuge tube and re-precipitate with 1/6 volume of PEG/NaCl (~17uL). Incubate on ice for 60 minutes. Microcentrifuge for 10 minutes at 4C. Discard supernatant, re-spin briefly, and remove residual supernatant with a micropipet.
11. Suspend the pellet in 200uL TBS, 0.02% NaN₃. Microcentrifuge for 1 minute to pellet any remaining insoluble matter. Transfer the supernatant to a fresh tube. THIS IS THE AMPLIFIED ELUATE.
12. Titer the amplified eluate on LB/IPTG/Xgal plates. Titer a small amount of the eluate (~1uL). Inoculate 10mL LB w/ ER2738
 - a. Check the inoculated LB media to see if it is at mid-log phase (OD₆₀₀~0.5)

- b. While cells are growing, melt Agarose Top in microwave and dispense 3mL into sterile culture tubes, one per expected dilution. Equilibrate tubes at 45C in water bath until ready for use.
- c. Pre-warm 1 LB/IPTG/Xgal plate per expected dilution at 37C in incubator until ready to use.
- d. Prepare 10-fold dilutions of phage in LB. Use a fresh pipet tip for each dilution.
 - i. Amplified phage culture supernatant: 10^8 - 10^{11} (Mineral – 10^9 - 10^{12} , Control 10^9 – 10^{11}). Be sure to vortex well.

	LB	Eluate	
$1:10^2$	99uL	1uL	A
$1:10^4$	99uL	1uL A	B
$1:10^6$	99uL	1uL B	C
$1:10^7$	18uL	2uL C	
$1:10^8$	99uL	1uL C	D
$1:10^9$	18uL	2uL D	
$1:10^{10}$	99uL	1uL D	E
$1:10^{11}$	18uL	2uL E	
$1:10^{12}$	99uL	1uL E	

- e. Once culture has reached mid-log phase, dispense 200uL culture into microfuge tubes, 1 for each phage dilution.
- f. Add 10uL of each dilution to each tube, vortex quickly, and incubate at RT for 1-5min.
- g. Lay out a couple of bench pads to keep the counter top warm. Else, the agar will clump. Work with no more than 4 plates at a time.
- h. One at a time, transfer the infected cells to a culture tube containing 45C Agarose Top, vortex quickly, and IMMEDIATELY pour onto a pre-warmed LB/IPTG/Xgal plate. Spread Agarose top by tilting plate.

- i. Allow plates to cool 5 minutes, invert, and incubate overnight at 37C.
- j. Inspect plates and count plaques on plates having $\sim 10^2$ plaques. Multiply each number by the dilution factor for that plate to get the phage titer in plaque forming units (pfu) per 10uL.

13. Store plates at 4C

Prep samples and control for round three.

Day Six

1. Carry out a third round of panning using 2×10^{11} pfu of the second round amplified eluate as input phage, again using 0.5% Tween in the wash steps.
2. Count blue plaques and determine the phage titer. Use this value to calculate an input volume corresponding to 2×10^{11} pfu. If the titer is too low, succeeding rounds of panning can be carried out with as little as 10^9 pfu of input phage.
3. Inoculate 10mL LB medium with a single clone of ER2738. This is the plating culture for titering. Incubate at 37C with vigorous shaking.
 - a. If amplifying eluted phage on the same day, inoculate 20mL LB medium in a 250mL Erlenmeyer flask. **Do not use a 50mL tube.** Incubate at 37C with vigorous shaking.
4. Pour off the coating solution from each plate and firmly slap it face down onto a clean paper towel to remove residual solution. Fill each plate or well completely with Blocking buffer. Incubate at least 1 hour at 4C.
5. Discard the blocking solution as in step 2. Wash each plate rapidly 6X with TBST (0.5%). Coat bottom and sides of plate or well by swirling, pour off the solution, and slap the plate face down on a clean paper towel each time. Work quickly to avoid drying out plates.
6. Pipet 2×10^{11} pfu of the second round amplified eluate onto coated plate and rock gently for 40 minutes at RT.
7. Discard nonbinding phage by pouring off and slapping plate face-down onto a clean paper towel.

8. Wash plates 10X with TBST (0.5%) rapidly Coat bottom and sides of plate or well by swirling, pour off the solution, and slap the plate face down on a clean paper towel each time to prevent cross-contamination. Work quickly to avoid drying out plates.
9. Elute bound phage with 1mL of general buffer (Glycine/HCl pH=2.2, 1mg/mL BSA). Rock gently for no more than 10 minutes at RT, Pipet eluate into a microcentrifuge tube. Neutralize with 150uL 1 M Tris-HCl (pH-9.1).
10. Titer a small amount of the eluate (~1uL). Plaques from the first or second round eluate titering can be sequenced if desired.
 - a. Check the inoculated LB media to see if it is at mid-log phase ($OD_{600} \sim 0.5$)
 - b. While cells are growing, melt Agarose Top in microwave and dispense 3mL into sterile culture tubes, one per expected dilution. Equilibrate tubes at 45C in water bath until ready for use.
 - c. Pre-warm 1 LB/IPTG/Xgal plate per expected dilution at 37C in incubator until ready to use.
 - d. Prepare 10-fold dilutions of phage in LB. Use a fresh pipet tip for each dilution.
 - i. Unamplified panning eluates: 10^1 - 10^4
 - e. Once culture has reached mid-log phase, dispense 200uL culture into microfuge tubes, 1 for each phage dilution.
 - f. Add 10uL of each dilution to each tube, vortex quickly, and incubate at RT for 1-5min.
 - g. Lay out a couple of bench pads to keep the counter top warm. Else, the agar will clump. Work with no more than 4 plates at a time.
 - h. One at a time, transfer the infected cells to a culture tube containing 45C Agarose Top, vortex quickly, and IMMEDIATELY pour onto a pre-warmed LB/IPTG/Xgal plate. Spread Agarose top by tilting plate.
 - i. Allow plates to cool 5 minutes, invert, and incubate overnight at 37C.

- j. Inspect plates and count plaques on plates having $\sim 10^2$ plaques. Multiply each number by the dilution factor for that plate to get the phage titer in plaque forming units (pfu) per 10uL.
11. Time the procedure so that the plates are incubated no longer than 18 hours. Store the remaining eluate at 4C.
12. Set up an overnight culture of ER2738 in LB-Tet from a colony, not by diluting the plating culture. Shake at 37C

Day Seven – Plaque amplification

1. Dilute the ER2738 overnight culture 1:100 in LB. Dispense 1mL dilute culture into culture tubes, one for each clone to be characterized. Stab 75 clones from the third round for mineral film, HA disk, and TCPS. Stab 20 clones from the streptavidin control sample.
2. Using a sterile pipet tip, stab a blue plaque and transfer to a tube containing diluted culture. **IMPORTANT: pick plaques from plates having no more than ~100 plaques. This will insure that each plaque contains a single DNA sequence.**
[Can only fit ~100 samples on shaker at one time, so have to do 2 batches]
3. Incubate tubes at 37C with shaking for 4.5-5 hours (NO LONGER!)
4. Transfer cultures to microcentrifuge tubes, centrifuge 30 seconds.
 - a. **If immediately going to prepare samples for rapid purification of sequencing templates for DNA sequencing, follow the inset letters. If not, continue to step 5. Takes about 1 hour for 24 samples [1.5 hours if you do 48 samples simultaneously].**
 - b. Transfer 500uL of the phage-containing supernatant to a fresh microfuge tube.
 - c. Add 200uL PEG/NaCl. Invert to mix, and let stand at RT for 10 minutes
 - d. Centrifuge 10 minutes, discard supernatant.
 - e. Re-spin briefly. Carefully pipet away any remaining supernatant.

- f. Suspend pellet thoroughly in 100uL Iodide Buffer and add 250uL ethanol. Incubate 10 minutes at RT. Short incubation at RT will preferentially precipitate single-stranded DNA, leaving most phage protein in solution.
 - g. Spin 10 minutes, discard supernatant. Wash pellet in 70% ethanol, dry briefly under a vacuum.
 - h. Suspend pellet in 20uL RNase-DNase free H₂O.
 - i. 5uL of the resuspended template should be sufficient for manual or automated cycle sequencing with dye-labeled dideoxynucleotides. More or less template may be required depending on the sequencing method used.
5. Transfer the supernatant to a fresh tube and re-spin. Using a pipet, transfer the upper 80% of the supernatant to a fresh tube. THIS IS THE AMPLIFIED PHAGE STOCK AND CAN BE STORED AT 4C FOR SEVERAL WEEKS WITH LITTLE LOSS OF TITER. For long term storage, dilute 1:1 with sterile glycerol and store at -20C.

Notes: Conversion factor for UV Spec: $A_{260} @ 1.000 = 33 \text{ ug/mL}$ for ssDNA.

Factor on UV spec to read OD is 9.3×10^8 .

Preparing DNA for DNA Core From Phage Display Library Kit 7-mer peptide (New England Biolabs) DNA Sequencing at DNA Core 2560 MSRBII

1. Transfer 500uL of the phage-containing supernatant to a fresh microfuge tube.
2. Add 200uL PEG/NaCl. Invert to mix, and let stand at RT for 10 minutes
3. Centrifuge 10 minutes, discard supernatant.
4. Re-spin briefly. Carefully pipet away any remaining supernatant.
5. Suspend pellet thoroughly in 100uL Iodide Buffer and add 250uL ethanol. Incubate 10 minutes at RT. Short incubation at RT will preferentially precipitate single-stranded DNA, leaving most phage protein in solution.

6. Spin 10 minutes, discard supernatant. Wash pellet in 70% ethanol, dry briefly under a vacuum.
7. Suspend pellet in 30uL TE buffer [10mM Tris-HCl (pH=8.0), 1mM EDTA].
8. 5uL of the resuspended template should be sufficient for manual or automated cycle sequencing with dye-labeled dideoxynucleotides. More or less template may be required depending on the sequencing method used.

General Notes: First try submitting prepared ssDNA for control and mineral (10 uL of each sample at 100ng/uL) [control: 2 samples, mineral: 5 samples]. DNA Core requests 10 uL of primer per sample, however will only submit 20uL of primer (1pmol/uL) A good time to stop if the experiment cannot be finished seven days in a row is at the PEG/NaCl precipitation. The phage is very stable at this point.

Peptide Adsorption Standard Curves Used in Peptide Quantification

UV Spectroscopy was determined the most feasible method of peptide detection for the adsorption studies. A standard curve for each peptide was determined at A205nm or A220nm. The peptides containing tryptophan (W), tyrosine (Y), or phenylalanine (F) were also read at A280nm, A274nm, and A257, respectively. The standard curves were forced through zero, and the best non-linear fit was determined for each curve. The initial peptide concentration introduced to the substrates was also read for each adsorption experiment conducted. An aliquot of the initial peptide concentration was sent for amino acid analysis, and the results were used to adjust the standard curve accordingly. Peptide standard curves are presented for short peptides from Chapter Two [A (Figure B.1), E (Figure B.2), S (Figure B.3), and V (Figure B.4)], long peptides from Chapter Three [D-VTK (Figure B.5), L-VTK (Figure B.6), RGDV (Figure B.7), RGEV (Figure B.8), E (Figure B.9)], and the phosphorylated peptide from Appendix C [VTK-phos (Figure B.10)].

Other options of peptide quantification include amino acid analysis (Dee et al., 1998; Fujisawa et al., 1997), radiolabeling of the amino acid tyrosine (Hern and Hubbell,

1998), fluorescent tagging (Sawyer et al., 2005b), x-ray photoelectron spectroscopy (Rezania et al., 1997), or protein quantification kits (e.g. bicinchoninic acid).

Developed Protocols for Peptide Adsorption and Cell Attachment

Peptide Adsorption Protocol

Materials Needed:

Millipore H₂O (ddH₂O)

Trizma buffer, sterile filtered (50mM, pH=7.5, Sigma pre-crystal packet #T7818)

24-well sterile tissue culture dishes

1000 μ L and 200 μ L sterile pipette tips

Polypropylene 1.5mL tubes, autoclaved

Microcuvette for the UV Spectrophotometer (Biorad, Model Smartspec 3000)

Mineralized films (5 Day soak in 1Xmodified SBF)

HA, CA5, and CA10 Disks, sonicated clean and autoclaved (as prepared in methods of Chapters Two and Three)

10mM HCl, sterile filtered

Standard Curve Methods:

1. Reconstitute the peptide in ddH₂O at a concentration of 10mg/mL.
2. Dilute the peptide in Trizma buffer to a concentration of 1 mg/mL to get a working amount of 1.5mL for the standard curve.
3. Perform serial dilutions according to Table B.1.
4. On the UV Spectrometer, run an absorbance curve over the wavelength range (200-300nm) to determine the optimum wavelength(s) to read each peptide.
5. After determining the optimum wavelength(s) to quantify the peptide with, read the standard curve samples, each sample in duplicate.
6. Plot the standard curve and use to determine the concentration of adsorbed peptide in the experiment.

Peptide Adsorption Methods:

1. Soak mineralized films in Trizma buffer overnight at 4°C in a humidifier box (plastic Tupperware container with wet lining paper towels).
2. Determine working concentration of peptide in solution. Use reconstituted peptide from Standard Curve Methods step 1 and dilute the peptide in Trizma buffer to an initial starting concentration of 750 µg/mL.
3. Soak samples in 1mL peptide solution for 3 hours with gentle agitation (LabLine Titer Plate Shaker at setting 2). Control samples receive 1mL of Trizma buffer devoid of peptide.
4. After 3 hours, transfer peptide solution into labeled polypropylene tubes.
5. Rinse the substrates 1X with Trizma buffer.
6. Demineralize films in 1mL of 10mM HCl solution for 18 hours with agitation (again on Lab-Line Titer Plate Shaker, setting 2-3). Samples should be demineralized in the same 24-well plate that the experiment was run.
7. Read a 100µL aliquot for each sample at the determined absorbances. (A205nm, A220nm). This is an indirect measurement of peptide adsorption. Blank UV Spectrometer with ddH₂O.
8. After 18 hours agitation in 10mM HCl, transfer demineralized peptide solution (1mL) into polypropylene tubes.
9. Read a 100µL aliquot for each sample at the determined absorbances. (A205nm, A220nm). This is the direct measurement of peptide adsorption. Blank UV Spectrometer with 10mM HCl. Use standard curves to determine amount of peptide adsorbed.

Cell Attachment Assay Protocol

Materials Needed:

hBMSCs

Millipore H₂O (ddH₂O)

Trizma buffer, sterile filtered (50mM, pH=7.5, Sigma pre-crystal packet)

24-well sterile tissue culture dishes

15mL sterile tubes

1000 μ L, 200 μ L, 50 μ L, and 10 μ L sterile pipette tips

Polypropylene 1.5mL tubes, autoclaved

Microcuvette for the UV Spectrophotometer (Biorad, Model Smartspec 3000)

Mineralized films (5 Day soak in 1Xmodified SBF)

HA, CA5, and CA10 Disks, sonicated clean and autoclaved (as prepared in methods of Chapters Two and Three)

α -MEM with glutamine and 20%FBS, 1% P/S

α -MEM with glutamine without any supplements

0.25% Trypsin/EDTA solution

Dulbecco's Phosphate Buffer Solution (PBS)

Denatured BSA (dBSA) (1g BSA in 50mL PBS, heat to 80°C and hold for 6 minutes)

WST-1 Premixed Reagent (Clonotech, #630118)

Hemocytometer

70% Ethanol solution

Peptide Adsorption:

1. Follow the Peptide Adsorption Protocol until step #5 (rinse substrates 1X with Trizma)
2. Add 1mL of dBSA per well and let sit without agitation for 1 hour at room temperature.
3. Remove dBSA solution, and rinse each well 1X with PBS.
4. During the dBSA incubation, prepare hBMSCs for seeding.
 - a. Trypsinize appropriate number of flasks with 0.25% Trypsin/EDTA. Incubate cells at 37°C with 5% CO₂ for 2 minutes (2mL Trypsin solution for a T75 flask). Add 2mL of α -MEM with glutamine and 20%FBS, 1% P/S.

- b. Spin the cell solution for 5 minutes at 1000rpm. Resuspend the cells in n mL of α -MEM with glutamine.
 - c. Count cells on hemacytometer. Determine the cell concentration by adding the cell numbers in all four quadrants on the hemacytometer, dividing by 4, and multiplying by $n \times 10^4$. Cell concentration =
$$\left(\frac{A+B+C+D}{4}\right) \times n \text{ mL used to resuspend} \times 10^4$$
5. Prepare two cell solutions: cell seeding solution and cell standard curve solution.
 - a. Cell seeding solution should contain enough cells to seed 5×10^4 cells in 500 μ L of α -MEM with glutamine per well.
 - b. Cell standard curve solution should suspend 5×10^5 cells in 1mL of α -MEM with glutamine in a 1.5mL polypropylene tube.
6. Seed cells on substrates (500 uL per sample; 50,000 cells/film) and let incubate at 37°C with 5% CO₂ for 1 hour.
7. Prepare a cell standard curve in α -MEM with glutamine according to Table B.2.
8. Seed cell standard curve in a 24-well tissue culture plate, n=2 for each cell concentration.
9. After allow cells to adhere for 1 hour at 37°C in 5% CO₂, remove liquid from wells in all samples except standard curve.
10. Centrifuge 24-well dishes upside down in a Eppendorf 5810R or equivalent for 5 minutes at 300rpm.
11. Rinse wells 1X with PBS.
12. Add 500 μ L α -MEM with glutamine per well.
13. Add 50 μ L of WST-1 premixed reagent (CloneTech #630118) to both centrifuged plates and plate with cell standard curve.
14. Allow WST-1 to incubate with cells for 2-3 hours.
15. Transfer 100 μ L to a 96-well plate from each well and read at 420nm on a UV Microplate reader.

General Notes:

When performing the cell attachment assay, it is best to also prepare wells in a separate 24-well dish to monitor α -MEM, α -MEM with WST-1, and n=4 initial seeding concentrations that all the substrates received. Additionally, be sure to prepare enough wells for both BLM and TCPS controls (n=6) that receive the dBSA blocking treatment, but do not have any peptide adsorbed. This background cell attachment varies from day to day, so it is best to run these groups every day the experiment is run.

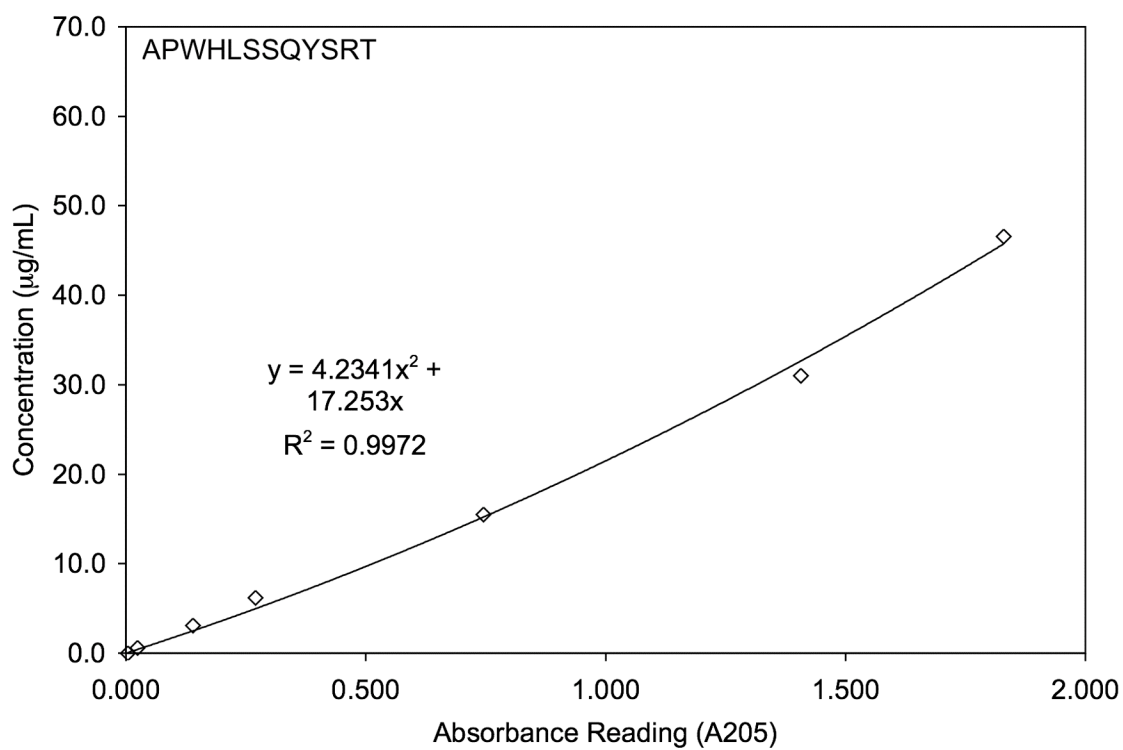


Figure B.1: Standard curve for peptide APWHLSSQYSRT [A] (MW = 1431.7 g/mol) determined via UV spectroscopy at A_{205} .

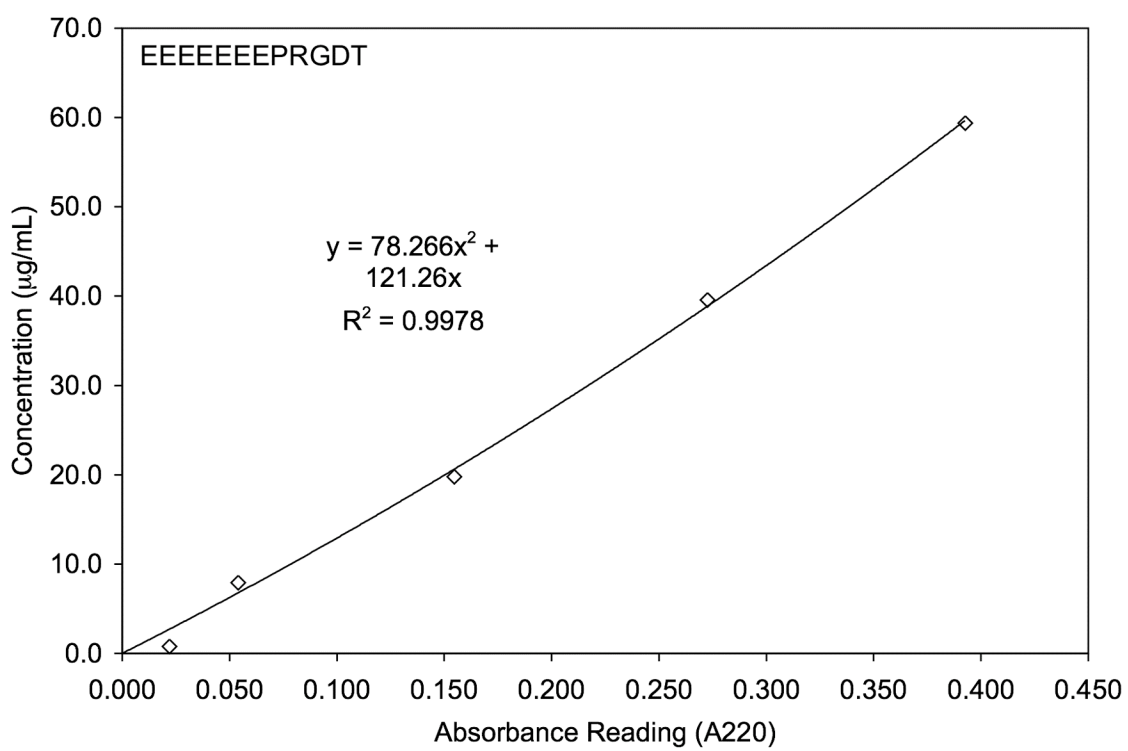


Figure B.2: Standard curve for peptide EEEEEEEPRGDT [E] (MW = 1447.6 g/mol) determined via UV spectroscopy at A220.

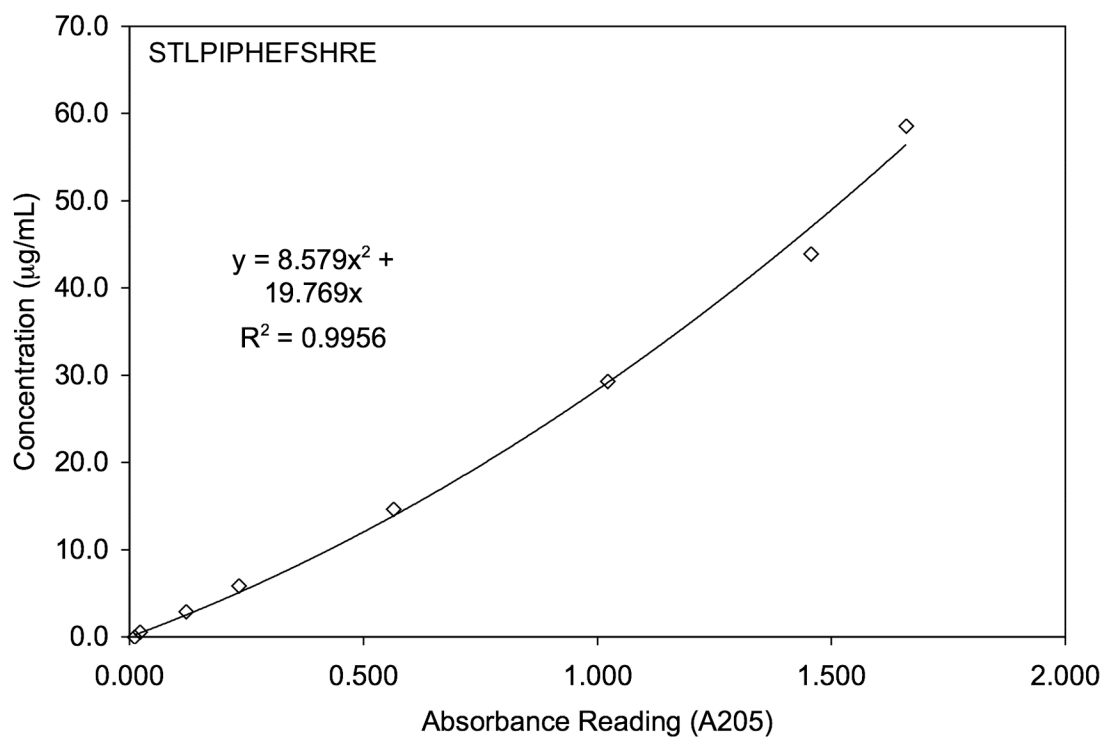


Figure B.3: Standard curve for peptide STLPIPHEFSHRE [S] (MW = 1411.7 g/mol) determined via UV spectroscopy at A205.

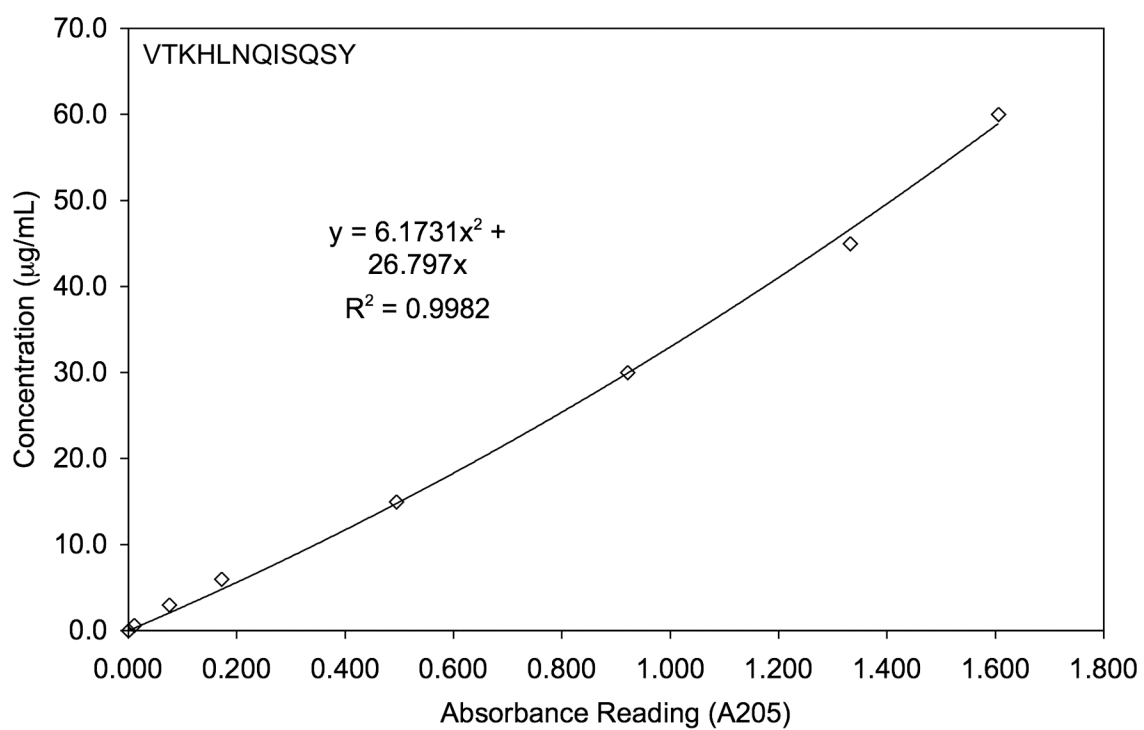


Figure B.4: Standard curve for peptide VTKHLNQISQSY [V] (MW = 1416.7 g/mol) determined via UV spectroscopy at A205.

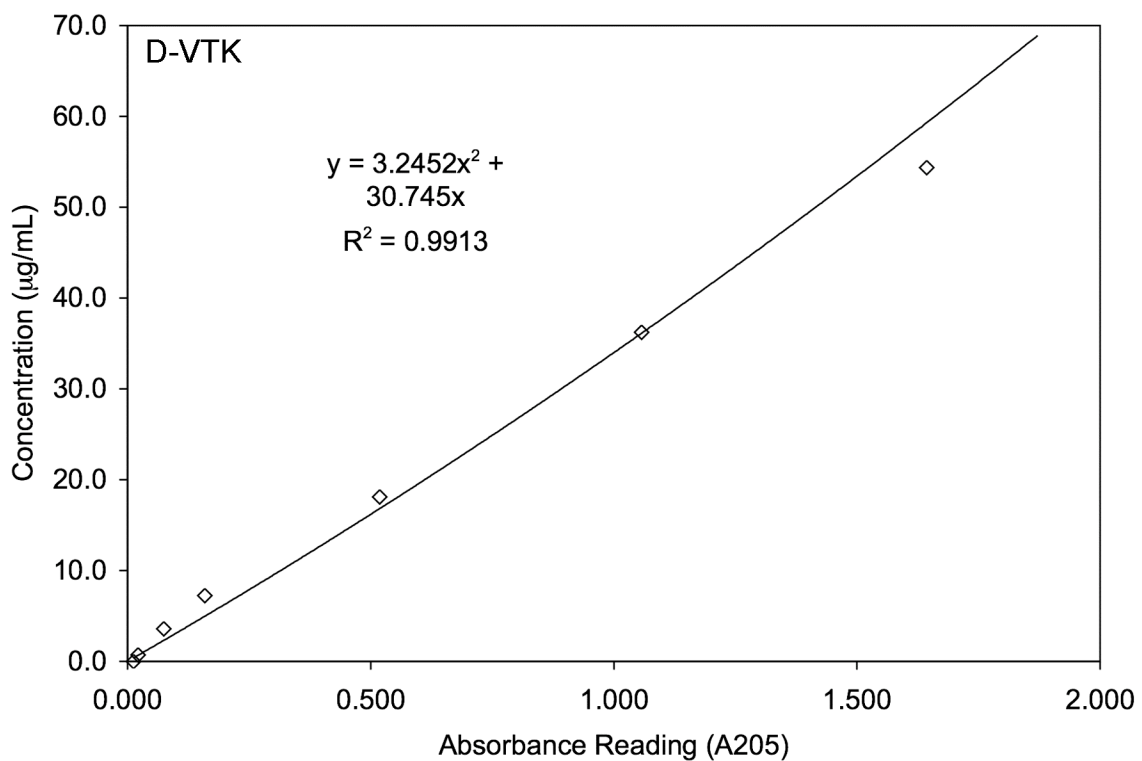


Figure B.5: Standard curve for peptide GGDPIYALSWSGMAGGGSVTKHLNQISQSY (MW = 3081.2 g/mol) determined via UV spectroscopy at A205.

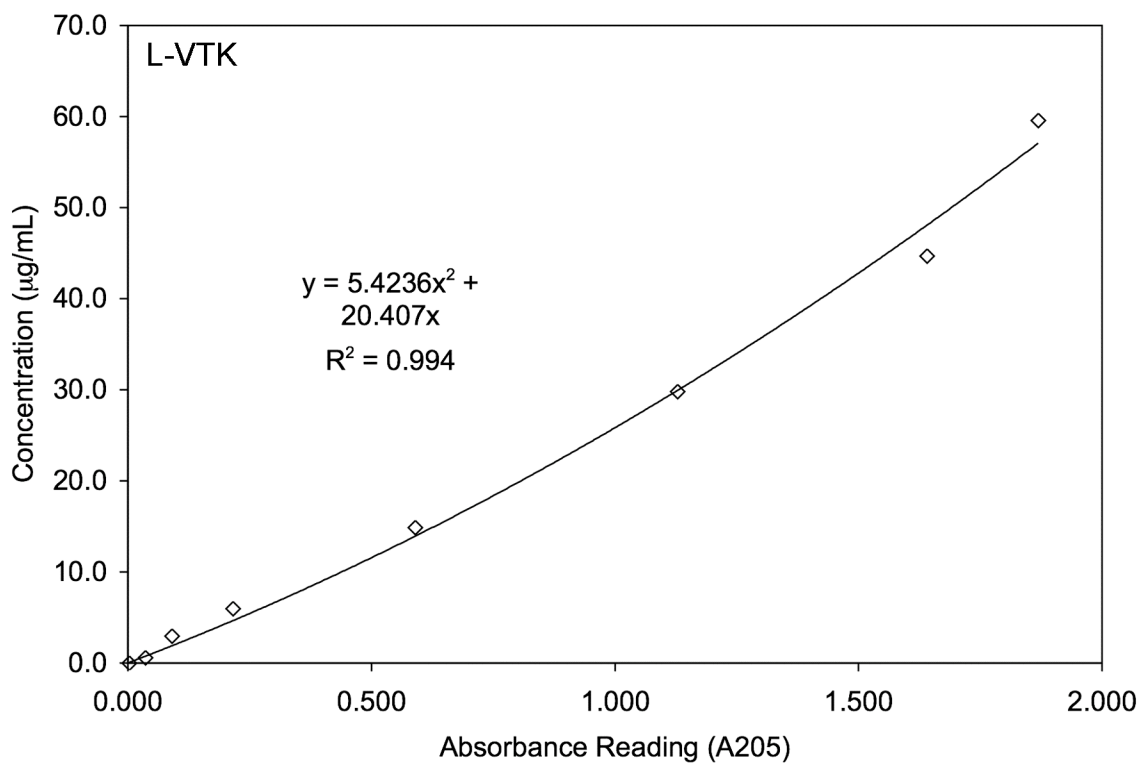


Figure B.6: Standard curve for peptide GLLADTTHHRPWTGGGSVTKHLNQISQSY (MW = 3218.0 g/mol) determined via UV spectroscopy at A205.

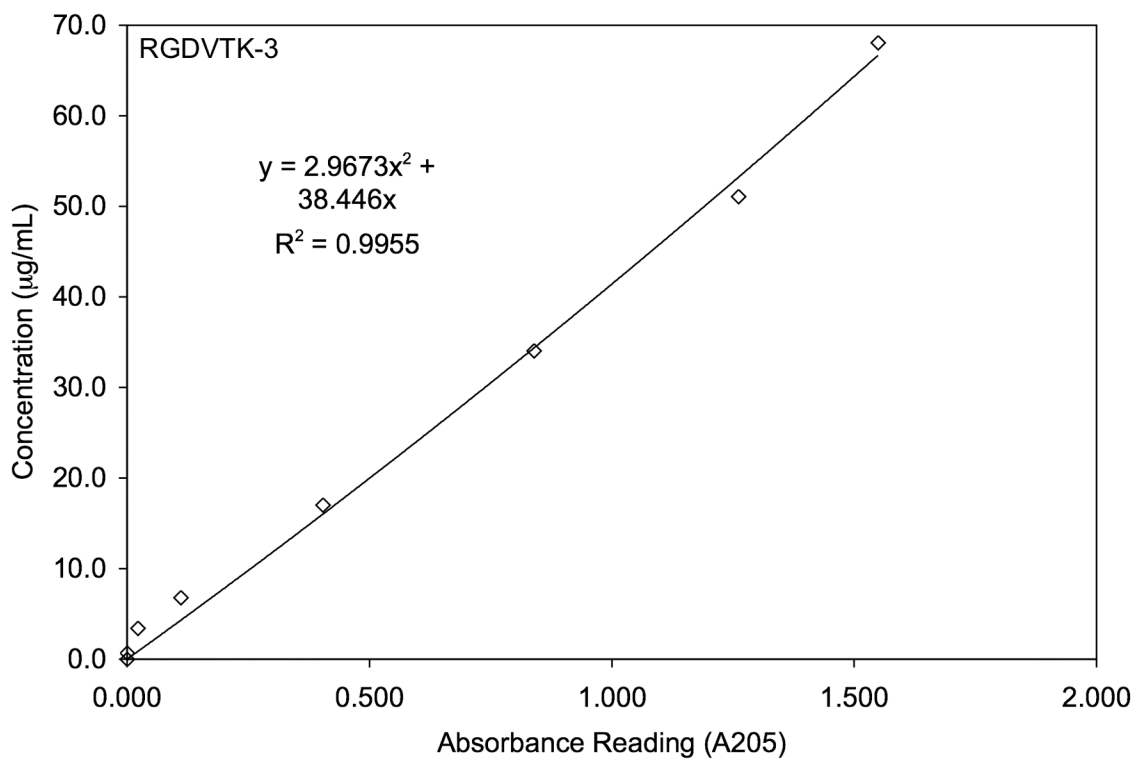


Figure B.7: Standard curve for peptide GGRGDGGGSVTKHLNQISQSY (MW = 2117.6 g/mol) determined via UV spectroscopy at A205.

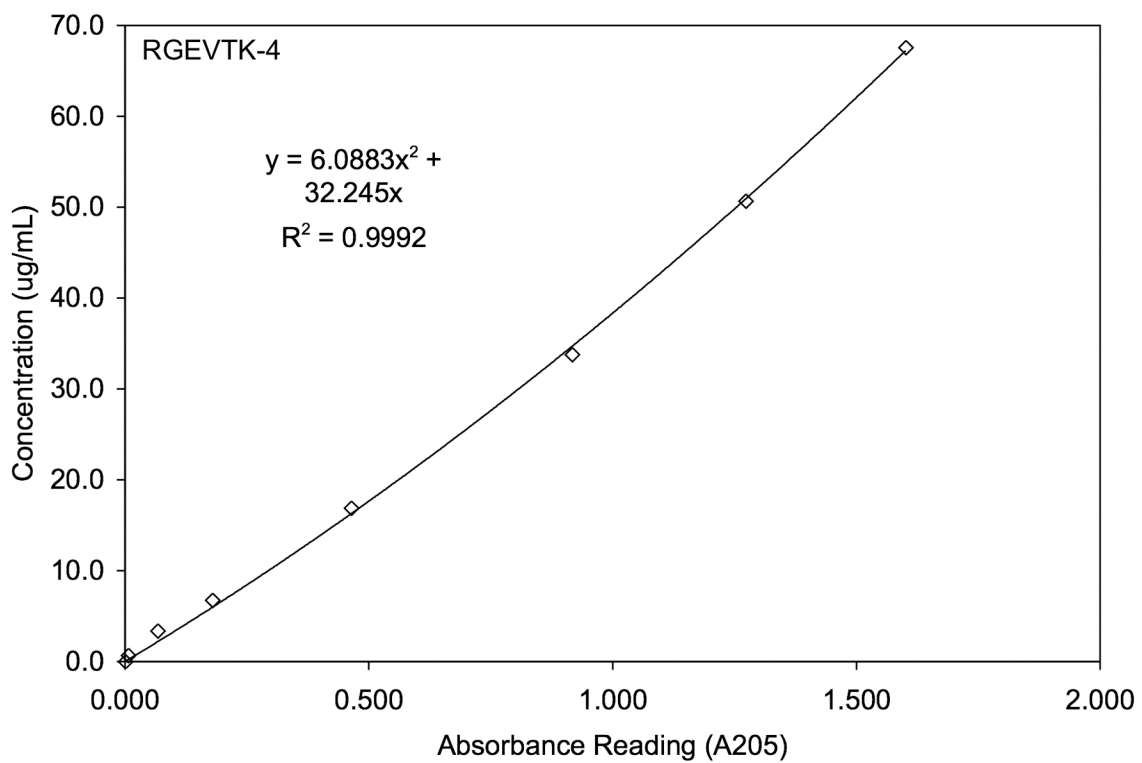


Figure B.8: Standard curve for peptide GGRGEGGGSVTKHLNQISQSY (MW = 2131.6 g/mol) determined via UV spectroscopy at A205.

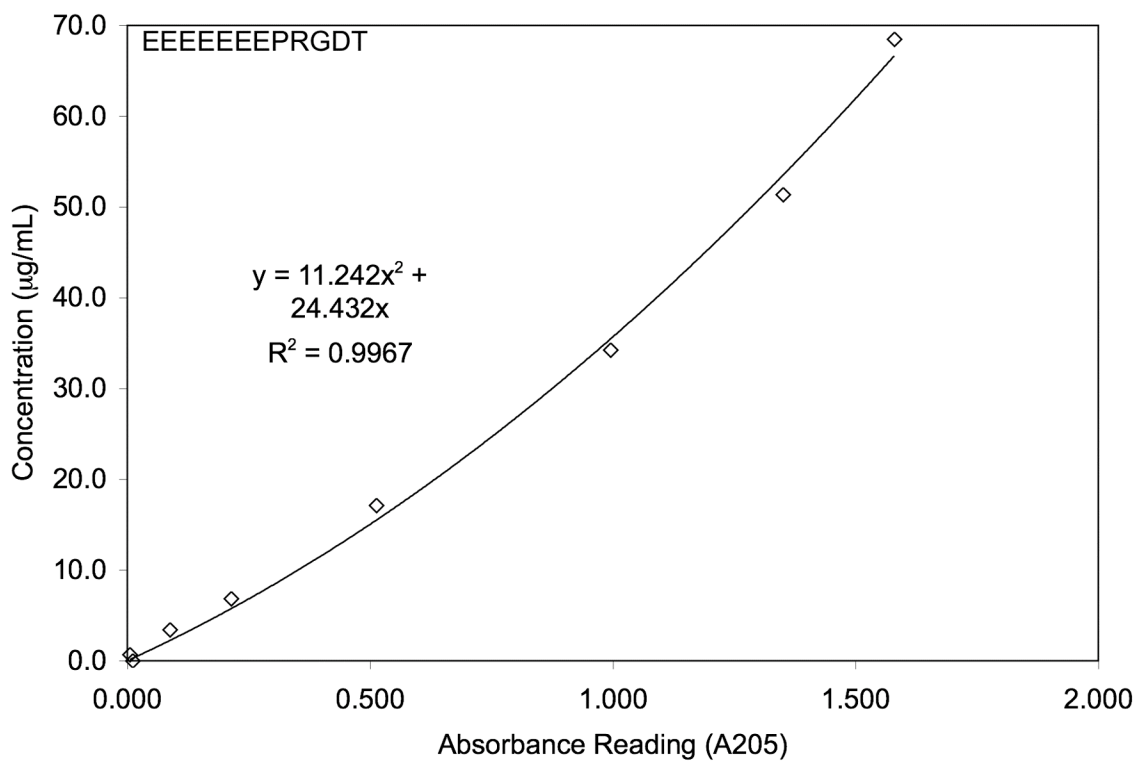


Figure B.9: Standard curve for peptide EEEEEEEPRGDT (MW = 1447.6 g/mol) determined via UV spectroscopy at A205.

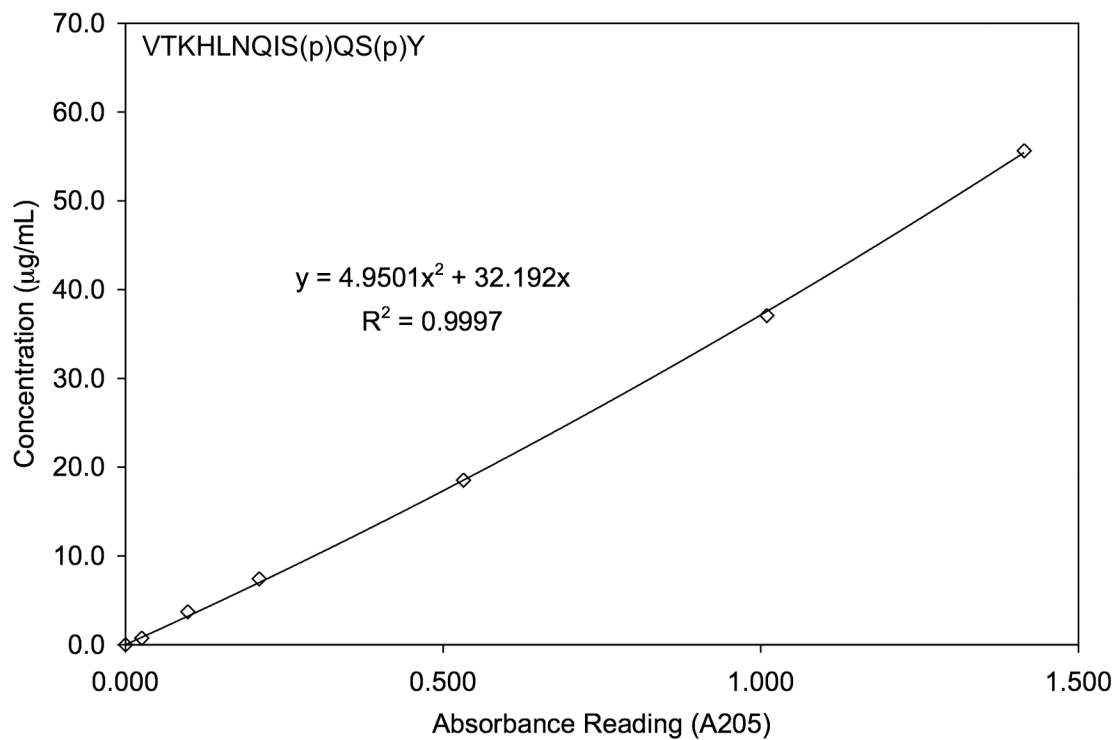


Figure B.10: Standard curve for peptide VTKHLNQIS(p)QS(p)Y (MW = 1576. g/mol) determined via UV spectroscopy at A205.

Table B.1: Standard Curve Dilution Scheme for Peptide Adsorption

Peptide Concentration	Amount of Stock Peptide Solution μL	Amount of ddH₂O μL	Name
1000	1500	0	A
750	375 A	125	C
500	500 A	500	B
250	125 A	375	D
100	100 B	400	E
75	50 C	450	
50	50 B	450	F
25	50 D	450	
10	50 E	450	G
5	50 F	450	
1	50 G	450	
0	0	500	

Table B.2: Cell Standard Curve Scheme for Cell Attachment Assay

Number of Cells	500,000 cells in 1mL (μL)	blank media (μL)	total volume (μL)
75000	300	700	1000
50000	200	800	1000
40000	160	840	1000
30000	120	880	1000
20000	80	920	1000
10000	40	960	1000
7500	30	970	1000
5000	20	980	1000
2500	10	990	1000
1000	4	996	1000
0	0	1000	1000

APPENDIX C

BIOREACTOR PROTOCOL AND MATLAB PROGRAM

Scaffold Mineralization using the Bioreactor Protocol

Materials Needed:

Aluminum cylinder*

Aluminum foil*

Aluminum shaft (with 3/16" 20 threading)*

3/16" 20 Alan Bolt*

8 x 8" glass baking pan*

4 small Petri dishes*

Aluminum base plate

4 large C-clamps

Circular 5 1/2" Delrin mold

1x Modified SBF with NaN_3 (The NaN_3 helps prevent bacterial contamination)

NaCl

PLGA/chloroform solution

Gloves

EtOH

Agitator plate

Stir/hot plate

Safety Glasses

Kimwipes

* - To be autoclaved daily (can autoclave on 'solids' setting at 250°F for 25min, cool down time of 20min)

Procedure:

1. Fabricate 3mm thick scaffolds in circular Delrin mold following scaffold fabrication protocol. For each scaffold use 375 μg NaCl and 288 μL PLGA/chloroform solution. (300mg NaCl, 236 μL PLGA/chloroform solution for 2.5mm scaffolds)
2. Autoclave aluminum base, Alen bolt, and aluminum foil (enough foil to cover opening on cylinder and plug screw holes in mold).
3. Filter and warm to 37C in hot water 1L 1x modified SBF (w/ NaN_3 0.05 g/L).
4. Sample 8 mL of filtered SBF in 15 mL Falcon tube to test pH.
5. Turn on water supply to Instron and power up the machine.
6. Calibrate any sensors that require calibration (most likely the load sensor). Sensors that need calibration will have a blinking green light.
7. Using gloves clean circular mold, o-ring, and aluminum plunger with 70% ethanol.
8. Plug screw holes in mold with autoclaved rubber stoppers. Secure thermocouple with dental rubberbands on the Delrin mold.
9. Jog the crosshead up to a position to attach the plunger with aluminum rod. Bolt mold into position on plunger with the flush side of the scaffolds facing down (the plunger, aluminum rod, can be removed/tightened by using the clamp control unit (behind the tower) and foot pedal (to the right of the tower).
10. Turn on hydraulics and actuator.
11. Put aluminum cylinder in position under the mold (w/o o-ring attached). Use knobs on front of machine to lower mold into and out of cylinder to align.
12. Make sure piston in positioned close enough to middle position to allow the machine to cycle.
13. Attach o-ring. Add 1L SBF. Using gloves wet insides of cylinder and o-ring with SBF on a Kimwipe.
14. Use knobs on front of machine to lower mold into cylinder. Be extra careful when moving o-ring into opening of the cylinder. Push down on sides of mold to ensure it goes in level.
15. Lower mold into position using knobs. It is in position when the bottom of the blue tape on the plunger is aligned with the rim of the cylinder (this step produces a large load on the mold, >1000 N, so be careful and wear safety glasses).
16. Use c-clamps to clamp aluminum cylinder to aluminum base plate.
17. Cover the top of the aluminum cylinder with autoclaved aluminum foil.

18. Set positional waveform on control panel: cyclic, triangular, 25.4 mm (this is the amplitude: the distance from the midline to the peak of the wave), 0.0011 Hz (this frequency corresponds to 1 cycle/15 minutes)
19. Turn on amplitude control by pressing the amplitude control button on the consol followed by the button corresponding to 'on'.
20. Plug in temperature controller.
21. Press start. Run Instron for 6 hours. Loads will be large for the first few cycles (~ 800 N) but should reduce to 300-500 N after a few cycles. Check on cycling periodically to troubleshoot any problems that may occur.
22. Clean Tupperware used for overnight soaks well with ethanol.
23. Make SBF (w/ NaN_3) if needed (every other day) following SBF protocol.
24. Filter and warm to 37C in hot water 1 L 1x modified SBF (w/ NaN_3).
25. Sample 8mL SBF in a 15mL Falcon tube after 6 hour run.
26. Place mold in cleaned Tupperware. Add 1L warmed SBF.
27. Leave in incubator set at 37C overnight.
28. Sample 8mL SBF in a 15mL Falcon tube from baking pan the next morning.
29. Repeat steps 2-27 each day for 5 days.
30. Rinse scaffolds in deionized water to remove excess salt.
31. Remove the scaffolds from the mold using a brass tube cutter and a spatula. Remove them gingerly, to keep the scaffolds intact.
32. Dry scaffolds under hood for 1-2 days.

General Notes: O-rings need to be replaced in the middle of a 5-6 Day run. Be sure to wipe them thoroughly with ethanol.

Coprecipitation on 3-Dimensional Scaffolds using the Bioreactor

Materials Needed:

Aluminum cylinder*

Aluminum foil*

Aluminum shaft (with 3/16" 20 threading)

Rubber stoppers*

3/16" 20 Alan Bolt

Aluminum base plate

4 large C-clamps

Circular 5 ½” Delrin mold

5x and 2x SBF with NaN_3 filtered with 0.22um sterile filter (The NaN_3 helps prevent bacterial contamination)

450-600um diam. NaCl

Latex and Nitrile Gloves

EtOH

Safety Glasses

Kimwipes

Plastic pitcher, 25mL syringe

FITC-BSA, BSA

10mM HCl

6-well culture plate dishes for demineralization

PLGA (85:15 from Alkermes), Chloroform (Sigma), and NaCl (Sigma) for casting scaffolds

Delrin mold with 8 salt-leached scaffolds & o-ring (McMaster-Carr, Buna 251)

Teflon mold with 8 salt-leached scaffolds

Scintillation vials for pH reading samples

pH meter (Mettler-Toledo)

Tupperware for Teflon mold

* - To be autoclaved (can autoclave on ‘solids’ setting at 250F for 25min, cool down time of 20min)

Procedure for Bioreactor:

1. Fabricate 2.5-3mm thick scaffolds in circular Delrin mold and Teflon mold following scaffold fabrication protocol. For each scaffold use 600 μg NaCl and 472 μL PLGA/chloroform solution.
2. Autoclave aluminum base, rubber stoppers, and aluminum foil (enough foil to cover opening on cylinder and plug screw holes in mold).
3. Filter and warm to 37C in hot water 1L 5xSBF (w/ NaN_3 0.05 g/L).
4. Sample 3 mL of filtered SBF in scintillation vial to test pH.
5. Turn on water supply to Instron and power up the machine.

6. Calibrate any sensors that require calibration (most likely the load sensor). Sensors that need calibration will have a blinking green light.
7. Using gloves clean circular mold, o-ring, and aluminum plunger with 70% ethanol.
8. Plug screw holes in mold with autoclaved rubber stoppers. Secure thermocouple with dental rubberbands on the Delrin mold.
9. Jog the crosshead up to a position to attach the plunger with aluminum rod. Bolt mold into position on plunger with the flush side of the scaffolds facing down (the plunger, aluminum rod, can be removed/tightened by using the clamp control unit (behind the tower) and foot pedal (to the right of the tower)).
10. Turn on hydraulics and actuator.
11. Put aluminum cylinder in position under the mold (w/o o-ring attached). Use knobs on front of machine to lower mold into and out of cylinder to align.
12. Make sure piston is positioned close enough to middle position to allow the machine to cycle.
13. Attach o-ring. Add 1L 5x-SBF. Using gloves wet insides of cylinder and o-ring with SBF on a Kimwipe.
14. Use knobs on front of machine to lower mold into cylinder. Be extra careful when moving o-ring into opening of the cylinder. Push down on sides of mold to ensure it goes in level.
15. Lower mold into position using knobs. It is in position when the bottom of the blue tape on the plunger is aligned with the rim of the cylinder (this step produces a large load on the mold, >1000 N, so be careful and wear safety glasses).
16. Use c-clamps to clamp aluminum cylinder to aluminum base plate.
17. Cover the top of the aluminum cylinder with autoclaved aluminum foil.
18. Set positional waveform on control panel: cyclic, triangular, 25.4 mm (this is the amplitude: the distance from the midline to the peak of the wave), 0.0011 Hz (this frequency corresponds to 1 cycle/15 minutes)
19. Turn on amplitude control by pressing the amplitude control button on the consol followed by the button corresponding to 'on'.
20. Plug in temperature controller.
21. Press start. Loads will be large for the first few cycles (~ 800 N) but should reduce to 300-500 N after a few cycles. Check on cycling periodically to troubleshoot any problems that may occur.
22. After 6 hours, replace 5x-SBF with another 1L of 5X-SBF. Take pH aliquots.

23. Start static mineralization of Teflon mold scaffolds in Tupperware, following same SBF regiment.
24. Sample 3 mL of filtered SBF in scintillation vial to test pH.
25. After 6 more hours, replace with pre-warmed 2x-SBF. Take pH aliquots.
26. After 12 hours, replace with pre-warmed FITC-BSA 2x-SBF. Take pH aliquots.
27. Repeat #26 for next 36 hours.
28. Stop the run after 72 hours.
29. Rinse scaffolds in deionized water to remove excess salt.
30. Remove the scaffolds from the mold using a brass tube cutter and a spatula. Remove them gingerly, to keep the scaffolds intact.
31. Dry scaffolds under hood for 1-2 days.

Demineralization and BSA Quantification:

1. Demineralize 4 scaffolds from experimental and control groups in 2mL of 10mM HCl in 6-well culture plate dishes. Cut up scaffolds using razor or microtome blade.
2. Agitate on LabLine Titer plate shaker at setting 3-3.5 (200rpm) for 24 hours. Cover plates with aluminum foil to protect from light.
3. Read BSA concentration on UV Spec.

MicroCT of Scaffolds:

1. 4 scaffolds from each group should be scanned on the MicroCT to determine % mineral volume. Scan using Polymer_Parker_15um protocol at 75mV, 75mA with 400planes.

SBF Needed for 3-Day Run:

	Instron Mold	Teflon Control Mold	Totals
Day One	2L 5x SBF (pH=6.2 @ RT) 1L 2x SBF (pH=6.8 @ RT)	1L 5x SBF (pH=6.2 @ RT) 0.5L 2x SBF (pH=6.8 @ RT)	3L 5x SBF 1.5L 2x SBF
Day Two	2L 2x SBF with BSA	1L 2x SBF with BSA	3L 2x SBF with BSA
Day Three	2L 2x SBF with BSA	1L 2x SBF with BSA	3L 2x SBF with BSA
			3L 5xSBF 1.5L 2xSBF 6L 2xSBF with BSA

Procedure for making FITC-BSA:BSA SBF Solution:

1. Weigh out BSA and FITC-BSA
 - a. Use a 1:5 ratio of FITC-BSA to BSA
 - b. 100mg FITC-BSA : 500mg BSA per day
 - c. per liter: 33mg FITC-BSA; 167mg BSA

[200ug/mL x 3000mL = 600mg per day x 2 days = 1.2g for entire experiment]
2. Add BSA:FITC-BSA into filtered 2x SBF and allow to mix for at least 30 min.
(protect solution from light; cover with Al foil. Might want to do this in 4L Nalgene bottle so you can filter and mix in same container)
3. Store in refrigerator until use; protected from light.

3mL Aliquots for pH and Initial protein concentrations in scintillation vials:

	Start	6hr	12hr	24hr	36hr	48hr	60hr	72hr	Total #
Day One	1pH	2pH	2pH	2pH 1BSA	2pH 2BSA	2pH 2BSA	2pH 2BSA	1pH 1BSA	14pH 8BSA

BSA concentrations must be read immediately on the UV Spec. Using the 1mL quartz cuvette. Wavelengths 280 and 494nm should be read. Save the remainder of the aliquot in the refrigerator protected from light.

Micro-Computed Tomography MATLAB Program for Mineral Distribution Throughout a 3-Dimensional Scaffold

```
[ImFileName,ImPathName] = uigetfile('*.*vff','MultiSelect','off'); %let the user select the path
ImToLoad=strcat(ImPathName,ImFileName); %form a string that has the path and filename combined
disp(['Reading the file: ' ImToLoad])
disp(' ')
[ImHeader] = readvff_header(ImToLoad); %Read the header from the .vff file
origin_ind = strmatch('origin=',ImHeader); %find the entry within the ImHeader cell array containing the origin
origin_str = char(ImHeader(origin_ind));%extract the cell containing the origin data and make it a string
start_ind = strfind(origin_str,'=')+1;%get the index number after the = sign
fin_ind = strfind(origin_str,';')-1;%get the index number before the ; sign
origin_str = origin_str(start_ind:fin_ind); %extract just the portion containing the numbers
origin_split = strsplit(origin_str,' '); %split it up into a 1x3 cell array
origin_coord1 = str2num(char(origin_split(1))); %get the x coordinate of the origin
origin_coord2 = str2num(char(origin_split(2))); %get the y coordinate of the origin
origin_coord3 = str2num(char(origin_split(3))); %get the z coordinate of the origin
ImOrigin = [origin_coord1 origin_coord2 origin_coord3]; %append all three of the origin coords together
clear start_ind fin_ind
elsize_ind = strmatch('elementsize=',ImHeader);
elsize_str = char(ImHeader(elsize_ind)); %extract the cell containing the data and make it a string
elstart_ind = strfind(elsize_str,'=')+1; %get the index number after the = sign
elfin_ind = strfind(elsize_str,';')-1; %get the index number before the ; sign
elsize_str = elsize_str(elstart_ind:elfin_ind); %extract just the portion containing the numbers
```

```

voysize=str2num(elsize_str);
if isempty(elsize_ind)
    elsize_ind = strmatch('spacing=',ImHeader);
    elsize_str = char(ImHeader(elsize_ind));
    elstart_ind = strfind(elsize_str,'=')+1;
    elfin_ind = strfind(elsize_str,');
    elsize_str = elsize_str(elstart_ind:elfin_ind);
    voysize=str2num(elsize_str)
end
size_ind=strmatch('size=',ImHeader);
size_str = char(ImHeader(size_ind));%extract the cell containing the origin data and make it a string
start_ind = strfind(size_str,'=')+1;%get the index number after the = sign
fin_ind = strfind(size_str,')-1;%get the index number before the ; sign
size_str = size_str(start_ind:fin_ind); %extract just the portion containing the numbers
size_split = strsplit(size_str,'); %split it up into a 1x3 cell array
size_coord1 = str2num(char(size_split(1))); %get the x coordinate of the origin
size_coord2 = str2num(char(size_split(2))); %get the y coordinate of the origin
size_coord3 = str2num(char(size_split(3))); %get the z coordinate of the origin
ImSize = [size_coord1 size_coord2 size_coord3]; %append all three of the origin coords together
clear start_ind fin_ind
percent_chg = input('Enter the percentage that ROI should shrink by, as a positive decimal (ex. 0.10): ');
%make sure the number is positive
if percent_chg <=0
    error(strcat('The number that was input was less than or equal to zero.',...
        'The number must be a positive decimal, so the program will now stop.))
end

remainder = rem(1,percent_chg); %Calculate a remainder
if remainder == 0 %i.e., when the percentage evenly divides into 1
    percent_vector = [(1-percent_chg) : -percent_chg : percent_chg];
else %when the percentage does not evenly divide into 1
    disp('WARNING: The percentage decrease that was input is not evenly divisible into 1!')
    disp('WARNING: The last increment will not equal the percent change input')
    disp(' ')
    percent_vector = [(1-percent_chg) : -percent_chg : percent_chg, percent_chg];
end
disp('The percentages that the ROI will be shrunk are:')
disp(percent_vector)
disp(' ')
[FileName,PathName] = uigetfile('*.*','MultiSelect','off'); %let the user select the path
FileToLoad=strcat(PathName,FileName); %form a string that has the path and filename combined
disp(['Reading the file: ' FileToLoad])
disp(' ')
[storage,transform_data,roi_transform_data] = AdvROI_Load(FileToLoad);
x_spline_pts = squeeze(storage(:,1,:));
xcnt = mean(nonzeros(x_spline_pts));
y_spline_pts = squeeze(storage(:,2,:));
ycnt = mean(nonzeros(y_spline_pts));
z_spline_pts = storage(:,3,:);
zmin = min(max(storage(:,3,:)));
zmax = max(max(storage(:,3,:)));
zcnt = mean([zmin zmax]);
centroid_array = [xcnt ycnt zcnt];
centroid_array = centroid_array./voysize-ImOrigin;
ImOrigin_matrix = ones(size(storage,1),1)*ImOrigin; %1D to 2D
for ctr=1:1:size(storage,3)
    ImOrigin_matrix(:,ctr) = ImOrigin_matrix(:,1);
end
clear ctr

```

```

zero_indices=find(storage(:,:,:))==0);
coord_matrix = (storage./voxsizes) - ImOrigin_matrix;
coord_matrix(zero_indices)=0;
[centroid_matrix] = centroid_3d(coord_matrix,centroid_array);
radius_matrix_orig = coord_matrix - centroid_matrix;
for BIGctr = 1:length(percent_vector)
    percent_scale = percent_vector(BIGctr);
    disp(['The algorithm is now running for the percentage at: ',num2str(percent_scale)])
    [radius_matrix] = CoordShrink_cyl(radius_matrix_orig,percent_scale);
    radius_matrix = round(radius_matrix);
    trial_array = zeros(size(radius_matrix,1),size(radius_matrix,3));
    trial_array(:,:) = radius_matrix(:,3,:);
    trial_array = trial_array(1,:);
    find_repeats = [1,diff(trial_array)];
    repeats = find(diff(trial_array)==0);
    if isempty(repeats)==0
        radius_matrix_corr = zeros(size(radius_matrix,1),size(radius_matrix,2),(length(trial_array)-length(repeats)));
        for ctr=1:size(radius_matrix,3)
            if find_repeats(ctr)==1
                index=min(find(radius_matrix_corr(1,1,:)==0)); %find the first non-zero entry in 'radius_matrix_corr'
                radius_matrix_corr(:,:,index) = radius_matrix(:,:,ctr);
            end
        end
    else
        radius_matrix_corr = radius_matrix;
    end
    centroid_matrix_corr = centroid_matrix(:,1:size(radius_matrix_corr,3));
    coord_matrix_new = radius_matrix_corr + centroid_matrix_corr;
    zero_indices=find(coord_matrix_new(:,:,:))==0);
    ImOrigin_matrix_corr = ImOrigin_matrix(:,1:size(radius_matrix_corr,3));
    key_frames = round(coord_matrix_new(1,3,1:size(coord_matrix_new,3)));
    coord_matrix_final = (coord_matrix_new + ImOrigin_matrix_corr) .* voxsizes;
    coord_matrix_final(zero_indices)=0;
    coord_matrix_final = fix2(coord_matrix_final,4);
    FileRootName=FileToLoad(1:strfind(FileToLoad,'.xml'));
    FileEndName=strcat(num2str(percent_scale*100),'percent.xml');
    FileToSave = strcat(FileRootName,FileEndName);
    disp(['Saving the file: ',FileToSave])
    disp(' ')
    AdvROI_Save(FileToSave,voxsizes,key_frames,coord_matrix_final,transform_data,roi_transform_data);
end
%-----
function [header] = readvff_header(fname)
fid = fopen(fname,'r','b');
fInfo = dir(fname);
endHeader = 0;
lineNbr = 1;
tline = fgetl(fid); % skip the ncaa line without a ;
header{lineNbr} = tline;
lineNbr = lineNbr + 1;
while(endHeader == 0)
    tline = fgetl(fid);
    if(tline(end) == ';')
        header{lineNbr} = tline;
        lineNbr = lineNbr + 1;
    else
        endHeader = 1;
    end
end
end

```

```

fclose(fid);
end
%-----
function [contour_data,transform_data,roi_transform_data] = AdvROI_Load(FileToLoad)
inputdata = xml_load(FileToLoad);
num_slices = size(inputdata,2); %find the number of slices with contours
for ctr=1:size(inputdata,2)
    rowsizes(ctr) = (size(inputdata(1,ctr).contour,2)); %create a vector to hold the x-coordinates for every slice
end
max_rowsize=max(rowsizes);
contour_data = zeros(max_rowsize,3,num_slices); %note, the second digit in this so
for slicectr = 1:1:num_slices %run this for every slice
    point_lim = max(size(inputdata(1,slicectr).contour)); %calculate the number of points at for each contour
    pt_data_cell = struct2cell(inputdata(1,slicectr).contour); %get the data containing the coordinates. every row is
stored as a string. format is as a cell
    for ptctr = 1:1:point_lim
        pt_data = cell2mat(pt_data_cell(:,ptctr));
        point=pt_data_cell(1,1,ptctr); %get the data into a 1x1 cell
        point=strsplit(char(point),'()'); %remove the (
        point=strsplit(char(point),' '); %remove the )
        point=strsplit(char(point),' '); %remove the commas, separating 'point' into a 1x3 cell
        coord1=str2num(char(point(1,1)));
        coord2=str2num(char(point(1,2)));
        coord3=str2num(char(point(1,3)));
        contour_data(ptctr,1,slicectr) = coord1;
        contour_data(ptctr,2,slicectr) = coord2;
        contour_data(ptctr,3,slicectr) = coord3;
    end
end
transform_data = inputdata(1,1).transform;
roi_transform_data = inputdata(1,1).roi_transform;
end
end
%-----
function [centroid_matrix] = centroid_3d(data_matrix,centroid_array)
zero_indices=find(data_matrix(:,,:)==0);
centroid_matrix = ones(size(data_matrix,1),1)*centroid_array;
for ctr=1:1:size(data_matrix,3)
    centroid_matrix(:,ctr) = centroid_matrix(:,1);
end
centroid_matrix(zero_indices)=0;
end
%-----
function [radius_matrix_new] = CoordShrink_cyl(radius_matrix_orig,percent)
radius_matrix_new = zeros(size(radius_matrix_orig)); %Create a new radius matrix to store all of the radii
for ctr1=1:size(radius_matrix_orig,3) %use to go slice by slice
    for ctr2=1:size(radius_matrix_orig,1) %use to go row by row
        temp_coords_cart = radius_matrix_orig(ctr2,:,ctr1)
        temp_x = temp_coords_cart(1);
        temp_y = temp_coords_cart(2);
        temp_z = temp_coords_cart(3);
        [theta,rad_old,z_old] = cart2pol(temp_x, temp_y, temp_z);
        rad_new = percent*rad_old;
        z_new = percent*z_old;
        [temp_x2,temp_y2,temp_z2] = pol2cart(theta,rad_new,z_new);
        radius_matrix_new(ctr2,1,ctr1) = fix2(temp_x2,4);
        radius_matrix_new(ctr2,2,ctr1) = fix2(temp_y2,4);
        radius_matrix_new(ctr2,3,ctr1) = fix2(temp_z2,4);
    end
end

```

```

refcoord3 = fix2(radius_matrix_new(1,3,ctr1),4);
ptcheck = find(((radius_matrix_new(:,3,ctr1))~=refcoord3) & ((radius_matrix_new(:,3,ctr1))~=0));
if isvector(ptcheck) %this should run where there are some points that don't match
    radius_matrix_new(ptcheck,3,ctr1)=refcoord3;
end
end
end
%-----
function AdvROI_Save(FileToSave,voysize,key_frames,contour_data,transform_data,roi_transform_data)
fid = fopen(FileToSave,'w');
fprintf(fid,'%s\n','<?xml version="1.0" encoding="UTF-8" ?>');
fprintf(fid,'%s\n','<!DOCTYPE MicroViewContours>');
fprintf(fid,'%s\n','<ROI mode="Spline" pane="0">');
fprintf(fid,'%s\n','<transform>');
fprintf(fid,'%s\n',transform_data);
fprintf(fid,'%s\n','</transform>');
fprintf(fid,'%s\n','<roi_transform>');
fprintf(fid,'%s\n',roi_transform_data);
fprintf(fid,'%s\n','</roi_transform>');
for ctr3=1:1:size(contour_data,3)
fprintf(fid,'%s\n','<contour slice="" num2str(key_frames(ctr3)) "" keyframe="1">');
    for ctr1 = 1:1:size(contour_data(:,:,ctr3),1)
        if (contour_data(ctr1,1,ctr3))~=0 %added so that the rows with zeros are not written into the output file
            outputrow = ['(' num2str(contour_data(ctr1,1,ctr3) ,%.4f) ...
                ' ' num2str(contour_data(ctr1,2,ctr3),%.4f) ...
                ' ' num2str(contour_data(ctr1,3,ctr3),%.4f) ')];
            outputrow2=xml_formatany(outputrow,'p');
            fprintf(fid,'%s\n',outputrow2);
        end
    end
    fprintf(fid,'%s\n','</contour>');
end
fprintf(fid,'%s\n','</ROI>');
fclose('all');
end
%-----
function b = fix2(a, n)
if nargin < 2 || ~any(n) || isempty(a)
    b = fix(a); return
end
% general case(round to n decimals )
if ~isscalar(a) && ~isscalar(n) && ~isequal(size(a),size(n))
    error('Non-scalar inputs must be the same size')
end
t2n = 10.^floor(n);
b = fix(a.*t2n)./t2n;
end

```

Protocol for Using the MATLAB ROIshrink Program

Using the ROIshrink Program

In MicroView

1. Open a .vff in MicroView
2. Using the 'Advanced ROI' tool, define contours of the sample at 10 slice increments. Save the contours (will save as an .xml files).

3. Interpolate the contours
4. Generate 3D ROI
5. In the Bone Analysis tab (original menu on MicroView), autothreshold at 1000 and check the BMD box.
6. Run the BMD analysis and record the analysis.
- 7.

In Matlab

1. Type in the command prompt: ROIShrink
2. A window will pop up to select a .vff file. Choose a .vff file to analyze.
3. Enter at the prompt 0.01 increment
4. Another window will pop up to select a .xml file (saved from the defined ROI using the Advanced ROI tool). Choose the .xml file that corresponds to the .vff file you opened in the second step.
5. Matlab will save incremental files into the folder that you opened the .xml file in step 4.

In MicroView

1. Go back to Microview and open up the original .vff file for the sample.
2. Under the 'Advanced ROI' tool, click on 'Load Contours'.
3. To analyze the sample in 15% increments, load the following files.

15% increment	Corresponding .xml file
100	v100
84	v925
67	v87
50	v795
34	v34
17	v53

4. Perform the BMD analysis on each of the 15% increments on the files. This means each file has to be separately opened in Microview under the 'Load Contours' button, then interpolate and generate 3D ROI for each file.

APPENDIX D

PAPERS AND PRESENTATIONS

Published:

Segvich S, Biswas S, Becker U, Kohn DH, “Identification of Peptides with Targeted Adhesion to Bone-Like Mineral via Phage Display and Computational Modeling,” Cells, Tissues, Organs, in press.

Segvich S, Luong LN, Kohn DH, Biomaterials and Biomedical Engineering, Chapter Title: Biomimetic Approaches to Synthesize Mineral and Mineral/Organic Biomaterials, 2008. Eds. Ahmed W, Ali N, Ochsner A.

Segvich S, Smith HC, Luong LN, Kohn DH, “Uniform Three-Dimensional Biomineralization of Protein Incorporated Mineral Layer on Porous Polymer Scaffolds,” Journal of Biomedical Materials Research: Part B, 84(2): 340-9, Feb 2008.

Schek RM, Taboas JM, Segvich SJ, Hollister SJ, Krebsbach PH, “Engineered Osteochondral Grafts using Biphasic Composite Solid-Free Form Fabricated Scaffolds.” Tissue Engineering 10(9-10): 1376-1385, Sept 2004.

In Preparation:

Segvich S, Smith HC, Kohn DH, “Investigation of Surface Adsorption Properties of Identified High Affinity Peptides on Apatite-based Materials,” Biomaterials, in submission 2008.

Segvich S, Smith HC, Kohn DH, “Improved Cell Adhesion on Bone-like Mineral using Dual Functioning Peptides Identified via Phage Display”, in preparation.

Presentations:

Segvich, S. “Design of Peptides with Targeted Apatite Adhesion for Bone Tissue Engineering,” 2008 Dr. Dziewiatkowski Award Seminar, UM Ann Arbor, MI.

Segvich, S, Smith HC, Kohn DH. “Identification of High Affinity Peptides on Apatite-Based Materials and hBMSCs,” 2008 Midwest Tissue Engineering Consortium, Cincinnati, OH.

Proceedings of the 2008 Annual Meeting of the Orthopaedic Research Society, Paper #111, San Francisco, CA. Segvich S, Smith HC, Kohn DH. “Surface Adsorption of High Affinity Peptides on Apatite-Based Materials with Varied Carbonate Compositions”

2007 9th International Conference on the Chemistry & Biology of Mineralized Tissues, Austin, TX. Segvich S, Biswas S, Becker U, Kohn DH. “Identification of Peptides with Targeted Adhesion to Bone-Like Mineral Biomaterials”

Segvich S, Biswas S, Becker U, Kohn DH. “Molecular Modeling of Bone Adhesion Peptides on Hydroxyapatite,” 2007 Midwest Tissue Engineering Consortium, Ann Arbor, MI.

Proceedings of the 2006 Annual Meeting of the Society of Biomaterials, Presentation #514, Pittsburgh, PA. Segvich S, Smith HC, Luong LN, Kohn DH. “Uniform Three-Dimensional Biomineralization of Protein Incorporated Mineral Layer on Porous Polymer Scaffolds”

Proceedings of the 2006 Annual Meeting of the Society of Biomaterials, Presentation #529, Pittsburgh, PA. Segvich S, Biswas S, Becker U, Kohn DH. “Molecular Modeling of Cell Adhesion Peptide Adsorption on Hydroxyapatite”

Proceedings of the 2006 Annual Meeting of the Orthopaedic Research Society, Poster #835, Chicago, IL. Segvich S, Kohn DH. “Surface Adsorption of Bone Sialoprotein-Derived Peptide on Biomimetic Apatite”

Segvich S, Smith HC, Biswas S, Luong LN, Kohn DH. “Development and Investigation of Peptide Laden Organic-Inorganic Hybrid Scaffolding for Bone Tissue Engineering,” Symposium for Tissue Engineering at Michigan, 2006.

Awards:

UM Dr. Dziewiatkowski Award Winner – 2008

Midwest Tissue Engineering Consortium, Outstanding Oral Presentation – April 2008

New Investigator Award, 9th ICCBMT Austin, TX – November 2007

UM Graduate Student Symposium, Best Oral Presentation – November 2007

Midwest Tissue Engineering Consortium, Outstanding Oral Presentation – April 2007

Tissue Engineering at Michigan Training Grant DE07057- September 2004-2006

BIBLIOGRAPHY

- Abe Y, Kokubo T, Yamamuro T (1990) Apatite Coating on Ceramics, Metals and Polymers Utilizing a Biological Process. *J Mater Sci -Mater Med* 1:233-238.
- Abiraman S, Varma HK, Umashankar PR, John A (2002) Fibrin glue as an osteoinductive protein in a mouse model. *Biomaterials* 23:3023-3031.
- Adams JC, Watt FM (1990) Changes in keratinocyte adhesion during terminal differentiation: reduction in fibronectin binding precedes alpha 5 beta 1 integrin loss from the cell surface. *Cell* 63:425-435.
- Adey NB, Mataragnon AH, Rider JE, Carter JM, Kay BK (1995) Characterization of phage that bind plastic from phage-displayed random peptide libraries. *Gene* 156:27-31.
- Alsberg E, Hill EE, Mooney DJ (2001) Craniofacial tissue engineering. *Crit Rev Oral Biol Med* 12:64-75.
- Anselme K, Linez P, Bigerelle M, Le Maguer D, Le Maguer A, Hardouin P, Hildebrand HF, Iost A, Leroy JM (2000) The relative influence of the topography and chemistry of TiAl6V4 surfaces on osteoblastic cell behaviour. *Biomaterials* 21:1567-1577.
- Aoki H, (1991) *Science and Medical Applications of Hydroxyapatite*. Tokyo: Takayama Press System Center Co., Inc.
- Astala R, Stott MJ (2005) First principles investigation of mineral component of bone: CO3 substitutions in hydroxyapatite. *Chem Mat* 17:4125-4133.
- Azevedo HS, Leonor IB, Alves CM, Reis RL (2005) Incorporation of proteins and enzymes at different stages of the preparation of calcium phosphate coatings on a degradable substrate by a biomimetic methodology. *Mater Sci Eng C-Biomimetic Supramol Syst* 25:169-179.
- Bancroft GN, Sikavitsas VI, Mikos AG (2003) Design of a flow perfusion bioreactor system for bone tissue-engineering applications. *Tissue Eng* 9:549-554.
- Barber TA, Harbers GM, Park S, Gilbert M, Healy KE (2005) Ligand density characterization of peptide-modified biomaterials. *Biomaterials* 26:6897-6905.
- Barralet J, Best S, Bonfield W (1998) Carbonate substitution in precipitated hydroxyapatite: An investigation into the effects of reaction temperature and bicarbonate ion concentration. *J Biomed Mater Res* 41:79-86.
- Barrere F, van der Valk CM, Dalmeijer RA, van Blitterswijk CA, de Groot K, Layrolle P (2003) In vitro and in vivo degradation of biomimetic octacalcium phosphate and carbonate apatite coatings on titanium implants. *J Biomed Mater Res* 64A:378-387.
- Bearinger JP, Castner DG, Healy KE (1998) Biomolecular modification of p(AAm-co-EG/AA) IPNs supports osteoblast adhesion and phenotypic expression. *J Biomater Sci Polym Ed* 9:629-652.

- Ben-Nissan B, Chai C, Evans L (1995) Crystallographic and Spectroscopic Characterization and Morphology of Biogenic and Synthetic Apatites. In: *Biogenic and Synthetic Apatites*, pp 191-221.
- Benoit DS, Anseth KS (2005) The effect on osteoblast function of colocalized RGD and PHSRN epitopes on PEG surfaces. *Biomaterials* 26:5209-5220.
- Biswas S (2008) Interactions of mineral surfaces and adsorbates: A computational modeling approach. PhD Thesis, University of Michigan (AAT 3304923).
- Boanini E, Torricelli P, Gazzano M, Giardino R, Bigi A (2006) Nanocomposites of hydroxyapatite with aspartic acid and glutamic acid and their interaction with osteoblast-like cells. *Biomaterials* 27:4428-4433.
- Boskey A, (1999) Mineralization, structure and function of bone. In: *Dynamics of Bone and Cartilage Metabolism*, (Seibel M.J., Robins S.P., Bilezikian J.P eds). San Diego: Academic Press.
- Bunker BC, Rieke PC, Tarasevich BJ, Campbell AA, Fryxell GE, Graff GL, Song L, Liu J, Virden JW, McVay GL (1994) Ceramic Thin-Film Formation on Functionalized Interfaces through Biomimetic Processing. *Science* 264:48-55.
- Cavalcanti-Adam EA, Shapiro IM, Composto RJ, Macarak EJ, Adams CS (2002) RGD peptides immobilized on a mechanically deformable surface promote osteoblast differentiation. *J Bone Miner Res* 17:2130-2140.
- Chen GP, Ushida T, Tateishi T (2000) A hybrid sponge of poly(DL-lactic-co-glycolic acid), collagen and apatite. *Bioceramics* 192-1:753-756.
- Chen RR, Mooney DJ (2003) Polymeric growth factor delivery strategies for tissue engineering. *Pharm Res* 20:1103-1112.
- Chen Y, Mak AF, Li J, Wang M, Shum AW (2005) Formation of apatite on poly(alpha-hydroxy acid) in an accelerated biomimetic process. *J Biomed Mater Res B Appl Biomater* 73:68-76.
- Choquet D, Felsenfeld DP, Sheetz MP (1997) Extracellular matrix rigidity causes strengthening of integrin-cytoskeleton linkages. *Cell* 88:39-48.
- Croll TI, O'Connor AJ, Stevens GW, Cooper-White JJ (2004) Controllable surface modification of poly(lactic-co-glycolic acid) (PLGA) by hydrolysis or aminolysis I: Physical, chemical, and theoretical aspects. *Biomacromolecules* 5:463-473.
- Cygan RT, (2001) *Molecular Modeling in Mineralogy and Geochemistry*. In: *Molecular Modeling Theory: Applications in the Geosciences*, Vol. 42 1st edition (Cygan RT, Kubicki JD eds) Washington DC: The Mineralogical Society of America.
- Dahlin S, Angstrom J, Linde A (1998) Dentin phosphoprotein sequence motifs and molecular modeling: conformational adaptations to mineral crystals. *Eur J Oral Sci* 106:239-248.

- Dalton BA, McFarland CD, Underwood PA, Steele JG (1995) Role of the heparin binding domain of fibronectin in attachment and spreading of human bone-derived cells. *J Cell Sci* 108(5):2083-2092.
- Damsky CH (1999) Extracellular matrix-integrin interactions in osteoblast function and tissue remodeling. *Bone* 25:95-96.
- de Groot K, Wolke JG, Jansen JA (1998) Calcium phosphate coatings for medical implants. *Proc Inst Mech Eng [H]* 212:137-147.
- de Leeuw NH (2004) A computer modelling study of the uptake and segregation of fluoride ions at the hydrated hydroxyapatite (0001) surface: introducing $\text{Ca}_{10}(\text{PO}_4)_6(\text{OH})_2$ potential model. *Phys Chem Chem Phys* 6:1860-1866.
- Dee KC, Puleo DA, Bizios R, (2002) *An Introduction to Tissue-Biomaterial Interactions*. New Jersey: John Wiley & Sons, Inc.
- Dee KC, Andersen TT, Bizios R (1998) Design and function of novel osteoblast-adhesive peptides for chemical modification of biomaterials. *J Biomed Mater Res* 40:371-377.
- Dettin M, Conconi MT, Gambaretto R, Bagno A, Di Bello C, Menti AM, Grandi C, Parnigotto PP (2005) Effect of synthetic peptides on osteoblast adhesion. *Biomaterials* 26:4507-4515.
- Ducheyne P, Qiu Q (1999) Bioactive ceramics: the effect of surface reactivity on bone formation and bone cell function. *Biomaterials* 20:2287-2303.
- Durrieu MC, Pallu S, Guillemot F, Bareille R, Amedee J, Baquey CH, Labrugere C, Dard M (2004) Grafting RGD containing peptides onto hydroxyapatite to promote osteoblastic cells adhesion. *J Mater Sci Mater Med* 15:779-786.
- Essler M, Ruoslahti E (2002) Molecular specialization of breast vasculature: a breast-homing phage-displayed peptide binds to aminopeptidase P in breast vasculature. *Proc Natl Acad Sci U S A* 99:2252-2257.
- Featherstone JD, Pearson S, LeGeros RZ (1984) An infrared method for quantification of carbonate in carbonated apatites. *Caries Res* 18:63-66.
- Feinberg SE, Aghaloo TL, Cunningham LL, Jr (2005) Role of Tissue Engineering in Oral and Maxillofacial Reconstruction: Findings of the 2005 AAOMS Research Summit. *J Oral Maxillofac Surg* 63:1418-1425.
- Feng QL, Cui FZ, Wang H, Kim TN, Kim JO (2000) Influence of solution conditions on deposition of calcium phosphate on titanium by NaOH-treatment. *J Cryst Growth* 210:735-740.
- Ferris DM, Moodie GD, Dimond PM, Giorani CWD, Ehrlich MG, Valentini RF (1999) RGD-coated titanium implants stimulate increased bone formation in vivo. *Biomaterials* 20:2323-2331.
- Fujisawa R, Kuboki Y (1998) Conformation of dentin phosphophoryn adsorbed on hydroxyapatite crystals. *Eur J Oral Sci* 106 Suppl 1:249-253.

- Fujisawa R, Kuboki Y (1991) Preferential adsorption of dentin and bone acidic proteins on the (100) face of hydroxyapatite crystals. *Biochim Biophys Acta* 1075:56-60.
- Fujisawa R, Mizuno M, Nodasaka Y, Kuboki Y (1997) Attachment of osteoblastic cells to hydroxyapatite crystals by a synthetic peptide (Glu7-Pro-Arg-Gly-Asp-Thr) containing two functional sequences of bone sialoprotein. *Matrix Biol* 16:21-28.
- Fujisawa R, Wada Y, Nodasaka Y, Kuboki Y (1996) Acidic amino acid-rich sequences as binding sites of osteonectin to hydroxyapatite crystals. *Biochim Biophys Acta* 1292:53-60.
- Gale JD, Rohl AL (2003) The General Utility Lattice Program (GULP). *Mol Simul* 29:291-341.
- Garcia AJ, Boettiger D (1999) Integrin-fibronectin interactions at the cell-material interface: initial integrin binding and signaling. *Biomaterials* 20:2427-2433.
- Garcia AJ, Ducheyne P, Boettiger D (1998) Effect of surface reaction stage on fibronectin-mediated adhesion of osteoblast-like cells to bioactive glass. *J Biomed Mater Res* 40:48-56.
- Garcia AJ, Gallant ND (2003) Stick and grip: measurement systems and quantitative analyses of integrin-mediated cell adhesion strength. *Cell Biochem Biophys* 39:61-73.
- Garcia AJ, Reyes CD (2005) Bio-adhesive surfaces to promote osteoblast differentiation and bone formation. *J Dent Res* 84:407-413.
- Geesink RG (2002) Osteoconductive coatings for total joint arthroplasty. *Clin Orthop Relat Res* 395:53-65.
- Gilbert M, Giachelli CM, Stayton PS (2003) Biomimetic peptides that engage specific integrin-dependent signaling pathways and bind to calcium phosphate surfaces. *J Biomed Mater Res* 67A:69-77.
- Gilbert M, Shaw WJ, Long JR, Nelson K, Drobny GP, Giachelli CM, Stayton PS (2000) Chimeric peptides of statherin and osteopontin that bind hydroxyapatite and mediate cell adhesion. *J Biol Chem* 275:16213-16218.
- Glimcher MJ (1984) Recent Studies of the Mineral Phase in Bone and its Possible Linkage to the Organic Matrix by Protein-Bound Phosphate Bonds. *Philos Trans R Soc Lond Ser B-Biol Sci* 304:479-508.
- Goldberg HA, Warner KJ, Li MC, Hunter GK (2001) Binding of bone sialoprotein, osteopontin and synthetic polypeptides to hydroxyapatite. *Connect Tissue Res* 42:25-37.
- Gunn C, (1996) *Bones and Joints: a guide for students*. New York: Churchill Livingstone.
- Habibovic P, Barrere F, van Blitterswijk CA, de Groot K, Layrolle P (2002) Biomimetic hydroxyapatite coating on metal implants. *J Am Ceram Soc* 85:517-522.
- Hauptmann S, Dufner H, Brickmann J, Kast SM, Berry RS (2003) Potential energy function for apatites. *Phys Chem Chem Phys* 5:635-639.

- Healy KE, Thomas CH, Rezanian A, Kim JE, McKeown PJ, Lom B, Hockberger PE (1996) Kinetics of bone cell organization and mineralization on materials with patterned surface chemistry. *Biomaterials* 17:195-208.
- Hennessy KM, Clem WC, Phipps MC, Sawyer AA, Shaikh FM, Bellis SL (2008) The effect of RGD peptides on osseointegration of hydroxyapatite biomaterials. *Biomaterials* 29:3075-3083.
- Hern DL, Hubbell JA (1998) Incorporation of adhesion peptides into nonadhesive hydrogels useful for tissue resurfacing. *J Biomed Mater Res* 39:266-276.
- Hersel U, Dahmen C, Kessler H (2003) RGD modified polymers: biomaterials for stimulated cell adhesion and beyond. *Biomaterials* 24:4385-4415.
- Hirano Y, Mooney DJ (2004) Peptide and Protein Presenting Materials for Tissue Engineering. *Adv Mater* 16:17-18-25.
- Hollister SJ, Lin CY, Saito E, Lin CY, Schek RD, Taboas JM, Williams JM, Partee B, Flanagan CL, Diggs A, Wilke EN, Van Lenthe GH, Muller R, Wirtz T, Das S, Feinberg SE, Krebsbach PH (2005) Engineering craniofacial scaffolds. *Orthod Craniofac Res* 8:162-173.
- Houseman BT, Mrksich M (2001) The microenvironment of immobilized Arg-Gly-Asp peptides is an important determinant of cell adhesion. *Biomaterials* 22:943-955.
- Hu Y, Winn SR, Krajchich I, Hollinger JO (2003) Porous polymer scaffolds surface-modified with arginine-glycine-aspartic acid enhance bone cell attachment and differentiation in vitro. *J Biomed Mater Res A* 64:583-590.
- Hubbell JA (1999) Bioactive biomaterials. *Curr Opin Biotechnol* 10:123-129.
- Huebsch JB, Fields GB, Triebes TG, Mooradian DL (1996) Photoreactive analog of peptide FN-C/H-V from the carboxy-terminal heparin-binding domains of fibronectin supports endothelial cell adhesion and spreading on biomaterial surfaces. *J Biomed Mater Res* 31:555-567.
- Hughes JM, Cameron M, Crowley KD (1990) Crystal-Structures of Natural Ternary Apatites - Solid-Solution in the $\text{Ca}_5(\text{PO}_4)_3\text{X}$ (X=f, Oh, Cl) System. *Am Mineral* 75:295-304.
- Hughes JM, Cameron M, Crowley KD (1989) Structural Variations in Natural F, Oh, and Cl Apatites. *Am Mineral* 74:870-876.
- Ignatius AA, Augat P, Claes LE (2001) Degradation behavior of composite pins made of tricalcium phosphate and poly(L,DL-lactide). *Journal of Biomaterials Science-Polymer Edition* 12:185-194.
- Ishaug SL, Yaszemski MJ, Bizios R, Mikos AG (1994) Osteoblast function on synthetic biodegradable polymers. *J Biomed Mater Res* 28:1445-1453.

- Itoh D, Yoneda S, Kuroda S, Kondo H, Umezawa A, Ohya K, Ohyama T, Kasugai S (2002) Enhancement of osteogenesis on hydroxyapatite surface coated with synthetic peptide (EEEEEEPRGDT) in vitro. *J Biomed Mater Res* 62:292-298.
- Keselowsky BG, Collard DM, Garcia AJ (2003) Surface chemistry modulates fibronectin conformation and directs integrin binding and specificity to control cell adhesion. *J Biomed Mater Res* 66A:247-259.
- Kilpadi KL, Chang PL, Bellis SL (2001) Hydroxylapatite binds more serum proteins, purified integrins, and osteoblast precursor cells than titanium or steel. *J Biomed Mater Res* 57:258-267.
- Kim H, Kim HW, Suh H (2003) Sustained release of ascorbate-2-phosphate and dexamethasone from porous PLGA scaffolds for bone tissue engineering using mesenchymal stem cells. *Biomaterials* 24:4671-4679.
- Kohn DH, Shin K, Hong SI, Jayasuriya AC, Leonova EV, Rossello RA, Krebsbach PH (2005) Self-Assembled Mineral Scaffolds as Model Systems for Biomineralization and Tissue Engineering. *Proceedings of the Eighth International Conference on the Chemistry and Biology of Mineralized Tissues* 216-219.
- Kokubo T (1996) Formation of biologically active bone-like apatite on metals and polymers by a biomimetic process. *Thermochimica Acta* 280:479-490.
- Kokubo T (1995) Apatite Formation on Organic Polymers by a Biomimetic Process. *European Journal of Solid State and Inorganic Chemistry* 32:819-827.
- Koo LY, Irvine DJ, Mayes AM, Lauffenburger DA, Griffith LG (2002) Co-regulation of cell adhesion by nanoscale RGD organization and mechanical stimulus. *J Cell Sci* 115:1423-1433.
- Koutsopoulos S (2002) Synthesis and characterization of hydroxyapatite crystals: a review study on the analytical methods. *J Biomed Mater Res* 62:600-612.
- Kriplani U, Kay BK (2005) Selecting peptides for use in nanoscale materials using phage-displayed combinatorial peptide libraries. *Curr Opin Biotechnol* 16:470-475.
- Ladner RC, Sato AK, Gorzelany J, de Souza M (2004) Phage display-derived peptides as therapeutic alternatives to antibodies. *Drug Discov Today* 9:525-529.
- Langer R, Vacanti JP (1993) Tissue engineering. *Science* 260:920-926.
- LeBaron RG, Athanasiou KA (2000) Extracellular matrix cell adhesion peptides: functional applications in orthopedic materials. *Tissue Eng* 6:85-103.
- Lee SW, Mao C, Flynn CE, Belcher AM (2002) Ordering of quantum dots using genetically engineered viruses. *Science* 296:892-895.
- LeGeros RZ (1991) *Calcium Phosphates in Oral Biology and Medicine*. New York: Karger.

- Leonova EV, Pennington KE, Krebsbach PH, Kohn DH (2006) Substrate mineralization stimulates focal adhesion contact redistribution and cell motility of bone marrow stromal cells. *J Biomed Mater Res A* 79:263-270.
- Liao CJ, Lin FH, Chen KS, Sun JS (1999) Thermal decomposition and reconstruction of hydroxyapatite in air atmosphere. *Biomed Sci Instrum* 35:99-104.
- Liu XH, Ma PX (2004) Polymeric scaffolds for bone tissue engineering. *Ann Biomed Eng* 32:477-486.
- Liu Y, de Groot K, Hunziker EB (2005) BMP-2 liberated from biomimetic implant coatings induces and sustains direct ossification in an ectopic rat model. *Bone* 36:745-757.
- Liu Y, Hunziker EB, Layrolle P, De Bruijn JD, De Groot K (2004) Bone morphogenetic protein 2 incorporated into biomimetic coatings retains its biological activity. *Tissue Eng* 10:101-108.
- Liu Y, Layrolle P, de Bruijn J, van Blitterswijk C, de Groot K (2001) Biomimetic coprecipitation of calcium phosphate and bovine serum albumin on titanium alloy. *J Biomed Mater Res* 57:327-335.
- Lobel KD, Hench LL (1998) In vitro adsorption and activity of enzymes on reaction layers of bioactive glass substrates. *J Biomed Mater Res* 39:575-579.
- Luong LN, Hong SI, Patel RJ, Outslay ME, Kohn DH (2006) Spatial control of protein within biomimetically nucleated mineral. *Biomaterials* 27:1175-1186.
- Ma PX, Langer R (1999) Fabrication of Biodegradable Polymer Foams for Cell Transplantation and Tissue Engineering. In: *Methods in Molecular Medicine, Vol 18: Tissue Engineering Methods and Protocols*, (Morgan JR, Yarmush ML eds) Totowa, NJ: Humana Press Inc.
- Maheshwari G, Brown G, Lauffenburger DA, Wells A, Griffith LG (2000) Cell adhesion and motility depend on nanoscale RGD clustering. *J Cell Sci* 113(10):1677-1686.
- Makowski L, Soares A (2003) Estimating the diversity of peptide populations from limited sequence data. *Bioinformatics* 19:483-489.
- Mandava S, Makowski L, Devarapalli S, Uzubell J, Rodi DJ (2004) RELIC--a bioinformatics server for combinatorial peptide analysis and identification of protein-ligand interaction sites. *Proteomics* 4:1439-1460.
- Mao C, Flynn CE, Hayhurst A, Sweeney R, Qi J, Georgiou G, Iverson B, Belcher AM (2003) Viral assembly of oriented quantum dot nanowires. *Proc Natl Acad Sci U S A* 100:6946-6951.
- Mardilovich A, Kokkoli E (2004) Biomimetic peptide-amphiphiles for functional biomaterials: The role of GRGDSP and PHSRN. *Biomacromolecules* 5:950-957.
- Marks C, Marks JD (1996) Phage libraries - A new route to clinically useful antibodies. *N Engl J Med* 335:730-733.

- Maskarinec SA, Tirrell DA (2005) Protein engineering approaches to biomaterials design. *Curr Opin Biotechnol* 16:422-426.
- Massia SP, Hubbell JA (1990) Covalent surface immobilization of Arg-Gly-Asp- and Tyr-Ile-Gly-Ser-Arg-containing peptides to obtain well-defined cell-adhesive substrates. *Anal Biochem* 187:292-301.
- McFarland CD, Thomas CH, DeFilippis C, Steele JG, Healy KE (2000) Protein adsorption and cell attachment to patterned surfaces. *J Biomed Mater Res* 49:200-210.
- Menko AS, Boettiger D (1987) Occupation of the extracellular matrix receptor, integrin, is a control point for myogenic differentiation. *Cell* 51:51-57.
- Mikos AG, Thorsen AJ, Czerwonka LA, Bao Y, Langer R, Winslow DN, Vacanti JP (1994) Preparation and Characterization of Poly(l-Lactic Acid) Foams. *Polymer* 35:1068-1077.
- Mkhonto D, de Leeuw NH (2002) A computer modelling study of the effect of water on the surface structure and morphology of fluorapatite: introducing a $\text{Ca}_{10}(\text{PO}_4)_6\text{F}_2$ potential model. *J Mater Chem* 12:2633-2642.
- Moradianoldak J, Frolow F, Addadi L, Weiner S (1992) Interactions between Acidic Matrix Macromolecules and Calcium-Phosphate Ester Crystals - Relevance to Carbonate Apatite Formation in Biomineralization. *Proc R Soc Lond Ser B-Biol Sci* 247:47-55.
- Morita Y, Mamiya K, Yamamura S, Tamiya E (2006) Selection and properties for the recognition of P19 embryonic carcinoma stem cells. *Biotechnol Prog* 22:974-978.
- Murphy WL, Kohn DH, Mooney DJ (2000) Growth of continuous bonelike mineral within porous poly(lactide-co-glycolide) scaffolds in vitro. *J Biomed Mater Res* 50:50-58.
- Murphy WL, Mooney DJ (2002) Bioinspired growth of crystalline carbonate apatite on biodegradable polymer substrata. *J Am Chem Soc* 124:1910-1917.
- Muschler GF, Midura RJ (2002) Connective tissue progenitors: practical concepts for clinical applications. *Clin Orthop Relat Res* (395):66-80.
- Naik RR, Brott LL, Clarson SJ, Stone MO (2002a) Silica-precipitating peptides isolated from a combinatorial phage display peptide library. *J Nanosci Nanotechnol* 2:95-100.
- Naik RR, Stringer SJ, Agarwal G, Jones SE, Stone MO (2002b) Biomimetic synthesis and patterning of silver nanoparticles. *Nat Mater* 1:169-172.
- Nesse WD (2000) *Introduction to Mineralogy*. New York: Oxford University Press.
- Niu XF, Wang YL, Luo YF, Xin J, Li YG (2005) Arg-gly-Asp (RGD) modified biomimetic polymeric materials. *J Mater Sci Technol* 21:571-576.
- Nowakowski GS, Dooner MS, Valinski HM, Mihaliak AM, Quesenberry PJ, Becker PS (2004) A specific heptapeptide from a phage display peptide library homes to bone marrow and binds to primitive hematopoietic stem cells. *Stem Cells* 22:1030-1038.

- Odermatt A, Audige A, Frick C, Vogt B, Frey BM, Frey FJ, Mazzucchelli L (2001) Identification of receptor ligands by screening phage-display peptide libraries ex vivo on microdissected kidney tubules. *J Am Soc Nephrol* 12:308-316.
- Ogino M, Ohuchi F, Hench LL (1980) Compositional dependence of the formation of calcium phosphate films on bioglass. *J Biomed Mater Res* 14:55-64.
- Okamoto K, Matsuura T, Hosokawa R, Akagawa Y (1998) RGD peptides regulate the specific adhesion scheme of osteoblasts to hydroxyapatite but not to titanium. *J Dent Res* 77:481-487.
- Oliveira AL, Malafaya PB, Reis RL (2003) Sodium silicate gel as a precursor for the in vitro nucleation and growth of a bone-like apatite coating in compact and porous polymeric structures. *Biomaterials* 24:2575-2584.
- Pallu S, Bareille R, Dard M, Kessler H, Jonczyk A, Vernizeau M, Amedee-Vilamitjana J (2003) A cyclo peptide activates signaling events and promotes growth and the production of the bone matrix. *Peptides* 24:1349-1357.
- Robey PG, Boskey AL (2003) Chapter 6: Extracellular Matrix and Biomineralization of Bone. In: American Society for Bone and Mineral Research.
- Pampena DA, Robertson KA, Litvinova O, Lajoie G, Goldberg HA, Hunter GK (2004) Inhibition of hydroxyapatite formation by osteopontin phosphopeptides. *Biochem J* 378:1083-1087.
- Pan HH, Tao JH, Xu XR, Tang RK (2007) Adsorption processes of Gly and Glu amino acids on hydroxyapatite surfaces at the atomic level. *Langmuir* 23:8972-8981.
- Parikh SN (2002) Bone graft substitutes in modern orthopedics. *Orthopedics* 25:1301-9.
- Parker SC, de Leeuw NH, Bourova E, Cooke DJ (2001) Application of Lattice Dynamics and Molecular Dynamics Techniques to Minerals and Their Surfaces. In: *Molecular Modeling Theory: Applications in the Geosciences*, Vol. 42 1st edition (Cygan RT, Kubicki JD eds) Washington DC: The Mineralogical Society of America.
- Pasqualini R, Koivunen E, Ruoslahti E (1995) A peptide isolated from phage display libraries is a structural and functional mimic of an RGD-binding site on integrins. *J Cell Biol* 130:1189-1196.
- Pelham RJ, Wang YL (1998) Cell locomotion and focal adhesions are regulated by the mechanical properties of the substrate. *Biol Bull* 194:348-349.
- Porter B, Zauel R, Stockman H, Guldberg R, Fyhrie D (2005) 3-D computational modeling of media flow through scaffolds in a perfusion bioreactor. *J Biomech* 38:543-549.
- Posner AS, Blumenthal NC, Betta F (1984) Chemistry and Structure of Hydroxyapatites. In: *Phosphate Minerals*, (Nriagu JO, Moore PB eds) Berlin: Springer Verlag.
- Prime K, Whitesides G (1991) Self-assembled organic monolayers: model systems for studying adsorption of proteins at surfaces. *Science* 252:1164-1167.

- Qiu SR, Wierzbicki A, Orme CA, Cody AM, Hoyer JR, Nancollas GH, Zepeda S, De Yoreo JJ (2004) Molecular modulation of calcium oxalate crystallization by osteopontin and citrate. *Proc Natl Acad Sci U S A* 101:1811-1815.
- Rappe AK, Casewit CJ, Colwell KS, Goddard WA, Skiff WM (1992) Uff, a Full Periodic-Table Force-Field for Molecular Mechanics and Molecular-Dynamics Simulations. *J Am Chem Soc* 114:10024-10035.
- Rappe AK, Goddard WA (1991) Charge Equilibration for Molecular-Dynamics Simulations. *J Phys Chem* 95:3358-3363.
- Rapuano BE, Wu C, MacDonald DE (2004) Osteoblast-like cell adhesion to bone sialoprotein peptides. *J Orthop Res* 22:353-361.
- Redey SA, Razzouk S, Rey C, Bernache-Assollant D, Leroy G, Nardin M, Cournot G (1999) Osteoclast adhesion and activity on synthetic hydroxyapatite, carbonated hydroxyapatite, and natural calcium carbonate: relationship to surface energies. *J Biomed Mater Res* 45:140-147.
- Reyes CD, Garcia AJ (2003a) A centrifugation cell adhesion assay for high-throughput screening of biomaterial surfaces. *J Biomed Mater Res A* 67:328-333.
- Reyes CD, Garcia AJ (2003b) Engineering integrin-specific surfaces with a triple-helical collagen-mimetic peptide. *J Biomed Mater Res* 65A:511-523.
- Rezania A, Healy KE (1999) Biomimetic peptide surfaces that regulate adhesion, spreading, cytoskeletal organization, and mineralization of the matrix deposited by osteoblast-like cells. *Biotechnol Prog* 15:19-32.
- Rezania A, Thomas CH, Branger AB, Waters CM, Healy KE (1997) The detachment strength and morphology of bone cells contacting materials modified with a peptide sequence found within bone sialoprotein. *J Biomed Mater Res* 37:9-19.
- Robey PG, Boskey AL (2006) Chapter 3: Extracellular Matrix and Biomineralization of Bone. American Society for Bone and Mineral Research Primer.
- Rodi DJ, Makowski L (1999) Phage-display technology--finding a needle in a vast molecular haystack. *Curr Opin Biotechnol* 10:87-93.
- Rodi DJ, Mandava S, Makowski L (2004) DIVAA: analysis of amino acid diversity in multiple aligned protein sequences. *Bioinformatics* 20:3481-3489.
- Rose FRAJ, Oreffo ROC (2002) Bone tissue engineering: Hope vs hype. *Biochem Biophys Res Commun* 292:1-7.
- Rosengren A, Pavlovic E, Oscarsson S, Krajewski A, Ravaglioli A, Piancastelli A (2002) Plasma protein adsorption pattern on characterized ceramic biomaterials. *Biomaterials* 23:1237-1247.
- Rouahi M, Gallet O, Champion E, Dentzer J, Hardouin P, Anselme K (2006) Influence of hydroxyapatite microstructure on human bone cell response. *J Biomed Mater Res Part A* 78A:222-235.

- Ruoslahti E (1996) RGD and other recognition sequences for integrins. *Annu Rev Cell Dev Biol* 12:697-715.
- Sahai N (2005) Modeling apatite nucleation in the human body and in the geochemical environment. *Am J Sci* 305:661-672.
- Samoylova TI, Ahmed BY, Vodyanoy V, Morrison NE, Samoylov AM, Globa LP, Baker HJ, Cox NR (2002) Targeting peptides for microglia identified via phage display. *J Neuroimmunol* 127:13-21.
- Samoylova TI, Petrenko VA, Morrison NE, Globa LP, Baker HJ, Cox NR (2003) Phage probes for malignant glial cells. *Mol Cancer Ther* 2:1129-1137.
- Samoylova TI, Smith BF (1999) Elucidation of muscle-binding peptides by phage display screening. *Muscle Nerve* 22:460-466.
- Sarig S (2004) Aspartic acid nucleates the apatite crystallites of bone: a hypothesis. *Bone* 35:108-113.
- Sarikaya M, Tamerler C, Jen AK, Schulten K, Baneyx F (2003) Molecular biomimetics: nanotechnology through biology. *Nat Mater* 2:577-585.
- Sawyer AA, Hennessy KM, Bellis SL (2005a) Regulation of mesenchymal stem cell attachment and spreading on hydroxyapatite by RGD peptides and adsorbed serum proteins. *Biomaterials* 26:1467-1475.
- Sawyer AA, Weeks DM, Kelpke SS, McCracken MS, Bellis SL (2005b) The effect of the addition of a polyglutamate motif to RGD on peptide tethering to hydroxyapatite and the promotion of mesenchymal stem cell adhesion. *Biomaterials* 26:7046-7056.
- Scott JK, Craig L (1994) Random peptide libraries. *Curr Opin Biotechnol* 5:40-48.
- Segvich S, Biswas S, Becker U, Kohn D (2008a) Identification of Peptides with Targeted Adhesion to Bone-Like Mineral via Phage Display and Computational Modeling. *Cell Tiss Org In Press*.
- Segvich S, Smith HC, Luong LN, Kohn DH (2008b) Uniform deposition of protein incorporated mineral layer on three-dimensional porous polymer scaffolds. *J Biomed Mater Res B Appl Biomater* 84:340-349.
- Seker UO, Wilson B, Dincer S, Kim IW, Oren EE, Evans JS, Tamerler C, Sarikaya M (2007) Adsorption behavior of linear and cyclic genetically engineered platinum binding peptides. *Langmuir* 23:7895-7900.
- Shaw WJ, Long JR, Campbell AA, Stayton PS, Drobny GP (2000a) A solid state NMR study of dynamics in a hydrated salivary peptide adsorbed to hydroxyapatite. *J Am Chem Soc* 122:7118-7119.
- Shaw WJ, Long JR, Dindot JL, Campbell AA, Stayton PS, Drobny GP (2000b) Determination of statherin N-terminal peptide conformation on hydroxyapatite crystals. *J Am Chem Soc* 122:1709-1716.

- Shea LD, Smiley E, Bonadio J, Mooney DJ (1999) DNA delivery from polymer matrices for tissue engineering. *Nat Biotechnol* 17:551-554.
- Sheu TJ, Schwarz EM, O'Keefe RJ, Rosier RN, Puzas JE (2002) Use of a phage display technique to identify potential osteoblast binding sites within osteoclast lacunae. *J Bone Miner Res* 17:915-922.
- Shimaoka H, Dohi Y, Ohgushi H, Ikeuchi M, Okamoto M, Kudo A, Kirita T, Yonemasu K (2004) Recombinant growth/differentiation factor-5 (GDF-5) stimulates osteogenic differentiation of marrow mesenchymal stem cells in porous hydroxyapatite ceramic. *J Biomed Mater Res A* 68:168-176.
- Shin H, Jo S, Mikos AG (2003) Biomimetic materials for tissue engineering. *Biomaterials* 24:4353-4364.
- Shin H, Jo S, Mikos AG (2002) Modulation of marrow stromal osteoblast adhesion on biomimetic oligo[poly(ethylene glycol) fumarate] hydrogels modified with Arg-Gly-Asp peptides and a poly(ethyleneglycol) spacer. *J Biomed Mater Res* 61:169-179.
- Shin H, Zygourakis K, Farach-Carson MC, Yaszemski MJ, Mikos AG (2004a) Attachment, proliferation, and migration of marrow stromal osteoblasts cultured on biomimetic hydrogels modified with an osteopontin-derived peptide. *Biomaterials* 25:895-906.
- Shin H, Zygourakis K, Farach-Carson MC, Yaszemski MJ, Mikos AG (2004b) Modulation of differentiation and mineralization of marrow stromal cells cultured on biomimetic hydrogels modified with Arg-Gly-Asp containing peptides. *J Biomed Mater Res Part A* 69A:535-543.
- Shin K, Jayasuriya AC, Kohn DH (2007) Effect of ionic activity products on the structure and composition of mineral self assembled on three-dimensional poly(lactide-co-glycolide) scaffolds. *J Biomed Mater Res A* 83:1076-1086.
- Simionescu A, Philips K, Vyavahare N (2005) Elastin-derived peptides and TGF-beta1 induce osteogenic responses in smooth muscle cells. *Biochem Biophys Res Commun* 334:524-532.
- Stayton PS, Drobny GP, Shaw WJ, Long JR, Gilbert M (2003) Molecular recognition at the protein-hydroxyapatite interface. *Crit Rev Oral Biol Med* 14:370-376.
- Stigter M, de Groot K, Layrolle P (2002) Incorporation of tobramycin into biomimetic hydroxyapatite coating on titanium. *Biomaterials* 23:4143-4153.
- Streuli CH, Bailey N, Bissell MJ (1991) Control of mammary epithelial differentiation: basement membrane induces tissue-specific gene expression in the absence of cell-cell interaction and morphological polarity. *J Cell Biol* 115:1383-1395.
- Tamerler C, Dincer S, Heidel D, Zareie MH, Sarikaya M (2003) Biomimetic multifunctional molecular coatings using engineered proteins. *Prog Org Coat* 47:267-274.

- Tamerler C, Sarikaya M (2007) Molecular biomimetics: Utilizing nature's molecular ways in practical engineering. *Acta Biomater* 3:289-299.
- Tanahashi M, Matsuda T (1997) Surface functional group dependence on apatite formation on self-assembled monolayers in a simulated body fluid. *J Biomed Mater Res* 34:305-315.
- Toh YC, Ho ST, Zhou Y, Hutmacher DW, Yu H (2005) Application of a polyelectrolyte complex coacervation method to improve seeding efficiency of bone marrow stromal cells in a 3D culture system. *Biomaterials* 26:4149-4160.
- Tosatti S, Schwartz Z, Campbell C, Cochran DL, VandeVondele S, Hubbell JA, Denzer A, Simpson J, Wieland M, Lohmann CH, Textor M, Boyan BD (2004) RGD-containing peptide GCRGYGRGDSPG reduces enhancement of osteoblast differentiation by poly(L-lysine)-graft-poly(ethylene glycol)-coated titanium surfaces. *J Biomed Mater Res* 68A:458-472.
- Uchiyama F, Tanaka Y, Minari Y, Toku N (2005) Designing scaffolds of peptides for phage display libraries. *J Biosci Bioeng* 99:448-456.
- VandeVondele S, Voros J, Hubbell JA (2003) RGD-grafted poly-L-lysine-graft-(polyethylene glycol) copolymers block non-specific protein adsorption while promoting cell adhesion. *Biotechnol Bioeng* 82:784-790.
- Verrier S, Pallu S, Bareille R, Jonczyk A, Meyer J, Dard M, Amedee J (2002) Function of linear and cyclic RGD-containing peptides in osteoprogenitor cells adhesion process. *Biomaterials* 23:585-596.
- Weber IT, Harrison RW, Iozzo RV (1996) Model structure of decorin and implications for collagen fibrillogenesis. *J Biol Chem* 271:31767-31770.
- Wen HB, de Wijn JR, van Blitterswijk CA, de Groot K (1999) Incorporation of bovine serum albumin in calcium phosphate coating on titanium. *J Biomed Mater Res* 46:245-252.
- Wen HB, Wolke JG, de Wijn JR, Liu Q, Cui FZ, de Groot K (1997) Fast precipitation of calcium phosphate layers on titanium induced by simple chemical treatments. *Biomaterials* 18:1471-1478.
- Whaley SR, English DS, Hu EL, Barbara PF, Belcher AM (2000) Selection of peptides with semiconductor binding specificity for directed nanocrystal assembly. *Nature* 405:665-668.
- Wierzbicki A, Cheung HS (2000) Molecular modeling of inhibition of hydroxyapatite by phosphocitrate. *Theochem-J Mol Struct* 529:73-82.
- Wiesmann HP, Joos U, Meyer U (2004) Biological and biophysical principles in extracorporal bone tissue engineering. Part II. *Int J Oral Maxillofac Surg* 33:523-530.
- Wopenka B, Pasteris JD (2005) A mineralogical perspective on the apatite in bone. *Mater Sci Eng C-Biomimetic Supramol Syst* 25:131-143.

Yamaoka T, Hotta Y, Kobayashi K, Kimura Y (1999) Synthesis and properties of malic acid-containing functional polymers. *Int J Biol Macromol* 25:265-271.

Yaszemski MJ, Payne RG, Hayes WC, Langer R, Mikos AG (1996) Evolution of bone transplantation: molecular, cellular and tissue strategies to engineer human bone. *Biomaterials* 17:175-185.

Zeng HT, Chittur KK, Lacefield WR (1999) Analysis of bovine serum albumin adsorption on calcium phosphate and titanium surfaces. *Biomaterials* 20:377-384.

Zhang J, Spring H, Schwab M (2001) Neuroblastoma tumor cell-binding peptides identified through random peptide phage display. *Cancer Lett* 171:153-164.

Zhang R, Ma PX (2004) Biomimetic polymer/apatite composite scaffolds for mineralized tissue engineering. *Macromol Biosci* 4:100-111.